UNIVERSITÀ
DEGLI STUDI
DI PADOVA

Head Office: Università degli Studi di Padova

Department of Cardiac, Thoracic, Vascular Sciences and Public Health

Ph.D. COURSE IN TRANSLATIONAL SPECIALISTIC MEDICINE "G.B. MORGAGNI"
CURRICULUM NEUROSCIENCES
SERIES XXXII

C. ELEGANS AS MODEL TO STUDY NEUROMETABOLIC CONDITIONS

Coordinator: Prof. Annalisa Angelini

Supervisor: Dr. Eva Trevisson

Ph.D. student : Valeria Morbidoni

CONTENTS

ABBREVIATIONS

Aβ: amyloid-β

Arg: arginine

ATG: autophagy-related gene

ATS: Alport syndrome

BN-PAGE: blue native polyacrylamide gel electrophoresis

bp: base pairs

CGC: *Caenorhabditis* Genetics Center

COX: cytochrome *c* oxydase

CRISPR: clustered regularly interspersed short palindromic repeats

crRNA: CRISPR RNA

DAB: 3,3'-diaminobenzidine

DEPC: diethyl pyrocarbonate

DSB: double-strand break

dsRNA: double-stranded RNA

EDTA: ethylenediamine tetraacetic acid

EMS: ethyl methanesulfonate

ETC: electron transport chain

Ex: exon

FITC: fluorescein-5-isothiocyanate

For: forward

FOX: Forkhead-box

gRNA: guide RNA

GIR: Gabarap interacting region

HDR: homology directed repair

HR: heat repeat

IFT: intraflagellar transport

IGF: insulin-like growth factor

Ins: insertion

Int: intron

IPTG: isopropyl β-D-thiogalactopyranoside

KO: knockout

LIR: LC3 interacting region

MAP: microtubule-associated protein

MKS: Meckel–Gruber syndrome

mRNA: messenger RNA

MT: microtubule

mtDNA: mitochondrial DNA

mtRFP: mitochondrial Red Fluorescent Protein

NF1: Neurofibromatosis 1

NGM: nematode growth media

NHEJ: non-homologous end joining

NMD: nonsense mediated mRNA decay

OMIM: Online Mendelian Inheritance in Man®

ORF: open reading frame

OXPHOS: oxidative phosphorylation

PAM: Protospacer Adjacent Motif

PAS: phagophore assembly site

PCR: polymerase chain reaction

PI3K: phosphatidylinositol 3-kinase

PQ: paraquat

RB: Retinoblastoma

Rev: reverse

RISC: RNAinduced silencing complex

RNAi: RNA interference

ROS: reactive oxygen species

rRNA: ribosomal RNA

siRNA: small interfering RNA

ssODN: single stranded DNA oligonucleotide

TCA: tricarboxylic acid

TMP: trimethyl psoralen

TOGARAM1: TOG array regulator of axonemal microtubules

Trp: tryptophan

tRNA: transfer RNA

tracrRNA: trans-activating crRNA

TTB: Tris Triton buffer

VUS: variant of uncertain significance

WES: whole exome sequencing

SUMMARY

The are several advantages in using *Caenorhabditis elegans* as organism model, among others its small size, the fast vital cycle and the easiness to maintain it in culture. Since between 60 and 80% of human genes have an orthologue in the worm genome, it has already been employed to investigate mitochondrial disorders, neurodegenerative diseases and also to search for neurotoxins and neuroprotective drugs.

During my PhD program I used *C. elegans* as a model to study genes whose function is unknown or not fully understood and potentially involved in neurometabolic diseases. At this purpose I performed RNA interference (RNAi) experiments and CRISPR/Cas9 genome editing to generate knockdown and knockout (KO)/knock-in worm models, that were then extensively phenotypically characterized.

Cytochrome *c* oxidase (COX) is the terminal enzymatic complex of the mitochondrial respiratory chain. Mutations in COX genes are responsible for COX deficiency, which is the most frequent cause of mitochondrial encephalomyopathies. *COX16* is a COX assembly factor, with a homologue in the worm genome, that is *cox-16*.

By a COX specific histochemical staining we found that *cox-16* is required for COX biogenesis and function, since its knockdown in nematodes causes COX deficiency. These results confirm what was previously obtained in a *COX16* KO cellular model, with the advantage of having a multicellular model that could be used for drug screening, since no cure is available so far for COX deficiencies.

MYTHO is a recently identified FOXO-dependent gene which seems to be involved in autophagy and has an orthologue in the *C. elegans* genome.

Since RNAi did not allow to detect a clearcut phenotype in nematodes, we therefore generated a KO model by CRISPR/Cas9 technology. KO animals did not show a significant reduction in survival after starvation, but manifested a precocious aging phenotype with locomotion impairment and reduced lifespan compared to controls. We are currently performing further experiments to analyze the autophagic flux in absence of *MYTHO* and characterize the pathway linking this gene to the IGF/Akt/FOXO signaling.

A novel genetic variant has been identified in a gene that belongs to Crescerin1 family of proteins regulating microtubule dynamics, in patients with a Meckel-Gruber-like phenotype. The worm orthologue *che-12* is expressed in the cilium of a subset of sensory neurons.

We generated worm lines harboring the novel missense variant found in patients by CRISPR/Cas9 technology. These were then characterized to explore potential effects on behaviors controlled by sensory neurons expressing *che-12*. We did not observe an impairment in chemotaxis ability on a NaCl gradient, nor a strong reduction of lipophilic dye-uptake frequency, however preliminary results indicate that the cilium of sensory neurons is shortened in *che-12* knock-in mutants. The demonstration of the pathogenic effect of the variant could establish an important link between mutations in this gene (that has not been so far associated with a human disease) and ciliopathies.

SECTION I

INTRODUCTION AND AIMS

1 *C. elegans* as a model organism

1.1 The history of *C. elegans* research

The use of the small round worm *Caenorhabditis elegans* as a model organism in laboratory dated back to the end of the 19th century . The work conducted during that century in the parasitic nematode *Ascaris* species set the stage for free-living nematodes (Nigon *et al*, 2017).

A key figure of this phase is Emile Maupas, who was the first to identify and name *Rhabditis elegans* and to adopt an experimental approach performing genetic crosses in order to unveil the mechanisms of sex determination (Maupas, 1900).

In 1940s two labs headed by Victor M. Nigon and Ellsworth C. Dougherty perfected the use of *C. elegans* as model organism and redefined experimental methods and culture conditions, increasing the reproducibility of experiments. Most importantly, the chromosomal basis of worm sex determination was determined using a tetraploid line (Nigon *et al*, 1951).

It was during 1960s that the employment of *C. elegans* as a model of choice to understand biologic questions had its most important phase with the work of Sidney Brenner. He used different nematode species and isolated many new strains before finally choosing *C. elegans* for his studies around 1966. He generated a lot of mutants using EMS (Ethyl methanesulfonate), and identified them scoring their phenotype (morphology and behavior). He could also locate many of the mutated genes in a genetic map thanks to linkage analysis (Brenner, 1974).

At that time molecular biology techniques were limited, however Brenner's work and the simplicity of the model set the basis for next important results, including the definition of the first and only entire cell lineage of a multicellular organism (Sulston *et al*, 1983), the discovery of apoptotic cell death (Hedgecock *et al*, 1983), the demonstration of the role of insulin pathway genes in regulating lifespan (Kenyon *et al*, 1993), the introduction of GFP as a biological marker (Chalfie *et al*, 1994), the discovery of gene silencing by RNA interference (Fire *et al*, 1998). Finally, *C. elegans* was the first metazoan to have its genome entirely sequenced in 1998 (*C. elegans* Genome Consortium, 1998).

Many scientists that contributed to these scientific discoveries, that were later adapted and applied to other biological systems, received recognition and awards, like the Nobel Prize (Brenner, Horvitz and Sulston in 2002, Fire and Mello in 2006 and Chalfie in 2008).

1.2 *C. elegans* natural history

Caenorhabditis elegans is a free-living nematode that can most easily be found in rotting vegetable matter (Barrière and Félix, 2014). The requirements for its growth are a humid environment, ambient temperature, atmospheric oxygen and bacteria as food.

In the lab *C. elegans* is grown on agar plates containing a lawn of *Escherichia coli*, where it moves with sinusoidal waves almost exclusively within a single, dorsoventral plane (White *et al*, 1986; Hope, 1999). This nematode is quite small: newly hatched larvae are 0.25 mm long and adults are 1 mm long, so they are observed with microscopes, often dissecting ones.

It grows at temperatures comprised between 12 and 25 °C, with a Q_{10} of ~2 (that is an increase of 10 °C speeds up growth twofold), making it possible to control the rate of its development changing growth temperature (Corsi *et al*, 2015). These nematodes exist almost exclusively as self-fertilizing hermaphrodites, with males present at a frequency less than 0.2%.

1.3 *C. elegans* life cycle

The life cycle is quite rapid and it takes more or less 3.5 days at 20 °C from an egg to an adult producing eggs and can last less than 3 days at 25 °C to 6 days at 15 °C. (Hope, 1999).

After fertilization, embryogenesis lasts approximately 16 hours at 20 °C. Embryos are retained inside the hermaphrodite until the 24-cell stage at which time they are laid. The embryo hatches with 558 nuclei thus becoming a first stage larva (L1). Worms begin to eat and grow through four larval stages, named L1, L2, L3 and L4; the L1 stage lasts ~16 hours at 20° C, while the others are ~12 hours long. Each stage is followed by a period of inactivity named lethargus, in which a new protective collagen cuticle is synthesized and replaces the old one. Approximately 12 hours after the L4 molt, adult hermaphrodites start to lay eggs (about 300 over a 4-day period) until they have utilized all of their self-produced sperm, but additional progeny can be generated by mating with a male. After the reproductive period, hermaphrodites generally live several weeks before dying of senescence (Corsi *et al*, 2015).

In absence of food and at high population density an alternative stage called “dauer” develops instead of the L3 stage after the second molt (Cassada and Russell, 1975; White *et al*, 1986). This stage is characterized by a cuticle that completely surrounds the animal, preventing it from feeding and protecting it from external dangerous agents. Dauers are able to survive several months and when food is newly available, they shed and resume their development.

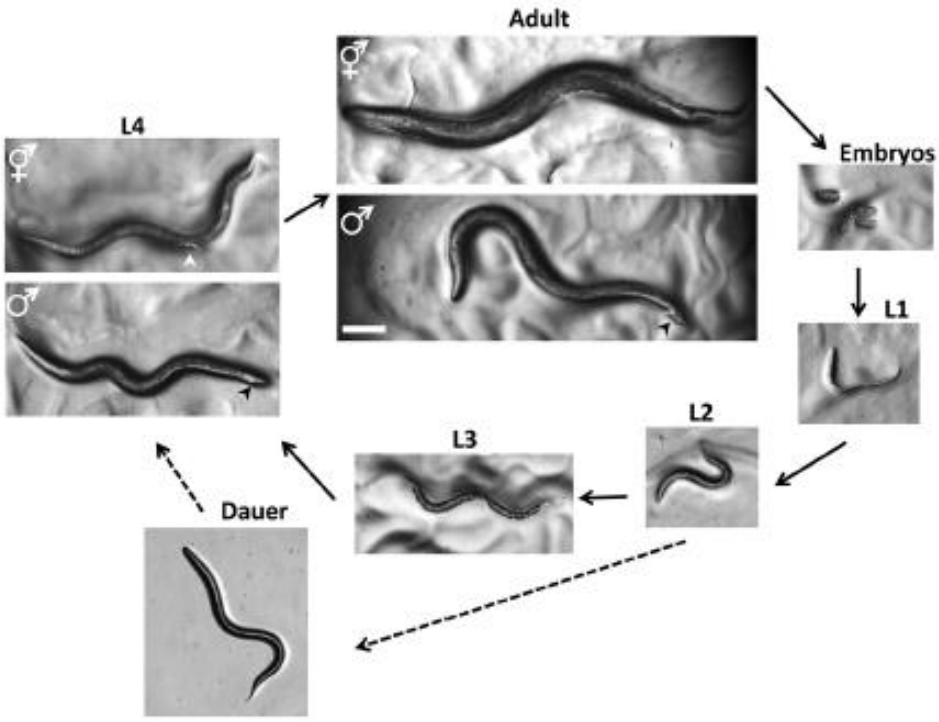

Fig. 1: Life cycle of *C. elegans*, consisting of four larval stages and an adult phase. An alternative L3 stage, called dauer, develops if food is absent and population density is high. Bar 0.1 mm (adapted from Corsi *et al*, 2015).

1.4 Anatomy

There are two sexes, the hermaphrodite and the male, both of which are diploid for the 5 autosomal chromosomes. The hermaphrodite has two XX chromosomes, while males possess only one X chromosome (the genotype of males is indeed referred as XO) and sex is determined by the X to autosome ratio (X:A) (Zarkower, 2006).

During the L4 stage hermaphrodites produce haploid ameboid sperm stored in the spermatheca. Later the germ line switches fate and produces oocytes. As said before, self-fertilization produces almost exclusively hermaphrodites.

Males arise only if meiotic non-disjunctions of the X chromosome happen (Corsi *et al*, 2015) for example after short exposures to higher temperatures (Sulston and Hodgkin, 1988; Fay, 2013).

If mated with males, hermaphrodites can lay up to 1000 eggs, instead of the approximately 300 produced by self-fertilization, indicating that the self-produced sperm is the limiting factor (Ward and Carrel, 1979). Besides, cross-fertilization produces hermaphrodites and males in equal proportions.

The general anatomy is shared by both sexes with males being a little shorter and thinner compared to hermaphrodites and consists of defined tissues. Adult *C. elegans* have an invariant number of cells, that is 959 in the hermaphrodite and 1031 in the male. The peculiarity of this organism is that the entire cell lineage, which has been traced, is identical between individuals (Sulston *et al*, 1983).

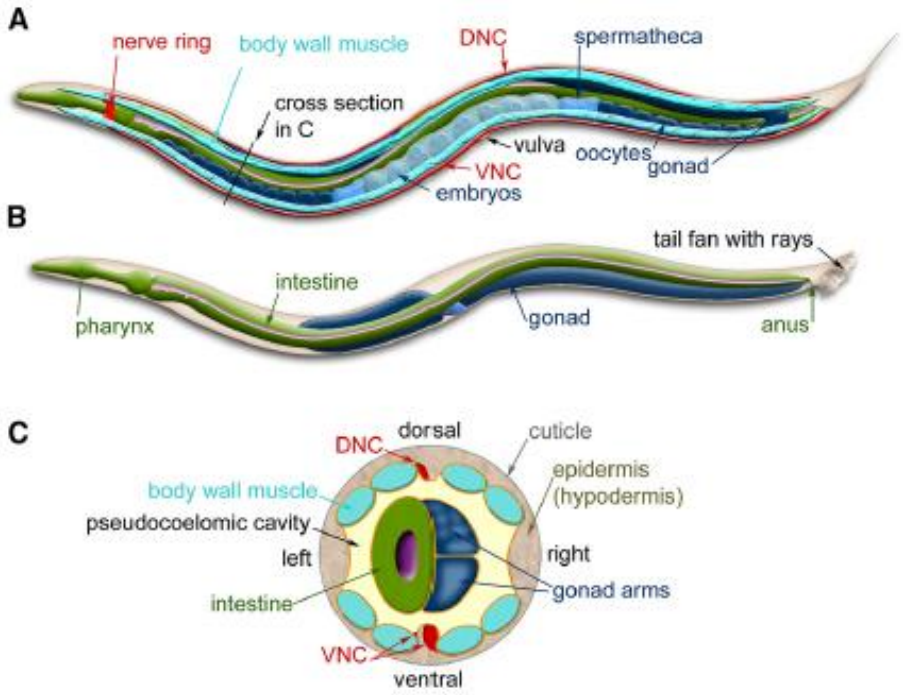

Fig. 2: Anatomy. of a hermaphrodite (A) and male (B) *C. elegans* viewed laterally. The dorsal nerve cord (DNC) and ventral nerve cord (VNC) run along the entire length of the animal starting from the nerve ring. Two of the four quadrants of body wall muscles are shown. (C) Cross-section through the anterior region of a hermaphrodite *C. elegans* highlighting the four muscle quadrants enclosed by the epidermis and cuticle with the intestine and gonad located within the pseudocoelomic cavity (adapted from Corsi *et al*, 2015).

The outer layer of cells is the epidermis, which encloses a pseudocoelomic cavity that contains the main worm organs. The epidermis consists of large multinucleated cells secreting the cuticle that covers the surface of the nematode and is composed by collagen, additional insoluble proteins termed cuticlins, lipids and glycoproteins (Corsi *et al*, 2015). Besides its role in defense against harmful agents, the cuticle defines the worm shape and provides anchoring points for muscle contraction.

Just below the epidermis, 95 body wall muscle cells are organized in four quadrants that run along the length of the body. Functional body wall muscle is required for the sinusoidal movement on semi-solid surfaces and develops during embryogenesis. Muscle cells are striated, mononucleated with multiple sarcomeres per cell (up to ten). Innervation of these cells is unusual, since muscles send extensions, called "muscle arms" to ventral and dorsal nerve cords to receive synapses (White *et al*, 1986). In addition to body wall muscle, *C. elegans* possesses muscles that control eating (20 pharyngeal muscles), egg-laying (8 vulval, 8 uterine muscles and 10 contractile gonadal sheath cells), digestion and defecation (2 stomatointestinal muscles, one anal sphincter and one anal depressor); besides, males possess 41 specific muscle cells (Gieseler *et al*, 2017).

Food enters worm through its mouth at the tip of the head and passes through the pharynx, a two-lobed neuromuscular pump, where it is grinded before entering the intestine for digestion. The pharynx

pumping depends on the availability and on the quality of the food: when worms are starving the pharynx pumps more (Avery and Shtonda, 2003).

The intestine consists of 20 big, polyploid epithelial cells that are arranged in pairs to form a tube that runs the animal longitudinally. During the first larval stage nuclei of intestinal cells divide, with subsequent rounds of DNA replication, but not nuclear division, in later larval stages (Hedgecock and White, 1985).

The hermaphrodite and the mail differ in the arrangement of the gonad and in the tail. The somatic gonad is located in the center of the body alongside the intestine and in the hermaphrodite it consists of two facing U-shaped tubes, while in the male it is a single U-shaped lobe (Corsi *et al*, 2015). Both sex gonads house the germline that will produce oocytes and sperm. Secondary sexual structures are the vulva in the hermaphrodite and the fan-shaped tail in the male. The vulva develops in the center of the epidermis on the ventral side of the hermaphrodite; male tails are flattened into a fan of cuticular material with 18 neuron projections and associated support cells called rays (Emmons *et al*, 2005).

C. elegans possesses also a rudimental immune system consisting of 6 cells (5 in the male) in the pseudocoelomic cavity, called coelomocytes, which function as scavengers in the body cavity. These cells are highly active in endocytosis and behave similarly to vertebrate macrophages, sorting and clearing material in the pseudocoelomic cavity of the animal (Hope, 1999; Corsi *et al*, 2015).

The excretory/secretory system, which is thought to be responsible for osmoregulation, consists of an excretory duct cell, an excretory pore cell, an excretory gland cell and the excretory cells all connected together (Hope, 1999).

1.4.1 The nervous system

For what concerns the nervous system of *C. elegans*, its overall general structure is a feature common to all nematodes. A nerve ring, consisting of annular neuropil and surrounding the neck of the pharyngeal muscle, is mainly composed of the axonal and dendritic processes of neurons whose cell bodies lie anteriorly and posteriorly to the nerve ring and contain only neuron cell bodies. All nematodes possess also a principal nerve cord that runs from head to tail along the ventral midline of the body. It contains cell bodies as well as processes, many of which project into the nerve ring establishing synapses with other neurons. Additional nerve cords (like the dorsal one) consist only of processes, since cell bodies reside in the ventral nerve cord and use circumferential commissures to connect to secondary nerve cords (Schafer, 2016).

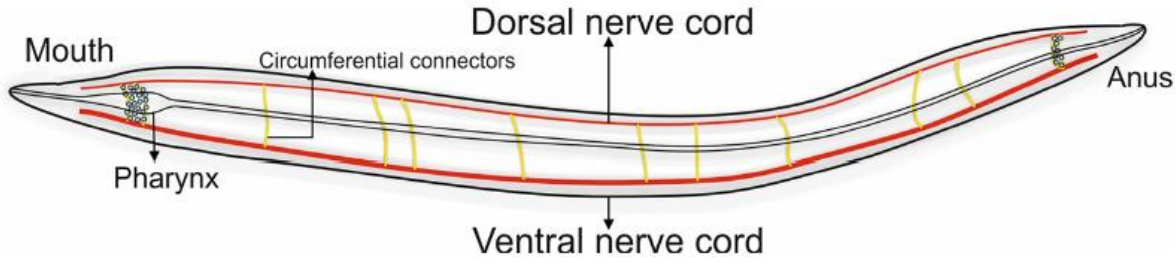

Fig. 3: The nervous system of nematodes consisting of the nerve ring, composed of axonal and dendritic processes, clusters of cephalic neuronal cell bodies ("ganglia"), a ventral nerve cord containing processes and motor neuron cell bodies, and a dorsal nerve cord and circumferential commissures (connectors) made exclusively of processes (adapted from Badhwar and Bagler, 2015).

The nervous system of an adult hermaphrodite consists of 302 neurons, while the male possesses 385 neurons and most of the extra nervous tissue is located in the tail. This number has been recently updated compared to the previous estimate of 383 male neurons after the discovery that sexual conditioning, a form of associative learning, requires two male-specific interneurons whose progenitors are fully differentiated glia (Sammut *et al*, 2015).

Neurons are generated at three main developmental periods: the first is during the proliferation phase of embryogenesis, the second at the late-L1 stage, and the third during the L2 stage (Altun and Hall, 2011).

Each of them has a peculiar combination of properties, such as morphology, connectivity and position, which could be reconstructed thanks to electron micrographs (White *et al*, 1986; see paragraph 10.1 for further details). Like in other vertebrates, neurons can be sensory neurons, interneurons or motoneurons. Most of them have a simple structure with one or two neurites that in the majority of cases cannot be distinguished as dendrites or axons, since they both give and receive synapses. In *C. elegans* there are also glia-like support cells, primarily associated with sensory neurons (Corsi *et al*, 2015). Contrary to the previously believed passive nature of nerve conduction, it has been recently demonstrated that AWA olfactory neurons, which are specialized in the detection of attractive odors gradients, reliably and reproducibly generate all-or-none action potentials under physiologically realistic conditions, as natural odor stimuli (Liu *et al*, 2018). Moreover, many common neurotransmitters, including acetylcholine, glutamate, ɣ-amino butyric acid (GABA), dopamine, and serotonin are present in *C. elegans* (Hobert, 2013).

Laser ablation has been applied to study the function of specific cells, and in particular of peculiar neurons, in *C. elegans* for decades. By killing individual or groups of cells with a UV laser, the subsequent abnormalities observed in development or behavior may provide answers to how cells interact with each other. The more recent invention of a near-infrared femtosecond laser system has enabled to reach surgical precision with laser ablation from the cellular level to the subcellular one to investigate for example the mechanisms of axon regeneration (Chiu *et al*, 2011).

1.5 Intermediary metabolism

Many enzymes involved in the principal pathways of intermediary metabolism are conserved in *C. elegans*. Energy is metabolized through pathways like glycolysis, tricarboxylic acid (TCA) cycle and oxidative phosphorylation, β-oxidation of fatty acids and degradation of branched amino-acids.
C. elegans is able to synthesize fatty and unfatty fatty acids *de novo* and it generally stores energy as lipids; carbohydrate stores consist primarily of glycogen. An alternative pathway to TCA, the glyoxylate pathway, is present only in nematodes among animals and uses small carbon compounds to build macromolecules (van der Bliek *et al*, 2017). Nitrogen and carbon are excreted respectively as ammonia and carbon dioxide or glycerol (Braeckman *et al*, 2009).
To cultivate this nematode in laboratory, the growth medium should contain exogenous cholesterol, since worms are not able to synthetize sterols *de novo* (Merris *et al*, 2004), a heme source (like hemoglobin or cytochrome *c*), several vitamins (thiamin, riboflavin, folic acid, niacinamide, pantothenic acid, pyridoxine, biotin and vitamin B_{12}) and amino acids (arginine, histidine, lysine, tryptophan, phenylalanine, methionine, threonine, leucine, isoleucine and valine). Energy sources like glucose and glycogen can be used, however it has been demonstrated that a high dietary glucose has a negative effect on worm lifespan (Schulz *et al*, 2007; Lee *et al*, 2009) and that is due to its accumulation as glycogen, that interferes with other antiaging signaling pathways (Gusarov *et al*, 2017).

1.6 Genetics

As mentioned above, *C. elegans* was the first multicellular eukaryote to have its genome completely sequenced in 1998 (*C. elegans* Genome Consortium, 1998). Its entire dimension is ~102 Mb (Tyson *et al*, 2018) and it contains 20,135 protein-coding genes (according to WormBase release WS272 in June 2019).
The nuclear genome is organized in five autosomal chromosomes named linkage group (LG) I, II, III, IV, and V plus the X chromosome. The functional organization of *C. elegans* chromosomes is different from that of vertebrate chromosomes, since they are holocentric, that is centromeres are along their entire length, and the distribution of active genes on autosomes is nonrandom, that is the density of active genes is higher in the center than along the arm (Cohen-Fix and Askjaer, 2017)
Genes are organized in 5' untranslated regions, open reading frames (ORFs) containing exons and generally small introns, and 3' untranslated regions. They possess alternative splicing mechanisms, with more than 90% of genes showing only one or two alternative spliced forms. *Trans*-splicing is common in this nematode, with more than half of pre-mRNAs receiving a SL1 leader sequence and 20% a SL2 (both SL1 and SL2 sequences are 22 nucleotides long). Worms are then peculiar among animals in having operons, polycistronic gene clusters containing two or more genes, accounting for ~15% of all genes (Hillier *et al*, 2005; Corsi *et al*, 2015).

The *C. elegans* mitochondrial DNA (mtDNA) is a circular molecule of 13,794 nucleotides in length and it encodes 36 genes: 2 ribosomal RNAs (12S rRNA and 16S rRNA), 22 transfer RNAs (tRNA), and 12 subunits of the mitochondrial respiratory chain. No introns are present and there are few or no non-coding nucleotides between genes; approximately 92% of the mitochondrial genome has coding function. (Lemire, 2005).

1.6.1 Forward and reverse genetics

C. elegans has been employed in genetic manipulations with an approach originally used by Sidney Brenner in his first experiments and called "forward genetics" (Brenner, 1974). Basically, worms were treated with mutagens, for example EMS, an alkylating agent that mainly causes GC-to-AT transitions or small deletions, and then interesting mutants were analyzed through classical genetic tools like linkage studies or, more recently, by whole genome sequencing to identify the chromosomal region harboring the mutation (Corsi *et al*, 2015).
With the more recently developed approaches, called "reverse genetics", a particular gene sequence is altered and the effects on development, morphology or behavior are analyzed (Ahringer, 2006).
Different methods can be used to perturb gene function in *C. elegans*.

1.6.1.1 RNA interference

The first, called RNA interference (RNAi) was originally discovered in 1998 by Fire and Mello (Fire *et al*, 1998). They found that the introduction of exogenous RNA into the nematode led to the interference with the function of a specific endogenous gene. This effect was surprisingly much more evident if dsRNA (double-stranded RNA) was used.
This phenomenon, believed to exist as a cellular defense mechanism against pathogens, is initiated by a cellular enzyme, the type III endoribonuclease Dicer, that cuts the intracellularly delivered dsRNA in small interfering RNA (siRNA). The 21-24 nucleotides long siRNA binds to the Argonaute (Ago) protein, which with other accessory factors forms the RNAinduced silencing complex (RISC) and then base pairs to the complementary cellular messenger RNA (mRNA). An enzyme of the RISC complex cleaves the target mRNA leading to its consequent degradation (Maillard *et al*, 2019).
Nowadays this technique is commonly used in laboratory to knock down gene function and can be carried out in three different ways: injection of dsRNA into young adult hermaphrodites; soaking of worms in a high concentrated dsRNA solution; feeding of worms with dsRNA expressed by *E. coli* on Nematode Growth Medium (NGM) plates. Remarkably, in *C. elegans* RNAi effect can be maintained for three or more generations and is heritable, since it can be transmitted with the single sperm (Grishok, 2005).
This technique is generally used for rapid screening of loss of function phenotypes. However, some precautions have to be taken. In fact, silencing produces a gene knockdown rather than a complete knockout and the results are often variable, the number of false negative results is high (about 30%)

and even if the level of the target mRNA is undetectable, the protein product could not be totally eliminated (Ahringer, 2006).

1.6.1.2 Genome-editing

During the last years, several advantages in genome-editing methods have been achieved and these techniques are also suitable to modify *C. elegans* genome by introducing point mutations or creating larger genomic rearrangements.

Among others, the clustered regularly interspersed short palindromic repeats (CRISPR)/Cas9 technology is now the most used for these purposes.

The name derives from the CRISPR loci, a microbial adaptive immunity system, that consists of a set of CRISPR-associated (Cas) genes and the CRISPR array, a series of repeat sequences (direct repeats) spaced by variable sequences (spacers) that have homology to various foreign DNA (*e.g.* viruses, mobile genetic elements). Cas genes are translated into proteins, while most CRISPR arrays are transcribed as a single RNA before being processed into shorter CRISPR RNAs (crRNA) that direct the activity of some Cas enzymes to degrade target complementary nucleic acids (Hsu *et al*, 2014).

So far six distinct bacterial CRISPR systems have been identified, with type I and III belonging to class I, while type II, IV, V and VI belonging to class II (Adli, 2018).

The type II system (often simply referred to as CRISPR) has been engineered from *Streptococcus pyogenes* to direct genome-editing in mammalian cells and is the basis for the current genome engineering technology available (Cong *et al*, 2013). A potential target sequence is valid if it contains a special Protospacer Adjacent Motif (PAM, which is NGG for this type) directly after the crRNA binding site. A key component in the biogenesis and processing of crRNA is a noncoding trans-activating crRNA (tracrRNA) that hybridizes with crRNA in order to facilitate RNA-guided targeting of Cas9. Then, Cas9 separates the double stranded DNA target and cleaves both strands after the PAM creating a double-strand break (DSB).

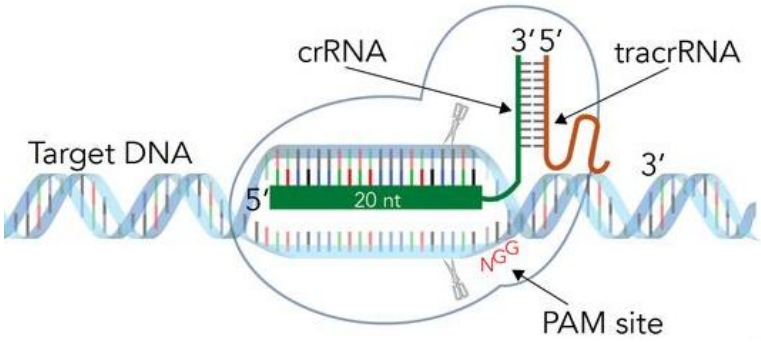

Fig. 4: A target sequence, complementary to the crRNA and followed by the PAM sequence (NGG), hybridizes with the crRNA-tracrRNA complex. The Cas9 enzyme is guided by this complex to the target site to create a DSB (adapted from the Integrated DNA Technologies web site, https://eu.idtdna.com/pages).

Cells can use NHEJ (Non-homologous end joining) or HDR (Homology directed repair) mediated genome repair mechanisms (Cong *et al*, 2013; Hsu *et al*, 2014). The error-prone NHEJ creates insertions/deletions (indels), while HDR uses a template sequence for a very precise repair of the DSB.

This technology has proven to be very accurate and efficient. CRISPR has been used in different cellular and animal models and it has also been optimized in *C. elegans* (Paix *et al*, 2017). Particularly, to improve genome-editing frequency while reducing off-targets effects, the new protocol introduced two innovations, the direct injection of CRISPR-Cas9 ribonucleoprotein complexes in the gonads of adult hermaphrodites and the use of linear DNAs with short homology arms as repair templates.

1.7 Advantages and limitations in using *C. elegans* as model organism

The use of this nematode as model for biological studies has several advantages.

First of all, its maintenance in lab is easy, since the size is small, the cultivation is cheap and the brood size is large. Moreover, it is quite innocuous for humans and strains can be cryopreserved.

The animal is transparent, thus enabling an easy visualization at the microscope and as said before both the number of somatic cells and neurons is invariant between individuals (Sulston *et al*, 1983; White *et al*, 1986). For these reasons *C. elegans* is a suitable organism for developmental studies and to investigate neuronal circuits and the genetic bases of behavior (Corsi *et al*, 2015).

Since its small size, many assays can be carried out in wells of a 96-well plate, enabling for example high-throughput for neurotoxins and drug screening (Kaletta and Hengartner, 2006).

An advantage for genetic analysis is the fact that *C. elegans* exists almost exclusively as self-fertilizing hermaphrodites. Actually, self-fertilization simplifies maintaining stocks in culture and tends to eliminate heterozygosis in the population. Genetic traits are inherited following standard Mendelian rules of segregation, so mutants can be easily identified. Moreover, genetic manipulation of nematodes and genetic crosses are commonly performed (Fay, 2013; Corsi *et al*, 2015)

As stated above, *C. elegans* was the first multicellular organism to have its genome completely sequenced in 1998 (*C. elegans* Genome Consortium, 1998). It has been shown that between 60 and 80% of human genes have an orthologue in the nematode genome and a subsequent comparison with the human genome confirmed that the majority of human disease genes and disease pathways are present in *C. elegans*. As a consequence, this nematode has been chosen to model and investigate different human genetic diseases and pathological conditions, providing physiologically relevant data derived from a whole-animal setting thus overcoming limitations derived from the use of *in vitro* cellular models (Kaletta and Hengartner, 2006).

Given the short and largely invariant lifespan and the fact that the somatic cells of the adults are post-mitotic, this nematode has become one of the most used organisms to study aging, a process that in *C. elegans* shares many characteristics with that in humans, such as muscle atrophy (sarcopenia), reduced

skin elasticity and increased susceptibility to infection. Besides, a large number of worms can be tested at the same time allowing the identification of mutants that shorten or lengthen lifespan even by 10-15% with statistical solidity (Panowski and Dillin, 2009; Tissenbaum, 2015).

However, as other model organism, also *C. elegans* shows some limitations. Worms have a simple body plan and lack many defined organs and tissues including a brain, blood, a distinct fat cell, internal organs and their small size makes the isolation of different tissues to perform biochemical analysis really challenging (Tissenbaum, 2015). Besides, worms are evolutionary distant from humans and some molecular pathways simply do not exist in *C. elegans*.

Therefore, it is important to define the purpose and potential restrictions before choosing a model. The use of *C. elegans* as a model organism to study a human genetic disease is a good choice if the disease can be defined on a molecular basis, however worm models usually do not recreate the complete pathophysiology of the human disease. Therefore, it is important that data obtained with *C. elegans* models are validated on higher organisms to ensure congruence between the model and specific aspects of the human pathology (Kaletta and Hengartner, 2006).

1.7.1 *C.elegans* as model of human diseases

Online Mendelian Inheritance in Man® (OMIM) is a comprehensive compendium of human genes and genetic phenotypes that is freely available and continuously updated. It contains information on all known Mendelian disorders and over 15,000 genes and focuses on the relationship between phenotype and genotype. The OMIM Morbid Map Scorecard (https://www.omim.org/statistics/geneMap, which was updated on September 13th, 2019) reports that 6,499 phenotypes are defined at the molecular basis, and 4,147 genes (among the about 20,000 human identified protein-coding genes) show phenotype-causing mutations.

Phenotypes include single-gene Mendelian disorders and traits, susceptibilities to cancer and complex diseases, variations that lead to abnormal but benign laboratory test values ("nondiseases") and blood groups and somatic cell genetic diseases with these statistics:

Class of Phenotype	Phenotype	Gene*
Single gene disorders and traits	5,442	3,766
Susceptibility to complex disease or infection	693	501
“Nondiseases”	147	116
Somatic cell genetic disease	226	127

Table 1: The Dissected OMIM Morbid Map Scorecard:*Some genes may be counted more than once because mutations in a gene may cause more than one phenotype and the phenotypes may be of different classes (adapted from the web site https://omim.org/statistics/geneMap).

This highlights the importance to establish genetic models to study human diseases and human genes, since many of them have an unknown function or have not been associated to a specific phenotype so far.

In the last years, *C. elegans* was employed as model organism to investigate several human diseases.

Mitochondrial diseases are heterogeneous in the age of onset and in clinical manifestations, since they are often multisystemic, but generally affect tissues with high energy demands, like brain, muscle and heart. They are caused by mutations in nuclear genes coding for mitochondrial proteins or in mitochondrial DNA, which encodes for subunits of the mitochondrial electron transport chain (ETC) and the structural RNAs necessary for their expression (Wallace, 2010).

Many mitochondrial genes have an orthologue in *C. elegans* genome. It has been demonstrated that mutations in these genes, collectively referred to as "*Mit*" mutations, can actually prolong the lifespan in this organism. Disruption in components of all five mitochondrial ETC complexes, their electron carriers, and the machinery necessary for their maintenance and assembly can in fact lengthen life in worms from 20% to 200% (Rea *et al*, 2007).

However some considerations have to be made, since not all mutations in the ETC lead to longer lifespan. Moreover, life extension can happen only with a moderate degree of mitochondrial dysfunction and it is associated with slowed larval development, small adult size and decreased fertility (Ventura and Rea, 2007). On the other side, when mitochondrial disruption is too severe significant larval arrest occurs, or adult animals are invariably sterile and lifespan is nevertheless shortened.

Despite this apparent difference between what happens in humans and worms, the opposite and distinct phenotypes that characterize *C. elegans* upon mild or severe mitochondrial damage represent a useful tool to mimic the progressive course and severity of mitochondrial diseases, enabling to investigate the phase of partial mitochondrial suppression that in human is likely asymptomatic, while in the worm model it is associated with peculiar and recognizable phenotypes (Maglioni and Ventura, 2016).

Neurons, with their high-energy demand, are particularly vulnerable to mitochondrial dysfunction and many mitochondrial diseases lead to neurodegeneration. *C. elegans* has been indeed used as model for neurodegenerative conditions such as Alzheimer's and Parkinson's diseases, genetic disorders, like Huntington's disease, Duchenne dystrophy and Friedreich's ataxia, but also to investigate molecular pathways involved in cancer (Kaletta and Hengartner, 2006; Maglioni and Ventura, 2016).

In some cases, the human disease gene does not have an orthologue in *C. elegans*. However, conserved responses or interactions can often be detected. The nematode models have also helped to elucidate disease pathogenesis and suggested new approaches for therapeutic interventions (Kaletta and Hengartner, 2006).

2 Aims of the work

Our research group focuses on the study of the molecular mechanisms underlying rare inherited neurometabolic conditions using *in vivo* models. During my PhD program, I have employed *Caenorhabditis elegans*, a transparent nematode, which is easy and fast to cultivate and combines the advantage of a significant genomic evolutionary conservation (between 60 and 80% of human genes have an orthologue in the nematode genome) with the possibility to obtain relevant data from a whole animal setting. We have used this animal model to:

1) explore in a multicellular context the function of *cox-16*, a cytochrome *c* oxidase (COX) assembly factor orthologue to human *COX16*, whose essential role for proper complex biogenesis and function was demonstrated in a cellular model devoid of this gene.

2) investigate the function of *MYTHO*, a recently identified FOXO-dependent gene involved in autophagy, through *T01G9.2* (the worm orthologue of *MYTHO*) knockdown and KO models.

2) examine the functional consequences of a novel genetic variant identified in *TOGARAM1* in patients with a Meckel-Gruber-like phenotype, by generating a knock-in model harboring the same variant in the worm orthologue gene *che-12*, which in nematodes is expressed in the cilium of a subset of sensory neurons.

The generation of KO and knock-in worm strains was performed in collaboration with Dr. Simone Martinelli, a *C. elegans* researcher who works at the Istituto Superiore di Sanità in Roma. I visited his lab and I was trained to use the microinjection system, essential to perform genome-editing in this animal model.
Experiments on *MYTHO* were performed in collaboration with Prof. Marco Sandri, who identified the gene and started its characterization using cellular and murine models.
To get some advice on *che-12* experiments we also collaborated with Prof. Kevin Slep, who works at University of North Carolina at Chapel Hill and is an expert in the analysis of proteins regulating microtubules dynamics.

SECTION II

MATERIALS AND METHODS

3.1 *C. elegans* strains, growth conditions and maintenance

Caenorhabditis elegans strains were grown monoxenically on Nematode Growth Medium (NGM) agar plates at 20 °C, feeding *E. coli* OP50 bacteria (Brenner, 1974). Where indicated, other culture media, food source and temperatures were employed for specific experimental needs.

Worm strains as well as OP50 bacteria were purchased from CGC (*Caenorhabditis* Genetics Center, University of Minnesota), unless otherwise specified. Bacterial cultures inoculated the day before in a rich medium like LB Broth (see table 3) were seeded on NGM plates and incubated overnight at 37°C. OP50 bacteria are uracil auxotrophs whose growth is limited on NGM plates, which are uracil-limited (Stiernagle, 2006).

To maintain stocks of worm strains, pieces of NGM agar were periodically cut and inverted on fresh new plates ("chunking"), thus enabling worms to leave the old agar pieces and to spread out onto the new bacterial lawn. If a precise number of nematodes was needed on a plate, worms were instead singularly picked up using a platinum wire.

To remove contaminants from plates or to synchronize a worm population, nematodes were treated with a solution containing 5 N NaOH and bleach ("bleaching") that kills everything but embryos, thus isolating eggs and synchronizing cultures at the first larval stage (Corsi *et al*, 2015).

As *Caenorhabditis elegans* can be frozen and stored indefinitely in liquid nitrogen (Brenner, 1974), once a new strain was obtained, some backup vials were conserved at -80 °C in a freezing solution containing glycerol at a final concentration of 15%.

The list of *Caenorhabditis elegans* strains used, their genotype, origin and methods of generation are displayed in the table below:

Table 2

Strain name	Genotype	Origin	Generation method	Number of outcrosses
Bristol N2	Wild-type isolate	CGC	Isolated from mushroom compost near Bristol	1
NL2099 (1)	*rrf-3(pk1426) II*	CGC	UV/TMP	2
DH26 (2)	*fer-15(b26) II*	CGC	EMS	2
DA2123 (3)	*adls2122 [lgg-1p::GFP::lgg-1 + rol-6(su1006)]*	CGC	Gamma Rays	7
Mytho KO	*T01G9.2*(*pan8*[S18Tfs*19]) *I*, *T01G9.2*(*pan9*[S18Tfs*19]) *I*, or *T01G9.2*(*pan10*[S18Tfs*19]) *I*	generated by Simone Martinelli's lab	CRISPR/Cas9	1

fer-15/Mytho KO	*T01G9.2*(*pan8*[S18Tfs*19]) *I*; *fer-15(b26) II* or *T01G9.2*(*pan9*[S18Tfs*19]) *I*; *fer-15(b26) II*	Our lab	Genetic cross	-
	adls2122 [*lgg-1p::GFP::lgg-1* + *rol-6(su1006)*]; *T01G9.2*(*pan8*[S18Tfs*19]) *I*	Our lab	Genetic cross	-
CB1370 (4)	*daf-2(e1370) III*	CGC	EMS	not indicated
CF1038 (5)	*daf-16(mu86) I*	CGC	UV/TMP	11
daf-2 /fer-15/Mytho KO	*T01G9.2*(*pan8*[S18Tfs*19]) *I; fer-15(b26) II; daf-2(e1370) III*	Our lab	Genetic cross	-
daf-16/ fer-15/Mytho KO	*T01G9.2*(*pan8*[S18Tfs*19]) *daf-16(mu86) I*; *fer-15(b26) II*	Our lab	Genetic cross	-
OH3192 (6)	*ntls1 [gcy-5p::GFP + lin-15(+)] V*	CGC	No mutagen	5
SP1620(7)	*che-12 (mn389) V*	CGC	EMS	2
LP177 (8)	*unc-119(ed3) III; che-12(cp26[Δ1-1282 + GFP + LoxP unc-119(+) LoxP]) V*	received from Kevin Slep	CRISPR/Cas9	not indicated
	che-12(*pan11*[R284W (AGA>TGG)]) *V*, *che-12*(*pan12*[R284W (AGA>TGG)]) *V*, or *che-12*(*pan13*[R284W (AGA>TGG)]) *V*	generated by Simone Martinelli's lab	CRISPR/Cas9	2
	ntls1 [gcy-5p::GFP + lin-15(+)] che-12 (mn389) V	Our lab	Genetic cross	-
	ntls1 [gcy-5p::GFP + lin-15(+)] che-11(*pan11*[R284W(AGA>TGG)]) *V*	Our lab	Genetic cross	-
	ntls1 [gcy-5p::GFP + lin-15(+)] che-12(*pan12*[R284W(AGA>TGG)]) *V*	Our lab	Genetic cross	-
	ntls1 [gcy-5p::GFP + lin-15(+)] che-12 pan12/cp26[Δ1-1282 + GFP + LoxP unc-119(+) LoxP] V	Our lab	Genetic cross	-

Table 2. Legend: (1) Simmer *et al*, 2002; (2) Hirsh *et al*, 1976; (3) Kang *et al*, 2007; (4) Kimura *et al*, 1997; (5) Kenyon *et al*, 1993; (6) Yu *et al*, 1997; (7) Bacaj *et al*, 2008; (8) Das *et al*, 2015; TMP (trimethyl psoralen).

The list and composition of media used is depicted below:

Table 3

***Caenorhabditis elegans* cultivation**	
Medium	**Composition**
NGM (*)	1.7% agar, 0.3% NaCl, 0.25% peptone, 25 mM KPO_4 buffer pH 6.0, 1 mM $CaCl_2$, 1 mM $MgSO_4$, 5 µg/mL cholesterol in ethanol.
NGM glucose (●)	1.7% agar, 0.3% NaCl, 0.25% peptone, 1% D-(+)-glucose, 25 mM KPO_4 buffer pH 6.0, 1 mM $CaCl_2$, 1 mM $MgSO_4$, 5 µg/mL cholesterol in ethanol
RNAi medium (◊)	NGM supplemented with 1 mM isopropyl β-D-thiogalactopyranoside (IPTG), 25 µg/mL of carbenicillin
High salt agar	2% agar, 5 mM KPO_4, 1 mM $CaCl_2$, 1 mM $MgSO_4$, with 60 mM NaCl

medium (#)	
Low salt agar medium (#)	2% agar, 5 mM KPO_4, 1 mM $CaCl_2$, 1 mM $MgSO_4$, without NaCl
Isocratic medium (#)	2% agar, 5 mM KPO_4, 1 mM $CaCl_2$, 1 mM $MgSO_4$, with 30 mM NaCl
M9 buffer (*)	0.3% KH_2PO_4, 0.6% Na_2HPO_4, 0.5% NaCl, 1 mM $MgSO_4$
S basal (*)	0.585% NaCl, 0.1% K_2HPO4 , 0.6% KH_2PO4, 5 µg/mL cholesterol in ethanol
1 M potassium citrate pH 6.0 (*)	2% citric acid monohydrate, 29.35% tri-potassium citrate monohydrate
Trace metal solution (*)	0.186% disodium EDTA, 0.069% $FeSO_4$•7 H_2O, 0.02% $MnCl_2$•4 H_2O, 0.029% $ZnSO_4$•7 H_2O, 0.0025% $CuSO_4$•5 H_2O
S medium (*)	1L S Basal, 10 mM potassium citrate pH 6, 10 mM trace metal solution, 3 mM $CaCl_2$, 3 mM $MgSO_4$
***Escherichia coli* cultivation**	
Medium	**Composition**
LB Broth (*)	1% Bacto-tryptone, 0.5% Bacto-yeast, 0.5% NaCl, pH to 7.0
LB agar (*)	1% Bacto-tryptone, 0.5% Bacto-yeast, 0.5% NaCL, 1.5 % agar, pH 7.5

Table 3. Legend: (*) Stiernagle, 2006; (●) Lee *et al*, 2009; (◊) Ahringer *et al*, 2006; (#) Das *et al*, 2015.

3.1.1 Genetic crosses

In order to increase the frequency of males, necessary to perform genetic crosses, 15-20 L4 hermaphrodites were incubated for 6-8 hours at 30 °C. In the F1 generation, some males were present due to X-chromosome missegregation in germ cells undergoing meiosis and the consequent production of nullo-X gametes (Sulston and Hodgkin, 1988; Fay, 2013). To perform a genetic cross several young males (up to ten) of one strain were seeded together with one or two L4 hermaphrodites of the other strain on NGM plates containing a small bacterial spot in order to favor mating, whose success is confirmed by the presence of approximately 50% of males in the progeny. F1 worms were then singled out on NGM plates and genotyped after deposition of eggs. The same procedure was repeated with F2 worms deriving from F1 worms that were heterozygous for both the genetic traits of interest, in order to find double homozygous worms resulting from the genetic cross of the two strains.

3.2 Molecular Biology

3.2.1 Genomic DNA extraction

For genomic DNA extraction, worms were collected from plates, washed with M9 buffer and centrifuged. The pellet was resuspended with 5 volumes of lysis buffer (100 mM NaCl, 10 mM Tris HCl pH 8.0, 10 mM ethylenediamine tetraacetic acid (EDTA), 1% SDS and 1% ß-mercaptoethanol) with proteinase K (Ambion™, ThermoFisher Scientific) added just before use and incubated at 65 °C overnight in agitation to favor tissue digestion.

The sample was mixed with one volume of phenol/chloroform/isoamyl alcohol (25:24:1) and centrifuged. The aqueous phase was then collected and phenol extraction was repeated. A volume of

chloroform was added and the total aqueous phase was precipitated with 2 volumes of 100% ethanol and 1/10 volume of sodium acetate 3 M, pH 5.2 for few hours at -20 °C.
The final pellet was washed two times with 70% ethanol and resuspended in TE (Tris-EDTA) buffer. DNA was incubated 30 minutes at 65 °C to help its solubilization.

3.2.2 Single worm lysis

For PCR (polymerase chain reactions) genotypization worms were singularly picked from plates with a platinum wire and placed in 4-6 µl of lysis buffer (50 mM KCl, 10 mM Tris pH 8.3, 2.5 mM $MgCl_2$, 0.45% NP-40, 0.45% Tween-20, 0.01% gelatin). After a quick freeze-thaw, an equal volume of lysis buffer supplemented with proteinase K at the final concentration of 120 µg/mL was added. Samples were incubated at 60 °C for 1 hour and then 15 minutes at 95 °C to inactivate proteinase K.

3.2.3 Total RNA extraction and cDNA synthesis

To extract total RNA, nematodes were collected from plates, washed with M9 buffer and pellet was resuspended in 400 µl of TRIzol™ (ThermoFisher Scientific) every 100 mg of worms. Samples were then snap-frozen in liquid nitrogen, thawed at 37°C and vortexed three times before being processed with a tissue grinder (Bhaskaran *et al*, 2011). The extraction was then carried out as previously described (Burdine *et al*, 1996). Briefly, after the addition of chloroform, the samples were vortexed and centrifuged at high speed to separate the phases. The aqueous one was then incubated for few hours at -20 °C with an equal amount of isopropanol to precipitate the RNA. The resulting pellet was washed few times with 75% ethanol and finally resuspended in DEPC (Diethyl pyrocarbonate) water (Ambion™, ThermoFisher Scientific).

SuperScript II reverse transcriptase (ThermoFisher Scientific) was used for cDNA synthesis starting from 1 µg of RNA and following manufacturer's instructions.

3.2.4 Polymerase chain reactions

PCR were performed with the high-fidelity Phusion Taq polymerase (NEB), using as template 100 ng of genomic DNA or cDNA and 4 µL of single worm lysates and following manifacturer's instructions. The HF buffer was generally adopted and for difficult amplicons 3% DMSO or 250 mM betain were included in the reaction mix. The primers used are listed in the table below:

Table 4

Name	Sequence (from 5' to 3')	Target gene	Application
-26 for	cttctAAGCTTgagtcgtgcggttcgtttaa	*cox-16*	Cloning in pL4440
368 rev	cttctCTCGAGggtcaatgtcggggatgttt	*cox-16*	Cloning in pL4440
-20 for	cttctAAGCTTacagctttgaatcatcgaaa	*T01G9.2*	Cloning in pL4440
1394 rev	cttctCTCGAGagggatgggtttctagcgaa	*T01G9.2*	Cloning in pL4440
5' UTR for	tgaaaagtcgataaaaattcagtagca	*T01G9.2*	Screening after CRISPR injections and

			backcross with N2
ex 2 rev	acctttttactgtacttcaattcgact	*T01G9.2*	Screening after CRISPR injections and backcross with N2 strain
Ins rev	ctcagtcgacggttattttgta	*T01G9.2*	Screening after CRISPR injections, specific for mutated sequence
20 for	tcacaaagaaaccatcaactgaa	*T01G9.2*	Analysis of target mRNA integrity
415 rev	catatgatcctggatgtgtcg	*T01G9.2*	Analysis of target mRNA integrity
ex 14 for	gattggagatttcggaatgg	*daf-2*	Screening of *daf-2* genotype in *daf-2/fer-15/Mytho* KO cross
ex 14 rev	tgatcggagggatcgtctta	*daf-2*	Screening of *daf-2* genotype in *daf-2/fer-15/Mytho* KO cross
int 1 for	ttgttggcactgaatttcaca	*daf-16*	Screening of *daf-16* genotype in *daf-16/fer-15/Mytho* KO cross
5' UTR for	catttttccgtctgcgtttc	*daf-16*	Screening of *daf-16* genotype in *daf-16/fer-15/Mytho* KO cross
int 2 rev	tttcactatctcttacctttgtagtcg	*daf-16*	Screening of *daf-16* genotype in *daf-16/fer-15/Mytho* KO cross
ex 5 for	gatcaagctggagtactcatgaaa	*che-12*	Screening after CRISPR injections and backcross with N2
ex 7 rev	cgccacgagattcacaaat	*che-12*	Screening after CRISPR injections and backcross with N2 strain
ex 6 for	cagaagacactgacgcaaacc	*che-12*	Screening after CRISPR injections, specific for mutated sequence
int 12 for	tggacctaattggattttgc	*che-12*	Screening of strain SP1620 genotype
ex 14 rev	cctgtccggaacgtagaaaa	*che-12*	Screening of strain SP1620 genotype
ex/int 13 rev	tttaccgcatgcttcaaagg	*che-12*	Screening of strain SP1620 genotype
gcy-6 for	ccccgaaaattctgaagaaaa	*che-12*	Screening of strain LP177 genotype
ex 1 rev	tcttgataatgcatcaaacagtga	*che-12*	Screening of strain LP177 genotype
GFP rev	tccagtgaaaagttcttctccttt	*che-12*	Screening of strain LP177 genotype

The reaction was performed as follows: initial denaturation at 98 °C for 30 seconds, a step consisting of 10 seconds at 98 °C, 20 seconds at the template melting temperature and 30 seconds at 72 °C, repeated 35 times and a final extension at 72 °C for 7 minutes.

PCR products were then run on 1% agarose gel and purified using Amicon® Ultra 0.5 mL 30k centrifugal filter devices (Millipore Merck) if a single specific band was obtained by the reaction. In case of multiple and aspecific bands, PCR was run on agarose gel, the correct band was excised by gel and purified using the QIAquick Gel Extraction Kit (QIAGEN).

3.2.5. Sanger Sequencing

The sequencing reactions were performed using the BigDye® Terminator v3.1 Cycle Sequencing Kit (Applied Biosystems) following manifacturer's instructions. Reactions were then purified using Centri-Sep spin columns (Princeton Separations) and 10 µL were run on 3500 Dx Genetic Analyzer (8-capillary, ThermoFisher Scientific).

3.2.6 RNA interference experiments

RNAi experiments were carried on *cox16* and *T01G9.2* genes, both of which are conserved in *C. elegans*.

3.2.6.1 Generation of constructs

To perform RNAi experiments, the coding sequence of target genes (*cox-16* and *TO1G9.2*) were cloned in the bacterial expression vector pL4440 (FireLab, Addgene) that carries two T7 sites flanking the insert and oriented in an antiparallel way and an ampicillin resistance gene.
Briefly, *cox16* and *T01G9.2* coding sequences were amplified using a forward primer carrying the site recognized by the restriction enzyme HindIII and a reverse one with the site recognized by XhoI (see table 4). The same sites are present in the Multiple Cloning Site of the vector. PCR reactions and the plasmid were digested in parallel with the two restriction enzymes (NEB), the products of the digestion were then purified with the QIAquick Gel Extraction Kit (QIAGEN) and ligated overnight at 16 °C using T4 DNA ligase (NEB). 5 µL of the ligations were used to transform Mach1 $T1^R$ bacteria (ThermoFisher Scientific) and plasmidic DNA was purified from single colonies using the QIAprep Spin Miniprep Kit (QIAGEN). The correctness of cloning was verified by Sanger sequencing.

3.2.6.2 RNAi feeding

The constructs were transformed in HT115(DE3) *E. coli* bacteria, a strain that expresses an IPTG-inducible T7 RNA polymerase, lacks RNAse III and is tetracycline resistant (Timmons *et al*, 2001). The genotype of the strain, which was purchased from the CGC, is: F-, mcrA, mcrB, IN(rrnD-rrnE)1, rnc14::Tn10(DE3 lysogen: lavUV5 promoter -T7 polymerase) (IPTG-inducible T7 polymerase) (RNAse III minus).
Single bacterial colonies were inoculated in LB Broth supplemented with ampicillin and tetracycline (Sigma-Aldrich) at the final concentration of 100 µg/mL and 13 µg/mL respectively and let grow overnight at 37 °C. The bacterial cultures were spread on NGM plates supplemented with IPTG (Euroclone) and carbenicillin (Sigma-Aldrich), as indicated in table 3 (Ahringer *et al*, 2006).
The *rrf-3* strain, which is sensitive to RNAi, was used for the experiments (Simmer *et al*, 2002). L4 hermaphrodites were seeded on RNAi plates minimizing the amount of OP50 bacteria transferred and, in order to eliminate eventual maternal effects, three worms generations were waited before proceeding to the analysis. In each experiment, a negative control, consisting of the pL4440 vector and a positive one, obtained feeding worms with bacteria carrying the pLT61 vector, were included. This plasmid contains 0.8 kb of *unc-22*, a gene whose silencing causes a visible shaking phenotype, inserted into the pL4440 vector.

3.2.7 CRISPR/Cas9 genome-editing

The Alt-R® CRISPR/Cas9 System (Integrated DNA Technologies, IDT) was used to perform genome editing in *C. elegans* and obtain a *T01G9.2* knockout strain and a *che-12* knock-in strain harboring a missense variant [p.(Arg284Trp)].

It pairs an a universal tracrRNA oligonucleotide with a target-specific crRNA oligonucleotide, having optimized length of 67 and 36 nucleotides respectively (Jacobi *et al*, 2017). The crRNA are chemically synthesized with modifications that protect them from degradation by cellular RNases and further improve target editing performance (Yin *et al*, 2017). We purchased the Cas9 protein purified from *Streptococcus pyogenes*, the tracrRNA, two different crRNA and two repair DNA templates each specific for one target gene from IDT.

crRNA and DNA templates were designed following recently published guidelines (Paix *et al*, 2017). Briefly crRNAs were chosen so that DSB (which happens 3 nucleotides before the PAM) was as close as possible to the desired edit and not further than 30 nucleotides away and had between 50 and 70% of GC content to be most efficient. Two or more mismatches in the first 15 nucleotides upstream the PAM were inserted to prevent Cas9 cleavage and reduce the chances of off-target mutations.

The DNA repair template, a single stranded DNA oligonucleotide (ssODN), contained the desired edit and two 35 nucleotides homology arms. It also included mutations to prevent re-cutting by Cas9 after editing and the sequence recognized by a restriction site to facilitate screening of point mutations.

Since it has been demonstrated that worms edited at one locus have a higher probability to be edited at a second locus, we also used a crRNA and a repair ssODN designed to introduce a missense mutation at the *dpy-10* locus, that causes a dumpy (Dpy) phenotype in worms when present in homozygosity, otherwise a roller (Rol) phenotype, when present in heterozygosity.

The crRNA and ssODN sequences are listed in the table below:

Table 5

Target gene	Type of molecule	Sequence (from 5' to 3')
T01G9.2	crRNA	tgaagaagatctgagcttca
T01G9.2	ssODN	catcgaaaatgaatggcaaacagcaagttacaaaaTAAccgtcgactgaggaagacctaagcttcacgtttgtttta aagtcaaaaaatcaataataa
che-12	crRNA	agtgtgggctttaattgctg
che-12	ssODN	cgtcttcgattcggaatagttccaagcttggtgtgcgcattgatcgcagaagacactgacgcaaaccagTGGatatc gggattagaaaaaatgaaacaagtagttga
dpy-10	crRNA	gctaccataggcaccacgag
dpy-10	ssODN	cacttgaacttcaatacggcaagatgagaatgactggaaaccgtaccgCATGCggtgcctatggtagcggagct tcacatggcttcagaccaacagcctat

Table 5. Legend: In uppercase the mutated nucleotides in ssODN that introduce a desired mutation, a stop codon for *T01G9.2* and a missense variant for *che-12*, that is p.(Arg284Trp), and for *dpy-10*, that is p.(Arg92Cys). Underlined the restriction sites used for worm genotyping, SalI for *T01G9.2* and EcoRV for *che-12*.

3.2.7.1 *In vitro* digestion with CRISPR/Cas9

Before proceeding with worm injections, the efficacy of the chosen crRNA was verified performing an *in vitro* digestion of target loci with the purified Cas9 protein. After genomic DNA extraction from worms, a PCR reaction was performed using forward and reverse primers that encompass the genomic region to be edited (see table 4). The mix contained the following components (whose final concentration is indicated between brackets): the purified PCR (20 ng/µL), the Cas9 protein (30 nM), the universal tracrRNA and the crRNA specific for the locus of interest (both 22 µM) BSA and NEB buffer 3 (NEB, 100 mM NaCl, 50 mM Tris-HCl, 10 mM $MgCl_2$,1 mM DTT, pH 7.9 at 25 °C) After 1 hour at 37 °C, proteinase K was added and the mix was incubated at 55 °C for ten minutes. Finally, the digestions were run on an agarose gel.

3.2.7.2 Worm injections with CRISPR/Cas9 components

After having verified the efficacy of the chosen crRNA to induce the Cas9-mediated digestion of PCR products *in vitro*, we proceeded with worm injections in collaboration with Simone Martinelli at the Istituto Superiore di Sanità in Roma, following a protocol modified from Paix *et al*, 2015.
The injections were performed in the distal gonad syncytium of young adult wild-type hermaphrodite animals with a mix containing: 750 ng/µL of Cas9 protein, 700 ng/µL of tracrRNA, 115 ng/µL of crRNA for *dpy-10*, 37.5 ng/µL of ssODN for *dpy-10*, 400 ng/µL crRNA for *T01G9.2* or *che-12* and 175 ng/µL of the ssODN for *T01G9.2* or *che-12*. For what concerns *che-12* experiments the mix was supplemented with the demethylating agent 5-azacytidine at the final concentration of 1 or 10 µM.

Worms were then recovered in M9 buffer and incubated at 20 °C. The F1 progeny was screened and animals with Rol or Dpy phenotypes were isolated, as well as pools of 5 wild-type worms from those plates. To identify mutant animals, PCR reactions were performed using three primers: a common (forward or reverse) primer and a couple of primers designed to discriminate wild type and mutated genotypes, since one anneals specifically with the wild-type sequence, the other with the mutated one (see table 4, primers used for screening after CRISPR injections). Homozygosity was confirmed by Sanger sequencing using standard techniques.

3.2.7.3 Strains generated by CRISPR/Cas9 technology

Four null strains for *T01G9.2* and three knock-in strains for *che-12* were generated by CRISPR/Cas9 technology. For each gene experiments were performed using one of the generated strains and results were confirmed on a second independent one, that is *T01G9.2*(*pan8*[S18Tfs*19]) and *T01G9.2*(*pan9*[S18Tfs*19]) for what concerns *T01G9.2*, and *che-12*(*pan11*[R284W (AGA>TGG)]) and *che-12*(*pan12*[R284W (AGA>TGG)]) in the case of *che-12*. Before proceeding to the analysis, strains were backcrossed to remove possible off-target mutations.

3.3 Assessment of cytochrome *c* oxidase activity in *C. elegans*

3.3.1 *C. elegans* COX histochemical staining

The staining was performed in worms where *cox-16* and *cco-1* genes were silenced by RNAi feeding and in control ones fed with empty pL4440 vector. All incubations were performed at room temperature, except where differently indicated, and with constant agitation.

Worms populations were synchronized and grown until adult age. They were then washed several times with M9 and kept in the same buffer for 30 minutes to empty their intestinal content and remove bacteria. Worms were consequently fixed and permeabilized before performing COX histochemical staining as previously reported with some modifications (Grad *et al*, 2007).

Briefly, each worm pellet was resuspended in one mL solution containing: 500 µL of ice cold 2X MRWB (Modified Ruvkun's witches brew, composed as follows: 160 mM KCl, 40 mM NaCl, 20 mM ethyleneglycol-bis-(ß-aminoethylether) *N,N,N',N'*-tetraacetic acid (EGTA), 10 mM spermidine HCl, 30 mM piperazine-*N,N'*-bis[2-ethanesulfonic acid] (PIPES), pH 7.4, 50% (v/v) methanol), 400 µL water and 100 µL of 20% (w/v) paraformaldehyde.

Worms were mixed by inversion and incubated for 35 min at 4°C. After two washes with Tris Triton buffer (TTB, composed as follows: 100 mM Tris-HCl pH 7.4, 1% (v/v) Triton X-100, 1 mM EDTA) samples were incubated in TTB containing 1% of –ß-mercaptoethanol for 15 minutes. Worms were then washed once with 1X borate buffer (diluted form the 40X borate buffer: 1 M H_3BO_3, 0.5 M NaOH) and then incubated with 0.9X borate buffer supplemented with 10 mM dithiothreitol (DTT) for 15 minutes. Nematodes were then washed with Tris-HCl 50 mM pH 7.4 before proceeding with the histochemical staining.

The following mix was prepared and kept in the dark: 0.1% (w/v) 3,3'-diaminobenzidine (DAB), 0.1% (w/v) cytochrome *c*, 0.02% (w/v) catalase in Tris-HCl 50 mM pH 7.4 (all reagents were purchased form Sigma-Aldrich). Worms were incubated with the assay mixture 75 minutes at 37 °C, and for each sample a tube containing 60 mM of sodium azide was added as negative control of the reaction. Nematodes were then carefully washed several times with water to remove excess stain, finally leaving a volume equal to that of the worm pellet.

3.3.2 Crude mitochondria extraction and in-gel activity for cytochrome *c* oxidase

Mitochondria extraction from wild-type *C. elegans* was performed as previously reported by Grad *et al*, with some modifications. All centrifugation steps were performed at 4 °C.

Worms were either cultivated on fresh NGM plates seeded with *E. coli* OP50 or in a liquid culture of S medium inoculated with a concentrated OP50 pellet made from 2-3 liters of an overnight culture.

After cultivation, worms were collected and pelleted. Several washes were performed until the supernatant was clear and devoid of bacteria and pellet was resuspended in a volume of 60% sucrose. The solution was mixed several times by inversion and centrifuged 5 minutes at 1100 g, in order to

separate alive worms in the upper phase, from dead ones, agar pieces and bacteria on the bottom of tubes. Worms were washed once with cold M9 buffer, then resuspended in the same buffer and kept at room temperature at constant agitation for at least 30 minutes to empty their intestine. The resulting pellet after centrifugation was resuspended in lysis buffer, composed as follows: 37mM Tris-maleate, 0.5 M sucrose, 2 mM $MgCl_2$ pH 6.4, or 220 mM mannitol, 70 mM sucrose, 5 mM 3-(N-morpholino) propanesulfonic acid (MOPS), 2 mM EDTA pH 7.4. Both were supplemented with 1X Protease Inhibitor Cocktail (PIC, Sigma-Aldrich), 1 mM phenylmethylsulfonyl fluoride (PMSF, Sigma-Aldrich) and 1 mM dithiothreitol (DTT, Sigma-Aldrich).

To break their cuticle, worms were first sonicated and then digested with the enzyme collagenase.

Samples were kept on ice while they were sonicated 4 or 8 times (40% amplitude with pulses every two seconds) with intervals of 1 minute, then a solution containing 33 mg/mL of collagenase type IV from *Clostridium histolyticum* (Sigma-Aldrich) and 5 mM of $CaCl_2$ in PBS was added and incubated 15 minutes at ambient temperature with constant agitation.

The reaction was blocked with 0.4% bovine serum albumin (Sigma-Aldrich) and samples were homogenized on ice with a glass-Teflon homogenizer for 5 minutes at 1600 rpm. Lysates were centrifuged for 20 minutes at 1000 g to eliminate undigested material, the supernatant was kept and centrifuged 10 minutes at 12000 g.

The resulting pellet was finally resuspended in lysis buffer and centrifuged at 15000 g for 30 minutes. In order to quantify the mitochondrial protein content with the BCA assay kit (Pierce), mitochondria were resuspended in a buffer containing sucrose 20% (w/v), 25 mM Tris-HCl, 1 mM EDTA pH 7.6.

The in-gel activity for complex IV was performed on worm mitochondria as reported by Suthammarak *et al* with some modifications. Briefly, 100 µg of mitochondrial proteins were submitted to solubilization by digitonin (ThermoFisher Scientific) with a detergent/protein mass ratio of 6/1 for one hour on ice.

Then samples were centrifuged for 20 minutes at 16000 g at 4 °C and NativePAGE™ 5% G-250 Sample Additive (ThermoFisher Scientific) was added to the supernatant to obtain a dye/detergent mass ratio of 4/1. Proteins were loaded in 3-12% Bis-Tris NativePAGE™ gels (ThermoFisher Scientific) and after 30 minutes of run, the first cathode buffer was replaced by the second cathode buffer that contained a 10-fold dilution of Coomassie Blue. Run continued for 90 minutes more and then complex IV activity was assayed directly on gel incubating it with 0.1% (w/v) 3,3' diaminobenzidine, 0.1% (w/v) cytochrome *c* and 24 units/ml catalase in 50 mM Tris-HCl pH 7.4 overnight at room temperature with constant agitation.

3.4 Phenotypical analysis and behavioral assays

3.4.1 Lifespan assay

The DH26 strain *(fer-15(b26)II)* was used to carry the experiments since it has a temperature-sensitive defect in spermatogenesis and adult worms are consequently sterile at 25 °C (Hirsch *et al*, 1976). In this way, lifespan of animals can be checked and recorded without any risk of misinterpretation due to the concomitant presence of progeny in the plates. So *Mytho* KO worms were crossed with *fer-15* animals and lifespan was analyzed as previously reported (Hsin and Kenyon,1999).
Briefly, 150 L4 *fer-15* and *fer-15/Mytho* KO hermaphrodites were seeded on agar plates and used as time zero for the analysis. Plates were maintained at 25 °C for the entire duration of experiments and monitored every day. Worms were judged to be dead when they ceased pharyngeal pumping and besides did not react to touching with a platinum wire. Worms that crawled off the plate or died as a result of extruded internal organs were censored. Survival curves were compared using the logrank test and the lifespan plots represent the composite of the three independent experiments performed.

3.4.2 Locomotion analysis

We measured locomotion in worms silenced for *T01G9.2* and their relative controls and in wild-type and *Mytho* KO nematodes. Worms were individually seeded on plates at the L4 stage and maintained at 20 °C or 25 °C and the analysis was carried after one or 5 days. Animals were tested in one or two separate intervals of 30 seconds each, paying attention not to mechanically stimulate plates during the analysis. The total number of body bends, reversals and duration of stillness periods were then calculated for each worm over the total period of observation as previously reported (Chiba and Rankin, 1990; Sawin *et al*, 2000). The experiment was performed three times and the results of the two worm strains were compared using the unequal variance *t*-test.

3.4.3 Survival analysis

3.4.3.1 Survival after prolonged starvation

We measured the survival capability after a prolonged period of starvation in worms silenced for *T01G9.2* and their relative controls and in wild-type and *Mytho* KO nematodes as reported (Kang *et al*, 2007) with some modifications. Following a bleaching treatment L1 larvae of each population were kept in M9 buffer at 20°C for the indicated time points and after that they were transferred on fresh NGM plates. After 48 hours at 20 °C the ability of worms to recover from starvation and survive was calculated as a ratio of worms alive to the total number of animals transferred to the plate. The experiments were performed two times and the results were analyzed using the unequal variance *t*-test.

3.4.3.2 Survival after oxidative stress

The resistance of wild-type and *Mytho* KO worms to oxidative stress was tested with two different variants of the same treatment.

In the first one, performed as indicated by Possik and Pause with some variations, 50 adult nematodes of each genotype were incubated in wells of a 96-well plate with 200 mM paraquat (PQ, Sigma-Aldrich) in M9 buffer at 20°C with constant agitation and survival was measured every hour during the incubation for 12 hours checking worms at the microscope. They were judged to be dead if not moving even after the touch with a platinum wire.

The second one was performed as previously described (Gusarov *et al*., 2017) with some modifications. Briefly, between 45 and 60 L4 *fer-15* and *fer-15/Mytho* KO worms were seeded on NGM plates and maintained at 25 °C for 5 days. Worms were then incubated in M9 buffer supplemented with PQ at the final concentration of 125 mM with constant agitation at 25 °C for 1 hour. To remove the oxidant, nematodes were washed three times in M9 buffer and transferred to fresh NGM plates that were incubated at 25 °C for the indicated time points at which survival was calculated as the ratio of worms alive to the total number of animals transferred to the plate after oxidant treatment.

Both kind of experiments were performed twice and the results were compared using the unequal variance *t*-test.

3.4.3.3 Survival after heat stress

30 5-days adult wild-type and *Mytho* KO hermaphrodite*s* were seeded on NGM plates and submitted to a heat-shock at 35 °C. Worm viability was measured at the indicated time points during the incubation checking worms at the microscope and touching them with a platinum wire if not moving and it was calculated as fraction on the total number of worms seeded on plates (longitudinal assay reported by Lithgow *et al*, 1995). The experiment was performed twice and the results of the two worm strains were compared using the unequal variance *t*-test.

3.4.4 Chemotaxis experiments

To measure the capability of different worm strains to chemotax on a linear NaCl gradient, plates were prepared as indicated by Das *et al* and as reported in table 3. Briefly two solutions containing 2% agar dissolved in chemotaxis buffer (5 mM KPO_4, 1 mM $CaCl_2$, 1 mM $MgSO_4$) one with 60 mM of NaCl (high salt agar medium) and the other one without (low salt agar medium) were used to create the linear NaCl gradient. Before pouring, plates were labeled to distinguish high and low salt agar ends and divided in 6 equal sectors perpendicular to the gradient axis. Then they were unvaryingly elevated at the low salt end and 20 mL of high salt agar medium were poured in the plate until agar hardened. Plates were finally laid flat and 20 mL of the low salt agar medium were poured in order to obtain a

horizontal surface. A 16-hour incubation allowed NaCl diffusion with the creation of a 0-60 mM NaCl gradient across agar surface.

Control isocratic plates were prepared pouring 20 mL of the same agar solution containing 30 mM of NaCl.

Wild-type worms, two knock-in strains for *che-12* (*che-12*(*pan11*[R284W (AGA>TGG)]) and *che-12*(*pan12*[R284W (AGA>TGG)]), a strain carrying a truncated CHE-12 protein (SP1620) and one where *che-12* was totally ablated by CRISPR/Cas9 (LP177) were assayed. Strains were synchronized with the bleaching technique and grown on NGM plates until adulthood was reached. Worms were washed off the plates with chemotaxis buffer and collected in a microcentrifuge tube. After a low speed centrifuge to remove bacteria and larvae, worms were washed and centrifuged two more times before being resuspended in a small aliquot of the same buffer and seeded on the plate center (both gradient and isocratic ones). The excess of buffer was dried with a small paper towel and time 0 was considered the moment in which worms started to move on agar. After 30 min, the plates were cooled to 4°C to paralyze animals and the number of worms in each sector along the plate's linear NaCl gradient was counted.

The normalized worm density for each sector, was calculated with the following formula:

$$\text{Normalized density} = \frac{\text{Number of worms on sector X}/\text{Total number of worms on the plate}}{\text{Area of sector X}/\text{Total area of the plate}}$$

3.4.5 Dye-uptake assay

Wild-type worms, two knock-in strains for *che-12* (*che-12*(*pan11*[R284W (AGA>TGG)]) and *che-12*(*pan12*[R284W (AGA>TGG)]), SP1620 and LP177 were assayed for the dye-uptake capability with two dyes, the Vybrant™ CM-DiI (3H-Indolium, 5-[[[4-(chloromethyl)benzoyl]amino]methyl]-2-[3-(1,3-dihydro-3,3-dimethyl-1-octadecyl-2H-indol-2-ylidene)-1-propenyl]-3,3-dimethyl-1-octadecyl-, chloride, ThermoFisher Scientific) and fluorescein-5-isothiocyanate (FITC) isomer I (Sigma-Aldrich) tested (Bacaj *et al*, 2008; Das *et al*, 2015).

Strains were synchronized with the bleaching technique and grown on NGM plates until adulthood was reached. Worms were then collected from agar plates with M9 buffer and centrifuged at low speed. Two more washes in M9 were performed in order to clean nematodes from bacteria. They were then resuspended in a small aliquot of M9 supplemented with the dye and a dilution of 1:1000 of CM-DiI was used, while for FITC first a stock solution (20 mg/ml) in N,N-dimethylformamide was prepared and stored at -20 °C and then diluted in M9 at a final concentration of 0.4 mg/ml.

Worms were incubated with each dye at ambient temperature with slow constant agitation for up to 4 hours. They were then pelleted and washed three times with M9 buffer to remove the excess dye.

3.5 Optical and fluorescence microscopy of *C. elegans*

Nematodes submitted to COX histochemical staining or to dye uptake assay were imaged at Zeiss Axio Imager M1 fluorescent microscope, while GFP signal of worms carrying this reporter fused with LGG-1 or GCY-5 proteins was acquired using confocal microscopy. The mounting procedure on glass slides was common to all of them: after three washes in M9 buffer, worm pellets were resuspended in M9 supplemented with 25mM sodium azide in order to anesthetize nematodes and they were mounted live on 2% agarose pads on glass slides.

For what concerns COX histochemistry, bright field images of whole worms or body portions were acquired (10x and 20x), while in the case of dye uptake assay the FITC signal and Vybrant ™ CM-DiI were acquired using FITC and rhodamine specific filters focusing on the worm head region where amphid neurons lie (40x).

Mytho KO animals were crossed with the strain carrying LGG-1 fused with GFP (DA2123 strain) (Kang *et al*, 2007) and adult worms of both genotypes were analyzed, focusing on the head and pharynx portions. Z-stack images were acquired using a Leica TCS SP5 scanning confocal microscope with 0.6 µm slice intervals at 63x, as previously described (Chang *et al*., 2017). GFP emission bandwidth was set to 496-557 nm and the sections in which the posterior bulb of the pharynx was visible were acquired as Z-stacks. The images were then collected and manually analyzed counting GFP::LGG-1 positive *punctae* in the posterior bulb of the pharynx. The *punctae* number per μm^2 was then calculated and results were normalized considering worms carrying the wild-type version of *Mytho* as 1. The experiment was performed twice and the results of autophagic pool sizes of both genotypes were compared using the unequal variance *t*-test.

Knock-in strains for *che-12* (*che-12*(*pan11*[R284W (AGA>TGG)]), (*che-12*(*pan12*[R284W (AGA>TGG)]) and hypomorphic mutants [*che-12*(*mn389)*, strain SP1620] were crossed with the strain carrying the *gcy-5* promoter fused with GFP (OH3192 strain, Yu *et al*, 1997), which was used as control in the experiments and adult worms were analyzed at a Zeiss LSM 800 confocal microscope. In particular 63x images were acquired zooming the head portion in order to locate the cilium of the ASER neuron and measure its length. The values for each genotype were then mediated, the strain carrying the wild-type version of *che-12* was considered as one 1 and the other strains were expressed as fractions compared to it. Results of different strains were compared using the unequal variance *t*-test.

3.6 Generation of a C2C12 *Mytho* KO cell line by CRISPR/Cas9 technology

C2C12 cells were purchased from ATCC and grown in Dulbecco's Modified Eagle Medium (DMEM) supplemented with 10% Fetal Bovine Serum (FBS, scomplemented at 55 °C for 1 hour), 1% Penicillin/Streptomycin and 1% L-Glutamine. All reagents were purchased from Gibco (ThermoFisher Scientific).

To generate the *Mytho* KO C2C12 line, cells were co-transfected with Transedit CRISPR all-in-one lentiviral expression vectors (pCLIP-ALL-EFS-Puro) containing two different CRISPR target sequences of *Mytho* (TEVM-1183975, with sequence CGACCCAATGCTGGACCTGG and TEVM-1251117, with sequence AGGAATGCCTCTGGCGCAGG, Transomic Technology), addressing exon 1 and exon 2, respectively. Cells were transfected in parallel with a non-targeting control gRNA (TELA1011, Transomic Technology) and transfections were performed using Lipofectamine® 2000 (ThermoFisher Scientific), according to the manufacturer's protocol.

After 24 hours cells were selected by the addition of puromycin (Gibco, ThermoFisher Scientific) at 1 µg/mL to the culture medium until the untransfected control cells were all dead. To isolate single clones, cells were serially diluted and seeded in 96-well plates. After growth and expansion of clones, genomic DNA was extracted from cells using standard protocols and fragments encompassing the CRISPR target sequences were amplified by PCR. Two different PCR reactions were performed, the first with primers upstream and downstream the first guide RNA (gRNA) target (forward primer 5′-CCACTTTTGCTGCAGTTGCT-3′ and reverse primer 5′-TGCTGAGACATCGCTGATCC-3′) and the second, that identifies clones in which the genomic portion between the two CRISPR target sequences has been deleted, with the same forward primer and as reverse an oligonucleotide downstream the second gRNA target (5′-TGAAAAGGCCCCCATGTGAA-3′), giving products of 502 and 568 base pairs (bp), respectively. PCR reactions were then sequenced and 4 clones harboring different mutations were mixed to reduce the consequences of possible CRISPR/Cas9-mediated off-target effects.

SECTION III

FUNCTIONAL CHARACTERIZATION OF THE WORM HOMOLOGUE OF HUMAN *COX16*

4 Introduction

4.1 The mitochondrial respiratory chain

Mitochondria perform crucial cellular functions, since they provide the majority of the cellular energy in the form of ATP, generate reactive oxygen species, buffer cytosolic calcium (Ca^{2+}) and regulate apoptosis through the permeability transition pore (Wallace, 2010).

The oxidative phosphorylation (OXPHOS) is the process responsible for ATP production in mitochondria. The mitochondrial respiratory chain is situated in the inner mitochondrial membrane and consists of five multimeric protein complexes (for each complex the number of subunits in human is indicated between brackets): reduced nicotinamide adenine dinucleotide (NADH) dehydrogenase–ubiquinone oxidoreductase (complex I, 45 subunits), succinate dehydrogenase–ubiquinone oxidoreductase (complex II, 4 subunits), ubiquinone–cytochrome *c* oxidoreductase (complex III, 11 subunits), cytochrome *c* oxidase (complex IV, 14 subunits), and ATP synthase (complex V, approximately 16 subunits). Two small electron carriers, that is ubiquinone (coenzyme Q10) and cytochrome *c*, are required by the respiratory chain.

ATP synthesis involves two coordinated processes. First, electrons (in the form of NADH and $FADH_2$ resulting from the oxidation of acetyl-coenzyme A in the Krebs cycle or during β-oxidation) are transported along the complexes to molecular oxygen, thereby producing water. At the same time, protons are pumped across the mitochondrial inner membrane to the intermembrane space by complexes I, III, and IV. ATP is generated by the influx of these protons back into the mitochondrial matrix through complex V (ATP synthase) (DiMauro and Schon, 2003).

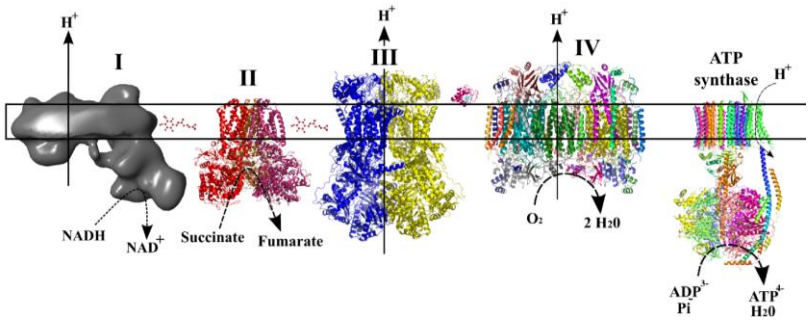

Fig. 5: The mitochondrial respiratory chain. Electrons are transported along the four complexes to molecular oxygen with the production of water. At the same time protons are pumped by complex I, III and IV to the intermembrane space and their consequent influx back into the mitochondrial matrix is used to produce ATP by complex V (adapted from Mourier and Larsson, 2011).

The organization of the mitochondrial respiratory complexes is a still debated issue, in origin discussed in terms of two extreme models, the "solid-state" and the "fluid-state" models.
In the solid-state model, the complexes that catalyze individual reactions are closely packed to guarantee high efficiency in electron transport. Coenzyme Q10 and cytochrome *c* transfer electrons along pre-defined and confined pathways between complexes. On the contrary, in the fluid-state model individual complexes are viewed as independent entities embedded and diffusing in the inner membrane, with coenzyme Q10 and cytochrome *c* moving randomly without restraint (Acin-Perez and Enriquez, 2014; Milenkovic *et al*, 2017). This second model was generally accepted until stable associations of respiratory complexes were purified and a reformulation of the solid model proposed that respiratory complexes are organized in larger structures called "supercomplexes": complexes IV and V can form dimers and oligomers; in addition, defined associations of complexes I, III and IV have been found in mitochondria from mammalian tissues, and it has been estimated that 85%–100% of complex I and 55%–65% of complex III, but only 15%–25% of complex IV are found in supercomplexes. Respirasomes are supercomplexes that contain complex I, III, and IV and are capable of NADH:O_2 oxidoreduction in vitro (Milenkovic *et al*, 2017; Signes and Fernandez-Vizarra, 2018).
The human mitochondrial DNA is a circular double-stranded molecule containing 37 genes, of which 2 are rRNAs and 22 are tRNAs , the remaining 13 encode subunits of the respiratory chain: seven subunits of complex I, one subunit of complex III, three subunits of cytochrome *c* oxidase and two subunits of ATP synthase (DiMauro and Schon, 2003).

4.1.1 The mitochondrial respiratory chain in *C. elegans*

OXPHOS is conserved in *C. elegans*. However, worm mitochondria show some differences compared to those human. First, the mitochondrial DNA copy number per cell is lower in nematodes, the *C. elegans* mitochondrial DNA contains 36 genes and lacks the ATP8 subunit of ATP synthase, and instead of coenzyme Q10, which has a chain of 10 isoprenyl repeats, worms, like rodents, primarily use coenzyme Q9 (van der Bliek *et al*, 2017). Despite these differences, worm mitochondria are really similar to mammalian ones. Many homologue subunits of each mitochondrial complex have been indentified and characterized in *C. elegans*: for complex I, 38 out of 45 human subunits, for complex II, 4 subunits out of 4, for complex III, 8 subunits out of 11, for complex IV, 9 subunits out of 14 and for what concerns complex V, 14 subunits out of 16 (Tsang and Lemire, 2003; van der Bliek *et al*, 2017).

4.2 Mitochondrial genetics and mitochondrial diseases

Mitochondrial genetics differs from the Mendelian one for some aspects. First of all mtDNA is inherited only by the mother, then, considering that thousands of mtDNA molecules are present in each cells and mutations are generally present only in part of them, cells possess both wild-type and

mutant mtDNA, a situation known as heteroplasmy. Besides, the mitotic segregation randomly distributes organelles during cell division, and if mutant mtDNA is present it will be inherited differently by daughter cells, with possible changes in phenotype (DiMauro and Schon, 2003).

Mitochondrial diseases are a broad spectrum of pathological conditions associated to defects in the mitochondrial respiratory chain that can be caused by mutations in genes encoded by mitochondrial DNA, as well as in nuclear genes that produce mitochondrial proteins (DiMauro, 2004; Ghezzi and Zeviani, 2012), They show variable age of onset, symptoms, progression and outcome and it has been reported that the prevalence of genetic OXPHOS defects is not less than 1:5,000 (Ghezzi and Zeviani, 2012).

The inheritance can be maternal or Mendelian, depending if the primary genetic defect is in the mtDNA or in nuclear DNA. Sporadic conditions, presumably caused by *de novo* mutations, are also known. Clinical manifestations can be restricted to lesions in single structures and tissues or multisystemic syndromes and the most common clinical presentations show involvement of skeletal muscle, heart and brain (that is postmitotic tissues with high energy demands) with neurodegeneration, cardiac defects and muscle alterations. The onset can vary from neonatal to adult life.

Concerning therapies for mitochondrial diseases, they are in the majority of cases restricted to exercise and dietary supplements. A successful example of therapy is the supplementation of coenzyme Q10 for primary and secondary forms of coenzyme Q10 deficiencies (Emmanuele *et al*, 2012).

In contrast, there has been remarkable progress in the understanding of the molecular genetic causes, pathological mechanisms, and clinical presentations of mitochondrial diseases. Due to these advances and emerging clinical trials, new treatment modalities are on the horizon.

4.3 Cytochrome *c* oxidase (COX)

Cytochrome *c* oxidase (COX), situated in the inner membrane of mitochondria, is the terminal enzyme of the respiratory chain in many aerobic organisms. It catalyzes electron transfer from cytochrome *c* to molecular oxygen with the consequent production of water and the reaction is accompanied by the pumping of four protons across the membrane. By coupling electron transfer with proton translocation from the mitochondrial matrix to the intermembrane space, COX contributes to energy accumulation as an electrochemical gradient that will be used by the OXPHOS system for the synthesis of ATP (Michel, 1998; Fontanesi *et al*, 2008).

COX contains four redox-active cofactors, two Cu atoms forming the so-called Cu_A, a low-spin heme *a* and a heme a_3-Cu_B binuclear center. Electrons from cytochrome *c* are first accepted by Cu_A and then are transferred via heme *a* to the binuclear center where oxygen reduction takes place (Michel, 1998; Pierron *et al*, 2012).

Human COX is formed by 14 subunits (Balsa *et al*, 2012), of which, COX1, COX2 and COX3 are large hydrophobic subunits that are encoded by mtDNA and form the enzymatic catalytic core, and the remaining are small subunits synthesized by nuclear DNA that surround the enzymatic core. They are

necessary for the assembly and stability of the holo-enzyme and for its dimerization (Fontanesi *et al*, 2008). COX assembly is a complex and regulated process, which has been recently proposed to happen following a modular assembly model (Vidoni *et al*, 2017). Briefly, COX1 together with the assembly factors COA3, COA1, COX14, CMC1 and SURF1 (MITRAC complex) joins COX4 and COX5A. A second module, composed by the structural subunits COX2, COX5B, COX6C, COX7B, COX7C and COX8A, is incorporated in the same step. Next, COX3 forms the late sub-assembly module together with COX6A, COX6B, and COX7A and finally, the last module is constituted by NDUFA4 and COX7A2L.

Many ancillary proteins take part in the assembly process in order to guarantee its correctness. They are encoded by nuclear genes and were originally identified in yeast studying respiratory-deficient *pet* mutant strains, but are still in part not characterized in human. Their roles include transcription and mRNA maturation, translation of COX mitochondrial genes, as well as import into mitochondria of nuclear encoded subunits or delivery of copper atoms (*e.g.* COX17 and COX19), insertion of subunits into the inner mitochondrial membrane (*e.g.* COX18, COX20 and OXA1L), heme *a* biosynthesis (*e.g.* COX15), copper homeostasis and insertion into the enzyme (*e.g.* SCO1, SCO2, COA6 and COX11) and formation of assembly intermediates (Fontanesi *et al*, 2008; Cerqua *et al*, 2018).

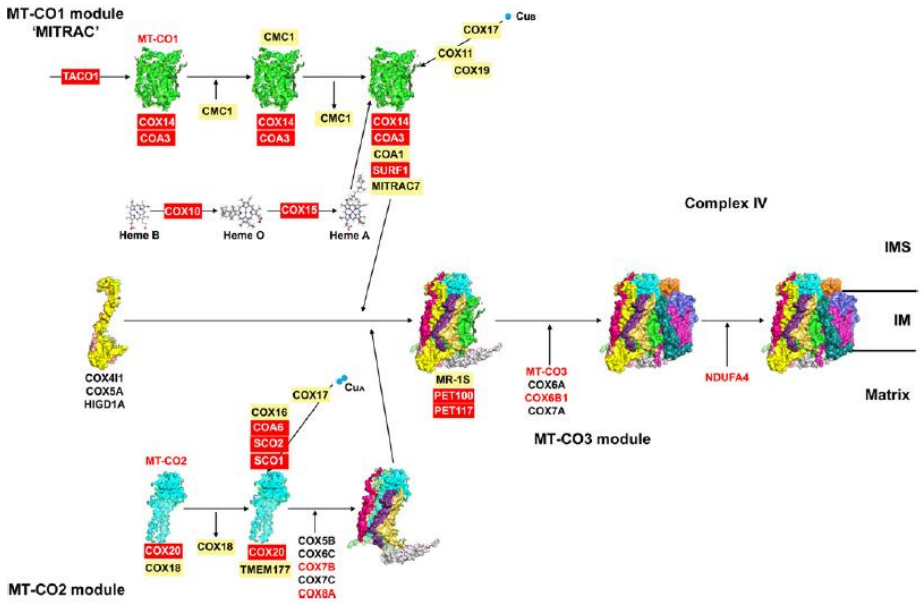

Fig. 6: The COX modular assembly model: Briefly, COX1 together with the MITRAC complex joins COX4 and COX5A. A second module, composed by the structural subunits COX2, COX5B, COX6C, COX7B, COX7C and COX8A, is incorporated in the same step. Next, COX3 forms the late sub-assembly module together with COX6A, COX6B, and COX7A and finally, the last module is constituted by NDUFA4 and COX7A2L (adapted from Signes and Fernandez-Vizarra, 2018).

COX is a ductile enzyme, whose activity can be modulated according to the energetic requirement of the cell. Tissue- and condition-specific isoforms have only been described for COX but not for other

OXPHOS complexes, suggesting a fundamental need to finely regulate the essentially irreversible reaction catalyzed by COX. Six COX subunits encoded by nuclear DNA are expressed as specialized isoforms in peculiar tissues including liver, heart, skeletal muscle, lung and testes (Sinkler *et al*, 2017). Then, another tissue-specific mechanism involves a cAMP-dependent phosphorylation of the enzyme with a consequent lowering of COX activity and ATP production (Hüttemann *et al*, 2012). In the presence of ADP, the binding affinity for cytochrome *c* to COX is increased by fivefold as compared to that of ATP, indicating that enzyme activity is modulated allosterically by the ATP/ADP ratio: when the ratio is elevated, the bound ADP is exchanged by ATP with consequent inhibition of oxygen consumption (Ramzan *et al*, 2012, Sinkler *et al*, 2017).

4.3.1 COX and neurons

Neurons are postmitotic cells that depend almost entirely on oxidative metabolism for their function and survival, making them extremely dependent on mitochondrial function. Neuronal activity precisely controls energy consumption to avoid any energetic wasting. Besides, every neuron compartment has different energy requirements: dendrites, being the principal receptive sites of incoming depolarizing input and whose membranes have to be continuously repolarized, consume the majority of energy, whereas axonal trunks, especially myelinated axons, consume very little energy.
COX subunit proteins, like the subunits of ETC complex I and III, come from two genomic sources. Neuronal dendrites and axons are rich in mitochondria, but can extend far from cell bodies where nuclear genome resides, thus making COX assembly really challenging. This process is strictly regulated and while the mitochondrial mRNAs are located inside mitochondria distributed throughout the neuron, the nuclear ones are restricted only in the cell bodies, so the translation of these subunits happens in the cell body. They are then inserted into mitochondria and targeted to their final destination (Wong-Riley, 2012).
Since the importance of a balanced energy production and expenditure for neurons homeostasis, among ETC enzymes cytochrome *c* oxidase can serve as a sensitive and reliable metabolic marker for neurons activity. In fact, all 14 subunits of cytochrome *c* oxidase are regulated by neuronal activity. Key factors in this regulation are the nuclear respiratory factors 1 and 2 (NRF-1 and NRF-2) and the mitochondrial transcription factor A (Tfam). Tfam controls transcription of mitochondrial DNA, and NRF-1 and NRF-2 are the primary transcription factors of nuclear DNA genes encoding mitochondrial proteins, including Tfam. NRF-1 and NRF-2 affect also the mitochondrial COX genes although in a indirect way. (Chicherin *et al*, 2019).

4.4 COX deficiencies

COX deficiencies (MIM# 220110) in humans comprehend a wide variety of disorders and represent the most frequent among mitochondrial diseases. In the past, especially in the pre-genomic era, too

many disorders were classified as COX deficiencies based on histochemical or biochemical criteria that did not consider the need for the selectivity of the enzyme defect. Parameters such as lactic acidosis in the blood or cerebro-spinal fluid and ragged-red fibers in adult skeletal muscle biopsies are characteristic of mitochondrial diseases although they are not specific to COX deficiencies (DiMauro *et al*, 2012; Rak *et al*, 2016).

Genotypically, isolated COX deficiencies could arise from mutations in any of the 3 subunits encoded in the mtDNA, from any of the 11 structural subunits encoded in the nucleus or from mutations in any of the assembly factors. Mutations in the same gene are expected to affect a common pathway in the same tissue and consequently have a similar outcome. However, what is observed in patients is an impressive heterogeneity of phenotypes independently if the mutation affects the biosynthesis or maturation of a mitochondrial or nucleus-encoded COX subunit or its assembly into the mature complex and ultimately supercomplex (Rak *et al*, 2016). Among others, a devastating progressive disease, generally affecting brain, skeletal muscle and heart, and that is usually fatal in the first years of life, has been reported.

Mutations in the 3 mtDNA encoded COX subunits can manifest in more than twenty different phenotypes and the degree of heteroplasmy in different tissues has been invoked as a possible factor to explain the large number of phenotypes associated.

Relatively few mutations have been reported in nuclear genes encoding COX structural subunits and it was suspected that such mutations were incompatible with life, until the discovery of the first mutation in *COX6B1* (Diaz, 2010).

The majority of the genetic defects related to COX deficiencies have been found in nuclear genes coding for auxiliary proteins and similarly to those in the structural genes exhibit a multiplicity of phenotypes (Rak *et al*, 2016).

The assembly factors so far identified and mtDNA genes constitute candidate genes to be screened to diagnose the causes of COX deficiency in patients. Recently, another gene that has been proposed for this purpose is *COX18*. Unfortunately, mutational screening of this gene in a large cohort of patients, with an unknown cause of COX deficiency and without mutations in other candidate genes, failed to reveal any sequence alteration in *COX18*, suggesting that mutations in this gene could be incompatible with life or not as frequent (Diaz, 2010).

The outcome of COX deficiencies is still poor because no treatment is currently available for this disorder (Rak *et al*, 2016). Previous works performed on patients' cell lines have shown that copper supplementation can correct COX defect due to mutations in *SCO2* (Salviati *et al*, 2002), however, copper toxicity limits the use of this treatment. Other molecules such as bezafibrate, a pan-PPAR agonist, and AICAR, an analog of adenosine monophosphate, have been tested in defective human cells (Casarin *et al*, 2012) or mouse models (Diaz *et al*, 2005).

4.4.1 *C. elegans* as model of COX deficiencies

C. elegans has been used as other organisms to model COX deficiencies in order to obtain a better comprehension of the pathophysiological mechanisms behind this heterogeneous group of disorders and to eventually develop better therapeutic approaches (Diaz, 2010).

In the work of Suthammarak *et al* the authors knocked down structural subunits COX-4 and COX-5A by RNAi and found that the silencing of each subunit caused in worms developmental delay (needing an extra day to become adults) and reduced fertility as in the case of many *Mit* mutants with moderate mitochondrial impairment (Ventura *et al*, 2007), but surprisingly it caused also the reduction of lifespan. COX deficiency was less than 50% of control values but the absence of these subunits affected also complex I activity although its protein levels were not altered. Finally, the formation of supercomplexes containing COX was also impaired (Suthammarak *et al*, 2009). This work has proven that a single primary defect can have wide ranging effects on function of multiple ETC different protein complexes. This is important mainly for correct diagnosis, since patients showing ambiguous multiple defects of electron transport involving complexes I and IV may, in fact, harbor a single genetic defect affecting complex IV.

In the last years my research group used a RNAi model to knock down the expression of several ancillary COX subunits and obtain a multicellular model of COX deficiency in order to investigate mitochondrial defects that are often observed in a tissue-specific fashion in patients.

The genes analyzed were the worm homologues of: *COX19* and *COX17* that encode two closely related metallochaperones involved in copper delivery to the mitochondrial inner membrane, *COX11* and *SCO1*, which act in the biogenesis of redox center Cu_A and Cu_B and *COX5B*, a structural subunit (*cco-1* in *C. elegans*).

We down-regulated the expression of these subunits thorough RNA interference and analyzed the phenotype of silenced worms: all of them displayed a COX-dependent decrease in respiration and an increase in lactate production, recapitulating the phenotype observed in patients with mutations in COX-assembly genes, an increase in lifespan and a reduced fertility.

By a COX specific histochemical staining, we also analyzed whether copper supplementation could rescue the phenotype (appreciable in this case as a decreased COX staining, indicating an impaired enzymatic activity), as it has been demonstrated in fibroblasts of patients with mutations in the *SCO2* copper chaperone and we found that in interfered nematodes the supplementation of copper sulphate in the growth medium allows a partial recovery of the pathological phenotypes (Trevisson *et al*, unpublished).

As said before, COX deficiency are a really heterogeneous group of diseases and the understanding of the pathomolecular mechanism at the basis is important for the development of therapies. *C. elegans* is an ideal organism to perform drug screening, since its easy and economic maintenance and the possibility to perform high-throughput testing of molecules. We investigated the effect of copper

supplementation on COX-deficient animals, which is specific for this kind of defect and could represent a realistic therapeutic option. To our knowledge, this is the first demonstration of the efficacy of copper supplementation in a multicellular system.

4.5 Identification and functional characterization of *COX16*

COX16 was originally discovered in *Saccharomyces cerevisiae* (Carlson *et al*, 2003). Mutations in this gene in yeast resulted in the inability to assemble COX. Moreover, *cox16* mutants were respiration-deficient. The authors also stated that like many COX assembly factors, Cox16p is an integral component of the mitochondrial inner membrane and seems to exist in a higher molecular weight complex. They also put some efforts in the identification of the human homologue *COX16*, whose cDNA was identified in a screen for novel proteins expressed in a hematopoietic cell line and led to the identification of the human gene on the long arm of chromosome 14. The ability of the human gene to complement the yeast *cox16* mutant on non-fermentable carbon sources was tested however with negative results.

With the purpose to characterize its expression and function, in the last few years my group began the study of human *COX16* with publication of results in 2018 in BBA Bioenergetics (Cerqua *et al*, 2018). The human *COX16* gene sequence was identified through the "cyber-screening" method, in a similar way for other COX assembly factors (Petruzzella *et al*, 1998). The *in silico* predictions were confirmed by the cloning of the entire coding region of the gene and subsequent sequencing and the obtained sequences were then aligned with those of human genomic DNA to establish the chromosomal localization. *COX16* (NCBI Reference Sequence: NM_016468.7) is localized on chromosome 14q24.1, confirming what was previously found by Carslon *et al*.

Software analysis predicted a protein of 106 aminoacids (sharing 28% of identity and 54% of similarity with the yeast protein sequence) and a mitochondrial localization with a single transmembrane domain and the C-terminus facing the intermembrane space.

Through northern blot analysis it was found that *COX16* transcript is present in all tissues tested, with the higher expression in skeletal muscle, heart and liver. Co-localization experiments evidenced that COX16 localizes in mitochondria and it was demonstrated with a proteinase K protection assay that the C-terminus of the protein is in the mitochondrial intermembrane space.

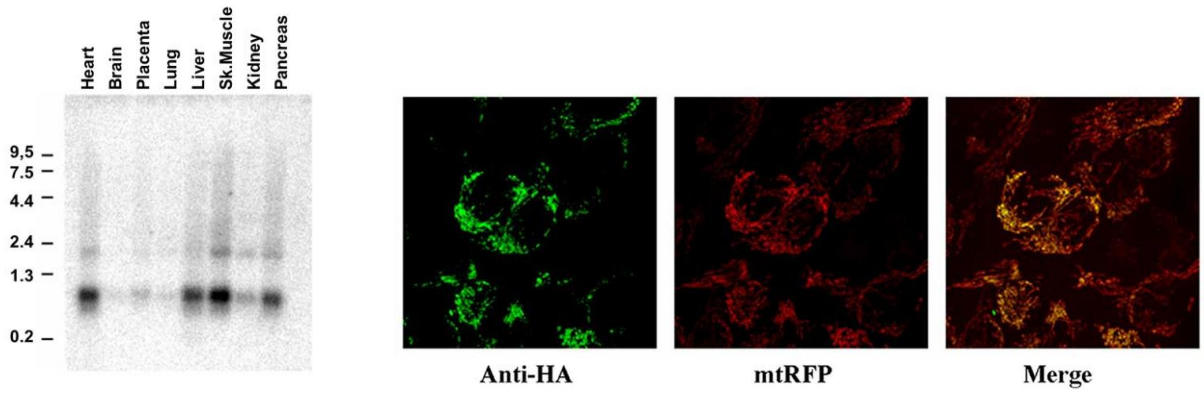

Fig. 7: On the left Northern Blot analysis of COX16 expression in different human tissues, on the right co-localization of COX16-HA and mitochondrial Red Fluorescent Protein (mtRFP). Cells expressing mtRFP were transfected with a plasmid expressing COX16-HA, and COX16 was detected using an anti-HA monoclonal antibody and a secondary antibody conjugated with FITC (adapted from Cerqua *et al*, 2018).

To elucidate *COX16* function, the functional complementation assay of the yeast *cox16*-null strain with the human protein was repeated, but, in order to exclude that the missed complementation of the deleted strain could be due to a faulty mitochondrial import of the human protein, a hybrid gene encoding the yeast targeting sequence and the transmembrane domain fused with the human soluble domain was generated. Differently from the yeast gene that could restore the growth of the deleted strain, no growth was detected with the human gene, as expected, but also with the hybrid construct.

We then turned to a mammalian cellular model and through CRISPR/Cas9 technology a KO HEK293 cell line for *COX16* was generated. Supernatants collected after the infection of a 293FT cell line with a empty lentiviral vector or containing the His-tagged *hCOX16* were used to transduce the *COX16* KO cells.

The activity of OXPHOS complexes was measured in *COX16* KO cells, in *COX16* KO cells repopulated with *COX16*-His and in parental HEK293 cells. Activities of all complexes were similar in the three cell types, whereas activity of complex IV was reduced in *COX16* KO cells compared to either *COX16* KO+*COX16*-His or parental cells.

The reduction of the steady-state levels of COX2, COX5B, and COX6B was then evidenced in *COX16* KO cells compared to parental cells, whereas levels of COX1, COX4 and COX5A remained stable, compatible with a block in the formation of the module containing COX2.

BN-PAGE analysis confirmed these data, showing the accumulation of a low-molecular weight intermediate containing COX1 and COX4, but not COX2 and the reduction of total Complex IV. Activity of complexes I and III was not affected, however the pattern of supercomplexes was abnormal with a reduction of those complexes containing complex IV.

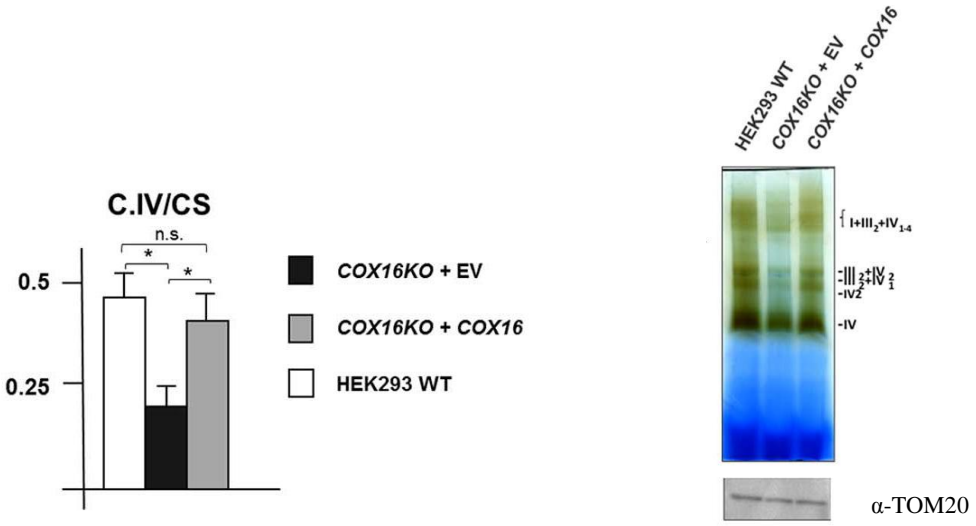

Fig. 8: On the left, complex IV activity of parental HEK 293 cells, *COX16* KO cells transduced with the empty vector (EV), or *COX16* KO cells transduced with *COX16*-His.*, p< 0.05. On the right COX in-gel activity. Cellular lysates of wild type HEK293 and *COX16* KO cells transduced with the empty vector or *COX16*-His were separated by BN-PAGE and stained overnight with 10 mg 3,3'-Diaminobenzidine, 10 mg cytochrome *c*, and 10 mg catalase (adapted from Cerqua *et al*, 2018).

A possible involvement of COX16 in copper delivery to COX2 was also investigated, since after the incubation of *COX16* KO cells with $CuCl_2$ for 10 days the COX enzymatic activity was in part recovered (from 40% to 80% compared to control cells). This result was also confirmed in yeast, given that the copper supplementation could restore the suboptimal growth on a non-fermentable carbon source of the *cox16*-null strain transformed with the yeast homologue of *COX16*.

Besides, immunoprecipitation experiments showed that COX16 interacts with COX2, supporting the idea that COX16 acts in a close relationship with COX2, however whether it directly binds copper ions through an unconventional motif, it stabilizes COX2 prior to copper delivery, or it is involved in recruiting soluble chaperones is still not known.

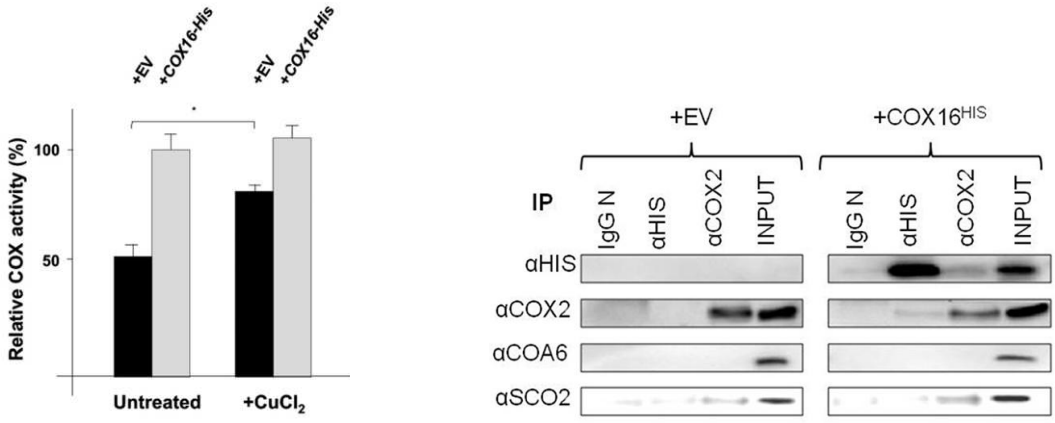

Fig. 9: On the left relative COX activity in *COX16* KO cells transduced with the empty vector or COX16-His after incubation with 200 μM CuCl2. *, p< 0.05. On the right co-immunoprecipitation (co-IP) experiments with anti-His and anti-

COX2 antibodies from HEK293 *COX16* KO+empty vector or *COX16* KO+*COX16*-His mitochondria. The IP eluates were analyzed with antibodies against COX2, COX16, SCO2 and COA6 (adapted from Cerqua *et al*, 2018).

We highlight the importance of other models apart from the yeast one. In fact the employed *cox16*-null strain did not reproduce the phenotype observed in human cells, which display partial COX deficiency, while the defect in yeast cells is complete. So results obtained in yeast should be extrapolated with caution to mammalian cells, as the assembly process is significantly different in these two models. However, the recent introduction of genome-editing techniques allows obtaining cellular KO models that can be used to specifically characterize gene function in mammalian cells.

Based on our results, copper supplementation could represent a possible therapeutic option if patients with mutations in *COX16* will be identified. This is not a remote possibility, since the ExAC variant databases list several potentially pathogenic recessive *COX16* mutations in different human populations (http://exac.broadinstitute.org/gene/ENSG00000133983).

These results were confirmed in the work by Aich *et al*, where authors demonstrate that in the COX2 biogenesis process, COX16 is required for SCO1 but not SCO2 association with COX2, implicating COX16 in Cu_A site formation and in the facilitation of COX2 association with the complex (Aich *et al*, 2018).

COX16 is conserved in *C. elegans*, so in parallel with the experiments conducted in the HEK293 cellular model we decided to use the nematode as a multicellular model to investigate the function of this ancillary COX subunit.

The worm *cox-16* gene was silenced by RNA interference and the effect on COX activity was explored through a specific COX histochemical staining similarly to what was previously done with worms silenced for other COX assembly factors (Trevisson *et al*, unpublished).

5 Results

The efforts made by my research group in the last years led to the identification and functional characterization of *COX16*, as an essential gene for COX assembly and function (Cerqua *et al*, 2018). The experiments performed on a HEK293 cell line KO for *COX16* enabled us to demonstrate that in absence of this gene, not only the activity of Complex IV is strongly reduced, but also the assembly of the complex itself.

Since immunoprecipitation experiments showed that COX16 interacts with COX2, a possible involvement of this factor in copper delivery to COX2 was also investigated with promising results in cell and yeast models.

Since *COX16* is also conserved in *C. elegans*, we decided to use the nematode as a multicellular model to investigate the function of this COX subunit.

The worm COX-16 protein is 115 amino acids long and shares 34% identity and 57% similarity with the human one.

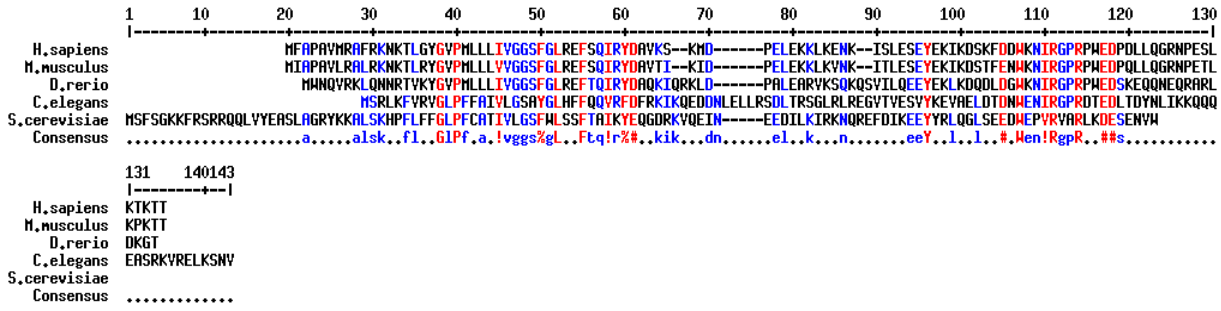

Fig. 10: A Multalin alignment (http://multalin.toulouse.inra.fr/multalin/) of protein sequences of COX16 from different species: *Homo sapiens* (NCBI Reference Sequence: NP_057552.1), *Mus musculus* (NP_079737.1), *Danio rerio* (NP_001017594.1), *Caenorhabditis elegans* (NP_001335555.1), *Saccharomyces cerevisiae* (NP_012531.1).

5.1 Knockdown of *cox-16* by RNA interference

With the same approach used with human *COX16*, we were able to reconstruct the worm *cox-16* coding sequence. The worm gene contains three exons and the coding region spans 348 bp.

cox-16 coding sequence was cloned in the pL4440 vector (see Table 4 for oligonucleotide details, Materials and methods), which carries two T7 sites flanking the insert and oriented in an antiparallel way. Once obtained, the construct was used to transform HT115(DE3) *E. coli* bacteria, that express an IPTG-inducible T7 RNA polymerase and lack RNAse III (Timmons *et al*, 2001).

To perform *cox-16* gene knockdown by RNAi, worm culture plates were prepared adding IPTG to the medium (see Table 3, Materials and methods) to induce the expression of the T7 RNA polymerase and the consequent production of dsRNA from the cloned insert in the pL4440 vector.

The *rrf-3* strain, which is sensitive to RNAi, was used for the experiments (Simmer *et al*, 2002), waiting three worm generations before proceeding to the analysis.
Considering that gene knockdown efficiency by RNAi is variable and influenced by several factors like temperature of incubation and IPTG induction, some controls were included in each experiment. Apart from a negative control, consisting of the empty pL4440 vector, a positive one was obtained feeding worms with bacteria carrying the pLT61 vector, that contains 0.8 kb of *unc-22* inserted into the pL4440 vector, with a resulting visible shaking phenotype of silenced worms.
cox-16 silencing was not lethal and enabled a normal development of worms that were phenotypically indistinguishable from their relative controls. Besides, worm movements were not impaired in absence of *cox-16*, nor were their behaviors altered, at least in a way that could be appreciated by visual inspection of worm plates.

5.2 *C. elegans* COX histochemical staining

The protocol developed by Grad *et al* was used with some modifications (see paragraph 3.3.1, Materials and Methods) to investigate worm COX activity *in vivo*.
The staining requires the incubation of fixed and permeabilized nematodes with a mix containing 3,3'-diaminobenzidine (DAB), cytochrome *c*, and catalase. Basically, if COX is functional in worm tissues the result is a visible brown staining, that is derived from DAB precipitation. In fact, following cytochrome *c* oxidation by COX enzymatic activity, DAB is in turn oxidized by cytochrome *c* and precipitates. Catalase is added to prevent the accumulation of hydrogen peroxide in the medium, while the use of exogenous cytochrome *c* may be useful in depleted tissues (Seligman *et al*, 1998).
The COX histochemical staining was performed on worms, to investigate the effects of the depletion of *cox-16* on COX assembly and function in a multicellular model.
Besides worms silenced for *cox-16*, and the control ones fed with bacteria expressing the empty pL4440 vector, also worms silenced for *cco-1*, that is the homologue of the human structural subunit *COX5B*, were stained. A negative control of the reaction was also included, adding to the reaction sodium azide, which inhibits COX activity, in order to ensure the specificity of the observed coloration.

A

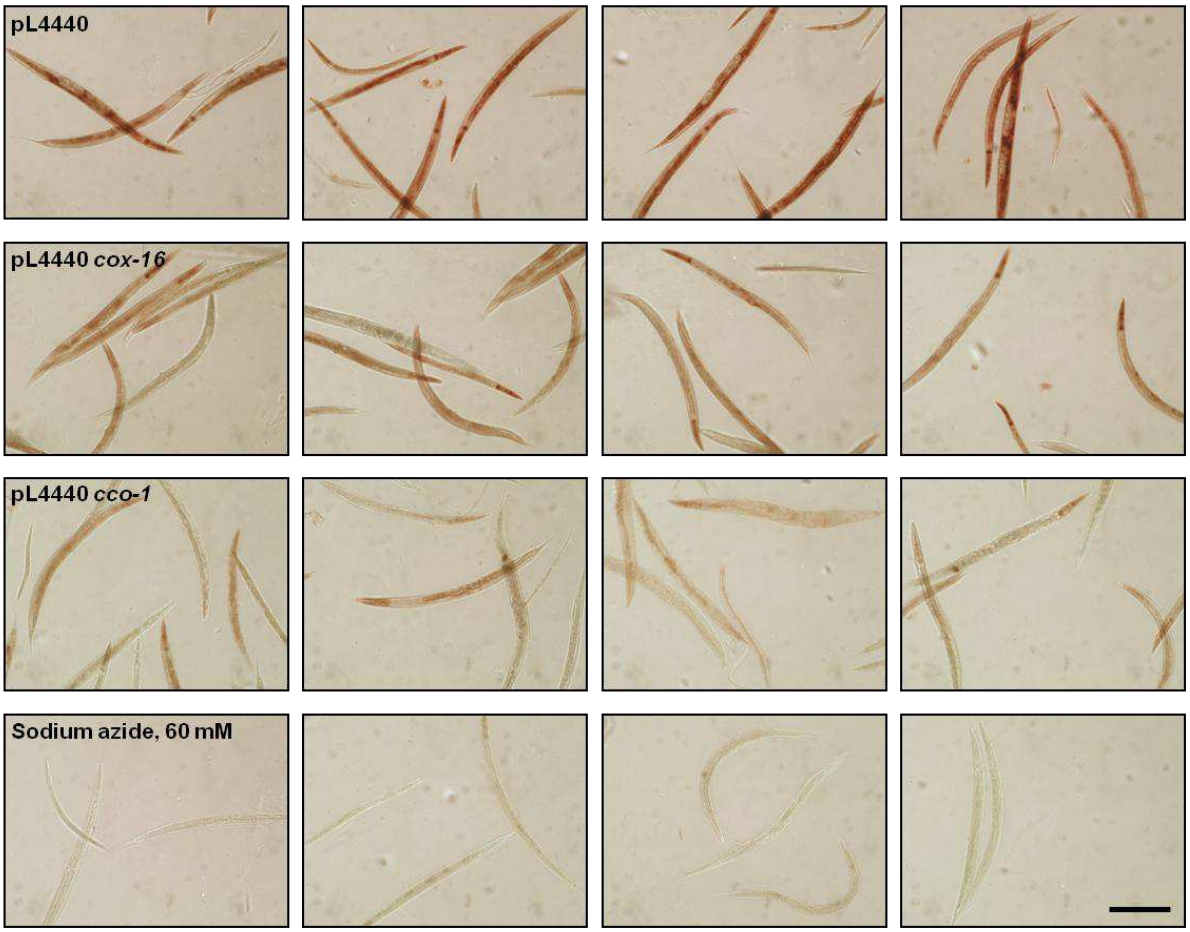

B

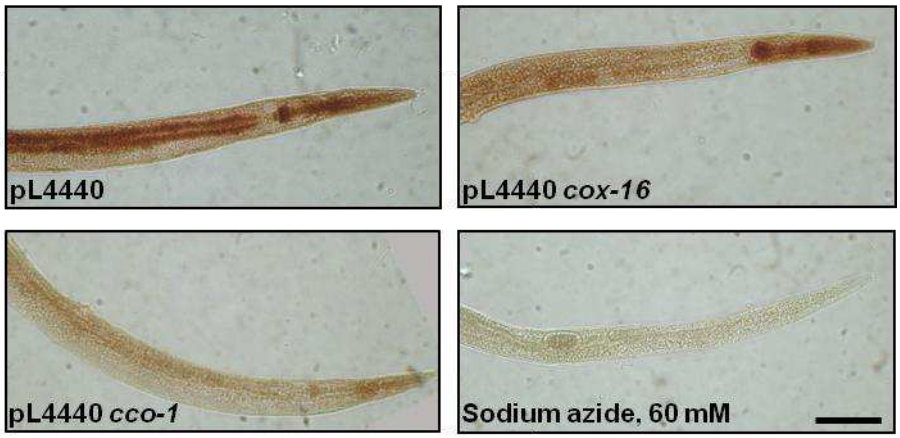

Fig. 11: COX histochemical staining for COX activity in *C. elegans*. Worms were fed with HT115DE(3) *E. coli* transformed with either the empty pL4440 vector, with pL4440 *cox-16*, or with pL4440 *cco-1*, which targets a structural subunit of COX (*COX5B*). Nematodes were fixed, permeabilized, and stained for COX and, as a further control, worms treated with 60 mM sodium azide were included. A) Photographs of four representative examples for experimental condition are shown. Scale bar 250 µm. B) Images taken at higher magnification. Each worm depicted was obtained by joining several partial photographs. Scale bar 100 µm.

As shown in figure 11, COX staining was intense and distributed all over nematode body in control worms fed with the empty vector. Conversely, worms incubated with sodium azide didn't stain, confirming the inhibition of COX activity and the specificity of the coloration observed in control worms.

The silencing of the structural subunit *cco-1* led, as already observed (Trevisson *et al*, unpublished) and expected, to a strong decrease of COX staining, compatible with a impaired assembly of the complex.

cox-16 silencing caused the reduction of COX staining as well, although the effect was lower and some body areas were spared, like the head and the pharynx.

5.3 In-gel activity for cytochrome *c* oxidase

We got also interested in the characterization of mitochondrial OXPHOS complexes and supercomplexes in *C. elegans*. Starting from already published protocols (Grad *et al*, 2007; Suthammarak *et al*, 2009), we performed mitochondria extraction from worms and complexes revelation through in-gel staining for COX activity, testing different conditions in order to find the one that gives the best mitochondrial yield, preserving their integrity (Table 6).

	1	2	3	4	5
Worms maintenance	Plate culture	Plate culture	Liquid culture	Liquid culture	Liquid culture
Lysis buffer composition	220 mM mannitol, 70 mM sucrose, 5 mM MOPS, 2 mM EDTA, pH 7.4	37 mM Tris-maleate, 0.5 M sucrose, 2 mM $MgCl_2$, pH 6.4	37 mM Tris-maleate, 0.5 M sucrose, 2 mM $MgCl_2$, pH 6.4	37 mM Tris-maleate, 0.5 M sucrose, 2 mM $MgCl_2$, pH 6.4	37 mM Tris-maleate, 0.5 M sucrose, 2 mM $MgCl_2$, pH 6.4
Sonication protocol	40% amplitude (4 times, 1′)	40% amplitude (4 times, 1′)	40% amplitude (4 times, 1′)	40% amplitude (8 times, 1′)	40% amplitude (8 times, 1′)
Collagenase treatment	33 mg/ml in 5 mM $CaCl_2$, 15′	33 mg/ml in 5 mM $CaCl_2$, 15′	33 mg/ml in 5 mM $CaCl_2$, 15′	33 mg/ml in 5 mM $CaCl_2$, 15′	33 mg/ml in 5 mM $CaCl_2$, 15′
Homogenization protocol	(1600 rpm 2 times, 5′)	(1600 rpm 2 times, 5′)	(1600 rpm 2 times, 5′)	(1600 rpm 2 times, 5′)	(1600 rpm once, 5′)
Complex IV IGA	+++	++	++	precipitated	precipitated

Table 6: Different conditions tested for the extraction of mitochondria from *C. elegans*. Both liquid and plate culture methods were used, two lysis buffers were employed and the sonication and homogenization protocols were performed with some variations between the different conditions. Based on the in-gel staining for COX activity condition 1 was chosen as the best.

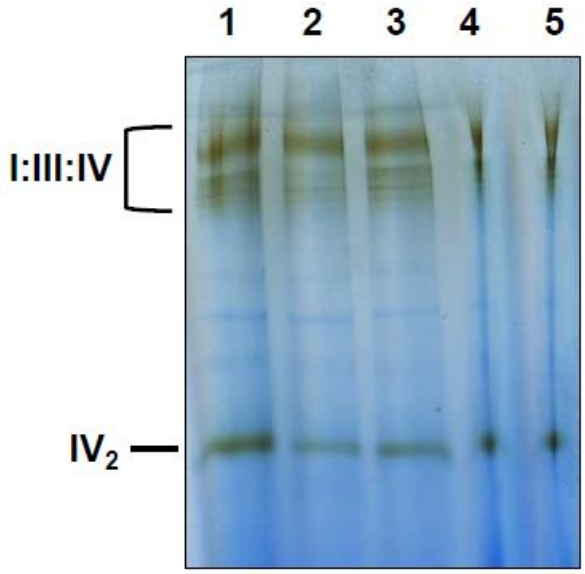

Fig. 12: After extraction from *C. elegans*, 100 µg of mitochondrial proteins were submitted to solubilization by digitonin with a detergent/protein mass ratio of 6/1 for one hour on ice. Then samples were centrifuged for 20 minutes at 16000 g at 4 °C and NativePAGE™ 5% G-250 Sample Additive was added to the supernatant to obtain a dye/detergent mass ratio of 4/1. Proteins were loaded in 3-12% Bis-Tris NativePAGE™ gels and after run complex IV activity was assayed directly on gel incubating it with 0.1 % (w/v) DAB, 0.1% (w/v) cytochrome *c* and 24 units/ml catalase in 50 mM Tris-HCl pH 7.4 overnight at room temperature with constant agitation.

We used both cultures grown in liquid medium, as well as on agar plates. We tested two different lysis buffers and performed sonication and homogenization protocols with some variations in their duration. 100 µg of extracted mitochondrial proteins were submitted to solubilization by digitonin and then loaded in 3-12% Bis-Tris NativePAGE™ gels. After run complex IV activity was assayed directly on gel overnight at room temperature with constant agitation (see paragraph 3.3.2, Materials and Methods).

Figure 12 shows the results of the different protocols tested for COX staining: condition 1 was the best, since conditions 4 and 5 led to mitochondrial protein precipitation and condition 2 and 3, although preserving mitochondria integrity, provided a lower protein yield resulting in attenuated COX staining compared to condition 1.

6 Discussion

COX16 was originally discovered in *Saccharomyces cerevisiae* (Carslon *et al*, 2003); using this model it was demonstrated that mutations in this gene resulted in a total inability for yeast cells to assemble complex IV.

The function of the human homologue remained elusive until my group began its study, confirming in a HEK293 *COX16* KO cellular model its important role for COX biogenesis and function. COX16 absence resulted in a strong reduction in COX activity and in the assembly of the complex itself, suggesting that the factor is involved in the formation of the COX2-containing module. The possibility that COX16 is required for copper delivery to COX2 was also investigated with promising findings in cell and yeast models (Cerqua *et al*, 2018). These results were confirmed by another group which performed similar experiments (Aich *et al*, 2018).

C. elegans was employed to demonstrate the essential role of *COX16* in COX assembly and function also in a multicellular model.

Through a RNAi interference model, we knocked down *cox-16* and *cco-1* in nematodes and we observed the effect on COX activity through a specific histochemical staining, that produces in worm tissues a brown precipitate if COX is active.

The strong reduction of COX staining in *cco-1* silenced worms is compatible with results reported by Suthammarak *et al*, who silenced in *C. elegans* two other structural subunits, COX-4 and COX-5A, leading to an impairment in COX assembly and enzymatic activity (Suthammarak *et al*, 2009).

Other examples of animal models in which COX structural subunits encoded by nuclear genes have been deleted or silenced confirmed their essential role in COX biogenesis and function. For example, a knockdown of the structural subunit *COX5A* was created using antisense morpholino oligonucleotides in *Danio rerio*, obtaining fishes with about 50% COX deficiency compared with control animals, that led to a series of developmental defects and eventually to early death (about seven days after fertilization) (Diaz, 2010).

Worms silenced for *cox-16*, instead, showed a partial preservation of COX activity, especially in some body portions. This result suggests that the function of this assembly factor is in *C. elegans* at least in part redundant and confirms data obtained with the HEK293 cellular model in which *COX16* was deleted with CRISPR/Cas9 technology causing the halving of COX enzymatic activity but not its total abrogation (Cerqua *et al*, 2018). However, the worm model was essential to prove the importance of this assembly factor for COX biogenesis and proper functioning also in a multicellular model.

We haven't performed further experiments on worms silenced for *cox-16*. However, given the results obtained by my group with the silencing of other COX assembly factors (Trevisson *et al*, unpublished), it would be interesting to carry out an extensive phenotypic characterization of worms after having knocked down *cox-16*.

It has been demonstrated that in *C. elegans* a moderate degree of mitochondrial dysfunction is generally associated with lifespan extension, larval development slowing and decreased fertility, while when mitochondrial disruption is too severe, significant larval arrest occurs, or adult animals are invariably sterile and lifespan is any case shortened (Ventura and Rea, 2007).

The RNAi approach was used by my group to knock down the expression of several ancillary COX subunits (*cco-1*, *cox-11*, *cox-17*, *cox-19* and *sco-1*) in nematodes, with a resulting COX-dependent decrease in respiration and an increase in lactate production, a prolonged lifespan and a reduced fertility.

A COX specific histochemical staining was performed also in these silenced worms, highlighting a decrease in staining, so in COX activity, for all of them, but evidencing different degrees of impairment and tissue predominance. The following supplementation of copper sulphate in the growth medium revealed beneficial and could restore COX activity.

The involvement of COX16 in copper delivery to COX2 was investigated in the HEK393 cellular model established by us and after having incubated *COX16* KO cells with $CuCl_2$ for 10 days, the COX enzymatic activity was in part recovered (from 40% to 80% compared to control cells). This result was also confirmed in yeast, given that the copper supplementation could restore the suboptimal growth on a non-fermentable carbon source of the *cox16*-null strain transformed with the yeast homologue of *COX16* (Cerqua *et al*, 2018). The treatment of *cox-16* silenced nematodes with copper sulphate, in a similar way to what was done with the other COX assembly factors, could confirm the results obtained in yeast and in a human cell line also in a multicellular model, pointing out possible tissue-specific effects.

The investigation of mitochondrial ETC complexes and supercomplexes assembly has been carried out in the last years also in *C. elegans* (Suthammarak *et al*, 2009; Suthammarak *et al*, 2010). we used a protocol developed by Grad *et al*, with some variations, in order to efficiently extract worm mitochondria, and performed an in-gel COX staining to reveal complex IV and supercomplexes containing it. We optimized the procedure using mitochondria derived from wild-type animals and chose a condition that enabled to get a good protein yield preserving at the same time mitochondria integrity (Table 6).

The pattern of bands observed is compatible with that obtained with a similar protocol by Suthammarak *et al*, with multiple high-molecular weight bands and a lower one.

Through Coomassie staining and mass spectrometry analysis of isolated single bands they demonstrated that the band with the lowest molecular weight corresponds to the dimeric form of complex IV, while the high-molecular weight bands contain subunits of supercomplex I:III:IV.

The analysis of silenced worms for different COX assembly factors could reveal an impairment in the formation of complex IV or supercomplexes. This has already been demonstrated in our cell model lacking *COX16*, in fact BN-PAGE analysis showed the reduction of total Complex IV and an abnormal pattern of supercomplexes with less of those containing complex IV (Cerqua *et al*, 2018).

C. elegans could be used as a model not only to confirm the results obtained for *COX16*, but also to investigate the degree of involvement in COX assembly of several other factors whose function is still elusive or not fully understood, given the simplicity to achieve a gene knockdown in the whole animal for each of them. The definition of an easy to obtain model of study has a primary importance also on the light of results of Suthammarak *et al* showing that single primary defect can have wide ranging effects on function of multiple different protein complexes of the ETC.

In fact, the knockdown of the structural subunits COX-4 and COX-5A by RNAi affected not only complex IV but also complex I activity, although the protein levels of this complex were not altered, proving that multiple defects involving complexes I and IV may depend on a single genetic defect affecting complex IV (Suthammarak *et al*, 2009). The same group demonstrated later that a structural defect of complex III, caused by a mutation in the iron sulfur protein, can reduce the amount of fully assembled complex I without a reduction in the amount of fully assembled complex III (Suthammarak *et al*, 2010).

The functionality and structural organization of complex IV could be studied also in double or even multiple *C. elegans* knockdowns for COX assembly factors, to investigate if and how the complex assembly is affected and the degree of resulting mitochondrial impairment and hence phenotype gravity. So the function of these factors could be better characterized, determining how they are involved in the general process of COX biogenesis and their mutual relationship. For example, since several COX assembly factors seem to be involved in copper metallation of the enzymatic complex, this approach could maybe explain the partially redundant function observed for COX-16.

COX deficiencies comprehend a wide variety of disorders and represent the most frequent among mitochondrial diseases. They can be associated with different phenotypes, including a devastating progressive disease, generally affecting brain, skeletal muscle and heart and that is usually fatal in the first years of life. The outcome is still poor because no treatment is currently available for this disorder (DiMauro *et al*, 2012; Rak *et al*, 2016).

RNAi for *cox-16* and the other COX assembly factors enabled us to obtain a multicellular model of COX deficiency that could be used in order to investigate mitochondrial defects in patients. In fact, no mutant strains are available in the *Caenorhabditis* Genetics Center (CGC) database (https://cgc.umn.edu/) for the COX assembly factors of our interest, except for two balanced lethal deleted strains isolated after mutagenesis, that is VC2734 for *cox-17* (*F40G9.2(ok1784)/sC1 [dpy-1(s2170)] III*) and VC3153 for *sco-1* (*sco-1(ok3770)/mIn1 [mIs14 dpy-10(e128)] II*), for which however ho phenotypic characterization is so far available (The *C. elegans* Deletion Mutant Consortium, 2012).

As already mentioned, since *C. elegans* size is quite small, many assays can be carried out in wells of a 96-well plate, enabling for example high-throughput for neurotoxins and drug screening (Kaletta and Hengartner, 2006). This simple multicellular model could help in the screening of a large number of molecules (copper, but also bezafibrate, AICAR) to target COX deficiencies, investigating the effect

on different animal tissues, an important advantage of this model compared to cell lines and yeast, since mitochondrial defects are often observed in a tissue-specific fashion in patients.

Moreover, the opposite and discrete phenotypes that appear in *C. elegans* upon mild or severe mitochondrial damage represent a useful tool to mimic the progressive course and severity of mitochondrial diseases, enabling to investigate trough RNAi models the phase of partial mitochondrial suppression that in human is likely asymptomatic, while in the worm model it is associated with peculiar and recognizable phenotypes (Maglioni and Ventura, 2016).

Patients with mutations in *COX16* have not been identified so far, however, this is not a remote possibility, since the ExAC variant databases list several potentially pathogenic recessive *COX16* mutations in different human populations. Given our results that indicate that *COX16* is essential for proper COX biogenesis and function, we highlight the need to include the screening of this gene in diagnostic panels.

SECTION IV

FUNCTIONAL CHARACTERIZATION OF A NEW GENE NAMED *MYTHO*

7 Introduction

7.1 Cellular and molecular mechanisms of autophagy

The term 'autophagy', derived from the Greek meaning 'eating of self', was first used by Christian de Duve over 40 years ago, and refers to the delivery of heterogeneous intracellular material to lysosomal digestion (Glick *et al*, 2010; Dikic and Elazar, 2018). The yeast *Saccharomyces cerevisiae* was the model of study that helped to define how autophagy is regulated and executed at the molecular level, however many key player genes have orthologues in other organisms ranging from worms to mammals, indicating the importance of autophagy across phylogeny (Glick *et al*, 2010).
This process can be activated by different cellular signals and has many physiological roles. It is active at basal levels in most cell types where it is thought to play a housekeeping role in maintaining the integrity of intracellular organelles and proteins and preserving the accumulation of damaged ones, but it also occurs in response to different forms of stress, including nutrient deprivation, growth factor depletion, infection and hypoxia (Mizushima, 2007; Rubinsztein *et al*, 2011; Dikic and Elazar, 2018).
Three types of autophagy have been identified: macro-autophagy, micro-autophagy and chaperone-mediated autophagy (CMA), and all of them cause the degradation of cytosolic content at lysosomes.
The term "autophagy" hereafter used indicates macro-autophagy unless otherwise specified.

7.1.1 The molecular autophagic machinery

The autophagic process begins with the recruitment of autophagy-related proteins (ATGs) to a specific subcellular location termed the phagophore assembly site (PAS) where a lipidic bilayer isolation membrane, probably derived from the endoplasmic reticulum, the Golgi or endosomes, nucleates with a cup-resembling structure. It then elongates and expands engulfing cytosolic cargos, such as protein aggregates, organelles and ribosomes and eventually seals in a double-membrane autophagosome enclosing the cytosolic material. After clearance of most ATGs and delivery of the autophagosome along microtubules to the lysosome, the outer membrane of the autophagosome fuses with the lysosomal membrane forming an autolysosome. This fusion results in the release of a single-membrane autophagic content into the lysosomal lumen and in the degradation of the autophagic body together with its cargo by lysosomal acid proteases. The products deriving from this degradation process are taken back to the cytoplasm by lysosomal permeases and transporters where they can be used to synthesize macromolecules or for metabolism (Glick *et al*, 2010, Dikic and Elazar, 2018).

From a molecular point of view, stimulating signals that induce autophagy recruit at the PAS Unc51-like-kinase (ULK1), which forms together with ATG13, ATG101, and focal adhesion kinase family-interacting protein of 200 kDa (FIP200) the ULK1 complex that is regulated in opposite manner by the mammalian target of rapamycin complex 1 (mTORC1) and AMP-dependent protein kinase (AMPK).
In high nutrients conditions, mTORC1 is activated and inhibits autophagy by binding to the ULK1 complex and phosphorylating both ATG13 and ULK1, thereby suppressing ULK1 kinase activity.
On the contrary, on low cellular energy levels, as in glucose starvation, the ATP/AMP ratio is sensed by AMPK that phosphorylates and activates ULK1.
Another key regulator of autophagy is TFEB (transcription factor EB), which is negatively regulated by mTORC1 and activated in anabolic conditions to regulate the expression of genes involved in lysosomal biogenesis and lipid catabolism (Menzies *et al*, 2017; Dikic and Elazar, 2018).
As anticipated, hypoxia, as well as starvation, stimulates autophagy and this action is mediated by genes induced by hypoxia-inducible factor (HIF), or by HIF independent mechanism that end up with TOR inhibition (Glick *et al*, 2010).
Once the ULK1 complex is active, VPS34 (vesicular protein sorting 34), a class III phosphatidylinositol 3-kinase (PI3K), is recruited to the PAS, where it produces phosphatidylinositol 3-phosphate (PI3P) while in a complex with VPS15, ATG14, and Beclin-1. It seems that PI3P aids the recruitment of WIPI [tryptophan-aspartic acid (WD) repeat domain phosphoinositide-interacting] proteins that, in turn, control the recruitment of other downstream autophagic factors. One established regulatory mechanism of this step is the interaction of Beclin-1 (encoded by *BECN1*) with Bcl-2, which disrupts that of Beclin-1 with VPS34 thus inhibiting autophagy; on the contrary AMBRA1 (activating molecule in *BECN1*-regulated autophagy protein 1) activates autophagy (Glick *et al*, 2010; Dikic and Elazar, 2018).
The ATG12 and ATG8/LC3 ubiquitin-like conjugation systems are then required for sustaining the expansion of the phagophore. In the first system, ATG12 is conjugated to ATG5 and the resulting complex binds to ATG16L1. ATG12-ATG5-ATG16L1 associates with pre-autophagosomal membranes and facilitates the recruitment of LC3. However, to make this possible LC3 has to be processed by the cysteine protease ATG4, which cleaves the C-terminus of LC3, exposing a glycine residue (LC3-I form), This enables the LC3-I conjugation to phosphatidylethanolamine (PE), leading to the formation of LC3-II, which is tightly associated with autophagosomal membranes. These events are crucial for phagophore membrane extension, which is also favored by mATG9, and for its sealing to form the mature autophagosome (Menzies *et al*, 2017; Dikic and Elazar, 2018).
This step-regulated maturation of LC3, which is expressed as the splice variants LC3A, LC3B, and LC3C with unique tissue distribution, makes it a key readout of levels of autophagy in cells. GABARAP [Gamma-aminobutyric type A (GABAA)-receptor associated protein] is processed in a similar way during autophagy and GABARAP-II co-localizes with LC3-II at autophagosomes (Glick *et al*, 2010).

Afterwards, a gradual clearance of ATGs happens with the concomitant recruitment of proteins responsible for lysosomal delivery and for autophagosome-lysosome fusion (Dikic and Elazar, 2018).
As mentioned above, autophagy can degrade cytosolic contents both in a selective way or randomly.
LC3-II, acting as receptor at the phagophore, interacts through its LIR (LC3-interacting region) with adaptor molecules on the target (*e.g.* protein aggregates, organelles) to promote their selective uptake and degradation. The best-characterized adaptor is p62/SQSTM1, a multi-functional molecule that promotes turnover of polyubiquitinated protein aggregates (Glick *et al*, 2010).

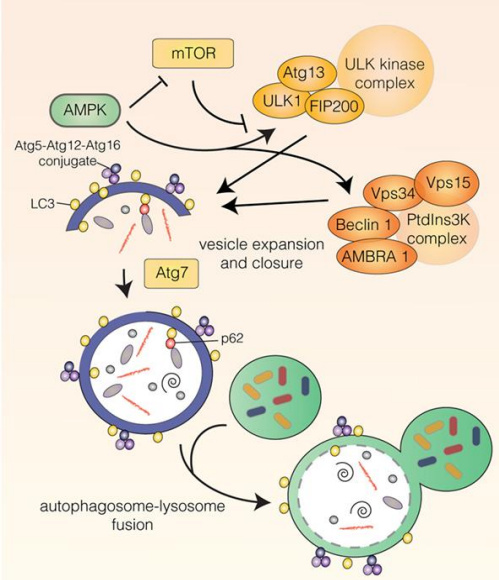

Fig. 13: The autophagic process, starting from autophagosome formation, proceeding with maturation and fusion with the lysosome. The main key player autophagic factors are represented (adapted from Mathiassen *et al*, 2017).

7.2 Autophagy regulation in neurons

The autophagic process is strictly regulated in neurons to ensure their homeostasis and survival.
Since neuronal morphology is quite elaborated, with highly branched dendrites and an axon that can extend very far from the cell body where most biosynthetic and degradative processes happen, the control of neuronal protein and organelles integrity is really challenging.
In the distal end of the axon autophagosomes originate by recruitment of core ATGs to specific sites of the endoplasmic reticulum and neuron-specific proteins regulate rates of autophagosome biogenesis in presynaptic terminals. Distal autophagosomes then begin to travel towards the soma and as they come closer to the cell body, their maturation proceeds. Once inside the soma, autophagosomes remain inside the somatodendritic region and are prevented from going back to the axon. This limitation facilitates their maturation into autolysosomes by promoting fusion with soma resident degradative lysosomes and ensures an efficient recycling of products derived from degradation. Recent evidence suggests that the axon may have a unique and specialized machinery for selective autophagy of ubiquitinated substrates. On the other side, dendritic autophagosomes are limited in

number, but upon enhanced synaptic activity their density can increase and their movements are not confined in one direction as in the axon (Kulkarni *et al*, 2018; Liang, 2019).

Moreover, neuronal autophagy plays an important role in synapse development, since synaptic components like synaptic proteins and vesicles, postsynaptic receptors and synaptic mitochondria are degraded by autophagy, thus contributing to synapses remodeling. It has been demonstrated that decreasing or increasing autophagy results in corresponding effects on synapse size and the modulation of this process may be required for different forms of synaptic plasticity and memory formation (Son *et al*, 2012; Liang, 2019).

Mitophagy assumes a crucial role as mitochondrial control quality mechanism at the synapse since synaptic activities are highly energetic processes that require proper calcium buffering capacity from mitochondria (Liang, 2019).

7.3 Autophagy in health and disease

Autophagy has several roles in cells. First of all, it is the most important process through which damaged organelles and polyubiquitinated protein aggregated are degraded. The amino acids deriving from protein degradation are used not only to synthesize new proteins but also as energy source in the TCA cycle and to produce glucose by gluconeogenesis in liver during starvation periods. Autophagy represents also a way to deliver cytosolic material to the lysosomes and to protect cells from endoplasmic reticulum stress. Finally, autophagy is a defense mechanism against microorganisms and viruses (Mizushima, 2007; Rubinsztein *et al*, 2011).

In the last years it has become evident that genetic or age-dependent perturbations in this process are implicated in different pathologic conditions, like cancer progression, neurodegenerative and immune diseases as well as aging.

The role of autophagy in cancer is controversial (Dikic and Elazar, 2018). It may have tumor-suppressive roles, like EMT (epithelial-mesenchymal transition) inhibition in several models of tumor or the degradation of crucial regulators of actin dynamics and cell migration, and its dysfunction has been associated with increased risk of cancer. However, it has also been reported that autophagy confers metabolic plasticity to premalignant cells enabling them to survive in stressful conditions, for example contributing to the remodeling of focal adhesions sites, a process essential for cell migration, and inhibiting *anoikis* (a specific form of apoptotic cell death).

Many current cancer clinical trials attempt to manipulate autophagy inhibiting it, but caution has to be taken since treatments may have unintended consequences by affecting other biological functions of autophagy (Thorburn, 2018).

Autophagy is important also for a proper immune defense, in fact autophagy-deficient animals are susceptible to infection and defects in this process are linked to autoimmune diseases. The therapeutic strategy so far adopted to combat bacterial infections activates autophagy (Dikic and Elazar, 2018).

7.3.1 Autophagy and neurodegenerative diseases

As mentioned above, autophagy is crucial for neuron homeostasis, so dysfunctions in this process are thought to be implicated in neurodegenerative diseases, considering that the major pathological phenotype of most late-onset neurodegenerative diseases are intraneuronal aggregates of misfolded proteins, which are substrates for autophagic degradation, when the proteasome is overloaded (Menzies *et al*, 2017).

The familial forms of neurodegenerative diseases allow to investigate the molecular mechanisms of pathology and for many of them autophagy-related genes are involved. However, the absolute contribution of autophagy dysfunction to disease progression has yet to be established and here some examples of what has been so far highlighted are reported.

An important clinical sign in Alzheimer's disease are extracellular amyloid β (Aβ) plaques, that may be autophagic substrates. However, autophagy could also play a role in plaque secretion into the extracellular space.

Parkinson's disease is characterized by loss of dopaminergic neurons in the *substantia nigra* and, typically, by the presence of α-synuclein (α -syn) inclusions, that affect autophagic process. In fact, although lysosomal function appears normal, autophagosome maturation and fusion with the lysosomes are decreased, resulting in impairment of protein degradation.

Moreover, mutations in *Parkin* and *PINK1*, that are two key players in mitophagy, are strongly associated with the early-onset form of Parkinson's disease. (Jiang and Mizushima, 2014; Dikic and Elazar, 2018).

Some neurological disorders are caused by mutant proteins with expanded glutamine repeats (polyQ) and autophagy perturbation is observed in several of them (Menzies *et al*, 2017). For example, in Huntington's disease (MIM# 143100), mutated huntingtin impairs efficient cargo recognition by autophagosomes, while in spinal bulbar muscular atrophy the mutated androgen receptor interacts with TFEB inhibiting its activation.

Most lysosomal storage disorders are caused by loss of function of specific lysosomal hydrolases, leading to the accumulation of the substrates of these enzymes and other autophagic substrates such as p62/SQSTM1, polyubiquitinated proteins, and damaged mitochondria, because of impaired autophagosome-lysosome fusion (Jiang and Mizushima, 2014).

Mutations implicated in neurodegenerative diseases have also been found in autophagic genes, both core and accessory ones (*e.g. ATG5*, *p62/SQSTM1*, *WIPI4*) (Jiang and Mizushima, 2014; Menzies *et al*, 2017).

It has been shown for many of these pathological conditions that the aggregate-prone proteins are autophagy substrates and that its induction reduces the levels of both the soluble and aggregated forms with beneficial effects. Many small molecules have been employed to induce autophagy and they act via mTOR-dependent (*e.g.* rapamycin) or mTOR-independent targets, signaling via AMPK (*e.g.*

trehalose, metformin) (Dikic and Elazar, 2018). Based on the available therapeutic options, recent efforts have been made in order to selectively activate only autophagy capable of removing aggregated proteins, but not the other types of autophagy, limiting in this way adverse effects (Thorburn, 2018).

7.3.2 Autophagy and aging

The decrease of autophagy with age has been reported in a variety of systems and model organisms were useful to identify autophagic genes involved in the aging process.
Many short-lived mutants with defects in autophagy were in fact identified in *S. cerevisiae*.
C. elegans mutants with loss-of-function of the homologues of human *ATG1*, *ATG7*, *ATG18* and *BECN1* display decreased lifespan and in mice the knockout of essential *ATG* genes is lethal during the early postnatal period because autophagy is crucial for mobilizing intracellular energy reserves during the transition from intrauterine metabolism to weaning.
Confirming this, ATG proteins or other proteins required for autophagy have reduced expression in human aged tissues, however how autophagy decreases with age remains unclear (Rubinsztein *et al*, 2011; Martinez-Lopez *et al*, 2015).
Recent studies have highlighted the role of ATG proteins not only in organelle quality control, but also in tissue differentiation and control of genome stability, so loss of these factors could accelerate aging by interfering with one or more of these mechanisms. It has been demonstrated that autophagy decreases during aging depending on hormone regulation and mTOR hyperphosphorylation (Martinez-Lopez *et al*, 2015).
Caloric restriction, that is a reduced food intake without malnutrition, is the key of anti-aging interventions that extends lifespan in most models so far tested. In fact, it induces autophagy through the activation of either of two energy sensors, AMPK and Sirtuin 1 (SIRT1, a NAD^+-dependent deacetylase), which engage in a positive forward loop of mutual activation, but also through the inhibition of insulin/insulin-like growth factor (IGF) signaling, resulting in TOR inhibition (Rubinsztein *et al*, 2011).

7.4 Autophagy in *C. elegans*

Many of the yeast genes encoding autophagy proteins have orthologues in the *C. elegans* genome. Genes that are distantly related homologues of yeast *ATG* genes or that have no yeast counterparts include the *epg* genes from *epg-1* to *epg-9*. Two homologues of yeast *ATG4*, *ATG16*, and *ATG8* (*lgg-1* and *lgg-2*) are present, conferring more complexity on the autophagic machinery (Meléndez and Levine, 2009; Zhang *et al*, 2015).
Many of the key signaling mechanisms for autophagy regulation appear to be conserved in *C. elegans*, where autophagy occurs in many cell types playing essential roles in developmental and physiological

processes, including survival of animals under nutrient restricted conditions, removal of a variety of protein substrates, dauer formation, the aging process, and prevention of bacterial infection.

It was found that in absence of food autophagy is activated in the pharyngeal muscles, and RNAi for *bec-1* (the worm homologue of human *BECN1*) or *atg-7* causes animal death, suggesting that autophagy provides the energy essential to maintain pharyngeal pumping efficiency and survival during starvation (Kang *et al*, 2007).

let-363 is the worm orthologue of mammalian TOR and a negative regulator of autophagy. Loss of *let-363* activity, through RNAi or mutation, causes developmental arrest at the L3 stage of larval development. Furthermore, RNAi inhibition of TOR, if performed from the L4 larval stage onwards, prolongs nematode lifespan, but the specific inhibition of autophagy shortens life of mutants, indicating that the autophagic machinery is indeed part of the mechanism by which TOR inhibition increases lifespan (Tóth *et al*, 2008; Meléndez and Levine, 2009).

In *C. elegans*, *daf-2*, which encodes for a hormone receptor similar to mammalian insulin and IGF-1 receptors, and *age-1*, whose protein product is the kinase PI3K, negatively regulate autophagy once activated (see paragraph 7.5). *daf-2* has two functions: it promotes growth to adulthood, and it shortens lifespan of adult animals.

Mutants for *daf-2* and *age-1* genes display an increase in adult longevity that requires the forkhead transcription factor DAF-16, the only worm homologue of mammalian FOXOs, which is crucial for the expression of stress resistance and longevity promoting genes. In conditions of low food abundance, high temperature, or overcrowding, nematodes can adopt an alternative fate becoming dauer larvae. Temperature-sensitive mutants of *daf-2* [for example, the extensively studied *daf-2(e1370)* allele] are constitutive dauers at restrictive temperatures also in presence of food (Kenyon *et al*, 1993; Kimura *et al*, 1997; Lin *et al*, 1997; Gems *et al*, 1998).

Interestingly, it was later found that autophagy inactivation by RNAi of *bec-1* decreases lifespan of *daf-2* mutant animals, without effects on wild-type worms. Moreover, in absence of *bec-1*, *daf-2* mutants can't form normal dauers, highlighting the importance of a functional autophagic process for survival under stressful conditions and lifespan extension (Meléndez *et al*, 2003).

As anticipated before, dietary restriction plays an evolutionarily conserved role in lifespan extension from worms to mammals. The increased lifespan observed in feeding-defective *C. elegans* mutants, *eat-2, eat-3* and *pha-3*, is accompanied by an increase of autophagy, suggesting that this process might be involved in dietary restriction-mediated lifespan extension. Besides, it was shown that the autophagic genes *bec-1, vps-34* and *atg-7* are essential for the lifespan extension of *eat-2* mutants (Meléndez and Levine, 2009).

Moreover, autophagy regulates the survival of newly hatched larvae that under food deprivation conditions arrest in the L1 stage. Not only a decreased autophagy activity caused by loss of function of essential autophagic genes, but also an excessive level of autophagy shortens L1 survival (Zhang *et al*, 2015; Palmisano and Meléndez, 2016).

In *C. elegans* autophagy is important also for the regulation of cell number during development, since 113 cells undergo apoptosis during embryogenesis, for lipid droplets degradation, in order to control the fat storage, for the cell fate specification of ASER/ASEL neurons and for the defense against bacterial infections (Zhang *et al*, 2015).

7.4.1 Monitoring autophagy in *C. elegans*

LGG-1 is by now the consolidated marker to monitor the autophagic process in nematodes, as its homologue LC3 is the standard choice for the evaluation of mammalian autophagy.

Fluorescent image analysis of the GFP::LGG-1 reporter or other autophagy reporters and LGG-1 lipidation analysis by western blot are the most common techniques employed for this purpose (Palmisano and Meléndez, 2016). Thanks to the GFP::LGG-1 reporter the autophagosomal pool can be visualized as GFP dots ("LC3 *puncta*") in several tissues of the nematode when autophagy is active (Kang *et al*, 2007).

At the same time, analogous cautions taken in mammalian autophagy analysis have to be considered. In fact, an increase in the number of autophagosomes does not necessarily reflect an induction of worm autophagy and it is therefore important to distinguish between induction of autophagy, increase in autophagic flux, and accumulation of autophagosomes due to inefficient or blocked autophagy (Klionsky *et al*, 2012).

A novel tandem tagged mCherry::GFP::LGG-1 reporter has been recently developed in order to evaluate the number of both autophagosomes and autolysosomes in the same body districts, with the first ones positive for both GFP and mCherry fluorescence, while the second ones emit only the mCherry signal due to quenching of GFP in the acidic environment (Chang *et al*, 2017).

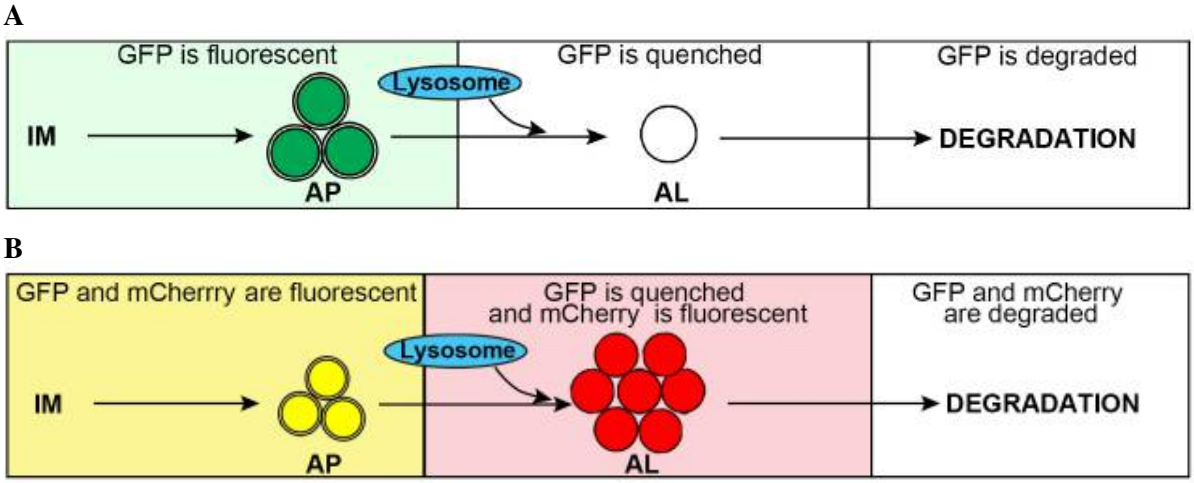

Fig. 14: The use of fluorescent reporters to evaluate autophagy in *C. elegans*. In A), a GFP::LGG-1 reporter is used to count the number of autophagosomes (AP) in nematode tissues. In autolysosomes (AL) GFP is quenched and no more visible. In B), a mCherry::GFP::LGG-1 reporter is employed to quantify both autophagosomes (yellow, both GFP and mCherry are visible) and autolysosomes (only red since GFP is quenched) in *C. elegans* (adapted from Chang *et al*, 2017).

Usually, it is useful to infer the turnover of autophagosomes in the presence and absence of lysosomal degradation. In *C. elegans*, this may be achieved by RNAi knockdown of genes with lysosomal function, such as *cup-5*, or the addition of inhibitors such as bafilomycin A1, or chloroquine, routinely used in mammalian cells. Bafilomycin A1 inhibits acidification of lysosomes and can be injected into adult wild type worms with a consequent increase in the number of autophagosomes in as few as 2 hours post-injection (Zhang *et al*, 2015; Palmisano and Meléndez, 2016).
Through the use of fluorescent reporters and pharmacological treatments to study autophagic flux it was found that, similarly to what happens in mammalian tissues, also in wild-type *C. elegans* autophagy decreases with age in the intestine, body-wall muscle, pharynx and nerve-ring neurons (Chang *et al*, 2017; Chang and Hansen, 2018).

7.5 *FOXOs* genes and the insulin pathway

The Forkhead-box (*FOX*) gene family of transcription factors in humans consists of at least 100 members that share the Forkhead domain, an approximately 100-amino acid, monomeric DNA-binding domain (Burgering, 2008; Martins *et al* 2016).
The human *FOXO* subclass consists of four members: *FOXO1*, *3*, *4* and *6*, of which *FOXO1*, *3* and *4* are ubiquitously expressed, however their levels of expression vary consistently between different cell types and organs, (Burgering, 2008; Zhang *et al*, 2011).
These factors are important for many cellular processes, controlling programs of gene expression that regulate cell metabolism, apoptosis, cell-cycle progression, oxidative stress resistance, autophagy and aging. As a consequence, genetic mutations in *FOXO* genes or altered expression of FOXO proteins are associated with diseases including diabetes and cancer or with reduced lifespan in mammals (Lee and Dong, 2017). The role of FOXOs in tumorigenesis was initially discovered by their involvement in chromosomal translocations found in human cancers (Burgering, 2008; Zhang *et al*, 2011).
Insulin and IGF pathways are essential for nutrient homeostasis as well as for growth and development. In mammals this signaling system includes three peptide hormones, insulin, IGF1 and IGF2, which are ligands for a series of receptors, among which only the IGF2 receptor acts as a signaling antagonist. Upon ligand binding, the insulin or IGF receptors autophosphorylate at tyrosine residues propagating signals through common pathways that include the insulin receptor substrate (IRS)/PI3K pathway. Once activated PI3K produces PIP3 (phosphoinositide (3,4,5)trisphosphate), recruiting the serine/threonine Akt, which in turn phosphorylates and inactivates FOXOs transcription factors. This post-translational phosphorylation of FOXOs in fact enables their interaction with 14-3-3 protein, resulting in FOXOs exclusion from nucleus and eventual ubiquitin proteasome pathway (UPP)-dependent degradation in the cytoplasm. Three of the four FOXOs (1, 3, and 4) are substrates of Akt while FOXO6 lacks some phosphorylation sites and exhibits a unique pattern of subcellular localization (Accili and Arden, 2004; Zhang *et al*, 2011). In addition to phosphorylation,

acetylation/deacetylation, methylation, or ubiquitination modifications have been shown to promote changes of subcellular localization, protein levels and transcriptional activity of FOXO factors (Martins *et al*, 2016).

7.5.1 *C. elegans* and the FOXO signaling pathway

In the last years many studies have been conducted to better elucidate FOXOs roles in cellular processes. As anticipated in paragraph 7.4, important contribution came from experiments conducted in *C. elegans* which demonstrated the involvement of FOXOs in aging and longevity patterns.
Temperature sensitive *daf-2* mutant animals are dauer-constitutive larvae at non permissive temperatures but show extended adult lifespan at lower ones. Both phenotypes require the activity of DAF-16. *daf-16* has two functions: under conditions that induce dauer, it promotes its formation, under conditions that do not favor dauer onset, it allows fertile adults carrying weak *daf-2* mutations to live twice as long as normal (Kenyon *et al*, 1993; Kimura *et al*, 1997; Lin *et al*, 1997; Gems *et al*, 1998). DAF-16 has been shown to regulate hundreds of genes in *C. elegans* including those related to stress response, antimicrobial activity, and metabolism, revealing its role as a central player of a complex network (Murphy *et al*, 2003).
It was also demonstrated that the overexpression of sirtuin gene *sir-2.1* activates DAF-16 by interacting with 14-3-3 proteins and that HSF-1, the worm heat-shock transcription factor, is required in *daf-2* mutants to extend lifespan. In fact, it acts with DAF-16 to promote longevity by activating specific longevity genes, including genes that encode small heat-shock proteins (Martins *et al*, 2016).
It has been recently shown that under stressful conditions DAF-16 and the transcription factor HLH-30 (homologue of human TFEB) translocate into the nucleus where they often form a complex and function in the same pathway to promote longevity and resistance to oxidative stress, while they oppose each other during dauer formation, with DAF-16 promoting it (Lin *et al*, 2018).

7.5.2 FOXOs and muscle homeostasis

The studies conducted in recent years have proven fundamental to unravel the role of FOXOs transcription factors in many cellular processes, and one of these is muscle homeostasis.
In skeletal muscles the two proteolytic systems, the proteasome and autophagy, are tightly regulated to ensure the removal of protein aggregates and damaged organelles. A group of genes named atrophy-related genes or atrogenes are commonly up- or downregulated in atrophying muscles during different catabolic conditions. They encode enzymes implicated in autophagy, protein degradation by the proteasome, ROS detoxification, DNA repair, mitochondrial function and energy balance pathways. The two atrogenes with the greatest induction are two muscle specific ubiquitin ligases, namely *atrogin1/MAFbx* and *MuRF1* (Milan *et al*, 2015).

It has been demonstrated that the IGF/PI3K/Akt signaling pathways regulates the expression of atrogenes in a murine muscular cell model through FoxOs transcription factors depending on nutrients availability. In presence of IGF-1 or insulin, the PI3K/Akt pathway enhances overall protein synthesis and blocks the expression of atrogenes by phosphorylating and inhibiting FoxOs, preventing so protein proteolysis. On the contrary, under anabolic conditions, like fasting, Akt is dephosphorylated enabling in this way the activation of FoxOs, which in turn stimulate the transcription of atrogenes, promoting muscle wasting (Sandri *et al*, 2004).

Moreover, it was found that in murine skeletal muscle FoxO3 regulates autophagy coordinating the proteasome with the autophagy-dependent clearance of organelles and that the *FoxO1* knockout mice shows partial protection from muscle loss during chronic kidney disease, supporting the key player role of FOXOs in muscle maintenance/loss (Mammuccari *et al*, 2007, Milan *et al*, 2015).

In an effort to explore more in detail the specific function of FOXOs transcription factors in gene regulation and muscle adaptation during catabolic conditions, Milan *et al* generated mice with adult skeletal muscle-specific deletion of *FoxO1*, *3* and *4* family members (Milan *et al*, 2015).

FoxO1, *3*, *4* null mice were indistinguishable in appearance from age-matched control mice and histological analysis of adult muscles revealed normal muscle architecture and absence of myopathic features. Then, mice were submitted to fasting to induce muscle wasting, since this is a condition known to induce nuclear translocation of FoxO members and their binding to target promoters. Interestingly, *FoxO1*, *3*, *4* null mice but not controls were spared from muscle loss after wasting, and this resulted also in muscular strength preservation, confirming that the absence of FoxO members prevents atrophy and profound weakening.

Moreover, autophagy was monitored in the same murine strains and it emerged that FoxO deletion had no effect on basal autophagic flux while after fasting the autophagy enhancement observed in control muscles was totally absent in FoxO-deficient ones, suggesting that FoxOs are essential for the induction and maintenance of a high autophagic flux, rather than for basal autophagy which appears to be under the control of mTOR.

At the same time, fasting resulted in the activation of the ubiquitin–proteasome system only in control muscles and not in *FoxO1*, *3*, *4* null ones.

As said before, the induction of atrogenes is FOXO-dependent. Since *FoxOs* deletion prevents muscle loss, the authors performed gene expression profiles of skeletal muscles derived from fed and starved control and *FoxO1*, *3*, *4* null mice to identify which genes are under FoxO regulation and these analyses revealed almost half of them require FoxO for their normal induction during fasting.

7.6 Identification and characterization of a new gene which was named *MYTHO*

When these transcriptomic profiles were later screened to find novel factors that regulate autophagy, a new gene was identified. In fact, among DNA sequences with unknown function that were upregulated during fasting but not in FoxO-deficient muscles, attention was paid to that having an ORF and for

being conserved in humans. To further reduce candidates, other adopted criteria were the presence of the autophagy-related LIR/GIR (Gabarap interacting region) domains in the coding region or the already known interaction with autophagy proteins in the published interactome.

This analysis resulted in only strong candidate, that is D230025D16Rik (mouse)/c16orf70 (human), which was named *MYTHO* (*Mytho* in mouse).

First of all, it was verified by quantitative RT-PCR that *Mytho* is induced during fasting in wild-type muscles, but not in *FoxO1*, *3*, *4* null ones. It was then found that *Mytho* expression is induced upon stress conditions, like absence of nutrients, loss of innervation or presence of tumor growth, and during aging.

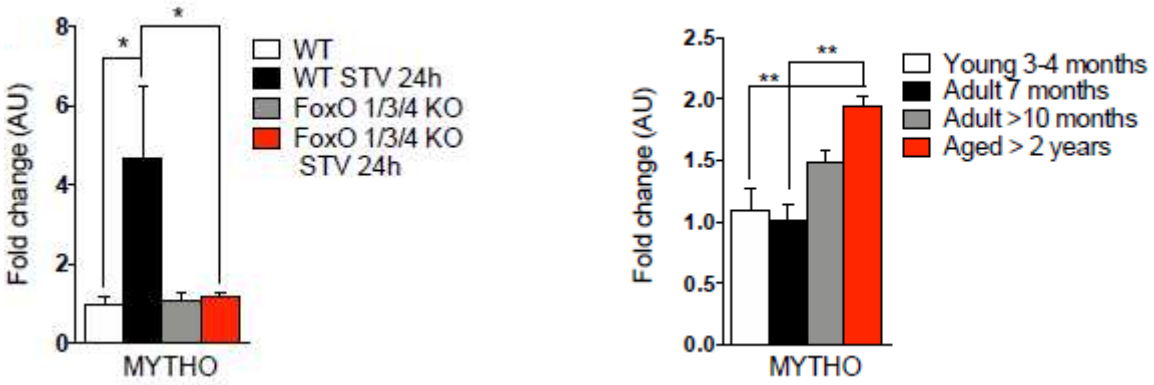

Fig. 15: On the left quantitative RT–PCR of *Mytho* from fed and 24-hour starved *tibialis anterior* of control and *FoxO1*, *3*, *4* null mice. On the right quantitative real time PCR of *Mytho* from mice of different age (3-4 months, 7 months, more than 10 months and more than 2 years old mice) (adapted from the manuscript in preparation).

The DNA sequence was then cloned in an expression vector and transfected into cells, resulting in a 48 kDa tagged protein compatible with the predicted 422 amino acids of the human protein. A polyclonal antibody was then generated against Mytho, revealing that it is expressed in different tissues, with the highest expression in lung, liver and heart.

Immunofluorescence analyses on transfected cells showed a *puncta* pattern of staining that was also present when *Mytho* was overexpressed *in vivo* in adult skeletal muscles. It was then verified that Mytho co-localized with LC3 and, although much less, with Lamp2 (a marker of lysosomes) confirming a recruitment of Mytho on autophagosomes and autophagolysosomes/lysosomes, which was also enhanced when autophagy was induced *in vivo* by the removal of nutrients.

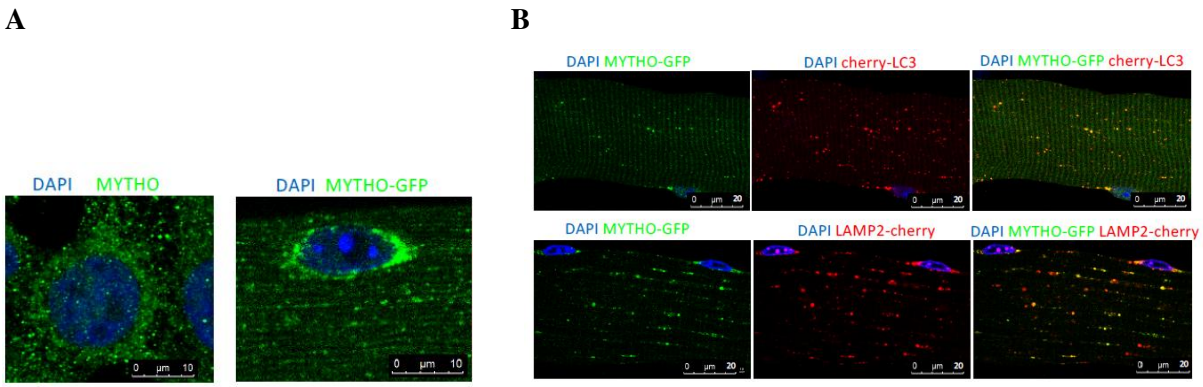

Fig. 16: A) On the left a representative images of HEK cells where endogenous MYTHO was stained using anti-C16orf70 antibody. On the right, myofibers from FDB muscles transfected with Mytho-GFP. B) Representative images showing the co-localization of Mytho-GFP and cherry-LC3 (upper panels) or Mytho-GFP with Lamp2-cherry (lower panels) in adult muscles of fed mice (adapted from the manuscript in preparation).

It was then demonstrated, blocking autophagosomes delivery to lysosomes by colchicine treatment that Mytho localization on lysosomes was a consequence of autophagosome-lysosome fusion, suggesting that Mytho requires autophagosomes for reaching lysosomes.

Then, *Mytho* was knocked down transfecting adult skeletal muscles with specific oligos and this resulted in the absence of LC3 puncta increase when nutrients were removed. Moreover, when autophagy flux was measured *in vivo* by blocking autophagosome-lysosome fusion via colchicine treatment, we found that inhibition of *Mytho* reduced basal autophagy flux and completely prevented the flux enhancement during fasting.

The results so far obtained indicate that *MYTHO* is a FOXO-dependent gene important for autophagy. Then, since many *C. elegans* RNAi models have proven that a functional autophagic process is essential for a healthy aging and for longevity (Meléndez *et al*, 2003; Kang *et al*, 2007; Meléndez and Levine, 2009), we asked ourselves what could be the functional and physiological implications in the deletion of this gene in an animal model. We chose *C. elegans* because the gene is extremely conserved across species having an orthologue also in the worm genome, that is *T01G9.2*, which displays two isoforms (a and b) differing of the three amino acids KFK, from position 21 to 23, that are present only in isoform a. As described in section I, nematodes can be easily maintained in laboratory and represent the ideal model organism to study aging (Tissenbaum, 2015).

8 Results

A comparative screening of transcriptomic profiles, obtained from skeletal muscles derived from fed and starved control and *FoxO1*, *3*, *4* null mice and performed to identify new genes that regulate autophagy, enabled to identify a new strong candidate gene, that is D230025D16Rik (mouse)/c16orf70 (human), which was named *MYTHO* (*Mytho* in mouse).

MYTHO is located on chromosome 16q22.1 and contains 19 exons; *Mytho* instead belongs to chromosome 8 and has 16 exons.

Since MYTHO possesses autophagy-related LIR/GIR domains and interacts with other autophagy-related proteins, it was investigated its involvement in the autophagic process.

8.1 Generation of a C2C12 *Mytho* KO cell line by CRISPR/Cas9 technology

To better elucidate *MYTHO*'s involvement in the autophagic process, we decided to generate a murine KO cell line devoid of this gene. We chose the myogenic C2C12 cell line (Blau *et al*, 1983), consisting of undifferentiated myoblasts that differentiate and fuse in large multinucleated myotubes if cultivated under low serum conditions, in order to use a cellular model as close as possible to skeletal muscle, where the role of *MYTHO* was originally investigated.

To obtain a *Mytho* KO C2C12 line, cells were co-transfected with Transedit CRISPR all-in-one lentiviral expression vectors containing two different CRISPR target sequences of *Mytho*, addressing exon 1 and exon 2 respectively, and in parallel also with a non-targeting control gRNA (Fig. 17 A).

Single clones were isolated and after their growth and expansion, genomic DNA was extracted and fragments encompassing the CRISPR target sequences were amplified by PCR (See Materials and methods, paragraph 3.6 for further details, Fig. 17 B). PCR reactions were then sequenced and 4 clones harboring different mutations (Fig. 17 C, D, E) were mixed to reduce the consequences of possible CRISPR/Cas9-mediated off-target effects.

A

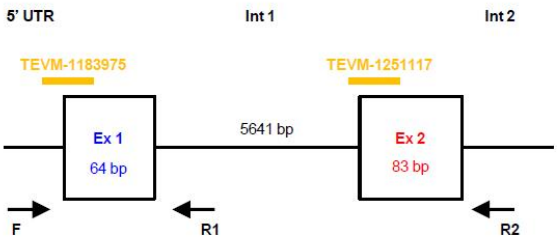

B

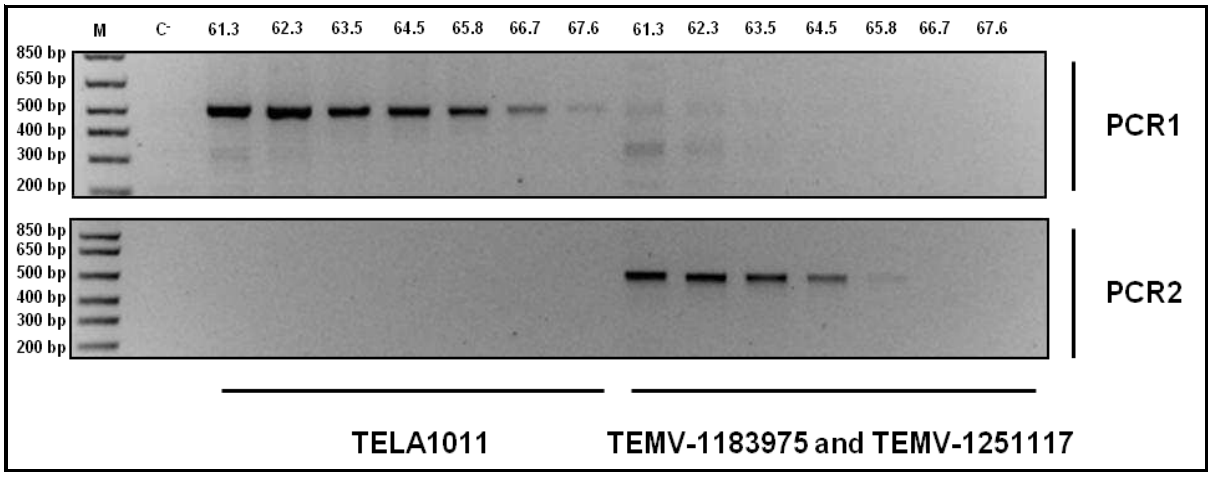
M
C-
61.3
62.3
63.5
64.5
65.8
66.7
67.6
61.3
62.3
63.5
64.5
65.8
66.7
67.6
850 bp
650 bp
500 bp
400 bp
300 bp
200 bp
PCR1
PCR2
TELA1011
TEMV-1183975 and TEMV-1251117

C

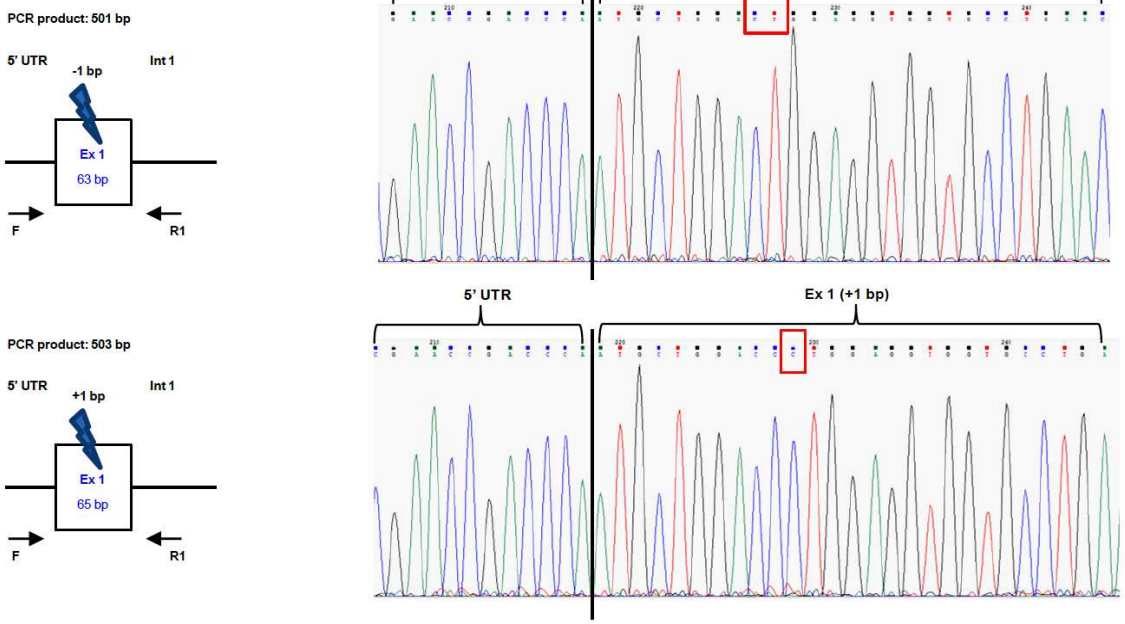
PCR product: 501 bp
5' UTR
Int 1
-1 bp
Ex 1
63 bp
F
R1
5' UTR
Ex 1 (-1 bp)
PCR product: 503 bp
5' UTR
Int 1
+1 bp
Ex 1
65 bp
F
R1
5' UTR
Ex 1 (+1 bp)

D

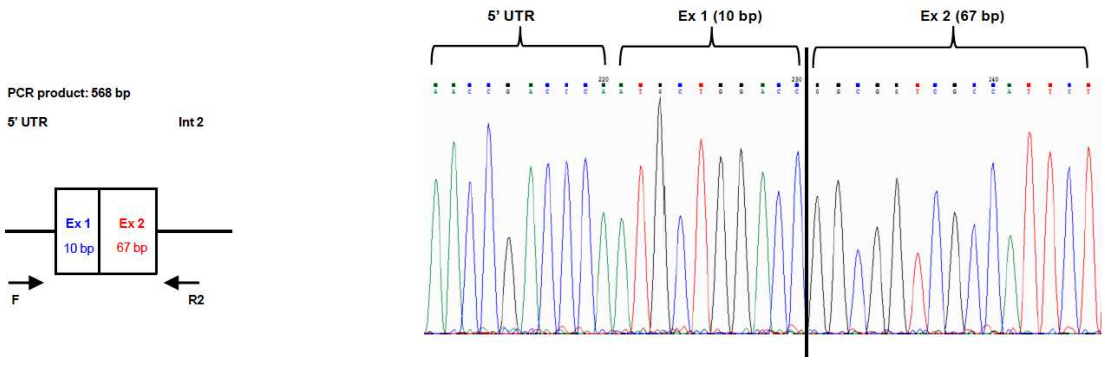
PCR product: 568 bp
5' UTR
Int 2
Ex 1
10 bp
Ex 2
67 bp
F
R2
5' UTR
Ex 1 (10 bp)
Ex 2 (67 bp)

E

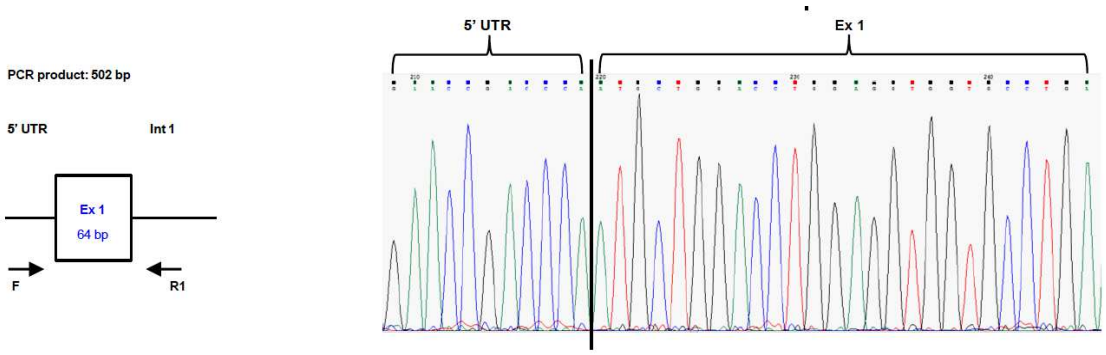

Fig. 17: Generation of a *Mytho* KO C2C12 cell line A) A schematic representation of the 5' portion of *Mytho* highlighting the two different CRISPR target sequences (TEVM-1183975 and TEVM-1251117, Transomic Technology) targeting exon 1 and 2 of *Mytho*, respectively. The arrows indicate forward (F) and reverse (R1 and R2) primers used for PCR genotyping. B) 1% agarose gel images showing both PCR reactions performed at different primer melting temperatures (indicated above gels). In particular two clones, the first obtained after cell transfection with a non-targeting control gRNA (TELA1011, Transomic Technology) and the second after cell co-transfection with TEVM-1183975 and TEVM-1251117 gRNA were used to set up the PCR conditions. A gradient was performed to eliminate aspecific products and for the first PCR reaction 64.5 °C was chosen as the melting temperature, while for the second one it was set at 61.3 °C. M, molecular marker (1 Kb Plus, ThermoFisher Scientific). C, D) Representative isolated cell clones harboring frameshift mutations: deletion (C, above) or insertion (C, below) of 1 base pair in exon 1, or a large deletion (D) between the target sequences of exon 1 and 2. E) A cell clone obtained transfecting cells with the control gRNA TELA1011. In C), D) and E) a schematic representation of genome editing outcome is depicted on the left, while Sanger sequencing of the PCR reaction performed for clone genotyping is shown on the right (adapted from the manuscript in preparation).

The experiments with *Mytho* KO C2C12 cell line were conducted in collaboration with the group of Prof. Marco Sandri. First of all, the absence of Mytho protein was verified by Western blot, using an anti C16orf70 antibody (Abcam), that also recognizes the murine homologue of MYTHO (Fig. 18 A). Then, *Mytho* KO C2C12 cells and control ones were treated with chloroquine to analyze the autophagic flux. The level of lipidated LC3 was measured by Western blot and the number of LC3 puncta was counted after the transfection of cells with a plasmid carrying mCherry tagged-LC3 (Fig. 18 A, B). The resulting reduced level of basal autophagy in absence of Mytho confirmed its importance in this cellular process. Conversely, overexpression of *Mytho* in cells was sufficient to increase autophagosome numbers and autophagy flux.

A

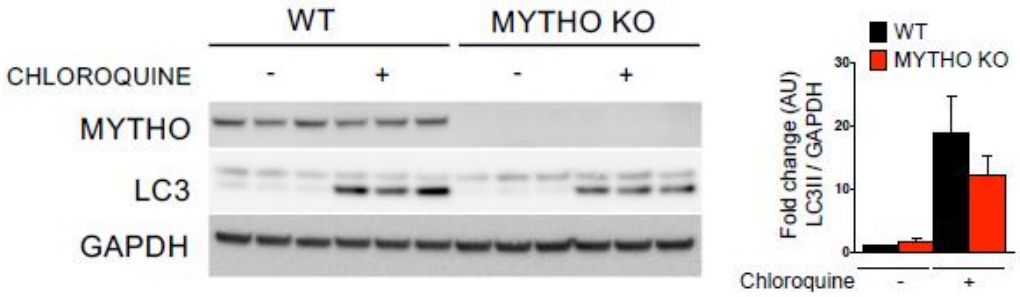

B

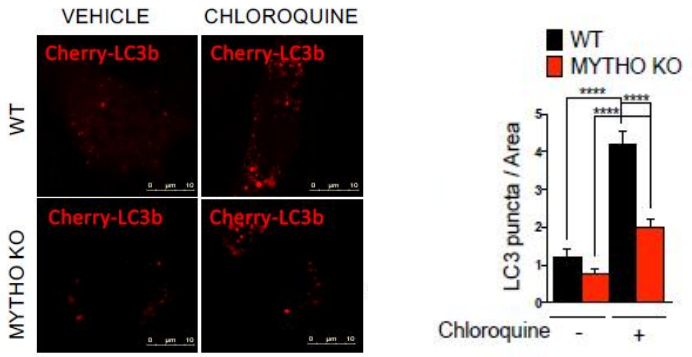

Fig. 18: A) C2C12 cell line in which *Mytho* gene was deleted by CRISPR/Cas9 technology. Control and *Mytho* KO cells were treated or not with chloroquine for autophagy flux measurements. Homogenates were loaded and analysed for LC3 lipidation (on the left). Quantification of LC3-II band on GAPDH is depicted on the right. B) Representative images of C2C12 KO and control cells transfected with Cherry-LC3 and treated with chloroquine or vehicle. The graph on the right shows the quantification of LC3 *puncta* in the different conditions (adapted from the manuscript in preparation).

8.2 Generation of a multicellular model devoid of *MYTHO*

The results so far obtained indicate that *MYTHO* is a FOXO-dependent gene important for autophagy. Then, since many *C. elegans* RNAi models have proven that a functional autophagic process is essential for a healthy aging and for longevity (Meléndez *et al*, 2003; Kang *et al*, 2007; Meléndez and Levine, 2009), we asked ourselves what could be the functional and physiological consequences of silencing this gene in a multicellular animal model. We chose *C. elegans* because the gene is extremely conserved across species having an orthologue also in the worm genome, that is *T01G9.2*, which is localized on chromosome 1, contains 12 exons and displays two isoforms (a and b) differing of the three amino acids KFK, from position 21 to 23, that are present only in isoform a.

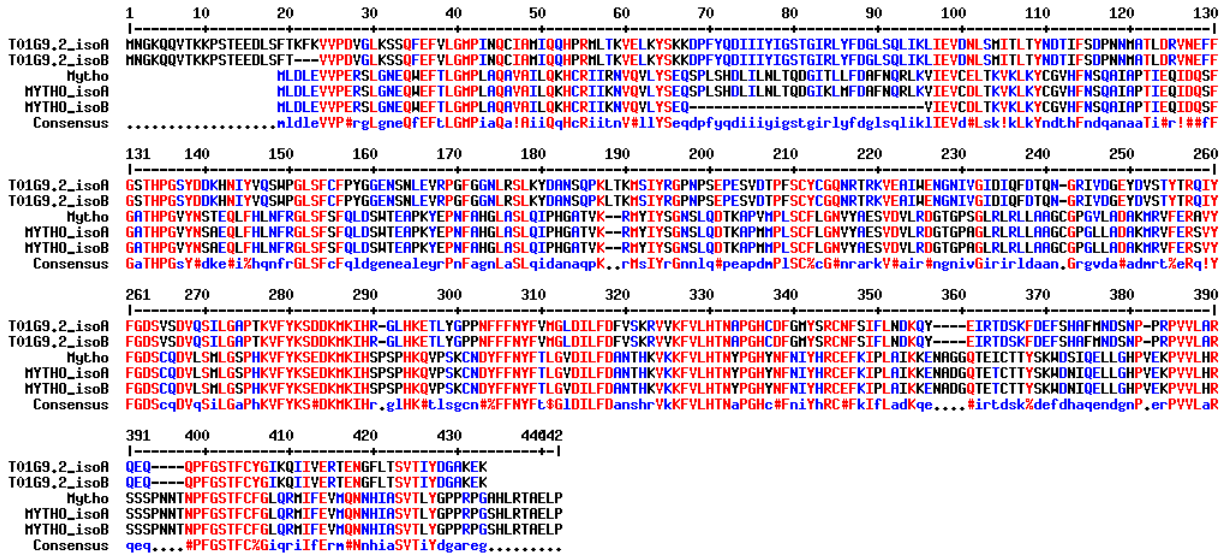

Fig. 19: A Multalin alignment (http://multalin.toulouse.inra.fr/multalin/) of protein sequences of MYTHO from different species: *Caenorhabditis elegans* isoform a (NCBI Reference Sequence: NP_740894.1), and b (NP_492252.1) which differ of the three amino acids KFK, from position 21 to 23, that are present only in isoform a, which is 422 amino acid-long; *Mus musculus* (NP_663579.2) that has a 422 amino acids-long protein; *Homo sapiens* isoform a (NP_001307469.1) which is 422 amino acids long and isoform b (NP_001307472.1) which has the same N- and C-termini of isoform a but it is shorter (394 amino acids). As highlighted by the red residues, regions of high conservation are concentrated in the second half of the alignment.

8.2.1 Knockdown of *T01G9.2* by RNA interference

To obtain a knockdown model of *T01G9.2* in *C. elegans*, the gene coding sequence (both isoform a and b, differing of the first nine nucleotides of exon 2 that are present only in isoforms a, see table 4 for primer sequences) was cloned in the pL4440 plasmid and the *rrf-3* worm strain was fed with HT115(DE3) bacteria transformed with the constructs and IPTG was added to the culture medium (see Table 3). The same negative (empty vector) and positive (pLT61 vector) controls were included in the experiments and three generations were waited before starting with the phenotypic characterization.

Worms silenced for *T01G9.2* developed normally and had not any evident anomaly in behavior. A pilot brood size assay (results not shown) didn't reveal any alteration in the timing of egg deposition and in the progeny number in silenced worms compared with pL4440 fed ones.

Since *Mytho* is a FoxO-dependent gene which seems to have an important role in muscle homeostasis and the worm orthologue is also expressed in body wall muscle cells (Meissner *et al*, 2011), we decided to analyze worm movements, focusing on easy measurable parameters, like the number of body bends, the frequency of reversals and the duration of stillness periods. To do so, we seeded single L4 worms on RNAi plates, kept them at 20 °C until the following day when we recorded and quantified movements of each worm (Fig. 20 A). No difference could be appreciated in body bends and in duration of stillness periods, however worms silenced for *T01G9.2* showed a lower frequency of reversals compared to controls.

Since the data obtained so far indicate that Mytho is important for autophagy and given that also in *C. elegans* starvation promotes autophagy induction in all tissues (Chapin *et al*, 2015), we submitted worm larvae silenced for *T01G9.2* and their relative controls to prolonged periods of starvation and measured how many of them survived two days after having been seeded on fresh RNAi plates (Fig. 20 B), but even after 7 days of starvation the survival fraction was decreased in a similar way in controls and silenced worms.

We then repeated the locomotion analysis after having kept worms at 25 °C for one day after seeding, in order to evidence possible temperature-dependent mechanisms. Every animal was scored in two separate intervals of 30 seconds each and the same parameters as before were considered (Fig. 20 C). No clear differences were perceivable between silenced worms and control ones, apart from a not significant lower trend in the number of body bends in worms devoid of *T01G9.2*.

A

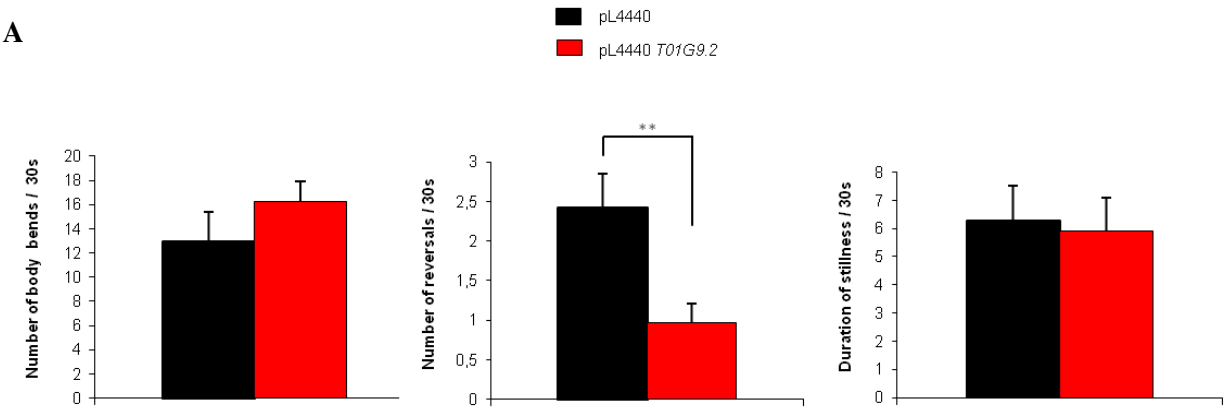

B

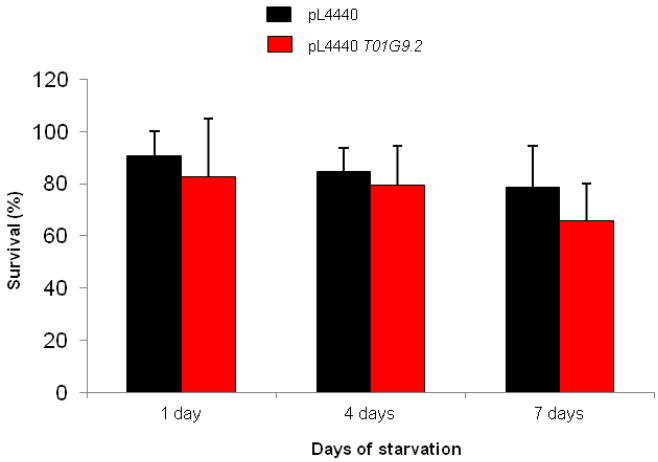

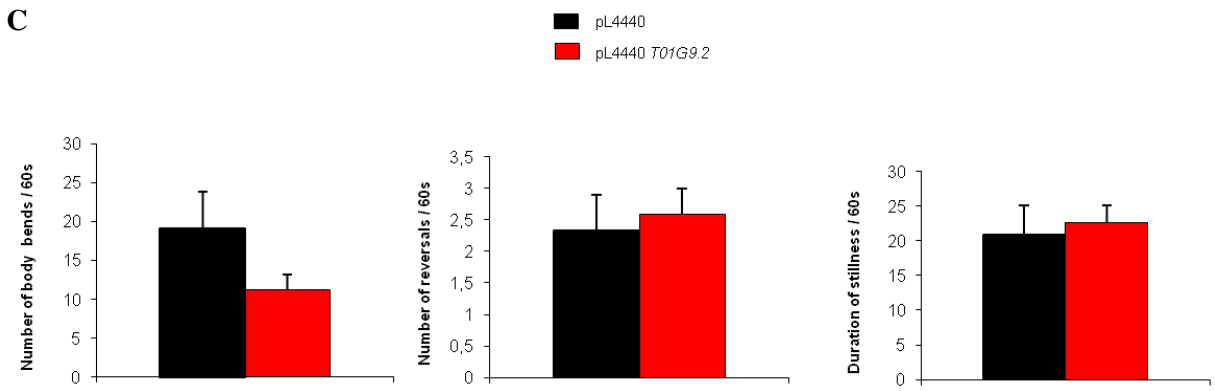

Fig. 20: A) Locomotion analysis in worms silenced for *T01G9.2* and their relative controls. Briefly, L4 worms were singularly seeded on RNAi plates, maintained at 20 °C and the following day their movements were measured for 30 seconds, counting the number of body bends, the frequency of reversals and the duration of stillness periods. The graph represents the mean of three independent experiments. The bars indicate the standard error of the mean and the results were compared using the unequal variance *t*-test. N = 14 for pL4440 controls and N =26 for pL4440 *T01G9.2*. **, p< 0.01. B) Survival fraction after a long period of starvation. Following a bleaching treatment, L1 larvae of each population were kept in M9 buffer at 20°C for the indicated time points. After 48 hours on fresh RNAi plates at 20 °C, the ability of worms to recover from starvation and survive was calculated as a ratio of worms alive to the total number of animals transferred to the plate. The experiment was performed two times and the bars represent the standard error of the mean. The results were compared using the unequal variance *t*-test. C) Locomotion analysis performed as in A), however worms were kept at 25 °C for one day before the analysis and every animal was scored in two separate intervals of 30 seconds each. The graph represents the mean of two independent experiments. The bars indicate the standard error of the mean and the results were compared using the unequal variance *t*-test. N = 6 for pL4440 controls and N =12 for pL4440 *T01G9.2*.

8.2.2 Deletion of *T01G9.2* by CRIPR/Cas9 genome editing

Considering the lack of a clearcut phenotype after RNAi, we decided to generate a KO strain for *T01G9.2* by CRISPR/Cas9 technology, in order to investigate the effects of a total gene ablation in the worm model.

We designed a crRNA targeting exon 1 of *T01G9.2* and a DNA repair template that introduces a stop codon at amino acid 10 of the protein, in order to knock out both isoforms (which differ of the first three amino acids of exon 2 that are present only in isoforms a, see table 5 for crRNA and ssODN sequences).

First of all, we verified the efficacy of the chosen crRNA with an *in vitro* digestion of the target locus with the purified Cas9 protein (Fig. 21 A), then worm injections were performed in collaboration with Dr. Martinelli at the Istituto Superiore di Sanità in Roma, following a protocol modified from Paix *et al*, 2015. We finally obtained four different strains, but all of them carried a different genomic edit from the expected one. In particular three of them had a frameshift mutation (exon 1 loses the final 8 base pairs with the concomitant insertion (Ins) of 63 nucleotides deriving from the *T01G9.2* KO ssODN), predicted to lead to the formation of a premature stop codon at position 36, *i.e.*, *T01G9.2*(*pan8*[S18Tfs*19]) *I*; *T01G9.2*(*pan9*[S18Tfs*19]) *I*; *T01G9.2*(*pan10*[S18Tfs*19]) *I*. The

fourth knockout strain carried a different frameshift mutation predicted to lead to the formation of a premature stop codon at position 22, *i.e.*, *T01G9.2*(*pan7*[T20Ffs*3]) *I*.

Mytho KO animals from strains *T01G9.2*(*pan8*[S18Tfs*19]) *I*, *T01G9.2*(*pan9*[S18Tfs*19]) *I* and *T01G9.2*(*pan10*[S18Tfs*19]) *I* were genotyped performing a PCR reaction that amplifies the region between primers located in the 5' UTR and exon 2 (Fig. 21 B, see table 4), giving a product of 580 bp, instead of 525 bp. PCR products were also sequenced to confirm the insertion (Fig. 21 C).

Since an antibody against T01G9.2 is not available, we extracted total RNA from *T01G9.2*(*pan8*[S18Tfs*19]) *I* and *T01G9.2*(*pan9*[S18Tfs*19]) *I* strains and performed RT-PCR to ensure that no wild-type transcript was produced. Indeed, in *Mytho* KO nematodes we found only aberrant products at higher molecular weights that can produce a truncated protein with a stop codon after 35 aminoacids, as predicted (Fig. 21 D). These two strains, simply referred to as *Mytho* KO onwards, were outcrossed to remove possible off-target mutations and used for subsequent phenotypic analyses.

A

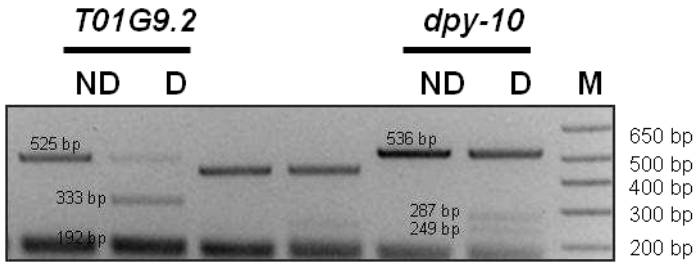

B

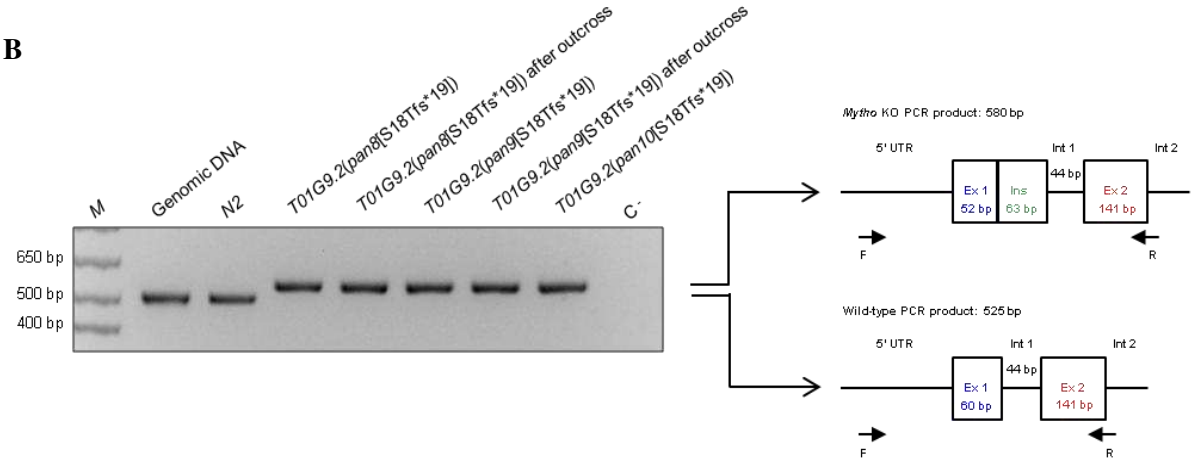

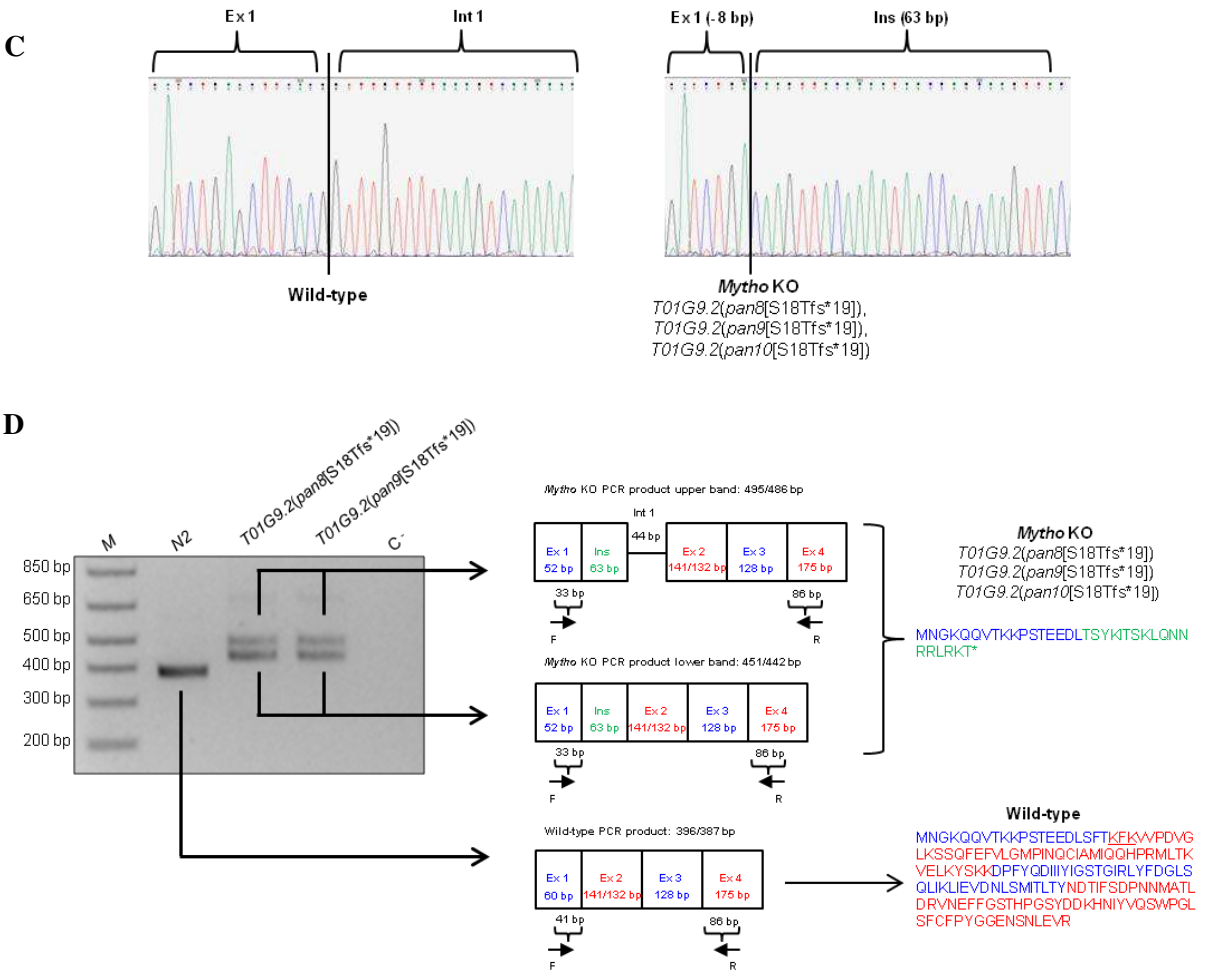

Fig. 21: A) *In vitro* digestion of *T01G9.2* and *dpy-10* CRISPR target loci with the purified Cas9 protein. After genomic DNA extraction from worms, a PCR reaction was performed using forward and reverse primers that encompass the genomic region to be edited and then incubated with the crRNA and Cas9 protein. A negative control was included in each reaction, consisting of the mix devoid of Cas9. The digestions were then run on a 2% agarose gel; M: 1 Kb plus molecular marker.
B) Genotyping of *Mytho* KO strains. On the left, an illustrative agarose gel image showing genotyping of strains *T01G9.2*(*pan8*[S18Tfs*19]) and *T01G9.2*(*pan9*[S18Tfs*19]), before and after outcrosses, and *T01G9.2*(*pan10*[S18Tfs*19]). On the right, a schematic representation of the 5' portion of *T01G9.2* showing the predictive genome editing outcome. In particular, exon 1 loses the final 8 base pairs with the concomitant insertion (Ins) of 63 nucleotides (nt) deriving from the *T01G9.2* KO ssODN. The arrows indicate forward (F) and reverse (R) primers used for PCR genotyping. The resulting *Mytho* KO PCR product is 580 bp, compared to the 525 bp long wild-type one. C) Sanger sequencing of *Mytho* wild-type and KO PCR products. On the left, the wild-type *T01G9.2* sequence pointing out exon1 - intron1 junction, while on the right, the same gene portion harboring the 63 nt insertion in *Mytho* KO strains. D) RT-PCR analysis of *Mytho* KO strains. After RNA extraction and cDNA synthesis, a PCR reaction was performed using forward (F) and reverse (R) primers designed on exon 1 and 4 of *T01G9.2*, respectively. PCR products were run on a 2% agarose gel (shown on the left) and bands were then excised from gel and sequenced. The results are depicted on the right and, as highlighted in the scheme, both isoforms of *T01G9.2*, differing of the first nine nucleotides of exon 2, are present in total worm RNA extracts. The resulting amino acidic sequences are shown next: the predicted protein sequence in *T01G9.2*(*pan8*[S18Tfs*19]), *T01G9.2*(*pan9*[S18Tfs*19]), and *T01G9.2*(*pan10*[S18Tfs*19]) strains displays a stop codon after 35 amino acids; the wild-type Mytho protein (the *N*-terminal portion up to amino acid 168), carrying or not amino acids KFK (position 21-23) is shown below (adapted from the manuscript in preparation).

8.2.2.1 Phenotypic characterization of *Mytho* KO worms

The advantage of CRISPR/Cas9-mediated genome editing is the possibility to genetically ablate *T01G9.2* and obtain a worm model knockout for this gene. Once *Mytho* KO strains were backcrossed, we started their phenotypic characterization. Worms developed normally, meaning that the ablation of *T01G9.2* has not lethal effects. By visual inspection of plates, no evident morphological differences were perceivable in *Mytho* KO worms compared to controls. A pilot brood size assay didn't show any overt alteration in egg laying timing and progeny number (results not shown).

In order to investigate the effects of gene knockout in locomotion and in survival capability after a long period of starvation, we performed preliminary experiments assaying a small number of *Mytho* KO worms, in a similar way to what we did with RNAi treated worms.

Therefore, we seeded single L4 worms on NGM plates with OP50 bacteria, kept them at 20 °C until the following day when we recorded and quantified movements of every worm. Unexpectedly, *Mytho* KO worms didn't show any impairment in body bends number, frequency of reversals or in duration of stillness periods (Fig. 22 A).

We decided to submit worms to stress conditions as starvation or a higher culture temperature.

In the first case synchronized L1 *Mytho* KO larvae and their relative controls were kept under prolonged periods of starvation and two days after the seeding on fresh NGM plates with OP50 *E. coli* their survival was measured (Fig. 22 B). The results confirmed what was obtained with worms silenced by RNAi: although a tendency was observed towards a reduction in survival after 7 and 9 days of starvation in *Mytho* KO worms compared to controls, no significant differences could be noticed between genotypes.

Locomotion was also investigated after the maintenance of worms at 25 °C for one day, considering the same parameters as before (Fig. 22 C). No significant differences were found between *Mytho* KO worms and control ones, although trends were noticed towards the reduction in the number of body bends and the increase of reversals frequency and of stillness periods duration in worms devoid of *T01G9.2*.

A

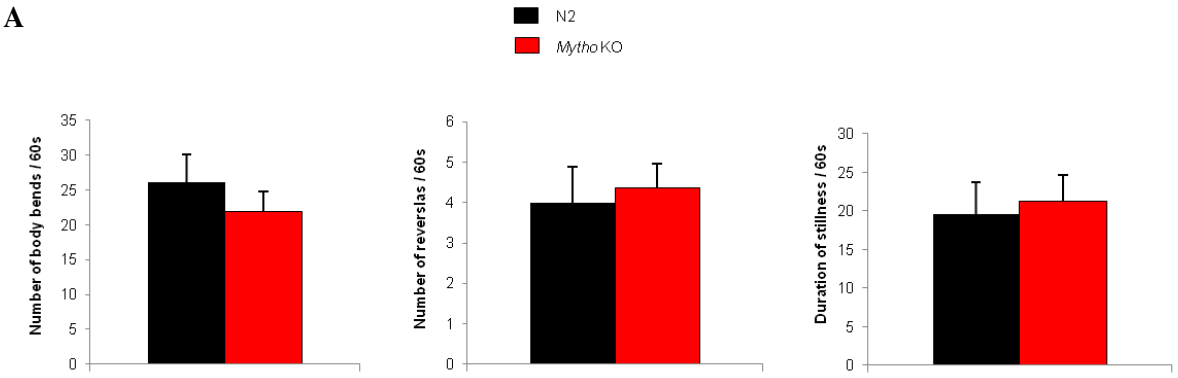

B

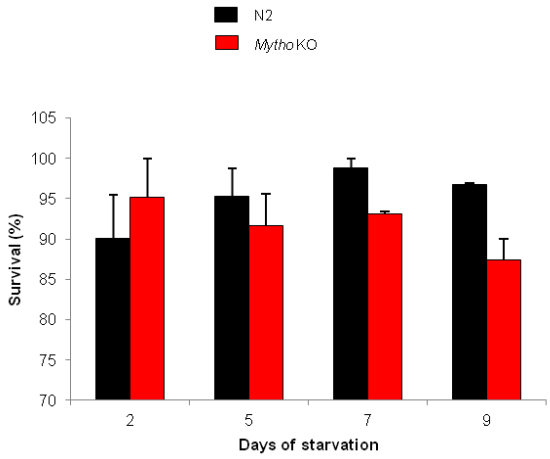

C

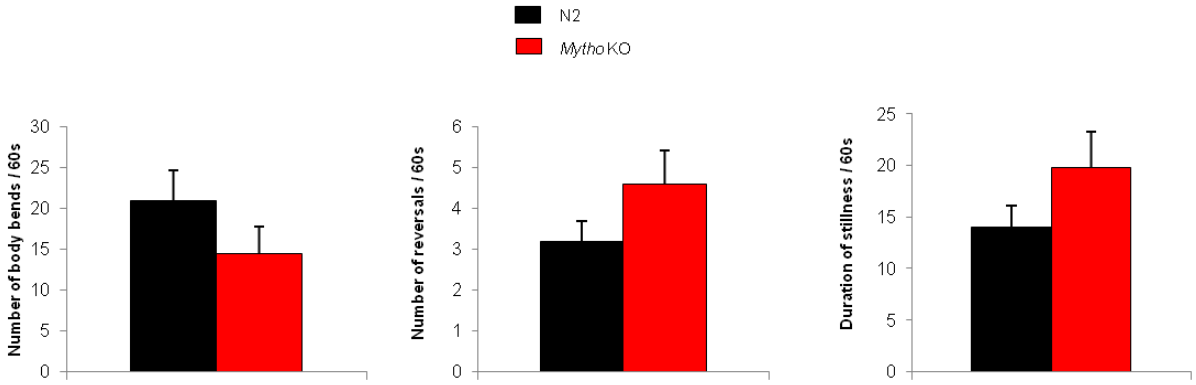

Fig. 22: A) Locomotion analysis in *Mytho* KO worms and their relative controls. Briefly, L4 worms were singularly seeded on NGM plates with OP50 bacteria, maintained at 20 °C and the following day their movements were measured during two separate intervals of 30 seconds each. The number of body bends, the frequency of reversals and the duration of stillness periods were counted and the graph represents the mean of two independent experiments. The bars indicate the standard error of the mean and the results were compared using the unequal variance *t*-test. N = 10 for N2 and N =8 for *Mytho* KO worms. B) Survival fraction after a long period of starvation. Following a bleaching treatment L1 larvae of each population were kept in M9 buffer at 20 °C for the indicated time points and after that they were transferred on fresh NGM plates with OP50 bacteria. After 48 hours at 20 °C the ability of worms to recover from starvation and survive was calculated as a ratio of worms alive to the total number of animals transferred to the plate. The experiment was performed two times and the bars represent the standard error of the mean. The results were compared using the unequal variance *t*-test. C) Locomotion analysis performed as in A), however worms were kept at 25 °C for one day before proceeding to the analysis. The experiment was performed once. The bars represent the standard error of the mean and the results were compared using the unequal variance *t*-test. N = 5 for N2 and *Mytho* KO worms.

Since many studies conducted in *C. elegans* proved fundamental to unveil the role of FOXOs in pro-survival and longevity pathways, we decided to investigate the effect of *T01G9.2* ablation on worm aging. To do so, we crossed *Mytho* KO worms with *fer-15* animals, that have a temperature-sensitive defect in spermatogenesis and are consequently sterile at 25 °C (Hirsch *et al*, 1976). We identified *Mytho* KO worms through a PCR reaction performed with primers located on the 5' UTR and exon 2 (see Fig. 21 B); then those worms that produced no or very few progeny at 25°C were selected.

150 L4 *fer-15* and *fer-15/Mytho* KO hermaphrodites were seeded on agar plates and used as time zero for the analysis. Plates were maintained at 25 °C for the entire duration of experiments and monitored every day. Interestingly *fer-15/Mytho* KO nematodes showed a reduced lifespan compared to controls and the difference became perceivable after 6 days from seeding, when some worms devoid of *Mytho* started to precociously die (Fig. 23 A).

Moreover, performing lifespan experiments we noticed that *Mytho* KO worms appeared older than controls and became lethargic after 4-5 days from the seeding. Therefore, we repeated the locomotion analysis performed on worms silenced for *T01G9.2* by RNAi or on *Mytho* KO animals one day after the seeding, but worms were kept at 25 °C for 5 days before the analysis. The number of assayed worms was comparable to those tested in similar experiments that were previously performed (Sawin *et al*, 2000).

We observed a significant decrease in body bends and reversals number and an evident increase in stillness periods duration in *Mytho* KO worms compared to control ones (Fig 23 B).

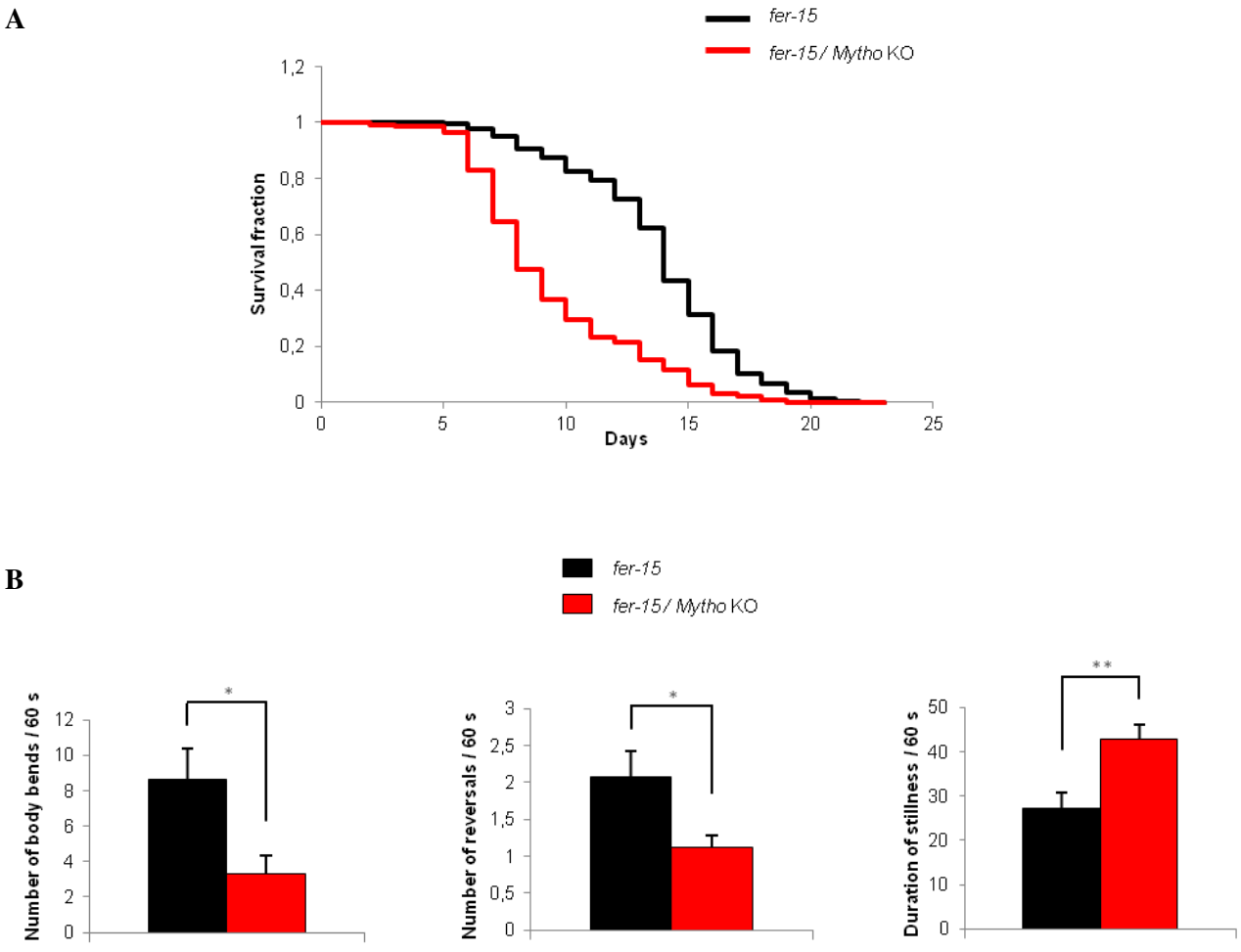

Fig. 23: A) Lifespan measurements. Survival curves of *fer-15* nematodes incubated at 25 °C were compared with that of *fer-15/Mytho* KO worms maintained at the same conditions. Curves were compared using the log rank test and the lifespan plots represent the composite of the three independent experiments performed. The difference is statistically significant with p

<0.0001. N = 150 for each genotype and experiment. B) Locomotion analysis in *fer-15/Mytho* KO animals and their relative controls. L4 worms were singularly seeded on NGM plates with OP50 bacteria, maintained at 25 °C for 5 days before proceeding to the analysis. The number of body bends, the frequency of reversals and the duration of stillness periods were counted during two separate intervals of 30 seconds each and the graph represents the mean of three independent experiments. The bars represent the standard error of the mean and the results were compared using the unequal variance *t*-test. N= 15 for *fer-15* worms and N= 17 for *fer-15/Mytho* KO worms. *, p< 0.05, **, p< 0.01 (adapted from the manuscript in preparation).

8.2.2.2 Investigation of autophagy in *Mytho* KO worms

Given the results obtained in cellular and murine models lacking *Mytho* that strongly suggest a role of this novel gene in autophagy, we investigated this possibility also in *C. elegans*, in light of previous results that indicate that a functional autophagic process is essential for a healthy aging and longevity (Meléndez *et al*, 2003; Kang *et al*, 2007; Meléndez and Levine, 2009).

LGG-1 is the worm orthologue of mammalian LC3 and fluorescent image analysis of the GFP::LGG-1 reporter by counting GFP positive *punctae* and LGG-1 lipidation analysis by western blot are the most common techniques employed to assay autophagy in nematodes (Palmisano and Meléndez, 2016).

So, we crossed *Mytho* KO animals with the strain carrying LGG-1 fused with GFP (DA2123 strain): *Mytho* KO worms were identified as previously (see Fig. 21 B); GFP worms were recognized thanks to the roller phenotype conferred by the *rol-6(su1006)* allele in the transgene (Kang *et al*, 2007) and adult worms of both genotypes were analyzed counting the number of GFP *punctae* (so of autophagosomes) in the posterior bulb of the pharynx (Fig. 24 A). We analyzed 20 or more worms per genotype as previously published (Chang *et al*, 2017) and we found that the *punctae* number is significantly decreased in *Mytho* KO animals compared to controls, suggesting an impairment of the autophagic process, at least in this body district, in absence of *Mytho* (Fig. 24 B, C).

A

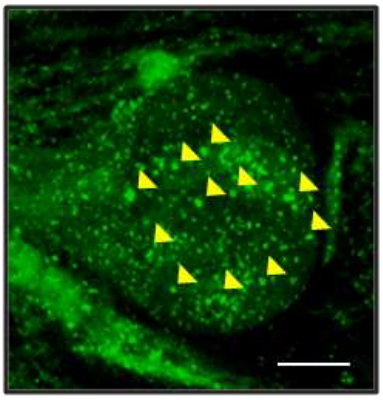

B

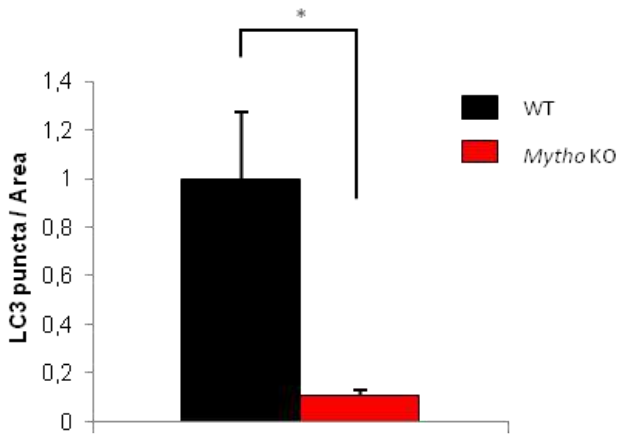

C

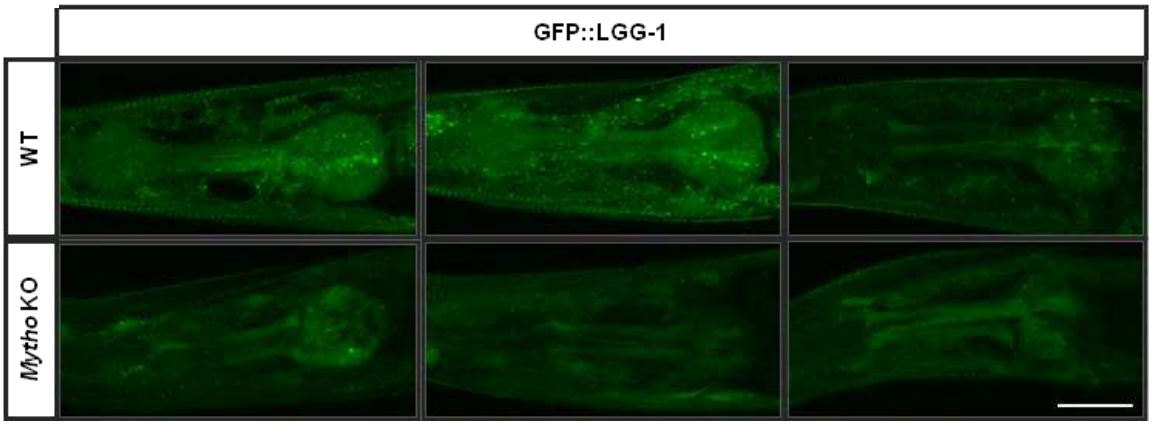

Fig. 24: Autophagosomal pool size analysis by confocal microscopy A) A detail representing the posterior bulb of pharynx of a worm carrying LGG-1 fused with GFP (DA2123 strain), that was chosen as the body district where GFP::LGG-1 positive *punctae* (yellow arrowheads) were counted. Scale bar 10 µm. B) *Mytho* KO animals were crossed with worms from strain DA2123, which was used as the control in the experiment. The sections in which the posterior bulb of the pharynx was visible were acquired as Z-stacks and images were then collected and analyzed counting GFP::LGG-1 positive *punctae* in the posterior bulb of the pharynx manually. The *punctae* number per μm^2 was then calculated and the graph corresponds to the mean of two different experiments, where wild-type worms were considered as 1 and *Mytho* KO ones represented as a fraction compared to it. The results of WT and KO autophagic pool sizes were compared using the unequal variance *t*-test and the bars indicate the standard error of the mean. N = 26 for WT worms and N = 20 for *Mytho* KO worms. *, $p < 0.05$. C) Representative images of three pharynxes from WT and KO adult worms. Scale bar, 25 µm (adapted from the manuscript in preparation).

8.2.2.3 Investigation of *Mytho* involvement in stress response pathways

FOXO transcription factors are involved in many cellular processes and in the response against several types of stress (Lee and Dong, 2017) and this cellular defense system is conserved also in *C. elegans* where it is orchestrated by the only *FOXO* homologue, that is *daf-16*, in cooperation with others factors that selectively intervene depending on the harmful condition (Martins *et al*, 2016; Lin *et al*, 2018).

To investigate the role of *T01G9.2* as FOXO-dependent gene, oxidative stress was induced by exposing *Mytho* KO and wild-type worms to paraquat (PQ, methyl viologen), which interferes with the electron transport chain to produce ROS (Possik and Pause, 2015). Adult worms for each genotype were incubated with 200 mM PQ at 20°C with constant agitation and survival was measured every hour during the incubation for 12 hours. As shown in Fig. 25 A, no difference could be appreciated between wild-type and *Mytho* KO worms.

We also tried a heat stress experiment, similarly to what was reported by Lithgow *et al* (longitudinal assay). 5-days adult wild-type and *Mytho* KO hermaphrodite*s* were seeded on NGM plates and submitted to a heat-shock at 35 °C. Worm viability was measured at the indicated time points,

however, also in this case, no difference could be observed in the survival fractions of the analyzed genotypes (Fig. 25 B).

Since performing lifespan assays we noticed a premature aging phenotype in *Mytho* KO worms, we decided to analyze the capability of stress resistance exposing nematodes to the harmful agent at the precise moment when the precocious aging becomes evident. So, L4 *fer-15* and *fer-15/Mytho* KO worms were seeded on NGM plates, maintained at 25 °C for 5 days and then incubated in M9 buffer supplemented with PQ at the final concentration of 125 mM with constant agitation at 25 °C for 1 hour. Nematodes were washed in M9 buffer and transferred to fresh NGM plates at 25 °C for the indicated time points at which survival was calculated. *fer-15/Mytho* KO worms survival was significantly decreased compared to relative controls (Fig. 25 C) and the difference between genotypes was more pronounced with respect to that observed at the same time point during the lifespan assay. Finally, since it is known that the addition of glucose to the culture medium decreases wild-type worms longevity (Schulz *et al*, 2007; Lee *et al*, 2009), we also performed a pilot test measuring the lifespan of *fer-15* and *fer-15/Mytho* KO nematodes at 25 °C on NGM plates with 1% glucose. As expected, we evidenced a viability decrease of *fer-15* worms grown in presence of glucose (grey line) compared to those cultivated in absence of it (black line). Surprisingly, lifespan of *fer-15/Mytho* KO nematodes was improved in presence of glucose in culture medium (pink line), and the final result is that viability of *fer-15* and *fer-15/Mytho* KO worms is very similar in presence of glucose (Fig. 25 D).

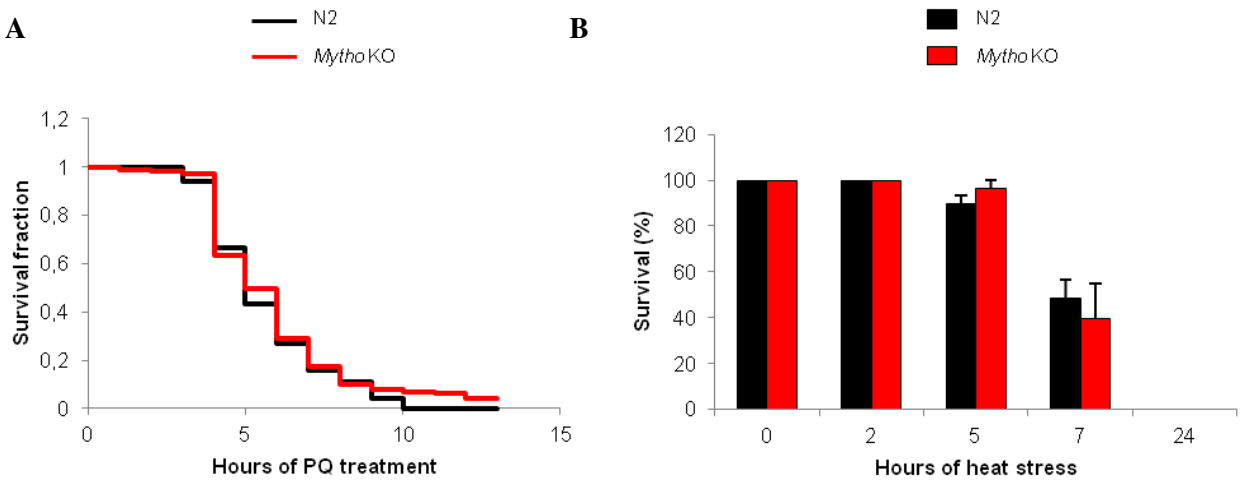

C

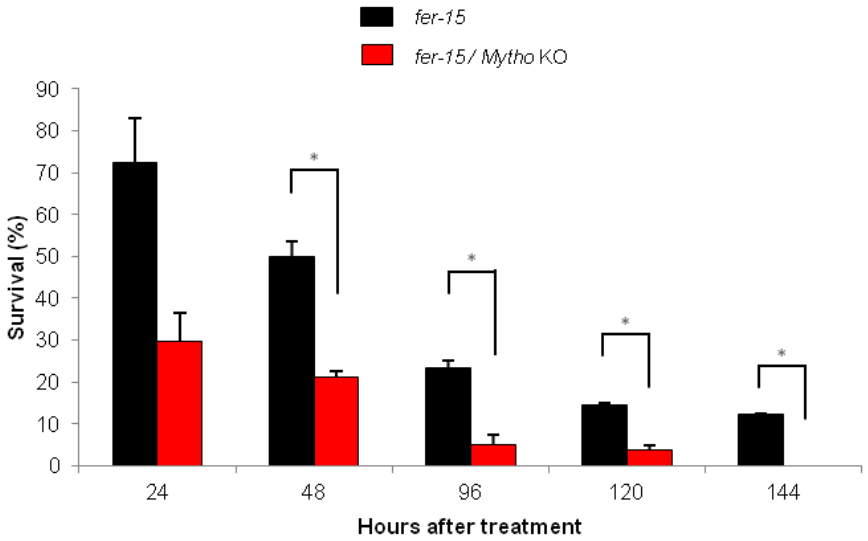

D

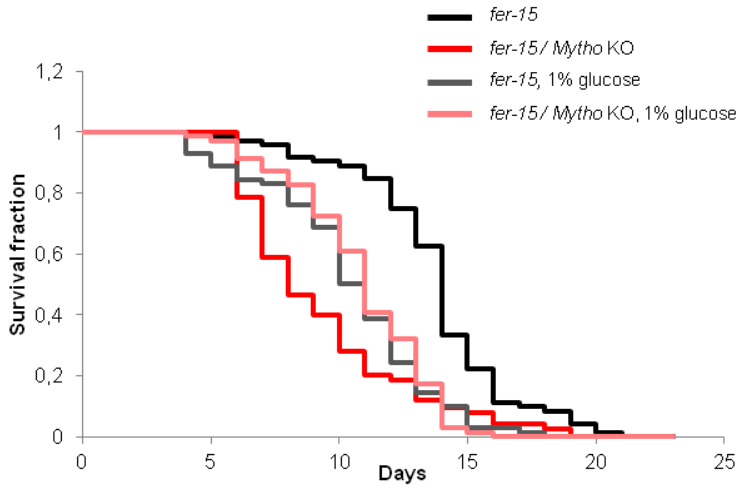

	p-value
fer-15 ND – *fer-15/Mytho* KO ND	p< 0.0001
fer-15 ND – *fer-15* GLU	p< 0.0001
fer-15 ND – *fer-15/Mytho* KO GLU	p< 0.0001
fer-15/Mytho KO ND – *fer-15/Mytho* KO GLU	p< 0.05
fer-15/Mytho KO ND – *fer-15* GLU	NS
fer-15 GLU – *fer-15/Mytho* KO GLU	NS

Fig. 25: Survival capability of wild-type and *Mytho* KO worms in presence of different stresses. A) Adult wild-type and *Mytho* KO nematodes were incubated in wells of a 96-well plate with 200 mM paraquat (PQ) in M9 buffer at 20 °C with constant agitation and survival was measured every hour for 12 hours checking worms at the microscope. The plots are the composite of the two independent experiments performed and represent the survival fractions of each genotype, that were compared at every time point using the unequal variance *t*-test. N = 50 for N2 and *Mytho* KO worms. B) 5-days adult wild-type and *Mytho* KO hermaphrodite*s* were seeded on NGM plates and submitted to a heat-shock at 35 °C. Worm viability was

measured at the indicated time points and represented as a fraction on the total number of worms seeded on plates. The experiment was performed twice and the results were compared using the unequal variance *t*-test. The bars indicate the standard error of the mean. N = 30 for N2 and *Mytho* KO worms. C) L4 *fer-15* and *fer-15/Mytho* KO worms were seeded on NGM plates, maintained at 25 °C for 5 days. and then incubated in M9 buffer supplemented with PQ at the final concentration of 125 mM with constant agitation at 25 °C for 1 hour. To remove the oxidant, nematodes were washed three times in M9 buffer and transferred to fresh NGM plates that were incubated at 25 °C for the indicated time points at which survival was calculated as the ratio of worms alive to the total number of animals transferred to the plate after oxidant treatment. The experiment was performed twice and the results were compared using the unequal variance *t*-test. The bars indicate the standard error of the mean. N= 95 for *fer-15* worms and N= 83 for *fer-15/Mytho* KO worms. *, $p < 0.05$ (adapted from the manuscript in preparation). D) Survival curves of *fer-15* nematodes incubated at 25 °C and maintained with or without 1% glucose in culture medium were compared with that of *fer-15/Mytho* KO worms kept at the same conditions. The experiment was performed once with N = 80 for each genotype. Curves were compared using the log rank test and the corresponding p-values are reported in the table. ND, normal diet; GLU, 1% glucose; NS, not significant.

8.2.2.4 Generation of *daf-2 /fer-15/Mytho* KO *daf-16/ fer-15/Mytho* KO worms

We crossed *daf-2(e1370)* and *daf-16(mu86)* mutants with *fer-15/Mytho* KO worms in order to perform lifespan assay and determine if the absence of Mytho could ablate *daf-2* mutants life extension or, conversely, worsen *daf-16* mutants phenotype.

We identified *Mytho* KO worms as before (see Fig. 21 B); then those worms that produced no or very few progeny at 25 °C were selected.

For what concerns the *daf-2* locus (chromosome III), the *e1370* allele carries a single nucleotide substitution in exon 14 (c.4252C>T) that leads to a missense mutation in the protein sequence (p.Pro1418Ser). A PCR reaction was performed using primers on exon 14 and products were sequenced in order to identify worms carrying the substitution (Fig. 26 A).

For what concerns the *daf-16* locus (chromosome I), the *mu86* allele carries a big deletion (10947 bp) in the coding sequence. This genetic cross was much harder to obtain since *T01G9.2* and *daf-16* localize both on chromosome 1. *daf-16* mutants were indentified through two different PCR reactions with a common reverse primer on intron 2 and two different forward primers, one localized in the 5'UTR, and the other in intron 1. In this way the region comprised between primers in 5'UTR and intron 2 can be amplified only if the gene is deleted. Conversely, the sequence between primers in intron 1 and 2 can be amplified only in wild-type worms (Fig. 26 B)

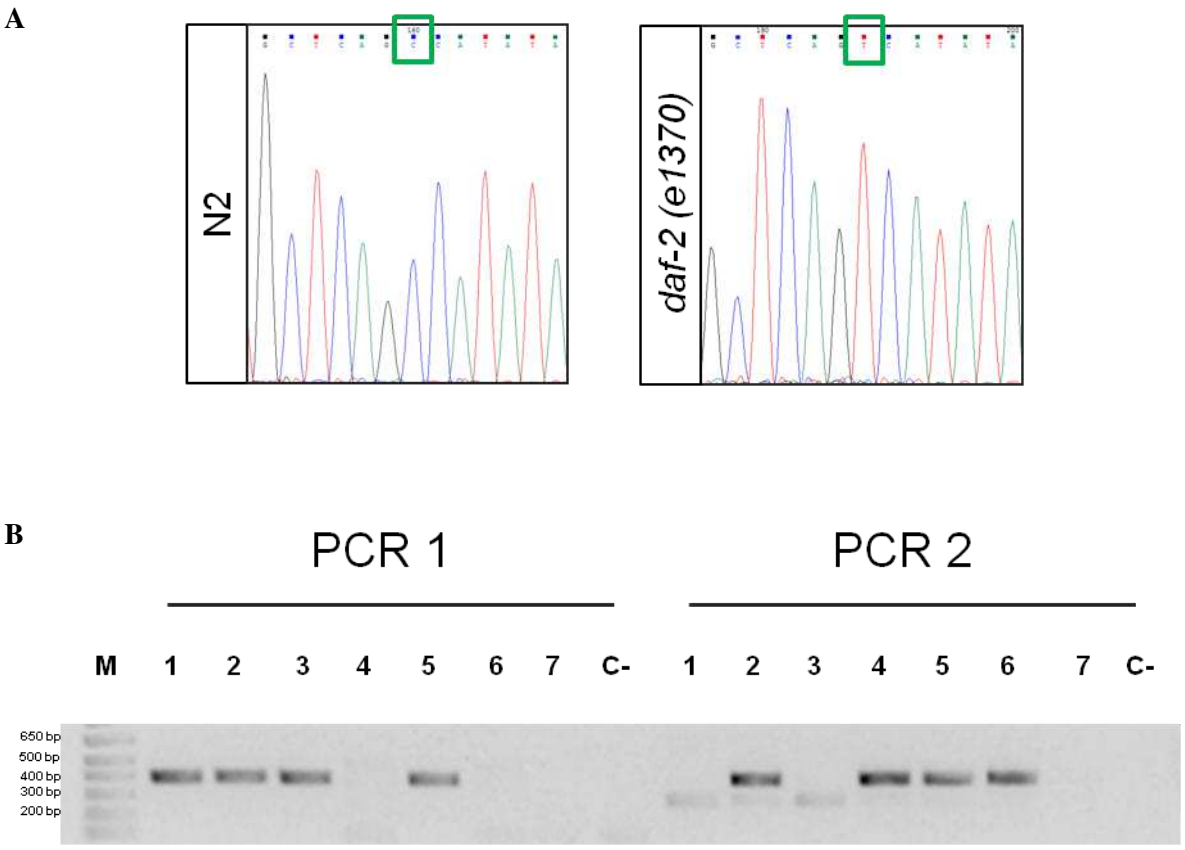

Fig. 26: Genetic cross of *daf-2(e1370)* and *daf-16(mu86)* mutants with *fer-15/Mytho* KO worms. A) To identify worms carrying the *e1370* allele in the *daf-2* locus, a PCR reaction was performed using primers on exon 14 and products were sequenced. A wild-type sequence is depicted on the left, while one carrying the c.4252C>T substitution is represented on the right. B) For what concerns the *daf-16* locus, two PCR reactions were performed in order to identify worms carrying the *mu86* allele in homozygosis. For the first one (PCR 1), that enables to recognize the wild-type allele, a forward primer in intron 1 and a reverse one in intron 2 are used, while for the second reaction (PCR 2), that identifies the mutated allele, a forward primer in the 5'UTR region and the same reverse primer in intron 2 are used. An exemplificative agarose gel image shows the screening of 7 *Mytho* KO worms. Worms 1 and 3 are wild-type for the *daf-16* locus, worms 2 and 5 are instead heterozygous for the same locus and worms 4 and 6 are homozygous for the *mu86* allele. Worm 7 could not be genotyped. M: 1 Kb plus molecular marker.

9 Discussion

The comparative screening of transcriptomic profiles obtained from skeletal muscles derived from fed and starved control and *FoxO1*, *3*, *4* null mice, which was performed to identify new genes that regulate autophagy, enabled the identification of a candidate one, that is evolutionary conserved and was called *MYTHO* (*Mytho* in mouse).

It was found that its expression is induced upon stress conditions, including absence of nutrients, loss of innervation or presence of tumor growth, and during aging, in line with the already established role of FoxOs transcription factors in many cellular processes (Lee and Dong, 2017).

MYTHO involvement in the autophagic process was investigated and it was demonstrated that the protein co-localizes with LC3 (an established marker of autophagosomes, Jiang and Mizushima, 2014) and, although much less, with Lamp2 (a marker of lysosomes) and it requires autophagosomes for reaching lysosomes.

The role of *Mytho* in autophagy was further investigated in a mouse cell model where *Mytho* was deleted. I was actively involved in this part of the project and I generated a C2C12 *Mytho* KO model through CRISPR/Cas9 technology (see paragraph 8.1, Results).Western blots for LC3 lipidation and immunofluorescence analyses for LC3 positive *puncta* revealed that the basal autophagic flux is reduced in the absence of Mytho. Conversely, overexpression of *Mytho* in cells or in adult skeletal muscle was sufficient to increase autophagosome numbers and the autophagic flux.

The results so far obtained indicate that *MYTHO* is a FOXO-dependent gene important for autophagy. Then, since many *C. elegans* RNAi models have proven that a functional autophagic process is essential for a healthy aging and for longevity (Meléndez *et al*, 2003; Kang *et al*, 2007; Meléndez and Levine, 2009), we asked ourselves what could be the functional and physiological implications of silencing this gene in a multicellular animal model and we chose *C. elegans* because the gene is extremely conserved across species having an orthologue also in the worm genome, that is *T01G9.2*.

T01G9.2 was originally identified as the *lin-10* locus, that, if affected by loss-of-function mutations, specifically prevents the induction of vulval cell lineages (Kim and Horvitz, 1990). However, more recent experiments demonstrated the existence of an alternate genomic region, located ~180 kb to the left of *T01G9.2*, that could rescue the *lin-10* vulvaless phenotype in transgenic experiments, generating animals that laid eggs and had an essentially wild-type vulval morphology. In contrast, *lin-10* animals that were transgenic for genomic clones containing *T01G9.2* showed weak rescue of the vulvaless phenotype and exhibited a protruding vulval phenotype (Whitfield *et al*, 1999).

In a recent study the authors focused their attention on genes known to be expressed in body wall muscle cells in *C. elegans* and orthologues of human ones with the aim of characterizing their sub-cellular localization. They expressed these proteins as GFP-tagged versions under the control of a worm muscle cell specific promoter, using the Gateway recombination cloning system. The constructs were microinjected and transgenic animals were analyzed by fluorescence microscopy in order to

determine the sub-cellular localization of GFP-tagged proteins. T01G9.2 belongs to the category of proteins that localize mainly to dense bodies, that correspond to the Z-lines in vertebrate striated muscle (Meissner *et al*, 2011).

To investigate *T01G9.2* function in *C. elegans* we initially performed RNAi experiments to knock down the gene in worm tissues. Silenced worms developed normally and had not any evident anomalies in behavior.

Since *Mytho* seems to have an important role in muscle homeostasis and the worm orthologue is also expressed in body wall muscle cells, we decided to analyze worm movements, focusing on easy measurable parameters (body bends number, reversals frequency and stillness duration). We analyzed worms seeded at the L4 stage after having kept them one day at 20 °C and found that those silenced for *T01G9.2* showed only a lower frequency of reversals compared to controls, suggesting that the knockdown of the gene only marginally affects worm movements.

Previous data showed that FOXOs are essential for the induction and maintenance of a high autophagic flux, rather than for basal autophagy which appears to be under the control of mTOR (Milan *et al*, 2015). Moreover, it has been reported that also in *C. elegans* starvation promotes autophagy induction in all tissues (Chapin *et al*, 2015). Given the importance of a functional autophagic process to worm survival (Kang *et al*, 2007), we submitted worm larvae silenced for *T01G9.2* and their relative controls to prolonged periods of starvation and measured how many of them survived two days after having been seeded on fresh RNAi plates. Even after 7 days of starvation the survival fraction was decreased in a similar way in controls and silenced worms, suggesting therefore that *T01G9.2* is not essential for worm survival after long starvation.

We then repeated the locomotion analysis after having kept L4 worms at 25 °C for one day, in order to evidence possible temperature-dependent mechanisms. Although 25 °C is still considered a physiological temperature for *C. elegans* culture, it has been demonstrated that the higher temperature of maintenance induces metabolic changes in worms (Gómez-Orte *et al*, 2017).

Even in this case, no clear differences were perceivable between silenced worms and control ones, apart from a not significant lower number of body bends in worms devoid of *T01G9.2*.

RNA interference is a fast and easy tool to silence a gene of interest in *C. elegans* and it is generally used to rapidly screen for loss of function phenotypes. However, some precautions have to be taken. In fact, the silencing produces a gene knockdown rather than a complete knockout and results are often variable, the number of false negative results is high (about 30%), and even if the level of the target mRNA is undetectable, the protein product could not be totally eliminated (Ahringer, 2006).

Considering these technical limitations, the lack of a clearcut phenotype after RNAi, we decided to generate a KO strain for *T01G9.2*, to investigate the effects of a total gene ablation.

We employed the CRISPR/Cas9 technology to get a *Mytho* KO model in *C. elegans* and we finally obtained four different strains, but all of them carried a different genomic edit from the expected one. Three of them showed a frameshift mutation predicted to lead to the formation of a premature stop

codon at position 36, *i.e.*, *T01G9.2*(*pan8*[S18Tfs*19]); *T01G9.2*(*pan9*[S18Tfs*19]); *T01G9.2*(*pan10*[S18Tfs*19]). The fourth knockout strain carried a different frameshift mutation predicted to lead to the formation of a premature stop codon at position 22, *i.e.*, *T01G9.2*(*pan7*[T20Ffs*3]).

Phenotypic analyses were conducted on strains *T01G9.2*(*pan8*[S18Tfs*19]) and *T01G9.2*(*pan9*[S18Tfs*19]), after having verified by RT-PCR that no wild-type transcript was produced from KO strains.

Worms developed normally, meaning that the ablation of *T01G9.2* has not lethal effects; besides, no evident morphological and behavioral differences were perceivable in *Mytho* KO worms compared to controls. We first of all repeated the same experiments performed with RNAi treated worms, in order to investigate the effect of gene knockout in locomotion and in survival capability after a long period of starvation.

Unexpectedly, *Mytho* KO worms didn't show any impairment in body bends number, frequency of reversals or in duration of stillness periods, nor keeping worms one day after seeding at 20 °C or at 25 °C. Moreover, synchronized L1 *Mytho* KO larvae and their relative controls were kept under prolonged periods of starvation and two days after the seeding on fresh NGM plates their survival was measured, confirming what was obtained with worms silenced by RNAi: the survival capability after long starvation is not influenced by *T01G9.2*.

These results obtained with the *Mytho* KO model argue against a role of this gene in autophagy and survival pathways in *C. elegans*, given the lack of clear phenotypes observed even with strong and challenging stimuli (for example, long periods of starvation).

It is now generally recognized that FOXOs are essential for a healthy aging and longevity (Burgering, 2008) and that *C. elegans* represented a crucial model of study to elucidate the function of these transcription factors, highlighting their role in pro-survival and longevity pathways (Martins *et al*, 2016). One keystone discovery was the finding that mutations in *daf-2*, cause a temperature-sensitive dauer-constitutive shift and extend animals longevity at lower temperature, however both phenotypes require DAF-16, which is crucial for the expression of stress resistance and longevity-promoting genes (Kenyon *et al*, 1993; Kimura *et al*, 1997; Lin *et al*, 1997; Gems *et al*, 1998).

Considering that *MYTHO* was identified as a *FOXO*-dependent gene, we decided to focus our attention on later stages of *C. elegans* vital cycle and to investigate if lifespan and aging are affected by *T01G9.2* ablation, owing to the fact that this nematode is an ideal model to study aging (Panoski and Dillin, 2009; Tissenbaum, 2015).

In order to analyze lifespan, we crossed *Mytho* KO worms with *fer-15* animals, that have a temperature-sensitive defect in spermatogenesis and are consequently sterile at 25 °C (Hirsch *et al*, 1976), and performed the experiment at this non permissive temperature.

Interestingly *fer-15/Mytho* KO nematodes showed a reduced lifespan compared to controls and the difference became perceivable after 6 days from seeding, when some worms devoid of *Mytho* started to precociously die.

We also noticed that *Mytho* KO worms appeared older than controls and became lethargic after 4-5 days from the seeding. Therefore, we repeated the locomotion analysis after having kept worms 5 days at 25 °C, observing a significant decrease in body bends and reversals and an evident increase in stillness periods in *Mytho* KO worms compared to control ones.

These results suggest that the absence of *T01G9.2* is responsible for a premature aging that impairs movements and leads to a shorter lifespan rather than for congenital defects in locomotion or development and represent the first demonstration of the essential role of *Mytho* for a healthy aging in a multicellular animal model.

We therefore tried to elucidate possible mechanisms that could be altered in *Mytho* KO animals leading to a precocious aging.

It is known that a functional autophagic process is linked as well as FOXOs to a healthy aging and longevity pathways (Dikic and Elazar, 2018). This was also demonstrated in *C. elegans*, since the RNAi inactivation of *bec-1* (the worm homologue of *BECN1*, which codes for Beclin-1) decreases lifespan of *daf-2* mutant animals, without effect on wild-type worms and impairs their ability to form normal dauers, highlighting the importance of autophagy for survival under stressful conditions and lifespan extension (Meléndez *et al*, 2003).

Recent detailed studies on autophagic flux in *C. elegans* revealed that autophagy is active in all major somatic tissues (intestine, muscle, pharynx and neurons) during aging, however autophagic activity appears to decrease with age. Moreover, it seems that autophagy is increased in certain tissues of long-lived *daf-2* mutants, suggesting the involvement of this cellular process in their increased longevity (Chang *et al*, 2017).

Therefore, we decided to investigate autophagy in absence of *T01G9.2*, and for this purpose we performed a preliminary experiment, counting GFP *punctae* in the posterior bulb of the pharynx of adult worms, after having crossed *Mytho* KO animals with the strain carrying LGG-1, that is the worm orthologue of mammalian LC3, a marker of autophagosomes, fused with GFP (DA2123 strain) (Kang *et al*, 2007). We found that the number of GFP *punctae* (so of autophagosomes) is significantly decreased in *Mytho* KO animals compared to controls, suggesting an impairment of the autophagic process, at least in this body district, in absence of *Mytho*.

This result, in line with what observed by our collaborators in cellular and murine models, differs from what obtained submitting young wild-type and *Mytho* KO larvae to long periods of starvation. In that case, no difference could be appreciated in survival fraction of the two genotypes, and considering that starvation induces autophagy also in *C. elegans* (Chapin *et al*, 2015), and that a functional autophagic process is crucial during starvation for worm survival (Kang *et al*, 2007) it argues against a role of *Mytho* in autophagy in a multicellular model.

However, the GFP *punctae* analysis was carried in adult worms, rather than during the first phases of development. In accordance with the results of lifespan analysis, it confirms our hypothesis that *Mytho* exerts its function during aging.

The autophagosomal pool analysis was carried on adult worms, however we couldn't wait 5 days keeping worms at 25°C similarly to other experiments, since nematodes (*Mytho* KO animals crossed with the DA2123 strain and control worms from this strain) precociously and unexpectedly died. We performed the analysis on 1-2 days-adult worms finding at this time point a significant difference between genotypes, meaning that it could be even stronger if investigated at later phases during aging. We have to consider that the experiment was carried out using a strain that enables to analyze only the autophagosomal pool, and in this way we can't discriminate if the autophagosomes impairment observed in *Mytho* KO nematodes is due to a decreased autophagic activity or to an increased fusion with lysosomes (Klionsky *et al*, 2012).

We plan to bypass this limitation by repeating the analysis with the recently developed tandem tagged mCherry::GFP::LGG-1 reporter in order to evaluate the number of both autophagosomes and autolysosomes in the same body districts, with the first ones positive for both GFP and mCherry fluorescence, while the second ones emit only the mCherry signal due to quenching of GFP in the acidic environment (Chang *et al*, 2017). This strain was deposited in the CGC consortium (https://cgc.umn.edu/, MAH215 strain).

Another possibility that could be exploited alone or in combination with the tandem tagged mCherry::GFP::LGG-1 reporter is to infer the turnover of autophagosomes in the presence and absence of lysosomal degradation, for example by injecting bafilomycin A1, which inhibits acidification of autolysosomes, into adult worms, with a consequent increase in the number of autophagosomes in as few as 2 hours post-injection (Zhang *et al*, 2015; Palmisano and Meléndez, 2016). With the recent acquisition of a microinjection facility for *C. elegans* by our research group we could address this issue in future.

It the impairment of autophagy will be confirmed in *Mytho* KO animals, it could also be interesting to elucidate if some tissues are preferentially affected. It has been reported for example that neurons appear to behave differently to other major tissues, with an earlier decline of autophagic activity during aging (Chang *et al*, 2017).

Microarray analysis and chromatin immunoprecipitation experiments enabled the identification of many downstream targets of DAF-16 in *C. elegans* and many of them are involved in stress resistance (*e.g.* the superoxide dismutase *sod-3*, catalases *ctl-1* and *ctl-2*, heat-shock proteins, the metallothionein *mtl-1*, and antibacterial lysozymes) (Murphy *et al*, 2003; Panoski and Dillin, 2009).

It was also shown that genes controlled by DAF-16 are upregulated in three long-lived *C. elegans* mitochondrial mutants (*clk-1*, *isp-1* and *nuo-6*) and that DAF-16 and multiple proteins interacting with it are required for the full longevity of these *Mit* mutants. The authors suggest that the activation of

DAF-16 results from elevated levels of ROS, strengthening the link between DAF-16 and oxidative stress response (Senchuk *et al*, 2018).

To investigate the role of *T01G9.2* as FOXO-dependent gene, oxidative stress was induced in *Mytho* KO and wild-type worms, by exposing them to paraquat (PQ, methyl viologen), which interferes with the electron transport chain generating ROS (Possik and Pause, 2015). Worms for each genotype were incubated with PQ and survival was measured every hour during the incubation for 12 hours, but no difference could be appreciated between genotypes.

So, we decided to analyze the capability of stress resistance exposing nematodes to the harmful agent at the precise moment when the precocious aging phenotype of *Mytho* KO animals becomes evident, that is after the maintenance at 25 °C for 5 days. After incubation with PQ for 1 hour, worms were transferred to fresh NGM plates at 25 °C and survival was calculated after 2 days onwards until all *Mytho* KO animal were dead.

Not only *fer-15/Mytho* KO worms survival was significantly decreased compared to relative controls but the difference between genotypes was also more pronounced compared to that observed at the same time point during the lifespan assay. For example, after 9 days in absence of PQ treatment the survival fraction of *fer-15/Mytho* KO animals was 0.37 compared to that of controls, which was 0.87 (corresponding to 42%), while after PQ exposure the values were respectively 0.24 and 0.05, lowering the ratio to 21%. This finding strongly suggests the involvement of *T01G9.2* in the response against oxidative stress and confirms that this gene exerts its function in adulthood after a specific time point.

It has been demonstrated that the heat-shock factor HSF-1 cooperates with DAF-16 in response to heat stress reducing insulin signaling to activate the expression of *shsp* genes, that code for small heat-shock proteins, and to promote pro-survival pathways (Hsu *et al*, 2003).

So, we also tried a heat stress experiment, similarly to what was performed by Lithgow *et al*, (longitudinal assay), seeding adult wild-type and *Mytho* KO hermaphrodite*s* on NGM plates and exposing them to a heat-shock at 35 °C. Worm viability was measured at different time points, and the results obtained for wild-type worms were comparable with what reported, although we noticed that worms started to die after 5 hours of incubation at 35 °C, while the authors saw a rapid decrease in the survival fraction only after 7 hours. However, also in this case no difference could be observed in the survival fractions of the analyzed genotypes.

We therefore performed a pilot test in a similar way to PQ treatment (data not shown): after 5 days at 25 °C *fer-15* and *fer-15/Mytho* KO worms were incubated 3 hours at 35°C , then maintained at 25° C and assayed for survival 24 hours later onwards. *fer-15/Mytho* KO worms survival was significantly decreased compared to relative controls and similarly to what observed with PQ treatment, the difference in survival fraction between genotypes is even more evident. For example, after 10 days in absence of heat stress the survival fraction of *fer-15/Mytho* KO animals was 0.29 compared to that of controls, which was 0.82 (corresponding to 35%), while after the incubation at 35 °C the values were respectively 0.56 and 0.11, lowering the ratio to 20%. Although only preliminary, this result suggests

the involvement of *T01G9.2* in the response to heat stress and corroborates our previous findings that the gene exerts its functions after a specific life time point.

Diet composition has dramatic effects on disease onset and life expectancy and studies conducted in *C. elegans* were fundamental to at least partially elucidate the mechanisms governing metabolism and healthy aging.

Schulz *et al* hypothesized a model in which the reduced availability of glucose induces mitochondrial respiration via *aak-2* (the worm homologue of AMPK), causing increased ROS formation, leading to mitohormetically increased catalase activity and stress resistance, cumulating in extension of life expectancy. On the contrary, increased availability of glucose may reduce mitochondrial activity, decreasing lifespan in nematodes (Schulz *et al*, 2007). It was then shown that the addition of glucose to the bacterial diet of *C. elegans* truly shortens its lifespan by inhibiting the activity of DAF-16 and heat-shock factor HSF-1 (Lee *et al*, 2009) and a more recent study linked the accumulation of dietary glucose in the form of glycogen to AAK-2 inhibition, DAF-16 repression and shortening of lifespan (Gusarov *et al*, 2013).

We therefore performed a pilot lifespan assay, maintaining *fer-15* and *fer-15/Mytho* KO worms also on NGM plates containing 1% of glucose. As expected, we found a viability decrease of *fer-15* worms grown in presence of glucose compared to those cultivated in absence of it, and this effect is in line with the already reported glucose-mediated inhibition of *daf-16*. Since *MYTHO* is a *FOXO*-dependent gene and *daf-16* is the only worm homologue of mammalian *FOXOs*, the block of DAF-16 translocation to the nucleus results in *C. elegans* in *Mytho* inhibition, and this suggests that the decreased lifespan in presence of glucose is at least in part due to the effects on *Mytho*.

Surprisingly, lifespan of *fer-15/Mytho* KO nematodes was improved in presence of glucose in culture medium, and the final result is that viability of *fer-15* and *fer-15/Mytho* KO worms is very similar in this culture condition. This unexpected result however needs to be confirmed with further assays.

Moreover, in order to explain this finding and to deepen the pathway linking IGF/Akt/FOXO to *MYTHO*, we decided to cross *daf-2(e1370)* and *daf-16(mu86)* mutants with *fer-15/Mytho* KO worms in order to determine by lifespan assays if the absence of Mytho could cancel the life extension shown by *daf-2* mutants or, conversely, worsen *daf-16* mutants phenotype. We obtained the two genetic crosses and longevity tests will be performed soon.

Our data collectively indicate that *MYTHO* is important for a healthy aging and longevity in a multicellular organism. Preliminary results indicate that in *C. elegans* it may have a role in autophagy as well and may be indeed essential as a FOXO-dependent gene to properly respond to several types of harmful stresses (at least oxidative, but probably also heat and metabolic stress). These findings strengthen what already observed in cellular and murine models, making MYTHO a novel protein coding gene at the crossroad between FoxO, autophagy and ageing (manuscript in preparation).

SECTION V

FUNCTIONAL CHARACTERIZATION OF A NEW VARIANT IDENTIFIED IN *TOGARAM1*

10 Introduction

10.1 Organization of the nervous system in *C. elegans*

In *C. elegans* a hermaphrodite invariantly has 302 neurons that belong to two distinct and independent nervous systems: a large somatic nervous system (282 cells plus 56 associated support cells) and a small pharyngeal nervous system (20 cells) (White *et al*, 1986). The male possesses instead 385 neurons, with the extra neurons located in the tail (Sammut *et al*, 2015).

Considering the peculiar combination of properties, such as morphology, connectivity and position of each neuron, White *et al* classified neurons in 118 classes with members of individual neuron classes mostly identified by their relative position to the anterior/posterior or left/right axis. Individual class components can be distinguished by subtle functional criteria or slightly distinct axodendritic projection patterns and are defined by the co-expression of terminal differentiation genes ("gene batteries") (White *et al*, 1986; Hobert, 2005).

Every *C. elegans* neuron name consists of either two or three uppercase letters representing class and in some cases a number. If the neurons are radially symmetrical, each cell has a three-letter name followed by L (left), R (right), D (dorsal), or V (ventral) (Altun and Hall, 2011).

This physical map has been recently updated, with the addition of a complete connectivity atlas also for the nervous system of male *C. elegans* (Cook *et al*, 2019).

10.2 Sensory neurons

A proper perception of the surroundings is essential for *C. elegans* chemotaxis, thermotaxis, aerotaxis and for escaping from harmful and noxious stimuli by avoidance behaviors. A hermaphrodite worm has a sensory nervous system comprised of at least 78 neurons of 34 types that are peculiar in their morphology, connectivity, and sensory properties and 60 of them are ciliated (Doroquez *et al*, 2014). The male possesses additional 48 ciliated neurons (Bae and Barr, 2008).

Many sensory receptors are arranged in *C. elegans* in groups of sense organs, known as sensilla.

Mechanical stimuli, temperature, many water-soluble and volatile chemicals, noxious substances, ambient osmolarity, oxygen levels, pH and light perception are perceived by a number of sensillar organs and various isolated sensory neurons, although some sensory functions, including oxygen sensation and mechanosensation, are also performed by nonsensillar neurons, like the non-ciliated touch cells (Starich *et al*, 1995; Altun and Hall, 2011).

A sensillum is a simple epithelial sense organ composed of dendrites of one or more sensory neurons surrounded by a channel formed by a single sheath cell and one or more socket cells.
At the end of its process, the socket cell forms a small tissue that envelops like a ring the distal ends of sensory dendrites, whereas the extreme distal portion of the sheath cell surrounds the lumen of the sensillar pouch just behind the socket cell.
Through laser ablation studies it was demonstrated that these cells, which are thought to be glial cells, have a role in neuronal development and function. In fact sheath cells regulate dendrite extension and, without them, associated sensory dendrites are not able to complete it, while socket cells are involved in navigating dendrites to specific sensory organs and their absence causes their infiltration in a different sensory organ (White *et al*, 1986; Altun and Hall, 2010).
The amphids are a pair sensilla in the head, open to the outside, situated at the sides of the lips that represent the largest chemosensory organs of *C. elegans*. Each of them comprises 12 neurons dendrites, a sheath and a socket cell.
Inner labial sensilia are found in a sixfold, symmetrically arranged manner at the top of each lip and every one contains two neuron dendrites, while each of the six outer labial sensilla, has only one outer labial sensory neuron dendrite. Both type contains one sheath and one socket cell.
Each cephalic sensillum is positioned adjacent to an outer labial sensillum in the lips and contains the dendrite of one of the four cephalic neurons, one sheath and one socket cell.
For what concerns anterior and posterior deirid sensilla, they are each bilaterally paired and are found at the posterior end of the pharyngeal bulb and slightly anterior to the anus.
The phasmids are located at the lateral sides of the tail, behind the rectum and they are similar to amphids in structure but they are smaller. They are composed of one sheath cell, two socket cells, and the ciliated dendrites of three neurons (Inglis *et al*, 2007; Altun and Hall, 2010; Doroquez *et al*, 2014).

10.2.1 Sensory cilia

Cilia are thin microtubule-based subcellular organelles that protrude from the cell surfaces of virtually all eukaryotic organisms and exist in two types, motile cilia (also known as flagella), used for locomotion or for the generation of fluid flow, and non-motile (primary) cilia, implicated in sensing the chemical and/or physical extracellular environments (Bettencourt-Dias *et al*, 2011).
Differently from many organisms, including humans, the only ciliated cell type in *C. elegans* is the sensory neuron, and none of the cilia in the nematode are motile (Inglis *et al*, 2007).
Worm cilia emanate from a transition zone, which typically possesses a circular set of doublet microtubules, as determined by ultrastructural analysis. In particular, in amphid and phasmid cilia the transition zone is followed by a so-defined “middle segment”, characterized by a classical arrangement of nine doublet microtubules around one to six single microtubules, that transforms into a “distal segment” made of singlet microtubules. These features may be different in some neurons.

Ciliogenesis, which occurs at around the midpoint of the threefold stage of embryogenesis, depends on the intraflagellar transport (IFT) of ciliary precursors from the transition zone, which localizes at the junction between the dendrite of the sensory neuron and the cilium, to the growing cilium (Inglis *et al*, 2007; Bae and Barr, 2008). It has been shown that in *C. elegans* amphids, two IFT motors, heterotrimeric kinesin-II and homodimeric OSM-3, move IFT-particles and probably ciliary precursor proteins from the base of cilium to their sites of incorporation; this anterograde IFT-machinery, and maybe also turnover products, are then transported back to the base of the cilium using the IFT-dynein motor. Kinesin-II and OSM-3 motors cooperate to assemble middle segments of cilia, while OSM-3 acts alone to build the distal segment.
Notably, some *C. elegans* neurons retain the ability to extend cilia in later stages, including the adult phase (Altun and Hall, 2010).

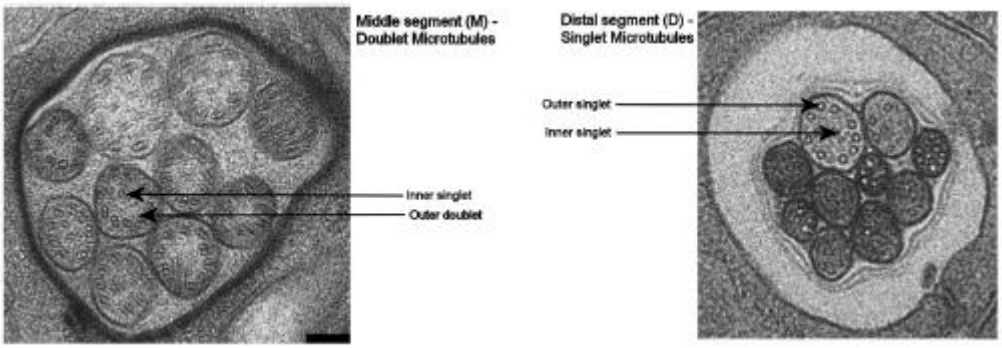

Fig. 27: Ultrastructures of cilia in the *C. elegans* hermaphrodite. The two panels show electron micrograph cross-sections of amphid cilia in the middle segment (microtubule doublets; left panel) and distal segment (microtubule singlets; right panel) (adapted from Inglis *et al*, 2007).

In *C. elegans* genes involved in ciliogenesis are under the transcriptional control of the transcription factor DAF-19 that recognizes a promoter element called "X box", which normally spans 14 nucleotides in length and is typically positioned ~100 nucleotides upstream from the start codon of the ciliary gene. Interestingly, an X box is found upstream of the *daf-19* gene itself, indicating that its activity is self-regulated and, consistent with the role of DAF-19 as a key regulator of ciliogenesis, cilia are totally absent in *daf-19* mutants. As expected, genes encoding IFT proteins also possess X boxes but disruption of these genes leads to truncated ciliary structures, rather to their complete disappearance (Perkins *et al*, 1986; Starich *et al*, 1995; Inglis *et al*, 2007).

10.2.2 Roles of sensory perception in *C. elegans*

As anticipated before, environmental stimuli are sensed by *C. elegans* through its sensory neurons that are in large part ciliated (Bae and Barr, 2008).
It has been estimated that roughly 5% of the *C. elegans* genome is devoted to chemical recognition. Many G protein-coupled receptors function as chemoreceptors in sensory neurons, where they are

differently expressed in left-right pairs of cells, although some receptors are present in multiple neuron types. At the same time, a single pair of neurons can express many different chemoreceptor genes. (Bargmann, 2006). Some soluble or volatile chemicals are attractive to worms and if present as gradient on a plate will stimulate worm movement towards that substance, while others are repulsive, inducing on the contrary escape behaviors.

C. elegans responds to various types of mechanical stimuli, including nose touch, or the viscosity of the bacterial food lawn.

The thermotaxis behavior is extremely sensitive and experience dependent. In fact, nematodes crawl to their culture temperature in a spatial temperature gradient within 0.1 °C. In addition, animals show short-term and long-term adaptation to the surrounding temperature.

Chemical and mechanical signals produced by hermaphrodites are also perceived by males during the mating process (Bae and Barr, 2008).

Besides its behavioral roles, chemosensation is important for some physiological processes, like entry and exit from the dauer larval stage. Food availability is sensed by ciliated sensory neurons, as well as animal density, since all worms constitutively secrete a pheromone, called daumone, and the ablation of some amphid sensory neurons leads to constitutive entry into the dauer stage, regardless of conditions (Bargmann, 2006).

Some sensory neurons have also a lifespan-regulatory role and control animal body mass.

10.3 Amphid and phasmid sensilla

Each amphid includes 12 sensory neurons (ADF, ADL, AFD, ASE, ASG, ASH, ASI, ASJ, ASK, AWA, AWB, AWC) as well as one sheath (Amsh) and one socket (Amso) cell. Amphid neurons possess axons that associate with the nerve ring while the dendrites extend to the anterior portion of the animal and end with ciliated structures. The phasmids are instead composed of one sheath cell, two socket cells, and the ciliated dendrites of PHA, PHB, and PQR neurons (only on the left side) (Inglis *et al*, 2007, Bae and Barr, 2008).

The majority of amphid neurons possess cilia shaped as single rods (ASE, ASG, ASH, ASI, ASJ, ASK) or pairs of rods (ADF, ADL), that extend in the channel formed by sheath and socket cells. Other amphids have cilia carrying membrane elaborations and peculiar shapes, like the wing neurons AWA, AWB, AWC and the amphid finger neuron AFD, in which a small cilium is surrounded by roughly 50 villi. These cilia are not exposed to the outside but are associated with the sheath cell. The lengths of amphid cilia range from ~7.5 μm (in the ASE, ASG, ASH, ASI, ASJ and ASK neurons) to ~1.5 μm for the AFD cilium.

Similar in structure to the single rod-like cilia found in amphids are the PHA and PHB phasmid cilia, that are located slightly posterior to the anus of the worm and are exposed to the external environment.

Amphid and phasmid neurons have roles in chemotaxis, mechanosensation, osmotaxis, and dauer pheromone sensation (Inglis *et al*, 2007; Altun and Hall, 2010).

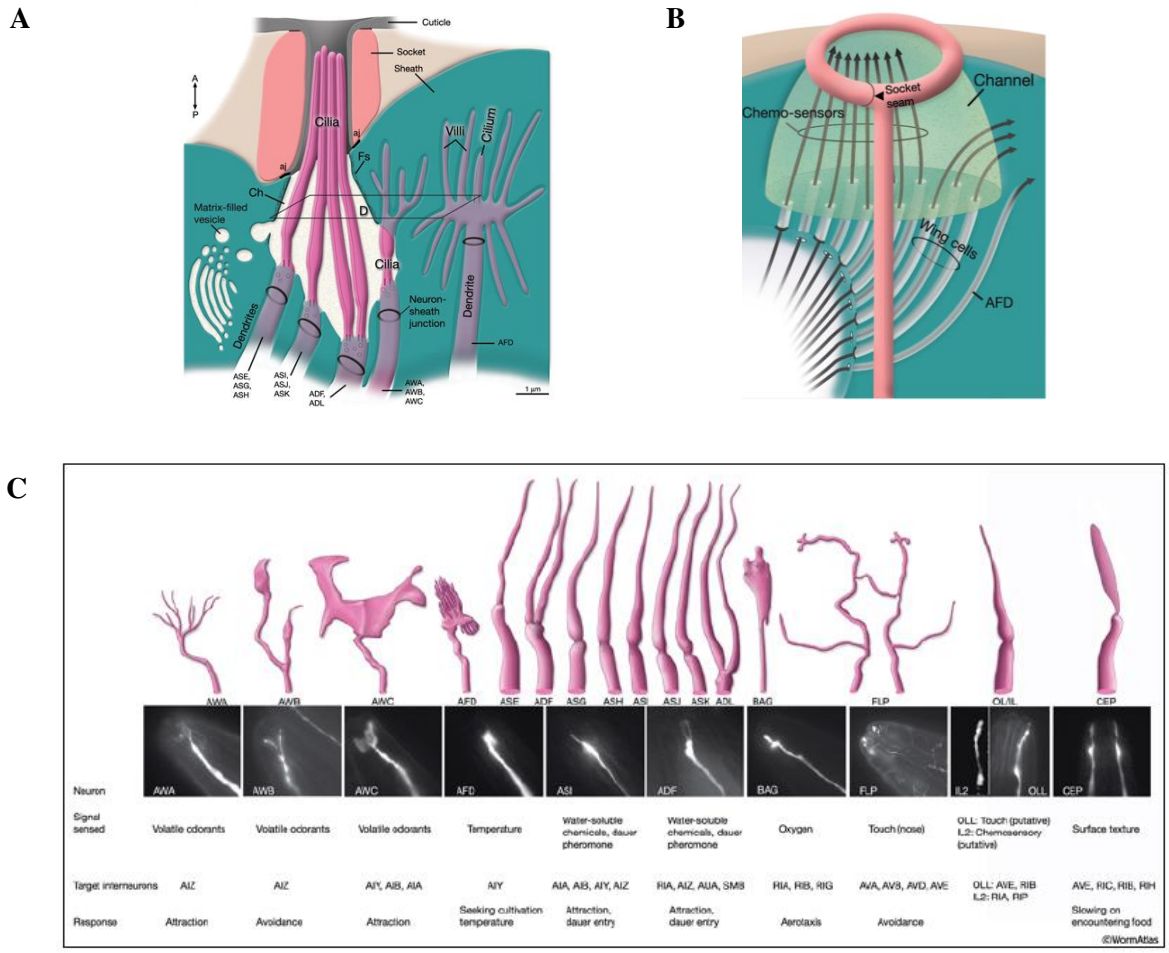

Fig. 28: A) The structure of the amphid is depicted longitudinally. The amphid channel (Ch) is defined by the cuticle in the distal socket part and an electron-dense lining supported by cytoskeletal filaments (Fs) in the anterior sheath part. The socket cell is connected to the hypodermis and the sheath cell by adherens junctions (aj). Adherens junctions are also present between the dendrites and sheath cell near to the level where the dendrites enter the channel. B) An illustration of invagination of the sheath-cell cytoplasm by amphid dendrites, longitudinally. The process of the AFD neuron stays embedded within the sheath cell, whereas all others enter the amphid channel. The cilia of AWA, AWB and AWC infiltrate back into the sheath cell, whereas the eight channel cilia are externally exposed through the pore. C) On the top panel illustrations of cilia of amphid neurons. On the middle panel fluorescent images of cilia. Although all chemosensory amphid cilia are similar in shape with one (ASE, ASG, ASH, ASI, ASJ, ASK) or two (ADF, ADL) finger-like cylinders, each of the amphid wing cilia (AWA, AWB, AWC) has a unique shape. On the bottom panel a table with the sensory cues detected by these neurons, the interneurons with which they synapse, and the behavioral response elicited (adapted from Altun and Hall, 2010).

10.3.1 The ASE neurons

The couple of amphid ciliated sensory ASE cells, ASER (right) and ASEL (left), were the first *C. elegans* neurons to be studied by direct electrophysiological recordings; they have voltage-regulated potassium currents and voltage-regulated calcium currents, but no voltage-activated sodium channels.
The function of ASE neurons in chemosensation was defined with laser ablation experiments. In fact, ASE-ablated worms show reduced chemotaxis to the water-soluble attractants sodium and chloride

ions, cAMP, biotin, lysine, and serotonin with a weak residual response distributed over numerous classes of neurons including ADF, ASG, ASI, ASK, and ASJ. Conversely the simultaneous ablation of all amphid and phasmid neurons except the ASE ones spares this behavior, indicating that the role of these neurons in water-soluble chemotaxis is unique (Bargmann, 2006).

ASER and ASEL neurons are functionally different. It is known, for example, that the ASER neuron preferentially senses chloride and potassium ions, while the ASEL one preferentially detects sodium ions. They have evolved particular regulatory devices recruiting a network of several homeobox genes and microRNAs to ensure their functional diversification.

Interestingly, these factors constitute a "bistable feedback loop" and the negative regulatory interaction between individual regulatory factors makes sure that the loop can exist in two states (hence "bistable"): in the ASEL cell, the result of the loop is the induction of a very specific subset of ASEL fate markers, while in the ASER cell, the loop operates with the "opposite" sign, thus causing the induction of the ASER fate. What determines the cell-type specific activity of the loop is currently unknown (Hobert, 2005; Bargmann, 2006).

10.4 Ciliary mutants

Many worm mutant strains that show peculiar phenotypes due to defects in cilia are available (Inglis *et al*, 2007).

Lipophilic dyes such as DiI (1,1'-dioctadecyl-3,3,3',3'-tetramethylindocarbocyanine perchlorate), DiO (3,3´-dioctadecyloxacarbocyanine, perchlorate) and FITC (fluorescein-5-isothiocyanate) fill 6 amphid (ASI, ADL, ASK, AWB, ASH and ASJ) and the two phasmid (PHA and PHB) neurons, but the mechanism of dye uptake is still unclear. Mutants that exhibited an abnormal dye filling (Dyf) phenotype were easily identified and analyzed to unravel the molecular perturbations causing the defect and it was found that not only abnormal cilia, but also an abrogated IFT could cause it (Starich *et al*, 1995). Besides, alterations to the ciliated neuron sheath and socket cells may also confer a Dyf phenotype, as for example in *daf-6* mutants whose cilia lose access to the environment. Caution has to be taken, since not always the lack of this phenotype implicates a proper cilium structure or function.

The osmotic avoidance abnormal (Osm) phenotype is characterized by the inability to avoid regions with high osmotic strength, such as 4 M NaCl or 8 M glycerol and is often associated with cilia defects in *C. elegans.*

As anticipated before, chemotaxis to both volatile and non-volatile compounds is dependent on cilia present at the tips of some sensory neurons and defects in this sensory process cause an abnormal chemotaxis (Che) phenotype (see next paragraph for details). Numerous *osm* and *che* mutants have been identified and it was discovered that they encode proteins essential for cilia structure and/or function.

Some ciliated sensory neurons have been connected to mechanosensation; in fact ciliary mutants *che-2*, *che-3*, *che-13*, *osm*-6*, che-12* and *osm-3* all show significantly reduced abilities to respond to a touch on the nose of the animal.

Several ciliary mutants display then abnormal responses to noxious temperatures, although the sensory neurons implicated in the response are still unidentified.

Moreover, male worms with defective cilia not only show compromised abilities in finding hermaphrodites, but also in locating the vulva and in ejaculation.

The abrogation of DAF-19 function, which leads to a complete loss of cilia (Perkins *et al*, 1986), results also in significantly longer-lived worms that constitutively enter the dauer stage, however it is not clear the mechanism linking DAF-19 and dauer phase, since only cilia-associated proteins have been shown to be regulated by this transcription factor (Inglis *et al*, 2007).

Moreover, laser ablation of certain ciliated neurons results in increased lifespan (Bargmann, 2006), and several ciliary mutants live longer, perhaps due to their altered sensory perception. The analysis of oxidative stress mutants showed that those resistant to paraquat frequently had defective cilia.

10.5 Functional characterization of *che-12*

Mutants in the nematode gene *che-12* were isolated in genetic screens for animals displaying dye uptake defects (Dyf phenotype), since their inability to hold FITC.

The *e1812* mutation in *che-12* was the first to be isolated and consists in a G-to-A transition that disrupts the predicted splice donor site of intron 16. It was reported that these mutants lacked matrix material normally secreted by the amphid sheath cell (Perkins *et al*, 1986)

The *che-12*(*mn389)* e the *che-12*(*mn399)* alleles were later identified after EMS treatment. The *mn389* allele has a 88-bp deletion that removes the last 47 nucleotides of exon 13; while the *mn399* allele harbors an 849-bp deletion, removing most of intron 12, exon 13, and the first 15 nucleotides of exon 14. Mutants displayed an abnormal dye filling phenotype (Starich *et al*, 1995).

Bacaj *et al* characterized nematodes carrying these mutations in homozygosis performing different staining and behavioral assays. They first of all found that one hundred percent of *che-12(e1812)*, *che-12(mn389)*, and *che-12(mn399)* animals failed to take up FITC in amphid neurons but only 2% of *che-12(e1812)* and *che-12(mn389)* mutants, and 51% of *che-12(mn399)* mutants failed to take up DiI and this different selectivity for dyes was not previously described.

They then reported an impaired chemotaxis of all *che-12* mutants toward the soluble attractant NaCl, a behavior controlled by the ASE amphid neuron and defects in avoidance of a high osmolarity 4 M fructose barrier, a phenotype mediated by the ASH amphid neuron. On the contrary mutant worms were normally attracted to the volatile odorants isoamyl alcohol (1%) and methyl pyrazine (1%), behaviors mediated by the AWC and AWA amphid neurons, respectively, and authors concluded that *che-12* is required for some, but not all, amphid cilia functions.

To determine the molecular basis of the Dyf and Che phenotypes showed by *che-12* mutants, the structure of the ASE neuron cilium was investigated, first of all with the use of the *gcy-5* pro::GFP ASER-specific reporter transgene (Yu *et al*, 1997). By fluorescent microscopy the length of the ASER cilium in *che-12(mn399)* animals was measured and it was found to be shortened compared to the corresponding wild-type controls (average length of 4.3 µm *versus* 6.1 µm).

The following analysis of *che-12(mn389)* mutants by electron microscopy revealed that the channel cilia of the analyzed animals lacked distal ciliary structures normally pervaded by singlet microtubules, however, the middle ciliary segment and the transition zone were intact.

The authors therefore suggested that *che-12* is important for the assembly of distal ciliary structures.

To characterize its expression, they generated a transgene bearing the 936-bp sequence located immediately upstream of the *che-12* translation start site fused to the gene encoding GFP and introduced it into wild-type animals. The analysis of the generated transgenic lines showed that *che-12* is expressed only in the subset of amphid neurons that lack wing- or finger-like ciliary extensions and in the two phasmid neurons, suggesting that this protein may only function in sensory neurons possessing simple cilia. Further experiments restricted *che-12* expression in the dendritic cilium.

The authors were also able to demonstrate that *che-12* is required both for development and for maintenance of a functional cilium, its expression is under the transcriptional control of DAF-19 and it requires a functional IFT to properly localize in the cilium, although it doesn't actively participate in IFT.

10.6 Identification and characterization of the Crescerin protein family

Colonic and hepatic tumor overexpressed gene (ch-TOG) and cytoskeletal linker protein 170–associated protein (CLASP) represent two distinct microtubule (MT)-associated protein (MAP) families that promote MT polymerization and pause, respectively. Both families use arrayed tubulin-binding TOG domains to regulate MT dynamics (Slep, 2009). A TOG domain consists of six HEAT repeats (HRs), elements that fold in pairs of antiparallel α-helices, forming an oblong, solenoid-like structure.

TOG domains bind tubulin using a series of intra-HEAT loops that are discontinuous in the primary sequence but line one face of the domain in the tertiary structure. The helices and intra-HEAT loops have significantly diverged in sequence during evolution, making the identification of new TOG domain–containing proteins really challenging.

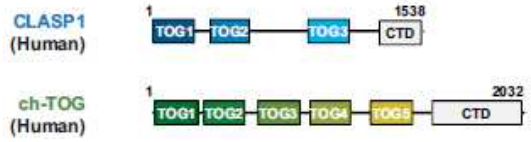

Fig. 29: Domain architecture of TOG family proteins ch-TOG and CLASP. CTD, C-terminal domain (adapted from Das *et al*, 2015).

Das *et al* investigated the presence of another TOG domain–containing protein family in eukaryotes and they found in the human proteome an uncharacterized protein, FAM179B (KIAA0423), that showed discontinuous sequence similarity to CLASP TOG1 and is a member of a protein family conserved in ciliated/flagellated eukaryotes ranging from mammals to unicellular eukaryotes, but absent in non-ciliated eukaryotes, including yeast. They named the protein family, whose only characterized member was so far the *C. elegans* CHE-12 protein, and its unnamed members Crescerin. Consistent with the expression of *che-12* already highlighted by Bacaj *et al*, they found that mammalian members of Crescerin1 subfamily, which contains four protein domains, localize at the primary cilium and basal body in cells.

They then cloned and purified all four conserved domains from mouse Crescerin1, to determine if the Crescerin family represents a novel TOG domain array–containing protein family.

Crystals were obtained for the second conserved domain (residues 332–620), and they demonstrated that it is a true TOG domain, consisting of 12 helices that pair into six tandem HRs (A–F) and stack, forming a 60-Å oblong solenoid.

So, this domain was designated a TOG domain, in particular as TOG2, confirming that Crescerin represents a third, unique TOG domain–containing protein family.

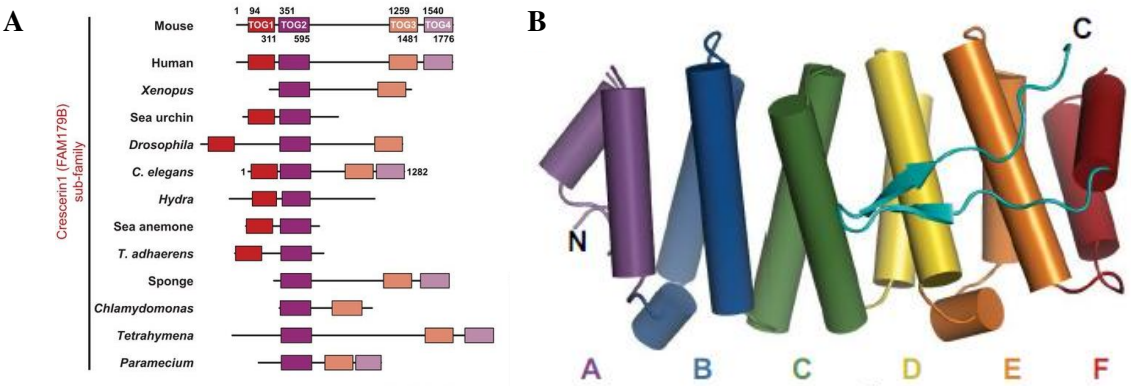

Fig. 30: A) Domain architecture of Crescerin family. Sequence analysis of Crescerin family proteins across species reveals a variable number of TOG domains and variable lengths of inter-TOG domain linkers. In each organism, the domains are colored according to the mouse Crescerin1 (FAM179B) TOG domain to which they are most similar in amino acid sequence. The Crescerin1 subfamily contains proteins with TOG domains similar to the N-terminal pair of TOG domains in mouse Crescerin1. Some organisms, including mammals, contain a separate gene (FAM179A) with two TOG domains that are similar to the C-terminal pair of TOG domains in mouse Crescerin1. These proteins are grouped under the Crescerin2 subfamily. B) Crystal structure of Crescerin1 TOG2. Each HR (A–F) and the C-terminal β-hairpin are shown in different colors (adapted from Das *et al*, 2015).

To determine whether Crescerin might regulate the MT cytoskeleton, the ability of mouse Crescerin1 TOG domains to influence MT polymerization *in vitro* was tested, and it was found that TOG2 and TOG4 dramatically increased the rate of MT polymerization while mutations in these domains

abrogated it, suggesting that they use canonical tubulin-binding determinants to induce MT polymerization.

To investigate how Crescerin affects cilia structure and function, *C. elegans* was used as a model system, given the difficulty to exercise precise temporal control on Crescerin expression in mammalian cells in a way that matches endogenous levels at different cell cycle stages.

The already characterized *che-12*(*mn389)* e the *che-12*(*mn399)* mutations truncate the CHE-12 protein after the second TOG domain and may not behave as null alleles. In order to evaluate the effect of complete loss of CHE-12 function, the authors employed the CRISPR/Cas9 technology to delete the entire *che-12* coding sequence and replace it with that of GFP.

As expected, the resulting Δ*che-12* animals expressed GFP primarily in the amphid and phasmid sensory neurons, with signal observed in the cell body and dendrite.

To probe the role of CHE-12 in cilia structure, they measured cilium length in ASER neurons, finding that Δ*che-12* cilia were dramatically shorter, with an average length of 3.2 μm, compared to those of wild-type worms (7.0 μm). The more severe 54% decrease in cilia length observed in Δ*che-12* animals compared to *che-12*(*mn389)* and *che-12*(*mn399)* mutants suggests that the hypomorphic strains may retain partial CHE-12 function.

To assay if CHE-12 uses canonical tubulin-binding determinants across its tetra-TOG domain array, Das *et al* used CRISPR/Cas 9 technology to mutate a conserved hydrophobic residue on the predicted tubulin-binding surface of each TOG domain HR A intra-HEAT loop (F34, A281, W815, W1073) to glutamate, naming this mutant as TOG-1′2′3′4′, and at the same time they introduced a GFP tag. After having verified that GFP was expressed at the cilia level, indicating that tubulin-binding via TOG domains is not necessary for CHE-12 cilia localization, they measured cilia length founding that it was dramatically reduced in the GFP::CHE-12 TOG-1′2′3′4′ mutant, with an average length of 3.4 μm. These results strongly suggest that CHE-12 promotes proper cilia structure and length through mechanistic use of its TOG array's tubulin-binding activity.

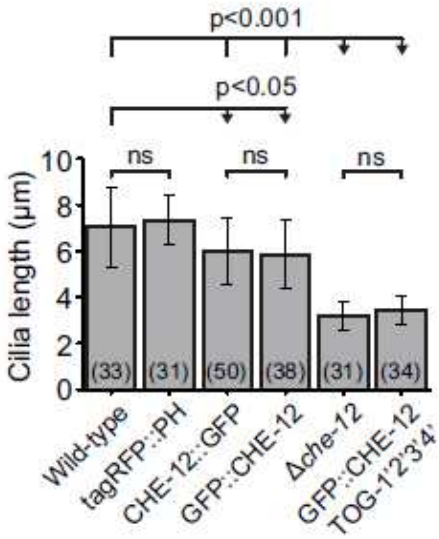

Fig. 31: ASER cilium length measurements. Values in parentheses indicate number of cilia measured for each strain; error bars indicate standard deviation. Besides wild-type and Δ*che-12* animals, GFP-tagged CHE-12 strains (both CHE-12::GFP and GFP::CHE-12), a control strain that expresses a labeled nonneuronal protein (tagRFP::PH) in the same genetic background, and GFP::CHE-12 TOG-1′2′3′4′ mutants (see above for details) were assayed (adapted from Das *et al*, 2015).

These results were then integrated with the ultrastructure analysis at electron microscopy. In contrast with wild-type worm cilia, those of Δ*che-12* and GFP::CHE-12 TOG-1′2′3′4′ mutant had poorly defined MT architecture at their proximal ends and no apparent MTs toward their distal ends.

Since it had already been shown that *che-12* hypomorphic mutants had an impaired ability to chemotax on a NaCl gradient, as well as to take up and hold lipophilic dyes (Perkins *et al*, 1986, Starich *et al*, 1995; Bacaj *et al*, 2008), the authors decided to investigate these behaviors also in case of complete deletion of *che-12* or mutations of the CHE-12 TOG domains.

Worms were placed in the center of agar plates containing either an isocratic 30 mM NaCl concentration (control plate) or a linear 0–60 mM NaCl concentration gradient and their migration was scored after 30 minutes.

Differently from wild-type worms, Δ*che-12* and GFP::CHE-12 TOG-1′2′3′4′ mutant worms were unable to sense and respond to the gradient, showing the same pattern of distribution of isocratic control plates.

Similar results were obtained using a dye-uptake assay to evaluate ciliary function, in which the Δ*che-12* and GFP::CHE-12 TOG-1′2′3′4′ mutant strains showed dramatically reduced dye-uptake frequencies compared with wild-type worms. Thus, the effects of mutating the CHE-12 TOG domains on cilia length and ultrastructure correlate with amphid cilia–mediated behavior in the whole animal.

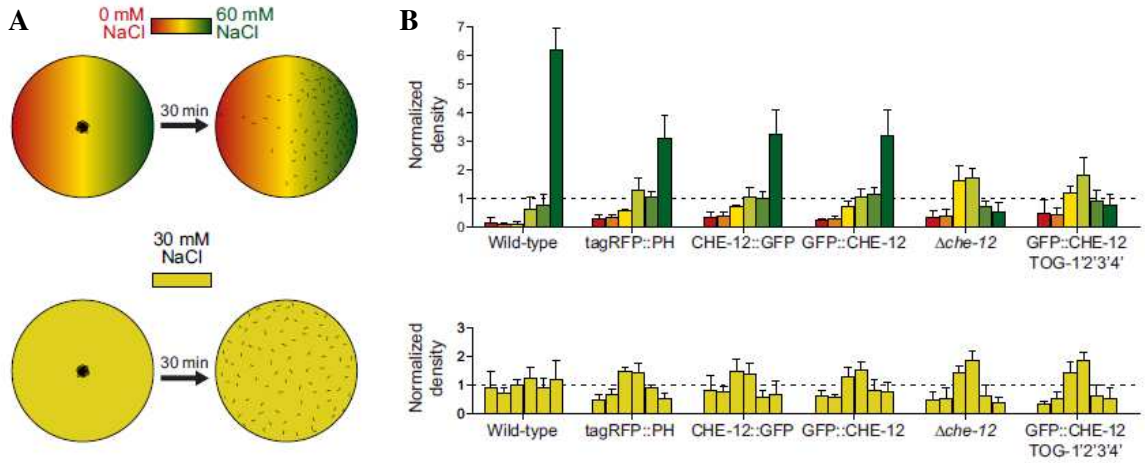

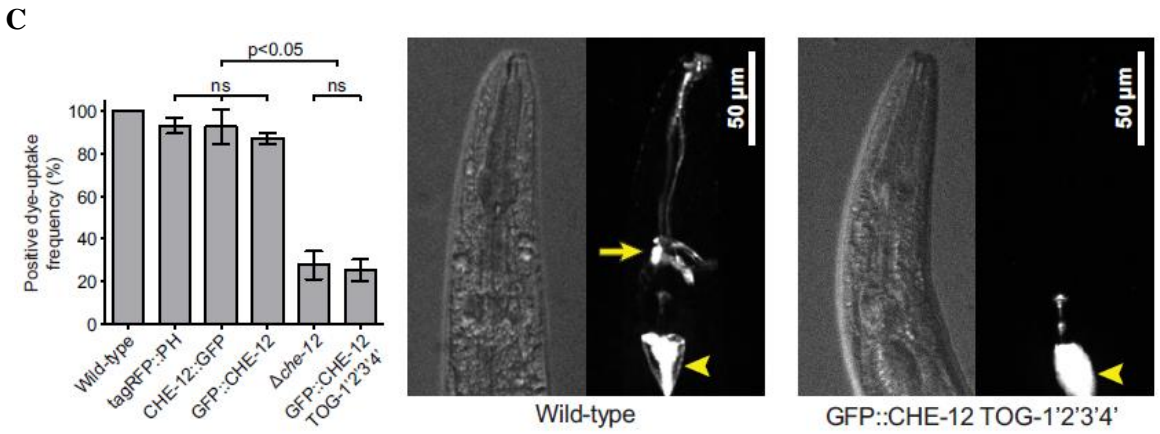

Fig. 32: A) Schematic diagram of *C. elegans* chemotaxis assay on a 0–60 mM NaCl gradient (red–green) or 30 mM NaCl isocratic (yellow) agar plates. B) Bar graph showing the normalized density of worms in different sections of the plate. Error bars indicate standard deviation. C) On the left quantification of DiI uptake assay in different worm strains. Error bars indicate standard deviation. On the right, images showing strong dye-filling in WT *C. elegans* amphid neurons (yellow arrow) and no dye filling in GFP::CHE-12 TOG-1′2′3′4′ amphid neurons. The gut staining due to feeding is indicated by a yellow arrowhead (adapted from Das *et al*, 2015).

Summarizing, the work of Das *et al* identified Crescerin as a novel TOG domain array–containing protein family. They found that Crescerin1 localizes to primary cilia in mammalian cells and uses its TOG domains array to promote MT polymerization *in vitro*. In *C. elegans* CHE-12 requires canonical TOG tubulin-binding determinants for correct sensory cilia development.

10.7 Ciliopathies

Ciliopathies comprise a group of disorders associated with mutations in genes that encode for ciliary proteins, leading to abnormal formation or function of cilia (Reiter *et al*, 2017). As cilia are a component of almost all cells, ciliary dysfunction can manifest as a spectrum of features that include primarily cerebral anomalies, retinal degeneration and renal disease. Additional symptoms include congenital fibrocystic diseases of the liver and pancreas, diabetes, obesity and skeletal dysplasias (Waters and Beales, 2011).

These group of disorders is highly heterogeneous and complex to comprehend both clinically and genetically (Thomas *et al*, 2019). Mutations in over 180 genes have been associated with ciliopathic features so far and considering the growing number of ciliome members (more than 420 proteins up until now), several other disorders associated with this broad range of clinical signs will likely be ascribed to mutations in newly identified ciliary genes (Reiter *et al*, 2017).

The notion of a "ciliopathic" disorder was first attributed to Bardet–Biedl syndrome (MIM# 209900), a multisystemic disorder characterized by retinal degeneration, cystic kidney disease or urinary tract malformation, cognitive impairment, diabetes mellitus, obesity, infertility, and postaxial polydactyly, when a mutation in *BBS8*, a member of the BBSome complex, was discovered (Waters and Beales,

2011; Thomas *et al*, 2019). Mutations in 21 genes are known to cause this syndrome (Suspitsin and Imyanitov, 2016).

Joubert syndrome (MIM# 213300) is characterized by hypotonia, ataxia, psychomotor delay, irregular breathing pattern and oculomotor apraxia with the distinctive "molar tooth sign" on brain MRI (Waters and Beales, 2011). It has been associated with mutations in over 30 genes, among which *NPHP6/CEP290*, a gene encoding a centrosomal protein, is most frequently mutated.

Meckel–Gruber syndrome (MKS; MIM# 249000) is an autosomal recessive disease that leads to perinatal death. Clinical features include occipital encephalocele and other posterior fossa defects, cystic dysplastic kidneys, hepatic bile duct proliferation, polydactyly and *situs inversus*. Mutations in 14 distinct genes have been reported in MKS to date, including *MKS1*, *MKS3*, *NPHP3*, *NPHP6/CEP290*, *NPHP8/RPGRIP1L*, *TMEM216*, and *CC2D2A* (Hildebrandt *et al*, 2011; Hartill *et al*, 2017).

Orofaciodigital syndrome type 1 (MIM# 311200) is a rare X-linked dominant disorder, whereby affected males die in utero. Characteristic features include malformation of the oral cavity, face and digits, in addition to central nervous system abnormalities and cystic kidney disease. Mutations in *OFD1*, which encodes a centrosomal protein localized at the basal body, have been described in patients (Waters and Beales, 2011), and more recently in other genes.

A spectrum of renal diseases has been described as a feature of several ciliopathic syndromes and includes a morphologically heterogeneous group of disorders (Waters and Beales, 2011; Hildebrandt *et al*, 2011).

Polycystic kidney disease is a group of monogenic disorders, characterized by the presence of multiple kidney and liver cysts, that can arise both in the neonatal period as well as in adulthood and are inherited in an autosomal dominant (MIM# 173900) or recessive (MIM# 263200) fashion. The dominant form is caused by mutations in *PKD1* (in the majority of cases) and *PKD2* genes, which respectively encode polycystin-1 and polycystin-2. In the recessive form pathogenic variants in *PKHD1*, which encodes for the protein fibrocystin, have been identified (Devlin and Sayer, 2019).

Nephronophthisis (MIM# 256100) is the most common genetic cause of chronic kidney disease within the first three decades of life and it is characterized by cysts that are mainly restricted to the corticomedullary junction. Mutations in more than 25 genes are associated with this ciliopathy, among which NPHP is most frequently affected, accounting for approximately 20% of cases. In roughly two thirds of cases the causative gene is unknown (Waters and Beales, 2011; Luo and Tao, 2018).

10.7.1 *C. elegans* as a model to study ciliopathies

Studies conducted in *C. elegans* were fundamental to link ciliopathies to cilia (Bae and Barr, 2008). In fact, the discovery that the orthologue protein of human polycystin-1 was expressed in worm ciliated

neurons raised the idea that dysfunction of nonmotile cilia might play a role in human disease (Barr and Sternberg, 1999; Hildebrandt *et al*, 2011).

Indeed the *C. elegans* genome contains many of the human ciliopathy disease genes, as those associated with defects in renal cilia function (Inglis *et al*, 2007; Bae and Barr, 2008).

Mutations in worm homologues of the polycystic kidney-disease loci *PKD1* and *PKD2*, *lov-1* and *pkd-2*, were shown to produce defects in male mating behavior. Additionally, it has been shown that *C. elegans* LOV-1 is required for the proper targeting of PKD-2 to the cilium of the male-specific neurons CEM, as well as eight pairs of ray neurons.

Studies in *C. elegans* also provided the first evidence that BBS proteins are essential ciliary proteins that contribute to IFT by stabilizing the association between kinesin motors and intraflagellar subcomplex assemblies. Notably, all but 3 of the 11 known human *BBS* genes possess worm orthologues, making the nematode an excellent model system to study Bardet–Biedl syndrome.

The worm *NPHP* homologues *nphp-1, nphp-2*, and *nphp-4* are expressed in the ciliated nervous system of males and hermaphrodites and *nphp-1* and *nphp-4* appear to play cell-type specific roles in cilia formation, ciliary length control, and sensory signal transduction. *nphp-2* encodes for a protein that localizes to the middle segment of sensory cilia and is partially redundant with *nphp-1* and *nphp-4* for cilia placement within the head and tail sensilla.

Two genes, *MKS1* and *MKS3*, associated with MKS, were recently cloned, and both of their *C. elegans* homologues (*mks-1/xbx-7* and *mks-3* respectively) were found to be specifically expressed in ciliated sensory neurons (Inglis *et al*, 2007).

It was also demonstrated that several genes, whose mutations cause nephronophthisis and MKS, form two distinct complexes that both localize to the cilia transition zone. Both complexes are required for proper function of the transition zone as a ciliary gate to regulate which proteins are present in the cilium. Accordingly, it was found in *C. elegans* that while individual *nphp* or *mks* mutants have mild defects in cilia structure and function, worms with mutations in both *nphp* and *mks* genes have severe ciliary defects that include malformed, misoriented, mispositioned and lacking cilia (Masyokova *et al*, 2016).

Furthermore, it has been shown that *nphp-2* genetically interacts with the worm orthologues of MKS ciliopathy genes, including *mks-1*, *mks-3*, *mks-6*, *mksr-1* and *mksr-2*, in a sensilla-dependent manner to control cilia formation and placement, but it is not required for correct localization of the NPHP- and MKS-encoded ciliary transition zone proteins or for IFT (Warburton-Pitt *et al*, 2012).

Thus, considering that *C. elegans* has proved a useful model to study genes whose mutations are involved in ciliopathies, we decided to examine the functional consequences of a novel genetic variant identified in the human gene *TOGARAM1* in patients with a Meckel-Gruber-like phenotype, by generating a knock-in model harboring the same variant in the worm orthologue gene *che-12*.

11 Results

11.1 Identification of a missense variant in *TOGARAM1* gene

TOG array regulator of axonemal microtubules 1 (*TOGARAM1*, MIM# 617618), also known as *FAM179B,* is the human orthologue of worm *che-12*.

The gene localizes on chromosome 14q21.2, it consists of 22 exons and codes for a protein of 1773 amino acids (NCBI Reference Sequence NP_001295049.1), which was recently identified by Das *et al*, through the discovery of Crescerin as a novel TOG domain array–containing protein family.

TOGARAM1 has never been associated with a human disease so far.

Recently, genetic analysis was carried on two siblings fetuses, with a familial history compatible with an autosomal recessive inheritance, both showing a severe malformation of the central nervous system compatible with a Meckel-Gruber-like phenotype.

Whole exome sequencing (WES) analysis identified two heterozygous variants in *TOGARAM1* in the DNA from the two affected siblings: a missense variant, that is [p.(Arg368Trp] leading to the substitution of an arginine residue with a tryptophan one, and a truncating allele, resulting in protein degradation. Segregation analysis showed that each variant was inherited from a healthy parent.

Prediction softwares suggested a pathogenic role of the missense variant since it could perturb the structure of the HR in the TOG2 region, with possible effects on protein folding; moreover, alignments of multiple protein sequences from different species showed that it affected a highly conserved arginine residue (Fig. 33).

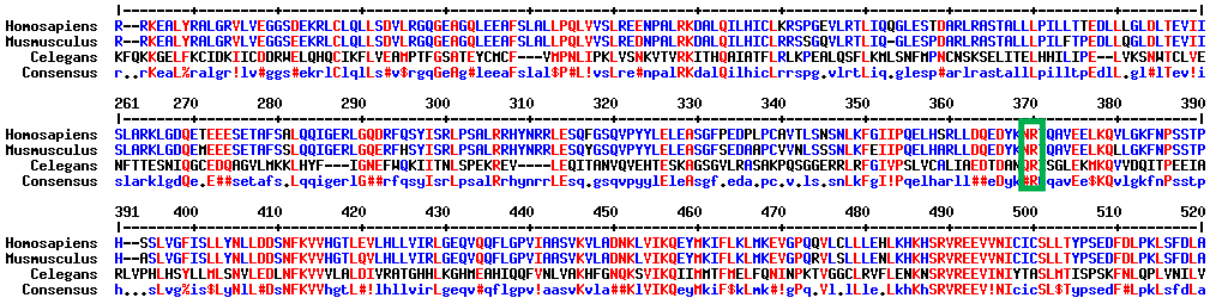

Fig. 33: Alignments of human (NP_001295049.1), mouse (NP_808473.2) and *C. elegans* (NP_001256204.1) TOGARAM1 protein sequences portions highlighting that the arginine residue of interest is conserved among species (green box).

The mutated arginine lies just under the first tubulin binding loop of the domain and the substitution of a tryptophan in that position could alter the binding loop's orientation, affecting as a consequence tubulin binding (Fig 34 A and B).

The demonstration of the pathogenicity of this variant could establish an important link between mutations in this gene and ciliopathies.

A

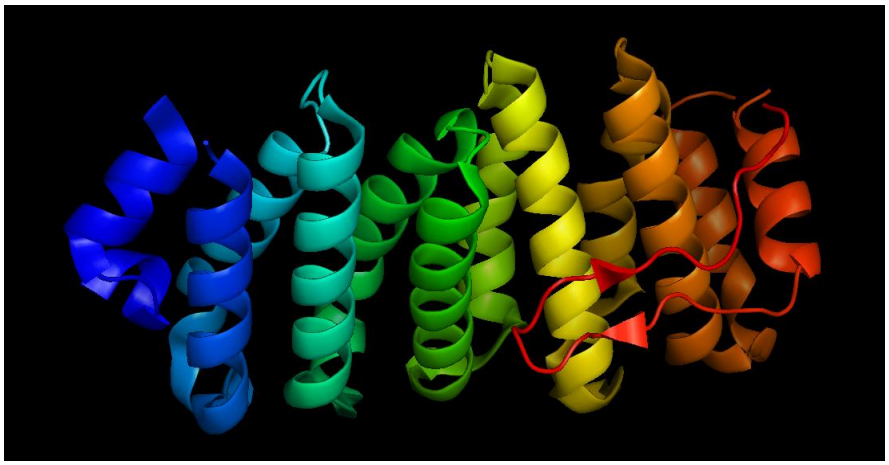

B

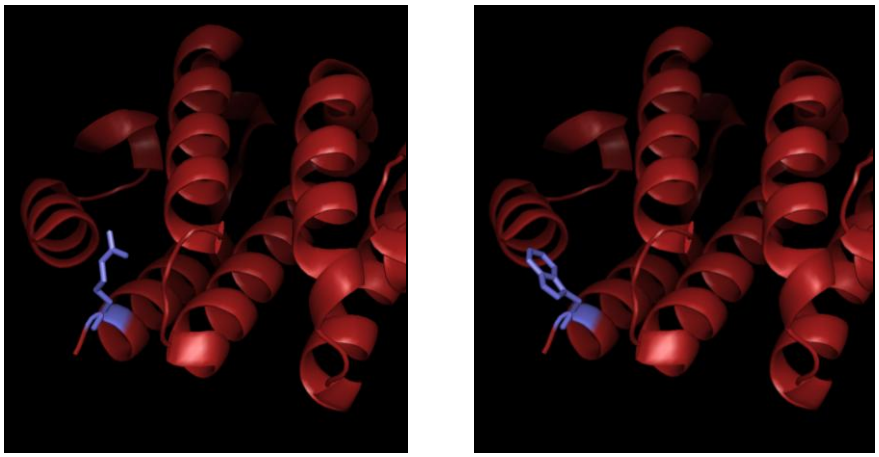

Fig. 34: A) The crystal structure of mouse TOG2 domain (PDB database, http://www.rcsb.org/, accession number 5DN7) with 12 helices that pair into six tandem HRs (represented in different colors) and a final C-terminal β-hairpin depicted in red. B) This structure has been used to model the missense mutation in analysis in the corresponding position of the mouse TOG2 domain (amino acid 367). On the left, the wild-type domain structure harboring an arginine in position 367, while on the right the domain carrying a tryptophan in the same position. The wild-type and mutated amino acids are depicted in violet.

11.2 Generation of a worm knock-in model to investigate the p.(Arg368Trp) variant in *TOGARAM1* gene

Since the worm homologue *che-12* was already characterized in worms, with mutants showing a peculiar and discernible phenotype and the novel mutation affects an extremely conserved residue across species, we decided to employ *C. elegans* as model to investigate the effects of this variant on *TOGARAM1* function.

CRISPR/Cas9 technology was chosen to generate the knock-in nematode strain harboring the same amino acidic substitution in the corresponding position of the worm orthologue, that is p.(Arg284Trp). We designed a crRNA to target in exon 6 the closest PAM sequence to the site of the desired edit. The repair DNA template contained the codon TGG to substitute the wild-type arginine residue (codon

AGA) with a tryptophan amino acid and some silent nucleotide changes in order to insert a restriction site for the EcoRV enzyme (-GATATC-), useful for mutant screening, and to prevent a second cut by Cas9 endonuclease.

After verifying the efficacy of the chosen crRNA with an *in vitro* digestion of the target locus with the purified Cas9 protein (Fig. 35 A), we performed worm injections in collaboration with Dr. Martinelli at the Istituto Superiore di Sanità in Roma, following a protocol modified from Paix *et al*, 2015.

We experienced some trouble to obtain the desired edit and eventually we succeeded adding to the protocol 1 or 10 µM of 5-azacytidine, namely a demethylating agent that decompacts chromatin. Three lines were obtained, *che-12*(*pan11*[R284W (AGA>TGG)]) *V*, *che-12*(*pan12*[R284W (AGA>TGG)]) *V* and *che-12*(*pan13*[R284W (AGA>TGG)]) *V*. The backcross with the wild-type strain was performed twice to eliminate possible off-targets effects introduced by CRISPR/Cas9 genome-editing. Worms were genotyped by an enzymatic digestion with the EcoRV restriction enzyme of the PCR products that include the region comprised between exon 5 and exon 7 of *che-12*, containing the variant of interest (Fig. 35 B, see table 4). The PCR were also sequenced to confirm the presence of the missense mutation (Fig. 35 C). Two independent lines, sometimes referred to as PAN11 and PAN12 in text and figures onwards, were used in the experiments.

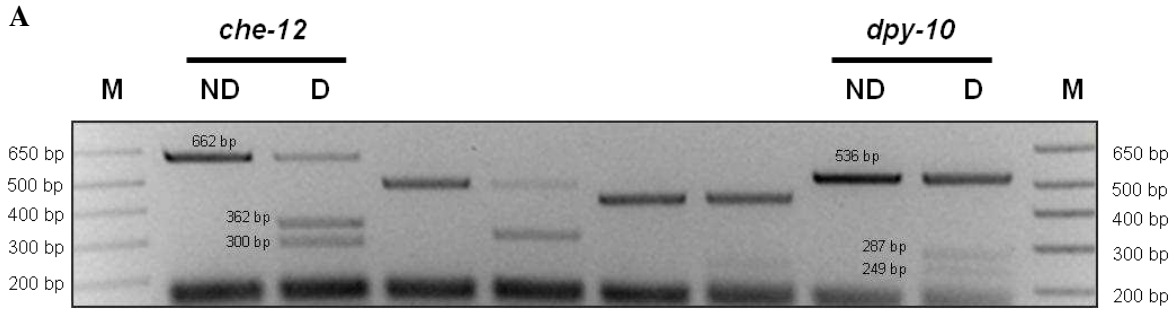

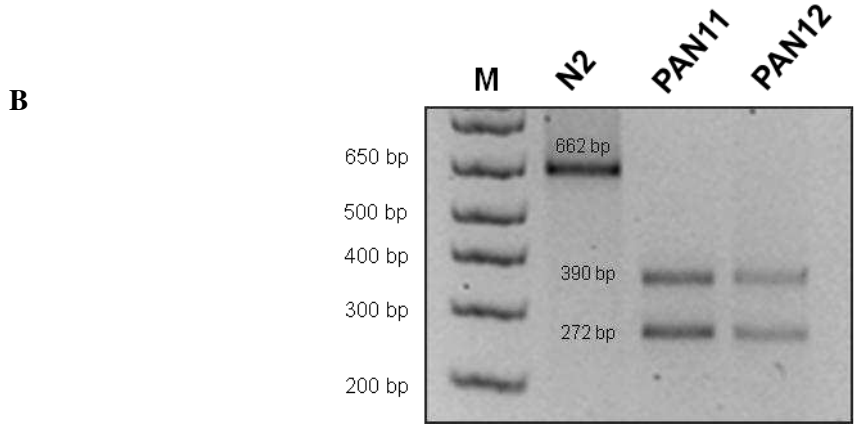

C

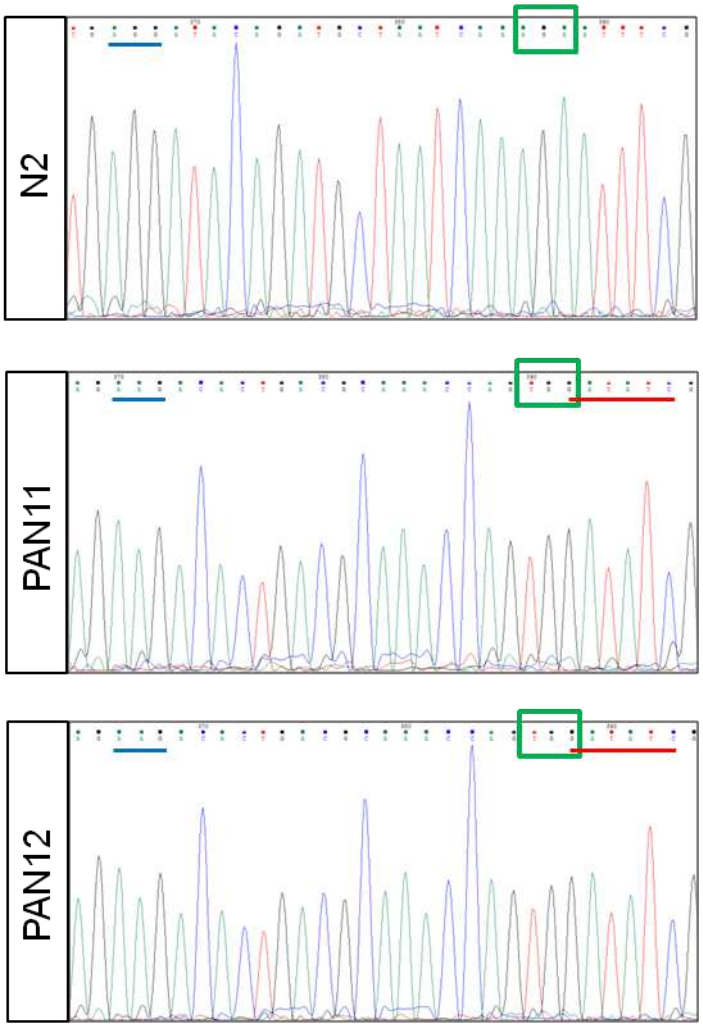

Fig. 35: A) *In vitro* digestion of *che-12* and *dpy-10* CRISPR target loci with the purified Cas9 protein. After genomic DNA extraction from worms, a PCR reaction was performed using forward and reverse primers that encompass the genomic region to be edited and then incubated with the crRNA and Cas9 protein. A negative control was included in each reaction, consisting of the mix devoid of Cas9. The digestions were then run on a 2% agarose gel; M: 1 Kb plus molecular marker. B) Genotyping of *che-12* knock-in worms. A PCR reaction was performed to amplify a portion of *che-12* locus comprised between exon 5 and exon 7 (662 bp) of the gene and then digested with the restriction enzyme EcoRV. The products were run on a 2% agarose gel and a representative agarose gel image is depicted, showing the genotyping of N2, PAN11 and PAN12 worms. The PCR obtained from N2 worms do not contain any EcoRV restriction site, while those from PAN11 and PAN12 lines not only harbor the variant of interest, but also the EcoRV restriction site in both alleles, so the result of digestion is the formation of two lower products (390 and 272 bp). C) Sanger sequencing from N2, PAN11 and PAN12 worms highlighting the PAM sequence (blue line), before (N2) and after (PAN11 and PAN12) editing, the introduction of the TGG (in PAN11 and PAN12) codon instead of AGA (in N2) (green box) and of the restriction site for EcoRV (red line, in PAN11 and PAN12).

11.3 Inclusion of hypomorphic and amorphic *che-12* mutants in phenotypic assays

Besides wild-type worms and two knock-in strains for *che-12* (*che-12*(*pan11*[R284W (AGA>TGG)]) *V* and *che-12*(*pan12*[R284W (AGA>TGG)]) *V*), a strain carrying a partially deleted CHE-12 protein

(SP1620) and one where *che-12* was totally ablated by CRISPR/Cas9 (LP177) were used in the phenotypic assays.

We purchased the SP1620 strain, that carries the *che-12*(*mn389)* allele, from CGC, while the Δ*che-12* strain was a kind gift from Prof. Kevin Slep (see table 2).

PCR reactions were performed in order to check strain genotype before proceeding to the experiments (see table 4) and an example is depicted in Fig. 36.

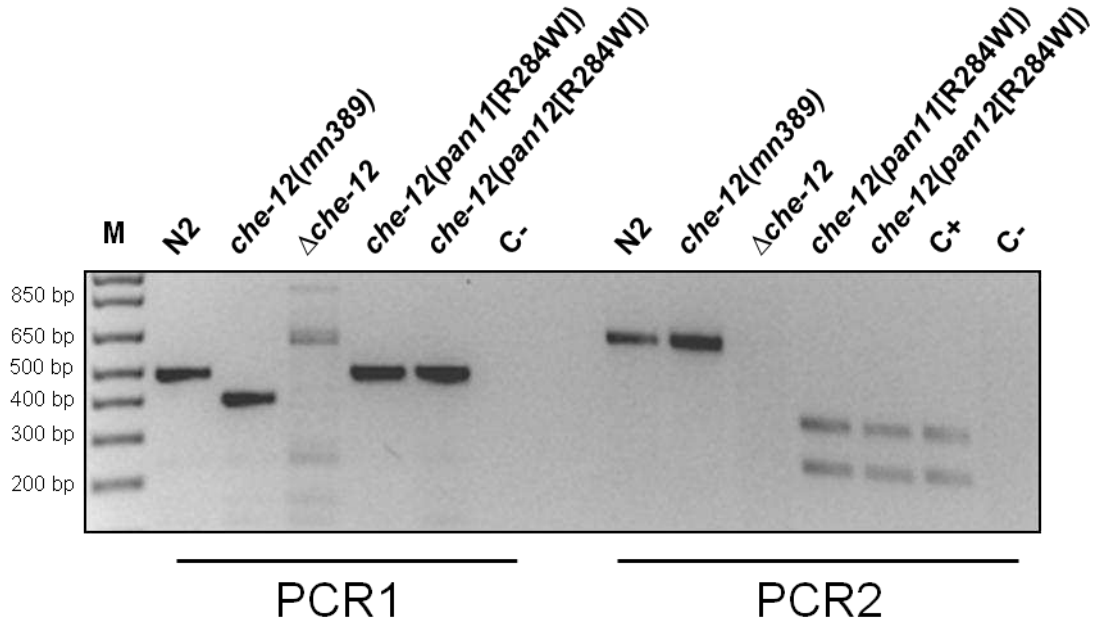

Fig. 36: An exemplificative agarose gel image of strain genotyping. Two PCR reactions were performed, the first using primers designed on intron 12 and exon 14 of *che-12*, the second with primers designed on exon 5 and 7 of the same gene. In the first reaction the wild-type product is 493 bp, while if the 88 bp deletion of allele *che-12(mn389)* is present the product is 405 bp. In the Δ*che-12* strain no PCR amplification is evident, apart from aspecific products, since the *che-12* locus is deleted. The product of the second reaction is 662 bp. PCR were then digested with EcoRV, in a similar way as depicted in Fig. 35 B. While products from N2 and SP1620 worms do not contain any EcoRV restriction site, those from PAN11 and PAN12 lines harbor the EcoRV restriction site in both alleles, so the result of digestion is the formation of two lower products (390 and 272 bp). As before, in the Δ*che-12* strain no PCR amplification is evident. M: 1 Kb molecular marker, C^+: a positive control for the digestion with EcoRV enzyme, C^-: negative control of PCR.

11.4 Chemotaxis assay

To measure the capability of *che-12* strains carrying the p.(Arg284Trp) missense variant to chemotax on a linear NaCl gradient, we performed the assay as reported by Das *et al*.

Adult synchronized worms were seeded on agar plates prepared to obtain a 0-60 mM NaCl gradient and on control isocratic plates containing 30 mM of NaCl.

After 30 min of free run, the plates were cooled to 4°C to paralyze worms and the number of worms in each of the 6 parallel sectors along the plate's linear NaCl gradient was counted. Finally the normalized worm density for each sector was calculated.

When worms were seeded on control isocratic plates, they did not sense any salt gradient and the direction of their movements was totally random. On these plates the normalized density of each sector should be 1. This was the case of N2, PAN11 and PAN12 strains, while the hypomorphic mutant [*che-12*(*mn389)*, strain SP1620] and the amorphic one (Δ*che-12*, strain LP177) showed lower density indexes in peripheral sectors (Fig. 37 A).

For what concerns gradient plates, wild-type worms efficiently sensed NaCl gradient and migrated towards the high-salt end, resulting in a high normalized density for sector 1, which has in fact the highest NaCl concentration. On the contrary, the hypomorphic and amorphic mutants were not attracted to zones with high salt concentration and their pattern of migration was very similar in gradient and control plates. The knock-in strains PAN11 and PAN12 behaved similarly to wild-type and were strongly attracted to the high-salt end (Fig. 37 B).

A

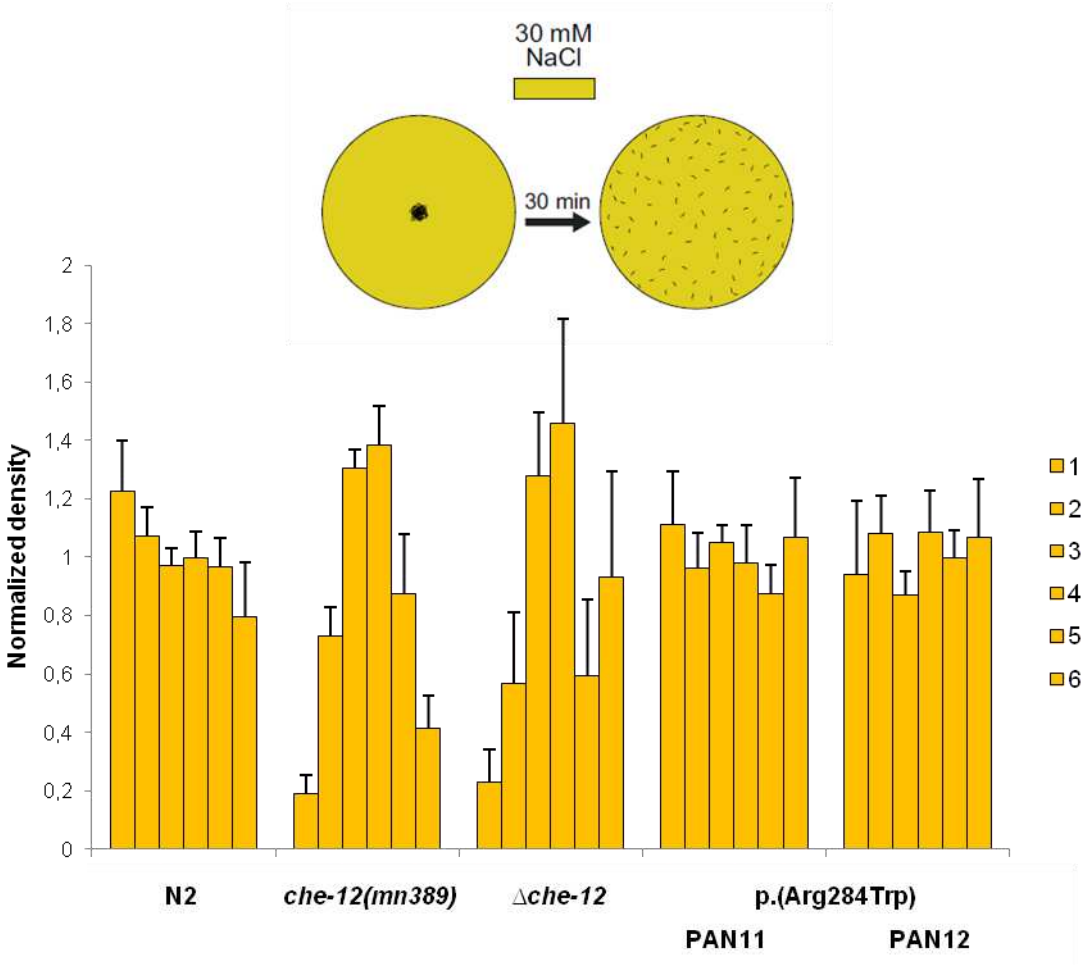

B

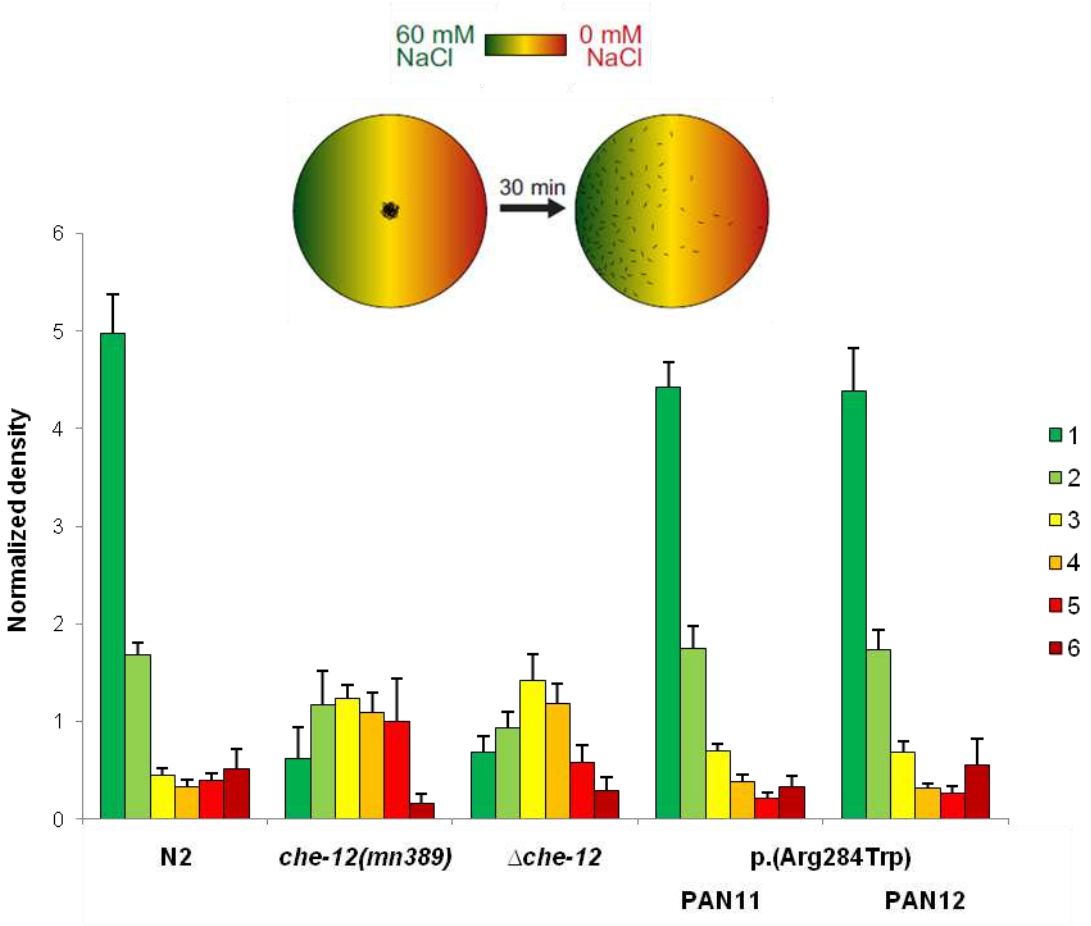

Fig. 37: Chemotaxis assay performed on N2 (wild-type), SP1620 [*che-12*(*mn389)*], LP177 (Δ*che-12*), PAN11 [p.(Arg284Trp)] and PAN12 [p.(Arg284Trp)] strains. Worm populations were synchronized and once adults they were seeded in the center of control isocratic plates prepared with 30 mM NaCl (A), or of plates with a linear 0-60 mM NaCl gradient (B). In both cases, after 30 minutes of free run, plates were cooled down at 4 °C in order to paralyze worms and the normalized density for each of the six parallel sectors of the plate was counted. In A) worms did not sense any gradient, as shown in the scheme above quantitations, so they moved in a random way and the normalized density was about 1 for all sectors. This value was lower in peripheral sectors in SP1620 and LP177 strains. In B) worms were exposed to a linear NaCl gradient, ranging from 0 mM at the low-salt end (sector 6), to 60 mM at the high-salt end (sector 1), as schematically depicted above quantitations. N2, PAN11 and PAN12 strains were attracted towards sector 1, which displays a high normalized density, and moved away from zones at low salt concentration resulting in very low normalized density values. On the contrary, SP1620 and LP177 strains behaved similarly to control isocratic plates, showing a tendency to stay in central sectors.

11.5 Dye-uptake assay

Wild-type worms, two knock-in strains for *che-12* (*che-12*(*pan11*[R284W (AGA>TGG)]) *V* and *che-12*(*pan12*[R284W (AGA>TGG)]) *V*), SP1620 and LP177 mutants were assayed for the dye-uptake capability with two dyes, the Vybrant™ CM-DiI (ThermoFisher Scientific) and FITC isomer I (Sigma-Aldrich), since it has been demonstrated that sensory amphid neurons can efficiently take up and concentrate lipophilic dyes (Bacaj *et al*, 2008).

Nematodes populations were synchronized, adult worms were collected in M9 and incubated with dyes (see paragraph 3.4.5) and then imaged at fluorescent microscope.

For what concerns Vybrant™ CM-DiI staining, about 95% of wild-type worms held the dye. Conversely, *che-12* hypomorphic and amorphic mutants displayed a reduced frequency of dye uptake, with the strain lacking CHE-12 showing a stronger impairment (63% and 30% of positive animals, respectively). Knock-in strains PAN11 and PAN12 were able to take up and hold DiI staining, although in a slightly reduced way compared to wild-type animals (86% and 93% of positive worms) (Fig. 38).

A

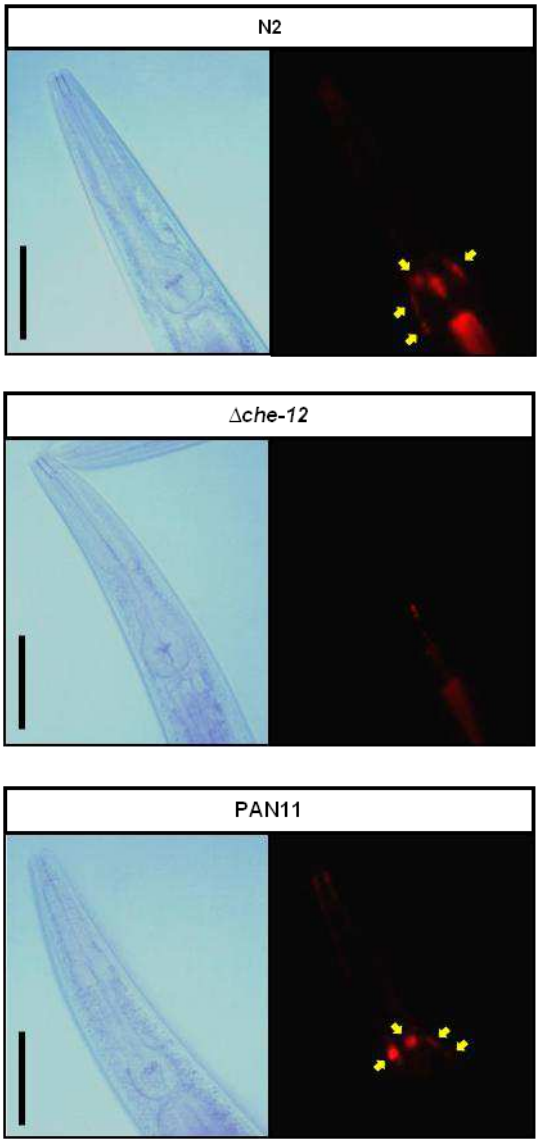

B

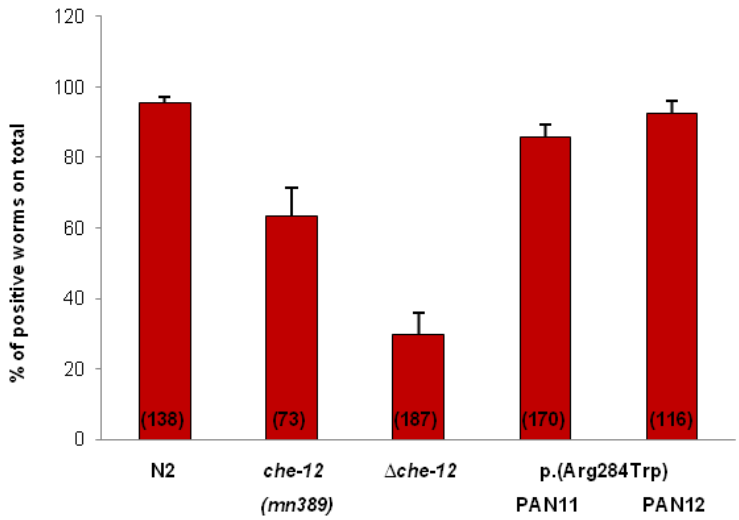

C

	p-value
N2 – *che-12(mn389)*	p< 0.01
N2 – Δ*che-12*	p< 0.001
N2 – p.(Arg284Trp) PAN11	p< 0.05
N2 – p.(Arg284Trp) PAN12	NS
che-12(mn389) – Δ*che-12*	p< 0.01
che-12(mn389) – p.(Arg284Trp) PAN11	p< 0.001
che-12(mn389) – p.(Arg284Trp) PAN12	p< 0.01
Δ*che-12* – p.(Arg284Trp) PAN11	p< 0.001
Δ*che-12* – p.(Arg284Trp) PAN12	p< 0.001
p.(Arg284Trp) PAN11– p.(Arg284Trp) PAN12	NS

Fig. 38: Vybrant™ CM-DiI staining. In A) representative images of DiI staining in N2, Δ*che-12* and PAN11 (*che-12*(*pan11*[R284W (AGA>TGG)]) *V*) worms. Yellow arrows indicate stained amphid neurons. Scale bar, 50 µm. In B) quantification of worms in each strain with stained amphid neurons. The graph represents the mean of two independent experiments and between brackets the total number of assayed worms is indicated. The bars indicate the standard error of the mean and the results were compared using the unequal variance *t*-test. In C) the results of the statistical analysis are reported. NS, not significant.

For what concerns FITC staining, 100% of wild-type worms held the dye. As in the case of Vybrant™ CM-DiI staining, *che-12* hypomorphic and amorphic mutants displayed a reduced frequency of dye uptake, with the strain lacking CHE-12 showing a stronger impairment (79% and 16% of positive animals, respectively). Knock-in strains PAN11 and PAN12 were able to take up and hold FITC staining, with percentages very similar to that of wild-type animals (97 and 99% of positive worms) (Fig. 39).

A

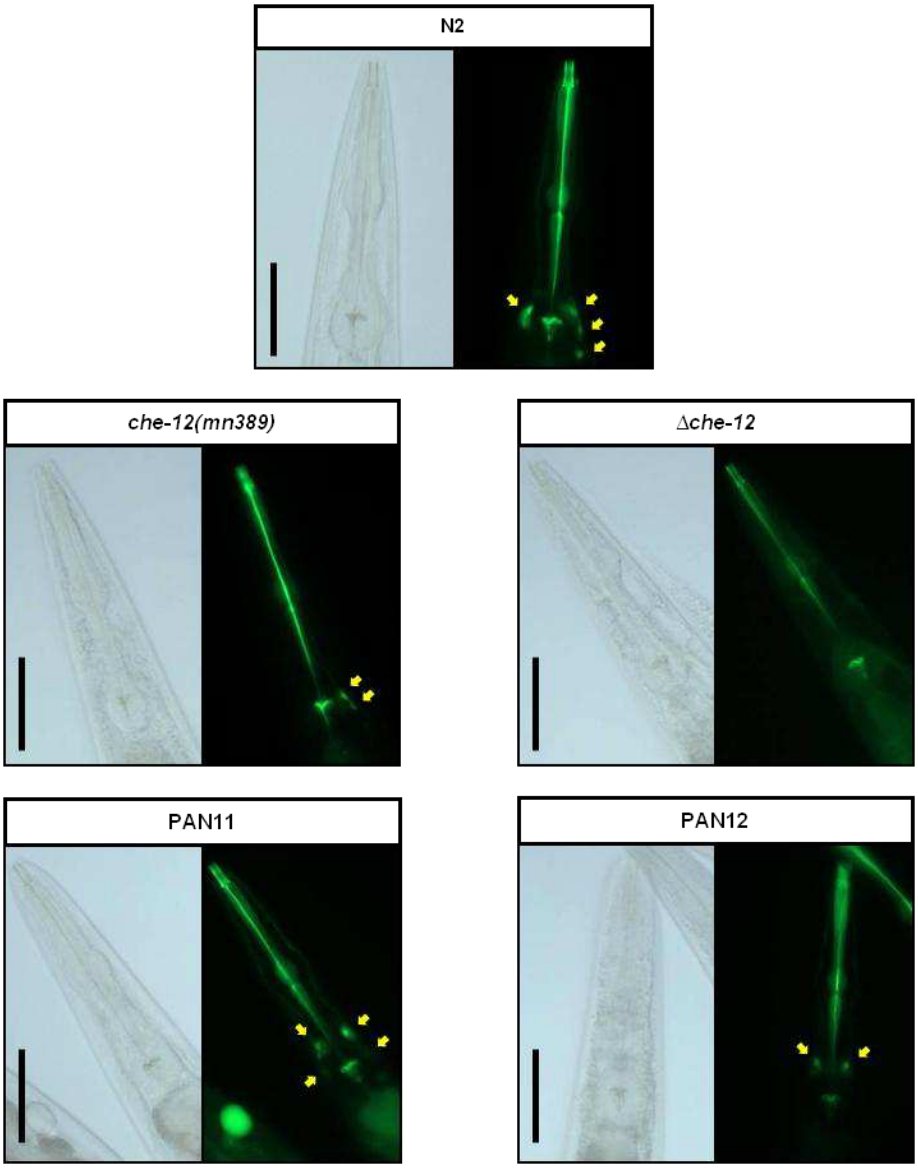
N2
che-12(mn389)
Δche-12
PAN11
PAN12

B

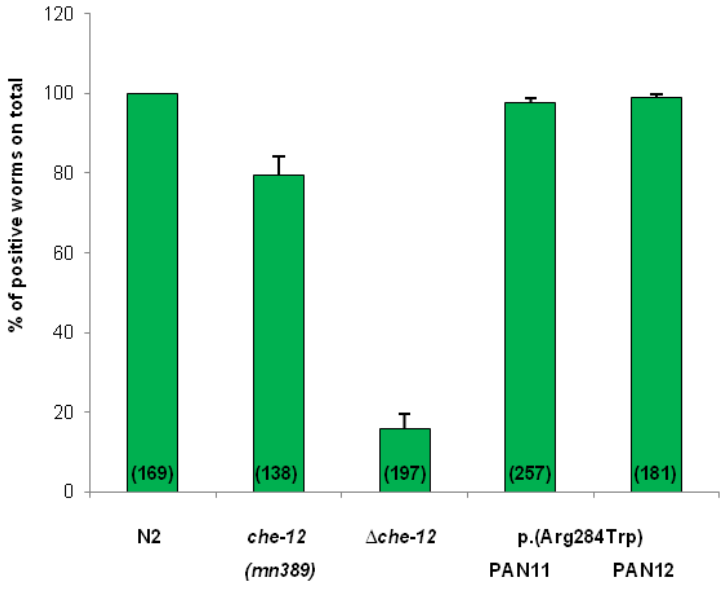
% of positive worms on total
120
100
80
60
40
20
0
(169)
(138)
(197)
(257)
(181)
N2
che-12
(mn389)
Δche-12
p.(Arg284Trp)
PAN11
PAN12

C

	p-value
N2 – *che-12(mn389)*	p< 0.001
N2 – Δ*che-12*	p< 0.001
N2 – p.(Arg284Trp) PAN11	p< 0.05
N2 – p.(Arg284Trp) PAN12	NS
che-12(mn389) – Δ*che-12*	p< 0.001
che-12(mn389) – p.(Arg284Trp) PAN11	p< 0.001
che-12(mn389) – p.(Arg284Trp) PAN12	p< 0.001
Δ*che-12* – p.(Arg284Trp) PAN11	p< 0.001
Δ*che-12* – p.(Arg284Trp) PAN12	p< 0.001
p.(Arg284Trp) PAN11– p.(Arg284Trp) PAN12	NS

Fig. 39: FITC staining. In A) representative images of FITC staining in N2, *che-12*(*mn389)*, Δ*che-12*, PAN11 (*che-12*(*pan11*[R284W (AGA>TGG)]) *V*) and PAN12 (*che-12*(*pan12*[R284W (AGA>TGG)]) *V*) worms. Yellow arrows indicate stained amphid neurons. Scale bar, 50 µm. In B) the quantification of worms in each strain with stained amphid neurons. The graph represents the mean of two independent experiments and between brackets the total number of assayed worms is indicated. The bars indicate the standard error of the mean and the results were compared using the unequal variance *t*-test. In C) the results of the statistical analysis are reported. NS, not significant.

11.6 Cilium length measurement

In order to measure the length of ASER neuron cilium in worms harboring the p.(Arg284Trp) missense variant, the two knock-in strains for *che-12* (*che-12*(*pan11*[R284W (AGA>TGG)]) *V* and *che-12*(*pan12*[R284W (AGA>TGG)]) *V*) were crossed with the OH1392 strain that carries the *gcy-5p::GFP* marker to specifically express GFP in the ASER neuron (Yu *et al*, 1997). Since it has been demonstrated that worms carrying the *che-12*(*mn389)* allele (strain SP1620) have a shorter cilium (Bacaj *et al*, 2008), this strain was also crossed with the GFP reporter and used as negative control in the experiments.

We crossed males from the OH1392 strain with L4 hermaphrodites from *che-12* knock-in and hypomorphic strains, selecting then GFP-positive nematodes in the F1 generation. The genetic screening was performed among GFP-positive worms of the F2 generation in search for worms carrying the p.(Arg284Trp) missense variant or the *che-12*(*mn389)* allele. Worms were then imaged at confocal microscope and the length of each cilium was measured. After having mediated values of each genotype, we considered the strain carrying the wild-type version of *che-12* as 1 and represented the other strains as fractions compared to it. We found that the *che-12* hypomorphic mutant has a shorter cilium (0.74), while the knock-in strains had intermediate values (0.90 for PAN11 and 0.86 for PAN12), that however were significantly lower compared to the wild-type one.

In order to obtain a worm model whose genotype recapitulates that found in patients we crossed the knock-out strain for *che-12* and the knock-in worms carrying the desired missense variant and expressing GFP in the ASER neuron, obtaining the hemizygous *ntls1 [gcy-5p::GFP + lin-15(+)] che-*

12 pan12/cp26[Δ1-1282 + GFP + LoxP unc-119(+) LoxP] V strain and we repeated the analysis, founding a further slight shortening of the ASER dendritic cilium (0.80).

A

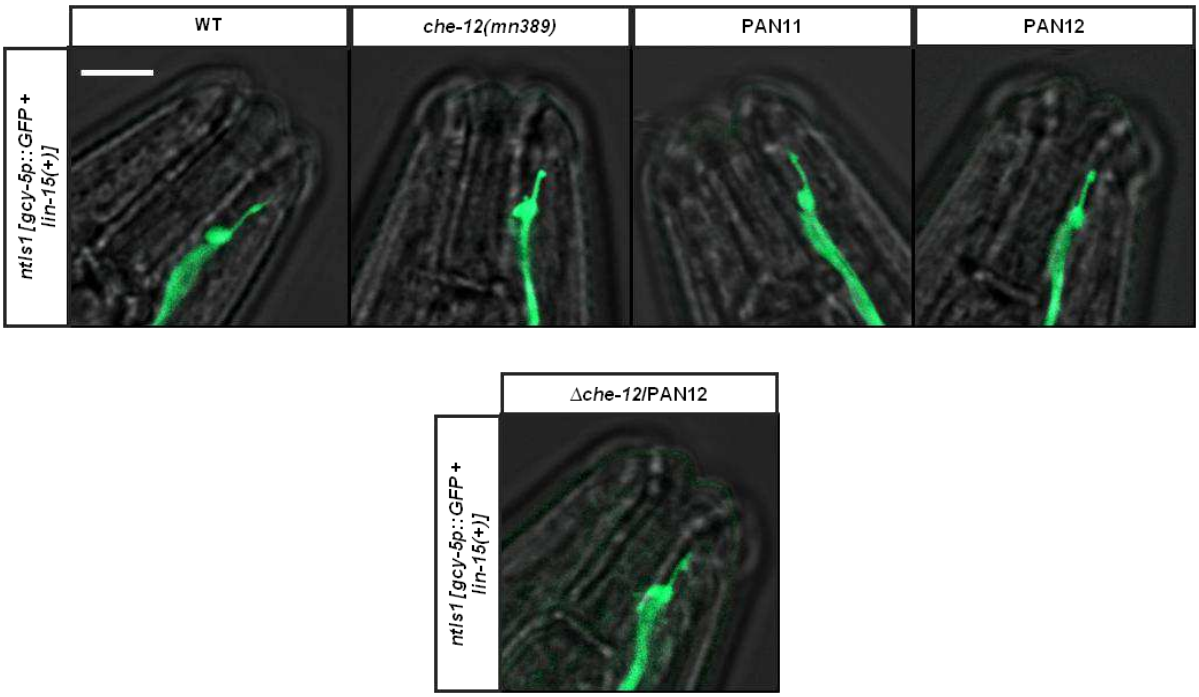

B

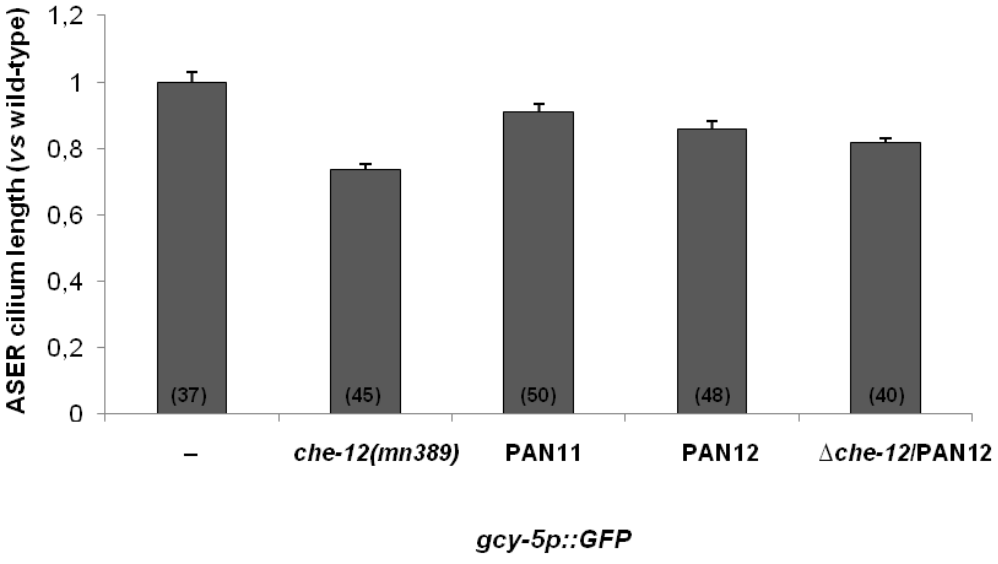

C

	p-value
N2 – *che-12(mn389)*	p< 0.001
N2 – p.(Arg284Trp) PAN11	p< 0.05
N2 – p.(Arg284Trp) PAN12	p< 0.001
che-12(mn389) – p.(Arg284Trp) PAN11	p< 0.001
che-12(mn389) – p.(Arg284Trp) PAN12	p< 0.001
p.(Arg284Trp) PAN11– p.(Arg284Trp) PAN12	NS
N2 - Δ*che-12*/p.(Arg284Trp) PAN12	p< 0.001
che-12(mn389) - Δ*che-12*/p.(Arg284Trp) PAN12	p< 0.001
p.(Arg284Trp) PAN11 - Δ*che-12*/p.(Arg284Trp) PAN12	p< 0.01
p.(Arg284Trp) PAN12 - Δ*che-12*/p.(Arg284Trp) PAN12	NS

Fig. 40: Cilium length measurement. Knock-in worms with the p.(Arg284Trp) missense variant and those harbouring the *che-12*(*mn389)* allele were crossed with the OH3192 strain that carries the *gcy-5p::GFP* marker. The knock-out strain for *che-12* and the knock-in worms carrying the desired missense variant [p.(Arg284Trp)] and expressing GFP in the ASER neuron were also crossed obtaining the hemizygous strain indicated as *Δche12*/PAN12. Worms were then imaged at the confocal microscope and the ASER cilium length of each strain was measured. A) Exemplificative images of ASER GFP reporter worms carrying, for what concerns the *che-12* locus, the wild-type version, the *che-12*(*mn389)* allele, or the p.(Arg284Trp) amino acidic substitution, either in homozygosis (PAN11 and PAN12) or hemizygosis (*Δche12*/PAN12). Scale bar 5 µm B) The graph represents the mean of cilium length measurements for each strain, where the wild-type *che-12* is considered as 1 and the other strains represented as a fraction compared to it. The number of assayed worms is reported between brackets and the bars indicate the standard error of the mean. The results were compared using the unequal variance *t*-test. In C) the results of the statistical analysis are reported. NS, not significant.

12 Discussion

In this work we performed the functional characterization of a novel human variant identified in *TOGARAM1*, encoding a protein required for cilia function, which has never been associated with a human disease so far.

TOGARAM1 (TOG array regulator of axonemal microtubules 1) was initially identified as a protein able to bind tubulin and to regulate MTs (formerly named FAM179B, KIAA0423) (Das *et al*, 2015): in fact, it shows discontinuous sequence similarity to TOG1 of CLASP MAPs and belongs to the Crescerin family, which is conserved in ciliated/ flagellated eukaryotes ranging from mammals to unicellular eukaryotes. Its murine orthologue Crescerin1, belonging to the subfamily 1 of proteins that possess 4 domains, was studied in detail and the crystal structure obtained from the second domain confirmed that it consists of 12 helices that pair into six tandem HRs and stack, forming a solenoid and conforming to a canonical TOG architecture with conserved intra-HEAT loops, homologous to the tubulin-binding determinants in ch-TOG and CLASP TOG domains. Consequently, it was designated as a TOG domain, in particular TOG2, proving that Crescerin represents a third, unique TOG domain–containing protein family.

Whole exome sequencing (WES by NGS technology) analysis identified two heterozygous variants in *TOGARAM1* in the DNA from two siblings fetuses affected by a severe malformation of the central nervous system resembling a Meckel-Gruber-like phenotype: a missense variant, namely [p.(Arg368Trp], and a truncating allele, resulting in protein degradation, and segregation analysis showed that each variant was inherited from a healthy parent. This substitution is classified as variant of unknown significance (class 3 according to ACMG criteria introduced by Richards *et al*, 2015) since it is extremely rare (not reported in the gnomAD, ExAC, dbSNP databases). Nevertheless, this residue is highly conserved through evolution and the predictive software support its probable pathogenicity due to the possible perturbation of HRs in TOG2 domain. In fact, the arginine residue lies just under the first tubulin binding loop of the domain and this made us hypothesize that a tryptophan in that position could alter the tubulin binding loop's orientation, thus affecting tubulin binding activity, if not the ability of the first and second HRs to correctly pack together.

In order to perform a functional characterization, we took advantage of the *C. elegans* CHE-12 protein, an already characterized member of the Crescerin family. Previous studies showed that *che-12* is expressed in the dendritic cilium of some amphid and phasmid neurons, a subset of sensory cells located in worm's head and tail, respectively. Both null and hypomorphic mutants are available and have been characterized in *C. elegans*. In fact, mutants harboring deletions at the C-terminal portion of the protein (alleles *e1812*, *mn389* and *mn399*) were identified through EMS mutagenesis experiments owing to their peculiar phenotype consisting of defects in behaviors normally controlled by amphid neurons (chemotaxis ability, amphid neuron staining, etc); moreover, a worm *che-12* knockout model (Δ*che-12*) and one harboring mutations in conserved hydrophobic residues on the predicted tubulin-

binding surface of the intra-HEAT loop in each HR A (TOG-1′2′3′4′) display more severe phenotypes, including shorter and more disorganized dendritic cilia compared to the mutants with C-terminal deletions, which thus retain partial CHE-12 function (Das *et al*, 2015).

Therefore, based on the evolutionary conservation of this gene (with an orthologue in the *C. elegans* genome, but not in non-ciliated organisms like yeast), the availability of *che-12* hypomorphic and amorphic mutants showing specific phenotypes (Bacaj *et al*, 2008; Das *et al*; 2015), and the fact that the mutated arginine residue is conserved among different species as well (see paragraph 11.1), we chose *C. elegans* to model the novel human variant in the corresponding *che-12* residue in order to investigate its functional consequences in this multicellular organism.

We took advantage of the recently developed protocol to perform genome-editing in *C. elegans* (Paix *et al*, 2015) and designed crRNA and ssODN to introduce the codon TGG (Trp) instead of AGA (Arg) in position 284. Since the first injections were successful only for the second edited locus, that is *dpy-10*, but not in obtaining the desired edit in *che-12*, we hypothesized that the genomic region of interest could consist of a highly compacted chromatin with a consequent reduced CRISPR editing efficiency. So we added to the injection mix 1 and 10 µM of 5-azacytidine, that is a demethylating agent that decompacts chromatin, and in both cases we were able to finally get the desired knock-in strains. Three lines were generated and all of them carried the desired missense substitution. After the backcross with wild-type animals, essential to eliminate possible off-targets effects due to CRISPR/Cas9 editing, we used the strains PAN11 and PAN12 to carry out the experiments.

First of all, we investigated the ASER-mediated capability of knock-in mutants to chemotax on a linear NaCl gradient, as reported by Das *et al*., including in the experiment as controls also wild-type worms, the SP1620 strain that carries a partially deleted CHE-12 protein at the C-terminus (*mn389* allele, purchased from CGC) and the one in which *che-12* was totally ablated by CRISPR/Cas9 (a gift from Prof. Kevin Slep).

Hypomorphic and amorphic mutants were not attracted to zones with high salt concentration, as already observed by Bacaj *et al* and Das *et al*. Their pattern of migration was very similar in gradient and control plates, and this is a consequence of their inability to sense NaCl gradients, however their peculiar concentration in the central sectors of the plates suggests that they are also a bit lethargic.

Wild-type worms efficiently sensed NaCl gradient and migrated towards the high-salt end and the knock-in strains PAN11 and PAN12 behaved similarly. As the chemotaxis towards high NaCl concentrations requires a proper ASER neuron functioning, this result suggests that the missense variant in analysis does not interfere with it.

However, since it was demonstrated by laser ablation experiments that ASE neurons are important not only to sense sodium and chloride ions, but also other soluble attractants such as cAMP, biotin, lysine, and serotonin (Bargmann, 2006), it could be interesting to assay chemotaxis of knock-in strains in presence of these substances, that have already be tested by Saeki *et al*.

Moreover, Bacaj *et al* reported that *che-12* hypomorphic mutants are defective in the avoidance of a high osmolarity 4M fructose barrier, a behavior mediated in wild-type animals by the ASH neurons. Therefore knock-in strains could be also assayed in avoidance tests like this, to evidence possible defects in other amphid neurons that express *che-12*.

Then, we analyzed the capability of *che-12* knock-in strains to take up and concentrate lipophilic dyes, which is mediated by amphid neurons, by staining the same strains analyzed in the chemotaxis assay, with Vybrant™ CM-DiI (a derivative of DiI, developed to ensure a uniform staining of cells) and FITC (isomer I) as reported by Bacaj *et al*.

For what concerns the Vybrant™ CM-DiI staining, about 95% of wild-type worms held the dye. Conversely, *che-12* hypomorphic and amorphic mutants displayed a reduced frequency of dye uptake, with the strain lacking CHE-12 showing a stronger impairment (63% and 30% of positive animals, respectively). This is in agreement with what found by Das *et al* for the *Δche-12* strain, with approximately 30% of worms stained with the dye, but contrasts with the percentage reported by Bacaj *et al* in *che-12*(*mn389)* mutants (100% DiI-positives). This discrepancy may be due to the somewhat different chemical structure of DiI and Vybrant™ CM-DiI.

Knock-in strains PAN11 and PAN12 were able to take up and hold DiI staining, although in a slightly reduced manner compared to wild-type animals (86% and 93% of positive worms).

Performing FITC staining, 100% of wild-type worms held the dye. As in the case of DiI staining, *che-12* hypomorphic and amorphic mutants displayed a reduced frequency of dye uptake, with the strain lacking CHE-12 showing a stronger impairment (79% and 16% of positive animals, respectively).

The significant decrease in FITC-positive *che-12*(*mn389)* worms compared to wild-type animals however contrasts with the total inability of these animals to hold the dye reported by Bacaj *et al*.

The authors could not explain why DiI and FITC stainings gave such different results in hypomorphic mutants (100% staining *vs* 0%, respectively). One possible explanation could be the quite different chemical structure of the dyes. In our hands, we found with both a stronger staining impairment in KO worms compared to the hypomorphic mutants and this could be due to the total ablation of *che-12* in the first case and the partial residual function of the protein in the second one, as suggested also by Das *et al*.

Knock-in strains PAN11 and PAN12 were able to take up and hold FITC staining, with percentages very similar to that of wild-type animals (97 and 99% of positive worms).

Although, in both stainings a significant difference was found between wild-type and PAN11 animals but not with PAN12 ones and this could be simply due to the higher number of PAN11 nematodes assayed. The FITC-positives PAN11 and PAN12 worms were almost 100%, while the Vybrant™ CM-DiI-positives ones were in the 85-95% range similar to the 95% of wild-type worms stained, indicating that the *che-12* missense variant in analysis doesn't impair in a significant way the ability of amphid neurons to take up and concentrate dyes.

As next step, we decided to analyze the length of the ASER dendritic cilium in knock-in strains, to explore if the variant could alter the CHE-12-mediated ability to induce MT polymerization. At this purpose, we crossed the PAN11 and PAN12 strains with the OH1392 strain that carries the *gcy-5p::GFP* marker to specifically express GFP in the ASER neuron (Yu *et al*, 1997).

Since it has been demonstrated that *che-12*(*mn389)* and *Δche-12* worms have a shorter cilium (Bacaj *et al*, 2008, Das *et al*, 2015), we decided to cross also these strains with the GFP reporter one in order to have negative controls in the experiments.

Unfortunately, the *che-12* locus and the *ntls1 [gcy-5p::GFP + lin-15(+)]* transgene are syntenic (chromosome V), making the obtainment of GFP animals that were at the same time mutants for *che-12* very challenging. Eventually we were able to get the cross for PAN11, PAN12 and *che-12*(*mn389)* worms, but not for the *Δche-12* ones, despite the very high number of genotyped worms.

Comparing strains carrying mutated versions of *che-12* with that harboring the wild-type one which was considered as 1, we found that the *che-12* hypomorphic mutant had a shorter cilium (0.74), similarly to what already reported (the *mn399* mutant had cilia that were 30% shorter compared to wild-type worms, Bacaj *et al*, 2008), while the knock-in strains had intermediate values (0.90 for PAN11 and 0.86 for PAN12), that however were significantly lower compared to wild-type one, but not as short as in the negative control. Then, in order to obtain a worm model whose genotype recapitulates that found in patients we crossed the knock-out strain for *che-12* and the knock-in worms carrying the desired missense variant and expressing GFP in the ASER neuron, obtaining at the F1 generation an hemizygous *ntls1 [gcy-5p::GFP + lin-15(+)] che-12 pan12/cp26[Δ1-1282 + GFP + LoxP unc-119(+) LoxP] V* strain and we repeated the cilium length analysis, founding a further slight shortening of the ASER dendritic cilium compared to wild-type (0.80).

These results suggest that the *che-12* missense variant is associated with a mild phenotype consisting in a shorter dendritic cilium, whose structure although is not compromised enough to impair the chemotaxis behavior on a NaCl gradient nor the ability to concentrate lipophilic dyes.

This is in agreement with unpublished data from our collaborators, hinting that mutations in TOG1 and TOG2 domains of CHE-12 are less penetrant compared to those in TOG3 and TOG4, however the high degree of conservation of the first two domains in Crescerin1 subfamily implies that they are important as well.

Further experiments are needed to elucidate the functional consequences of the p.Arg284Trp substitution on CHE-12. For example, electronic microscopy could be useful to dissect at ultrastructural level MT organization in order to evidence lack or disorganization of their distal structures.

Moreover, *in vitro* MT polymerization experiments are ongoing using purified murine wild-type and mutated (p.Arg367Trp) TOG2 domains that will be mixed with tubulin, monitoring their polymerization at 37 °C with a light scattering assay, in a similar way to what was done by Das *et al*.

The demonstration of an impairment in MT assembly in presence of the missense variant could in fact confirm and consolidate the result obtained measuring cilium length at the confocal microscope.
Cilium ultrastructure in knock-in mutants could be also investigated at earlier life stages, in light of the morphological defects found at the early stages of development in Meckel-Gruber syndrome.
It was found that the *MKS1* and *MKS3* genes, that if mutated are associated with this ciliopathy, have orthologues in the *C. elegans* genome (*mks-1/xbx-7* and *mks-3* respectively), which were interestingly found to be specifically expressed just in ciliated sensory neurons (Inglis *et al*, 2007).
It was also demonstrated that several MKS genes form a complex that localizes to the cilia transition zone, functioning as a gate to regulate what proteins should be present in the cilium. Moreover, individual *mks* mutants have mild defects in cilia structure and function (Masyokova *et al*, 2016), similarly to the so far subtle phenotype identified in our *che-12* knock-in mutants.
Finally, the missense variant will be also investigated at *TOGARAM1* transcript level, to prove that it is a *bona fide* missense variant, thus excluding possible effects on its maturation, which could reduce the amount of the mutant protein (Cartegni *et al*, 2002).
The demonstration of the variant pathogenicity could establish a link between *TOGARAM1* and ciliopathies, contributing to its definition as a new human disease gene.

SECTION VI

GENERAL CONCLUSIONS OF THE WORK

During my PhD program, I was involved in several projects aimed at the characterization of genes whose function is still unknown or not fully understood and may be potentially implicated in neurometabolic conditions. I employed *Caenorhabditis elegans* as model of study, generating gene knockdown strains by RNA interference and knockout (KO)/knock-in worm lines by CRISPR/Cas9 technology.

The main results obtained in the three research projects are listed below.

1) We performed the silencing of *cox-16,* a cytochrome *c* oxidase (COX) assembly factor orthologue to human *COX16* in *C. elegans*: through a RNAi interference model, we knocked down this gene in nematodes and observed the effect on COX activity through a specific histochemical staining. Silenced worms for *cox-16* showed a partial preservation of COX activity, especially in some body portions. This result suggests that the function of this assembly factor is in *C. elegans* at least in part redundant.

However, the worm model was essential to prove the importance of this assembly factor for COX biogenesis and proper functioning also in a multicellular model that could be used to screen a large number of molecules to target COX deficiencies and to investigate the effects on different animal tissues; this is an important advantage of this model compared to cell lines and yeast, since mitochondrial defects are often observed in a tissue-specific fashion in patients.

Given our results that indicate that *COX16* is essential for proper COX biogenesis and function, we highlight the need to include the screening of this gene in diagnostic panels.

The investigation of mitochondrial ETC complexes and supercomplexes assembly has been carried out in the last years also in *C. elegans.* We modified an already published protocol in order to efficiently extract worm mitochondria and perform in-gel COX staining to reveal complex IV and supercomplexes containing it. This approach could be used to investigate the degree of involvement in COX assembly of several factors whose function is still elusive or not fully understood, given the simplicity to achieve a gene knockdown in the whole animal for one or multiple COX genes.

COX deficiencies comprehend a heterogeneous group of disorders and represent the most frequent among mitochondrial diseases. The outcome is still poor because no treatment is currently available for these conditions. Patients with mutations in *COX16* have not been identified so far, however, this is not a remote possibility, since the ExAC variant databases list several potentially pathogenic recessive *COX16* mutations in different human populations.

2) The role of *MYTHO*, a recently identified FOXO-dependent gene which seems to be involved in autophagy, was investigated through *T01G9.2* (the worm orthologue of *MYTHO*) knockdown and KO models.

   Since RNAi experiments did not detect a clearcut phenotype and considering the intrinsic limitations of this approach, we generated a KO model by CRISPR/Cas9 technology, obtaining worm strains that carried a genomic rearrangement which was different from the one expected, but effective to prevent the production of a functional T01G9.2 protein, given the formation of a premature stop codon after 35 amino acids.

   We performed an extensive phenotypic characterization of *Mytho* KO worms, and while no impairment in development and in worms behaviors during the first vital stages could be observed, we highlighted a precocious aging phenotype which resulted in movement impairment and eventually in reduced lifespan in KO animals compared to controls.

   We started to investigate autophagy in absence of *Mytho* and found in adult animals a significant decrease in the number of autophagosomes in the posterior bulb of the pharynx, a body district where this process is active and declines during aging. Although the necessity to perform autophagic flux analysis through the use of fluorescent tandem-tagged reporter strains and of inhibitors of the autophagosome-lysosome fusion, these preliminary data are in line with what obtained in mammalian models (manuscript in preparation).

   Further experiments suggest that *Mytho* may be indeed essential as a FOXO-dependent gene to properly respond to several types of harmful stresses (at least oxidative, but probably also heat and metabolic stress). Given the necessity to elucidate the pathway linking IGF/Akt/FOXO to *MYTHO*, we crossed *daf-2(e1370)* and *daf-16(mu86)* mutants with *fer-15/Mytho* KO worms in order to determine by lifespan assays if the absence of Mytho could eliminate the life extension shown by *daf-2* mutants or, conversely, worsen *daf-16* mutants phenotype. The two genetic crosses have been obtained and longevity tests will be performed soon.

   Overall, our data identified *MYTHO* as a novel autophagy-related gene under FOXO regulation that plays a major role in controlling lifespan and stress resistance in a multicellular organism.

3) The *TOGARAM1* gene that belongs to Crescerin1 family of proteins that regulate microtubule dynamics has never been associated with a human disease so far. However, a genetic analysis was recently carried on two siblings fetuses that showed a severe malformation of the central nervous system with a Meckel-Gruber-like phenotype. WES analysis identified two heterozygous variants in *TOGARAM1* in the two affected siblings: a missense variant, that is [p.(Arg368Trp], leading to the substitution of an arginine residue with a tryptophan one, and a truncating allele, leading to protein degradation.

   Considering that this gene is highly conserved, having an orthologue also in the *C. elegans* genome, that is *che-12*, whose hypomorphic and amorphic mutants have been deeply characterized (Bacaj *et al*, 2008; Das *et al*; 2015), we used CRISPR/Cas9 technology to get a

nematode knock-in model that reproduces the variant in analysis in the corresponding *che-12* residue in order to investigate its functional consequences in a multicellular organism. After some technical difficulties, we were able to obtain the desired edit (p.Arg284Trp) thanks to the addition of a demethylathing agent to the injection mix. Two of the three generated lines were backcrossed to eliminate possible off-targets effects and used for the phenotypic characterization of mutants.

We were not able to detect in knock-in strains an impairment in behaviors controlled by the sensory neurons in which *che-12* is expressed, that is the ability to chemotax on a linear NaCl gradient or to concentrate lipophilic dyes (DiI, FITC), that are instead strongly decreased in strains harboring protein deletions at the C-terminus (*e.g.* the *mn389* allele) or completely devoid of *che-12*. On the contrary, thanks to a genetic cross with a reporter strain that specifically expresses GFP in the amphid ASER neuron, we could highlight in this sensory cell shortening of the dendritic cilium in worms harboring the missense variant in analysis. So knock-in strains show a mild phenotype, namely a shorter dendritic cilium, whose structure although seems not to be compromised enough to impair the chemotaxis behavior on a NaCl gradient nor the ability to concentrate lipophilic dyes. In the hemizygous strain, obtained from the genetic cross between the knock-out strain for *che-12* and the knock-in worms carrying the desired missense variant and expressing GFP in the ASER neuron, we found a further slight shortening of the dendritic cilium.

Further experiments are needed to elucidate the functional consequences of the p.Arg284Trp substitution on CHE-12. For example, electronic microscopy could be useful to dissect at ultrastructural level MT organization in order to evidence lack or disorganization of their distal structures. Moreover, we are analyzing *in vitro* how the mutated TOG domain regulates MT polymerization.

Finally, the missense variant will be also investigated at *TOGARAM1* transcript level, to exclude possible effects on its maturation.

The demonstration of the variant pathogenicity could establish a link between *TOGARAM1* and ciliopathies.

Collectively these results confirm the usefulness of *C. elegans* as model to study new genes or to investigate in a multicellular context the function of others that have been only characterized in a cellular context. Moreover, we are confident in the possibilities offered by this nematode for *de novo* discovery of human disease genes and pathways and to develop models of human disease, as already demonstrated for other pathological conditions.

SECTION VII

APPENDIX

13 Use of hybrid minigenes to analyze genomic variants potentially affecting splicing

The introduction of next generation sequencing (NGS) techniques in recent years has led, as a direct consequence, to the identification of a huge number of genomic variants whose functional meaning is largely unknown. In order to get a proper comprehension of its clinical meaning, the effects of a genomic variant on gene function and the possible pathological phenotypes associated should be determined.

It has been reported that mutations that affect splicing mechanism of the immature mRNA account for at least 15% of disease-causing mutations with up to 50% of all mutations described in some genes (Ars *et al*, 2000; Caminsky *et al*, 2014).

The splicing machinery is responsible for the generation of correct and mature mRNAs and requires the coordinated action of five small nuclear (sn)RNAs (U1, U2 and U4–U6) and more than 60 polypeptides for the correct individuation and joining of exons (Cartegni *et al*, 2002).

The process involves the recognition of key sequence components, that is the donor site, defined by the three terminal nucleotides of each exon and the first seven bases of the downstream intron, and the acceptor site that spans the first two bases of the exon and the last 26 bases of the upstream intron. These sequences (especially the dinucleotides immediately intronic to the exon) are not absolutely invariant. In fact, although highly conserved, they can vary not only between different genes, but also within a single one. The particular combination of nucleotides at each position within the same splice site determines its overall strength and the probability to be recognized by splicing factors (Caminsky *et al*, 2014).

In addition, the branch site is located in introns generally near the 3' end and contains an adenine that functions as branching point. Notably, binding sites for splicing regulatory elements have been shown to reside distant from the corresponding natural splice sites, both in exons (exonic splice enhancers or silencers), and in introns (intronic splice enhancers or silencers).

Alternative splicing is responsible for the production of multiple isoforms from the same gene. It has been estimated that ~60% of genes are represented by two or more transcripts, contributing to the complexity of the proteome despite the relatively low number of human genes.

Genomic variants can be also found in spicing regulatory sequences with possible consequences on the mRNA maturation. In fact, exons can be skipped, or conversely pseudo-exons can be wrongly included in the mature transcript, introns or portions of them can be retained and not properly excised

and also the efficiency of splicing mechanism can be negatively affected. The result is the production of an aberrant mRNA, that is either unstable or codes for defective or deleterious protein isoforms.

Mutations that potentially alter splicing are not only confined in intronic regions, but they can hit also exonic sequences. Point mutations in the coding sequence are generally classified as nonsense, missense or silent mutations, depending on their effect on the protein (introduction of a stop codon, substitution of an amino acid, no effect), but this interpretation needs to be supported by characterization at the mRNA level, since exonic variants can affect first immature mRNA splicing with a profound effect on the translated product and pathological consequences (Cartegni *et al*, 2002).

Therefore, the determination of the molecular mechanism(s) through which a mutation causes a specific phenotype is crucial for the development of novel therapeutic approaches.

Since the high processivity of new sequencing techniques and the individuation of a huge number of genomic variants with a not yet defined molecular meaning, *in silico* prediction methods have been developed in order to support variants classification. Software programs for splicing analysis use a wide variety of bioinformatic approaches and different algorithms: for example, some of them compare the predicted mutant sequence to a consensus sequence, based on a set of functional acceptor or donor splice sites. A limitation to this kind of approach is that low-frequency nucleotides present in functional splice sites are not represented, leading to misinterpretation and false-positive mutation predictions. This is especially the case of regulatory sequences located deeply inside introns that are hardly identified with prediction tools since their low degree of conservation (Caminsky *et al*, 2014).

It is always recommended to use multiple prediction software, since each of them has advantages or limitations due to the employed algorithm. Anyway, the results obtained by these *in silico* tools must be compared with those obtained by experimental validation, especially when the variant is investigated in clinical environment.

The two most widely used methods for validating mutant mRNA splicing isoforms are RT-PCR analysis of patient mRNA, and transfection of minigene constructs expressing the variant into cell lines, followed by RT-PCR. Both techniques show some limitations, since these approaches can't reveal relative abundance of each isoforms and, most of all, the introduction of premature stop codon in the mature mRNA may result in nonsense-mediated mRNA decay (NMD), leaving no evidence of the mutated isoforms with risk of misinterpretation of splice variants.

Experimental methods, like the use of puromycin, have been developed to stabilize transcripts with premature termination of translation, thus inhibiting NMD and restoring aberrant splice forms. Furthermore, certain mutations proximate to the penultimate exon evade NMD (Cartegni *et al*, 2002; Caminsky *et al*, 2014).

The minigene approach shows several advantages compared to the RT-PCR analysis of patient mRNA: first of all, it analyzes the transcript produced by a single allele, enabling the identification of mutations that allow the partial production of the wild-type transcript, behaving so as hypomorphic

alleles. On the contrary, the analysis of the patient cDNA detects the effect of both alleles on the resulting transcript and does not allow to discriminate the transcripts produced by each allele.

Moreover, the minigene assay requires only the patient DNA (or if not available, the variant to analyze may be inserted into the minigene backbone by site-specific mutagenesis), with no need for RNA, which can be often difficult to obtain.

During my phD course, I was also involved in the functional characterization through a hybrid minigene approach of several genomic variants found in patients affected by rare genetic diseases in *NF1*, *COL4A4*, *COL4A5*, *RB1*, *BRCA1* and *BRCA2* genes.

I used the ß-globin minigene, that was previously generated in our lab (Forzan *et al*, 2009) and was obtained by the cloning of the ß-globin gene inside a pcDNA™3.1/Hygro$^{(+)}$ vector (ThermoFischer Scientific), which is used for expression in mammalian cells. A polylinker containing the restriction sites for enzymes XhoI, NotI and HindIII was then subcloned in the intron 2 of ß-globin gene, to facilitate the following cloning steps.

Briefly, the patient DNA carrying the variant to analyze is first amplified with primers opportunely designed to carry the same restriction sites present in the polylinker in order to enable the subsequent cloning of the gene portion inside the ß-globin minigene. The PCR product generally contains the exon closest to the intronic variant to analyze, or the mutated exon in case of exonic variants, and a portion of at least 100 bp of flanking intronic regions upstream and downstream.

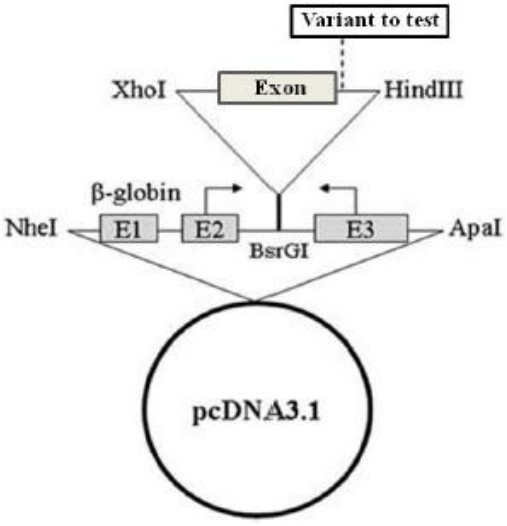

Fig. 41: A schematic representation of the ß-globin minigene, with the ß-globin gene, that consists only of three exons, cloned inside a pcDNA™3.1/Hygro$^{(+)}$ vector. A polylinker containing the restriction sites for enzymes XhoI, NotI and HindIII was then subcloned in the intron 2 of ß-globin gene and used to clone inside the vector genomic portions carrying the variant to test and amplified from patient DNA using primers with the same restriction sites as in the polylinker. In the depicted example, the intronic variant lies near the splicing donor site; the DNA portions has been cloned inside the ß-globin minigene using restriction enzymes XhoI and HindIII.

Both PCR product and vector were digested with the restriction enzymes (NEB) present in the polylinker and in the primers used for the amplification. The vector was then dephosphorylated with the Shrimp Alkaline phosphatase (rSAP, NEB) to prevent its recirculation and insert and vector were opportunely ligated using the T4 DNA lisase (NEB). A portion of the ligation reaction was used to transform the chemically competent bacteria Mach1 $T1^R$ bacteria (ThermoFisher Scientific) and screening was performed on single bacterial colonies to individuate those carrying the desired insert inside the ß-globin vector. The plasmidic DNA was purified using the QIAprep Spin Miniprep Kit (QIAGEN) and the correctness of cloning was verified by Sanger sequencing. For each tested variant, a construct carrying the wild-type sequence and one with the variant were used for the following transfection experiments.

HEK293 cells, that do not express ß-globin, were generally used to analyze the expression of the minigene constructs. However, when possible, a cell line deriving from the tissue where the gene of interest is majorly expressed or where the pathology primarily manifests its phenotype is chosen, as in our case we did with the human retinoblastoma cell line Y79, derived by explant culture of an eye primary tumor to investigate the effects of variants found in the *RB1* gene.

Cells were transfected with the construct carrying the variant of interest, with the corresponding wild-type one and with the empty ß-globin vector, as negative control. After 24 hours, the total RNA was extracted with TRIzol™ (ThermoFisher Scientific), retrotranscribed using SuperScript II reverse transcriptase (ThermoFisher Scientific) and the resulting cDNA was amplified using specific primers for the ß-globin gene, designed on exon 2 (forward) and exon 3 (reverse), in order to avoid eventual interference from the endogenous gene.

13.1 *NF1*

The *NF1* gene, localized on chromosome 17q11.2, encodes for the protein neurofibromin, that controls cell growth and proliferation by regulating the proto-oncogene Ras and cyclic adenosine monophosphate (AMP). It has been demonstrated that this gene shows a complex pattern of splicing with an elevated number of splicing isoforms.

Heterozygous mutations in the *NF1* gene cause Neurofibromatosis 1 (NF1, MIM# 162200), a neurocutaneous disease affecting approximately 1 in 3000 people that has a major impact on the nervous system, eye, skin, and bone. Individuals with NF1 have a predisposition to benign and malignant tumor formation and the hallmark lesion is the neurofibroma, a benign peripheral nerve sheath tumor. Most of the clinical symptoms of the disease are age-dependent and considerable phenotypic variability has been described both between and within families (Ars *et al*, 2003; Ferner and Gutmann, 2013).

Given the huge dimensions of the gene that with its 60 exons spans more than 300 kb of genomic DNA, the determination of the mutational spectrum has been complex with more than 3,000 genomic

variants reported so far found along in the entire gene, that can be point mutations or account for small *inframe* or *frameshift* deletions/insertions, as well as whole gene or multi exons deletions (Wallis *et al*, 2018).

We decided to investigate the possible effect on splicing of a series of uncharacterized variants in the *NF1* gene, and since the patient mRNA was not available in the majority of cases, we employed the hybrid minigene assay, including in the study some variants that were previously reported in literature or for which the RNA had already been analyzed as a control of the system reliability.

We analyzed 26 variants, with 20 of them localized in introns (among which only 8 concerned canonical splicing sites) and the remaining in exons.

We were able to clarify the effect on transcript maturation for all of the tested variants, highlighting an effect on splicing for 14 of them (12 intronic and 2 exonic). Interestingly, in 6 cases intronic variants were found outside the canonical sites, confirming the complex regulation of the splicing mechanism, while the two exonic variants resulted in the partial production of the wild-type construct, behaving so as hypomorphic alleles.

Using the minigene assays we were also able to show that distinct variants in the same position may have different effects on transcript maturation, because the combination of nucleotides at each position within the same splice site determines its overall strength and the probability to be recognized by splicing factors, in according to what was previously published (Caminsky *et al*, 2014).

This system has proven reliable and reproducible, since for one exonic and three intronic variants we obtained concordant results with what was published in literature or with RNA analysis.

We couldn't detect any effect for three variants on transcript splicing with our minigene system in disagreement with what was reported in databases. We therefore conducted further analysis on the clinical cases in our laboratory and we were able to confirm the benign nature of the variants, further emphasizing the power of minigenes in analyzing the effects of genomic variants on splicing.

The results of all variants tested have been collected and some of them are depicted in figure 42.

A manuscript is currently in preparation.

In the meantime we also analyzed with the minigene assay the missense mutation p.(Arg1038Gly) that segregates in seven patients from two unrelated families who all manifest a mild form of Neurofibromatosis type 1 without neurofibromas or other NF1 complications and proposed a novel genotype–phenotype correlation, which adds to the previously established three ones (Trevisson *et al*, 2019).

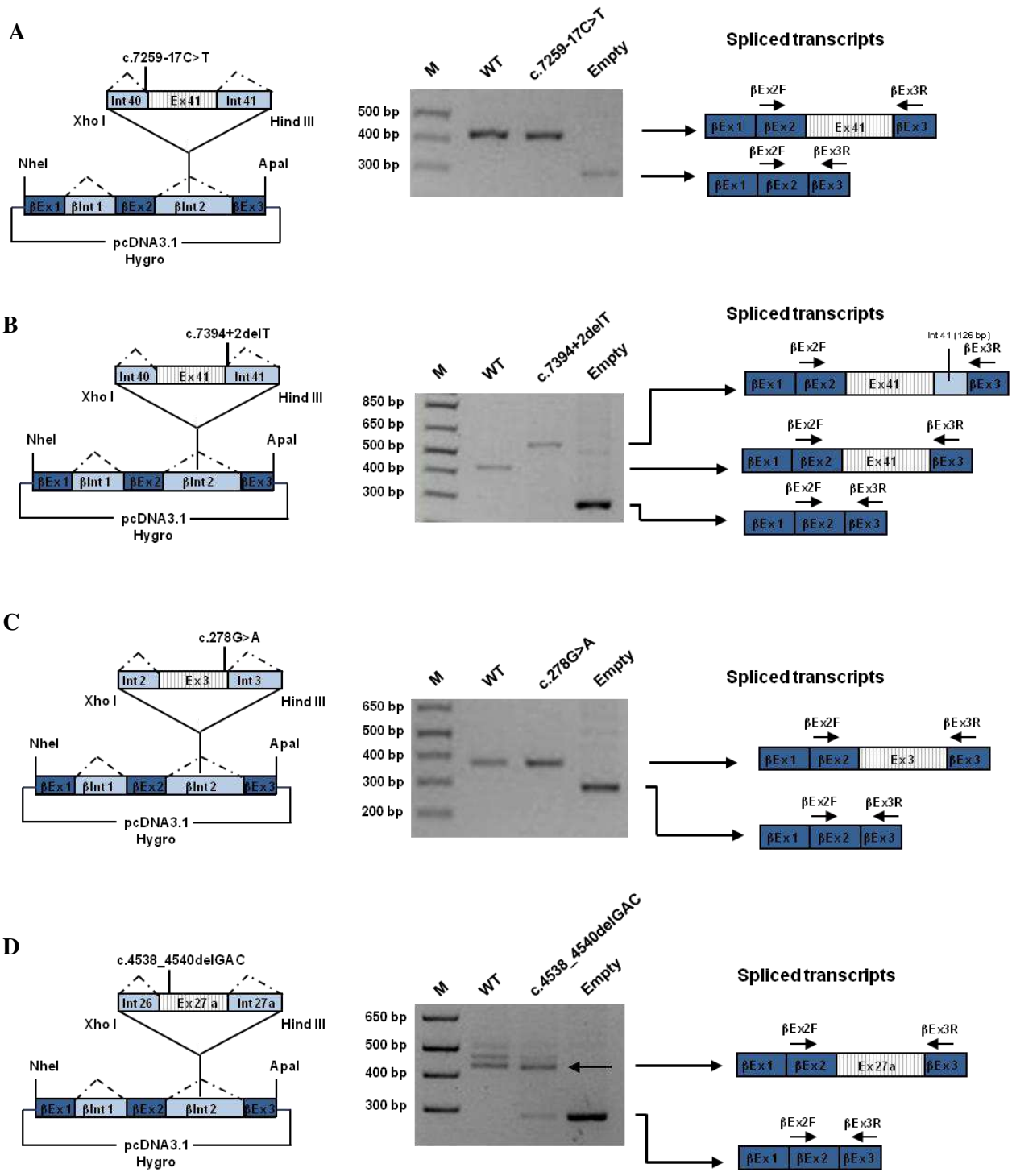

Fig. 42: Characterization of NF1 intronic (A and B) and exonic (C and D) variants through the hybrid minigene system. A schematic representation of the hybrid minigene constructs is depicted on the left with the dotted lines indicating normal splicing, while on the right the results of RT-PCR performed are shown. Each band was then extracted from gel and sequenced. Legend: M, 1 Kb plus molecular marker (ThermoFisher Scientific); Empty, empty β-globin-pCDNA3.1 vector; WT, wild type construct; c.7259-17C>T, c.7394+2delT, c.278G>A, c.4538_4540del GAC constructs containing the c.7259-17C>T, c.7394+2delT, c.278G>A, c.4538_4540del GAC variants, respectively. In A) and C) splicing is not affected, while variants cause exon skipping in B) with partial production of the wild-type allele in D). A manuscript collecting the results of *NF1* variants characterization is in preparation.

13.2 *COL4A4* and *COL4A5*

Alport syndrome (ATS) is a clinically heterogeneous nephropathy that is caused by mutations in collagen IV genes encoding the α 3-4-5 heterotrimer, which is produced by podocytes and represents the major constituent of the mature glomerular basement membrane (Hudson, 2004).

In ATS, failure to substitute the immature form (α 1-2-1 chains) of collagen IV with the α 3-4-5 chains results in progressive kidney injury and ultimately end-stage renal disease, associated with glomerular sclerosis and tubulo-interstitial fibrosis, inflammation and reorganization of the extracellular matrix (Gubler, 2008). Three classic models of Mendelian inheritance have been reported in ATS: semidominant X-linked due to mutations in *COL4A5* (XLAS; MIM# 301050), autosomal recessive (ARAS; MIM# 203780) and autosomal dominant (ADAS; MIM# 104200) caused by mutations in *COL4A3* or *COL4A4* genes (Fallerini *et al*, 2014).

Genotype–phenotype correlations have been established, particularly in the more frequent X-linked form, where truncating mutations closer to the 5' end are associated with a more severe phenotype. However, given the wide spectrum of phenotypic variability associated with ATS even within the same family, more complex inheritance patterns have been hypothesized and the existence of a digenic inheritance in ATS with two mutations in the α 3-4-5 collagen IV genes was recently demonstrated (Mencarelli *et al*, 2015).

This model may explain the variable expressivity of ATS disease better than simple Mendelian inheritance and preliminary results suggest that individuals with heterozygous mutations in two different collagen IV genes develop renal failure later than those with X-linked or autosomal recessive ATS in line with molecule stoichiometry of the disruption of the type IV collagen triple helix.

During my phD course, I was involved in a project aimed at the characterization of genomic variants found in α 3-4-5 collagen IV genes in several families affected by ATS, in order to better define the genetic mechanism of inheritance. We used the hybrid minigene system for three intronic variants (c.931-2A>G and c.976-56A>G in *COL4A4* and c.780+5G>A in *COL4A5*) to overcome the limitation of an undetectable expression level of *COL4* transcripts in blood samples.

For what concerns *COL4A4*, we cloned in the ß-globin minigene vector a gene portion containing both exon 16 and 17 and part of the flanking upstream and downstream introns and we used HEK293 cells to express wild-type and mutated minigene constructs.

We found that the c.931-2A>G variant in intron 15 hits the canonical splicing acceptor site and leads to an aberrant splicing product with a complete skipping of exon 16, as expected (Fig. 43 A, Cartegni *et al*, 2002).

On the other side the c.976-56A>G single substitution in intron 16 produces the same splicing pattern as the wild type, indicating that the variant behaves as a benign nucleotide change (Fig. 43 A). The result was confirmed by Sanger sequencing of PCR products.

In the case of *COL4A5*, we cloned exon 13 and part of flanking introns in the same backbone as before. The c.780+5G>A variant in intron 13 yielded two products, the first corresponding to that produced by the wild-type construct, as confirmed by Sanger sequencing, and the second resulting from the skipping of exon 13. Also in this case the splicing mutation presents with a 'leaky effect', in line with the hypothesis of an hypomorphic allele mutation (Fig 43 B).

These experiments helped not only in the functional characterization of unknown intronic variants found in the α 3-4-5 collagen IV genes in families affected by ATS but also in the definition of inheritance mechanisms of this pathology, whose individuation is critical for accurate genetic counseling, with a correct assessment of recurrence risks and prognostic considerations. The results of this study have been recently published (Fallerini *et al*, 2017).

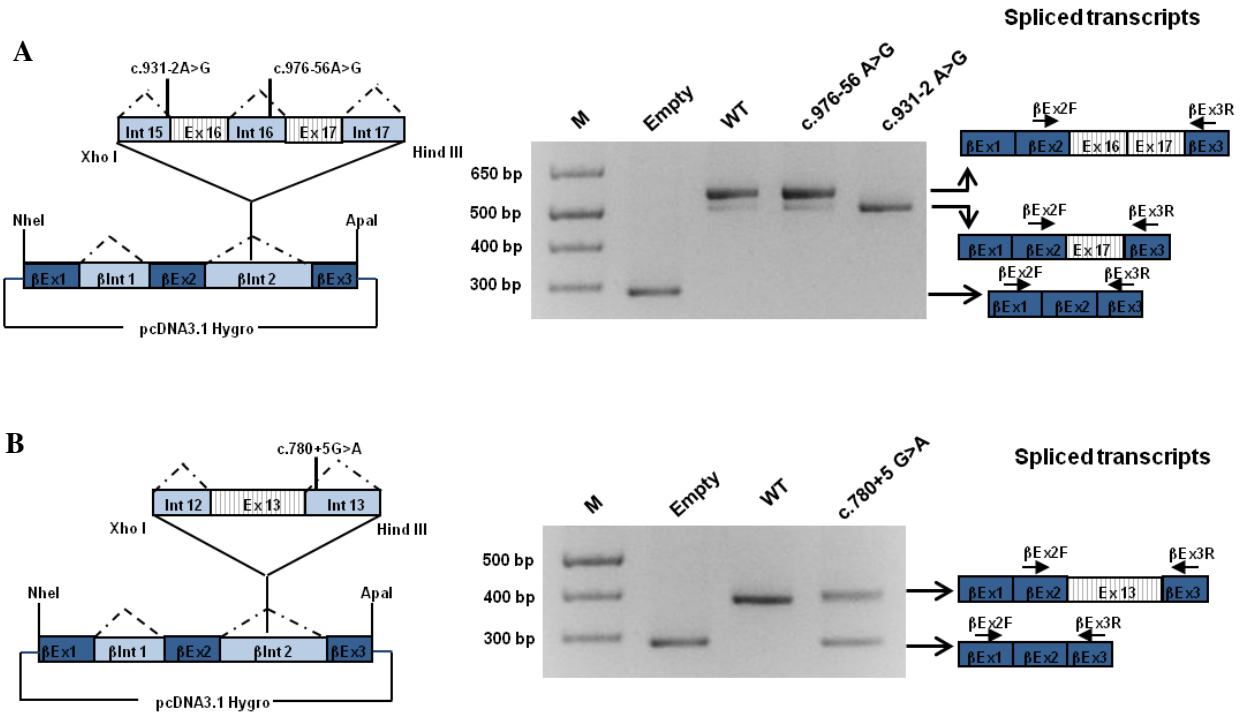

Fig. 43 RT-PCR analysis of the *COL4A4* and *COL4A5* minigene constructs expressed in HEK cells using vector specific primers. As above, a schematic representation of the hybrid minigene constructs is depicted on the left and on the right the results of RT-PCR are shown. Legend: M, 1 Kb plus molecular marker (ThermoFisher Scientific); Empty, empty β-globin-pCDNA3.1 vector; WT, wild type construct; c.976-56A>G, c.931-2A>G and c.780+5G>A constructs containing the c.976-56A>G, c.931-2A>G or c.780+5G>A variants, respectively (adapted from Fallerini *et al*, 2017).

13.3 *RB1*

The *RB1* gene, the first characterized tumor suppressor gene (Friend *et al*, 1986), is located on chromosome 13q14.2 and encodes a nuclear phosphoprotein, pRb, that, when hypo-phosphorylated, acts as a transcriptional cofactor and represses the proliferation-promoting activities of a subset of E2F transcription factors. Otherwise, when phosphorylated by activated cyclin-dependent kinases its

activity is repressed. In addition to control the G1-S cell cycle transition, pRb has important roles in embryogenesis and maintenance of trophoblast stem cells (Kanber *et al*, 2009).

The biallelic inactivation in this gene causes retinoblastoma (RB; MIM# 180200), the most common pediatric intraocular tumor, affecting about 1 in 15,000–20,000 live births.

In the non-hereditary form (60% of cases) both inactivating events occur in cells of the developing retina, tumor is confined to a single eye (unilateral) and develops after the first year of life. On the other side, in the hereditary form (40% of cases) a germline mutation predisposes to RB and a subsequent somatic inactivation of the other allele, mostly occurring through mitotic recombination/nondisjunction or large deletions, triggers the onset of pathology, that is anticipated compared to the other form and usually involves both eyes (bilateral) (Dimaras *et al*, 2012).

Pathogenic variants reducing *RB1* expression or partially inactivating pRB activity have been associated with milder phenotypic expression. Then, the description of low-penetrant families bearing classical "null" variants and the observation that a reported penetrance of 90% can in reality vary significantly between and within families with identical pathogenic variants has led to hypothesize that other mechanisms may be determinant, and one of them is mosaicism. The expressivity of the pathology can be also influenced by the gender of the transmitting parent (parent-of-origin effect), for example by genomic imprinting. In fact, it has been demonstrated that the RB1 maternal transcript is expressed 3-fold compared to the paternal one due to the insertion of a truncated, processed pseudogene, which acquired a differentially methylated CpG island (Kanber *et al*, 2009). As a consequence, maternally inherited pathogenic variants with hypomorphic effect may retain sufficient suppressor activity to prevent tumor development.

During my phD program, I was involved in a project aimed at the characterization of genomic variants found in the *RB1* gene in order to explain the mechanism behind the low penetrance found in familial RB. In particular we used the hybrid minigene system to unravel possible leaky effects of splicing mutations, with partial production of the wild-type transcript.

The variants analyzed were: c.608–16_608del in intron 6, c.718+2T>C in intron 7, c.1960+5G>C in intron 19, c.2106+2T>C in intron 20 and c.2663+2T>C, in intron 25. As control of the reliability of the system, we included in our study also the already published c.1331A>G variant that hits the last nucleotide of exon 13 (Genuardi *et al*, 2001).

The assay was performed on a human retinoblastoma cell line (Y79 cells) in order to mimic the tumoral context with its splicing factors landscape as close as possible. Our results highlighted that all the five intronic variants resulted in aberrant splicing, without the formation of the wild-type transcript, proving that they exert a severe effect on mRNA maturation (Fig. 44 A-E). The low penetrance showed by RB patients was further investigated and eventually explained by mosaicism mechanisms or by a combination of the production of partially functional pRB and the parent-of-origin effect.

Moreover, the minigene assay proved crucial to demonstrate the hypomorphic nature of variant c.1331A>G, strengthening the hypothesis that the low penetrance observed in the family could be due to a parent-of-origin-effect, with the higher levels of expression of the maternal hypomorphic variant representing a protective factor in RB development (Fig. 44 F).

The comprehension of the mechanisms through which the pathology manifests has important implications for genetic counseling, allowing to provide a better estimation of the recurrence risk, a more accurate prognostic assessment, prenatal diagnosis options and optimal medical surveillance in all at-risk individuals.

Also in this case, the results of this study have been recently published (Imperatore *et al*, 2018).

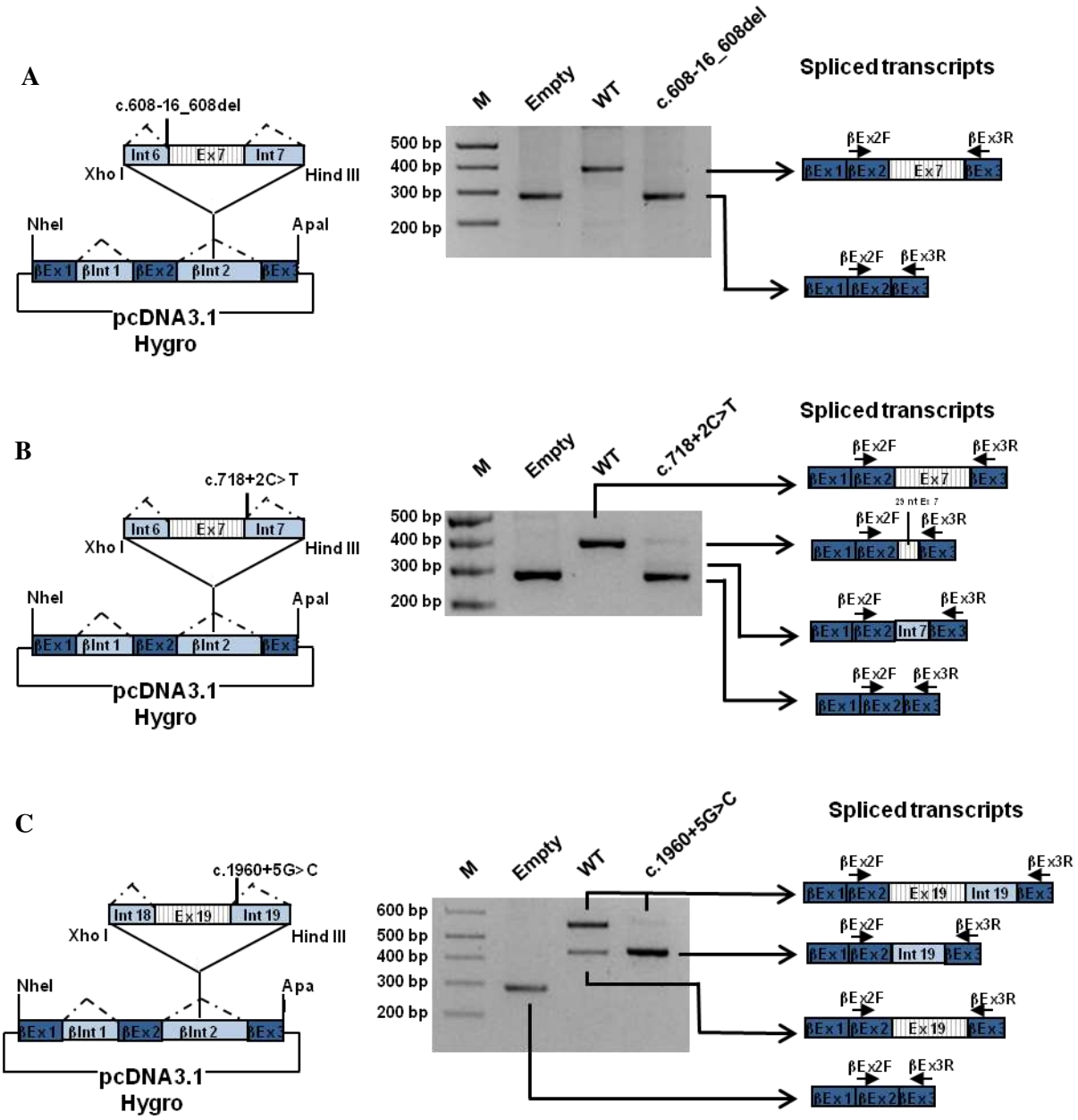

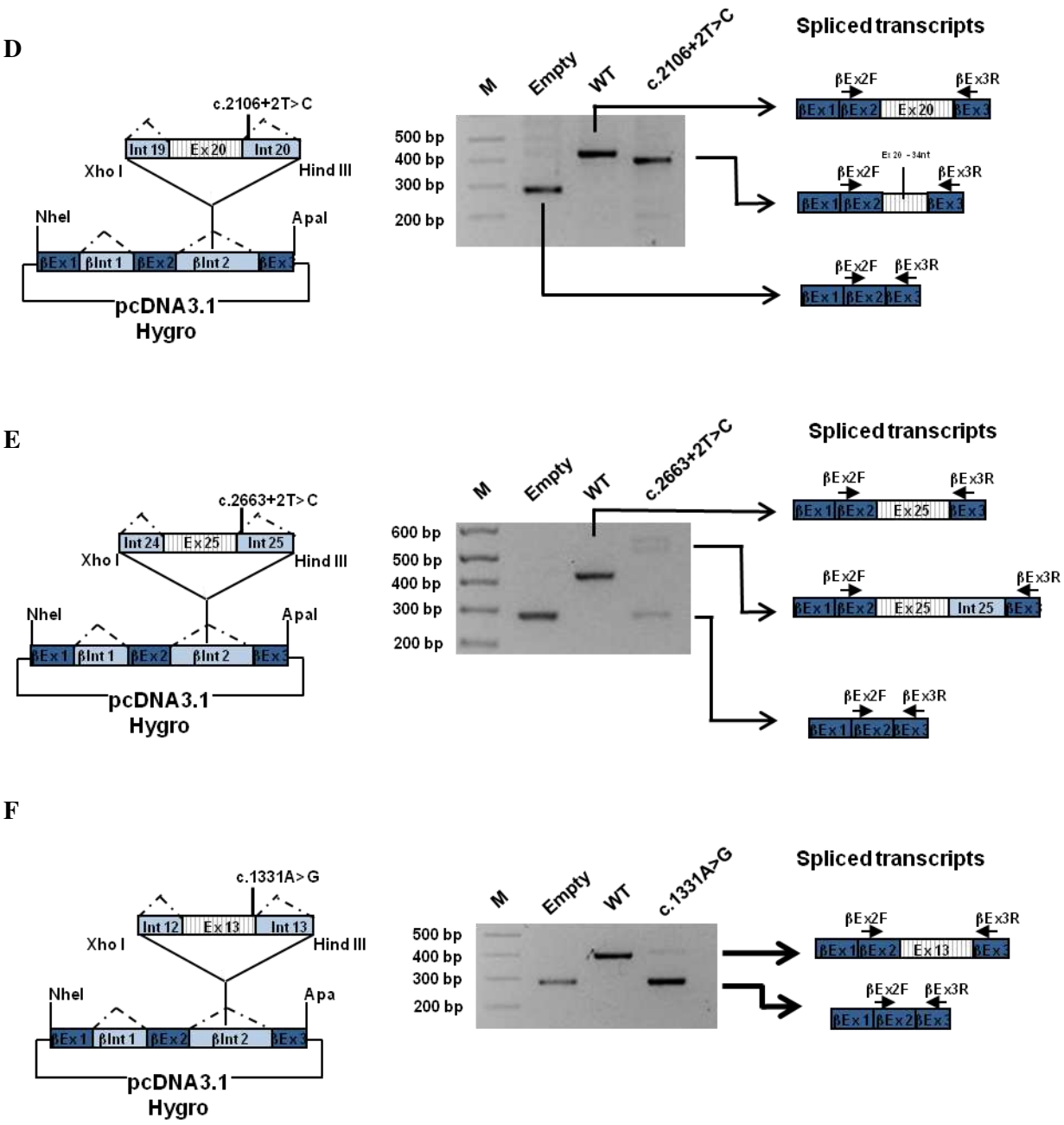

Fig. 44 RT-PCR analysis of the *RB1* minigene constructs expressed in Y79 cells using vector specific primers. Each construct, schematically depicted on the left, contains the exon close to, or harbouring the variant of interest and part of the upstream and downstream introns of *RB1* gene. In A and B) the construct contains the exon 7 of the *RB1* gene. Legend: M, 1 Kb plus molecular marker (ThermoFisher Scientific); Empty, empty β-globin-pCDNA3.1 vector; WT, wild type construct; c.608-16_608del and c.718+2C>T constructs containing the c.608-16_608del or the c.718+2C>T variant, respectively. In C), the construct contains exon 19 of the *RB1* gene. Legends as above, c.1960+5G>C, construct containing the c.1960+5G>C variant. In D), the construct contains exon 20 of the *RB1* gene; c.2106+2T>C, construct containing the c.2106+2T>C variant. In E), the construct contains exon 25 of the *RB1* gene; c.2663+2T>C, construct containing the c.2663+2T>C variant. In F), the construct contains exon 13 of the *RB1* gene; c.1331A>G, construct containing the c.1331A>G variant. All the tested variants (except for the c.1331A>G variant, which was used as control) resulted in aberrant splicing, without the formation of wild-type transcript (adapted from Imperatore *et al*, 2018).

13.4 *BRCA1* and *BRCA2*

BRCA1 (MIM# 113705) is located on chromosome 17q21.31, while *BRCA2* (MIM# 600185) on chromosome 13q13.1. The cumulative breast cancer risk estimates to age 70 years range from 40% to 87% for *BRCA1* and from 27% to 84% for *BRCA2* carriers. The corresponding ovarian cancer risks vary from 16% to 68% for *BRCA1* and from 11% to 30% for *BRCA2* carriers (Kuchenbaecker *et al*, 2017). *BRCA* gene mutations may also predispose to the development of other cancers, such as endometrial, pancreatic, colorectal, gastric, and skin cancer.

Next-generation sequencing techniques have allowed the collection of an elevated amount of sequence data, through the analysis of multi-gene panels, thus decreasing the time required for genetic testing. However, the clinical implications of many gene variants have yet to be established. In fact, despite the testing of hundreds of thousands of patients worldwide, there is a significant percentage (5–20%) of *BRCA1/2* sequence changes that are classified as VUS, *i.e.*, alterations for which there is insufficient evidence of the effects on gene function and on disease risk.

It has been previously demonstrated that many *BRCA1/2* variants affect mRNA and generate abnormal splicing products (Sanz *et al*, 2010). The demonstration of a dysfunctional effect on splicing for a variant of interest can overcome the need for additional data required for multifactorial likelihood analysis, a method that has proved useful in quantitative assessment of variant pathogenicity for multiple cancer syndrome genes (Parsons *et al*, 2019).

Identification of a pathogenic *BRCA1* or *BRCA2* variant is important clinical information that directs medical management of an individual, including strategies aimed at prevention (risk reducing surgery or medication), early detection (presymptomatic screening), and more recently personalized treatment with PARP-inhibitors.

I was involved in a project aimed at the characterization through the hybrid minigene system of some gene variants never investigated in patients' mRNA. This approach allowed to comprehend for each of them which transcripts were produced only by the mutated allele enabling a correct classification of variants following the guidelines of the ENIGMA consortium.

The variants analyzed were, for what concerns *BRCA1*, c.213-14G>C in intron 5, c.302-5T>C in intron 6 and c.441G>C in exon 7, while in the case of *BRCA2,* c.68-5A>G in intron 2 and c.7618-2A>G in intron 15. Any splicing aberration was excluded in case of the c.302-5T>C variant in *BRCA1* and the subsequent analysis after cell treatment with puromycin, performed to prevent potential degradation of unstable transcripts via NMD, confirmed the presence of only the full-length transcript (Fig. 45 B). The variant was classified as likely benign (class 2). The minigene assay demonstrated a total spliceogenic effect in case of c.7618-2A>G variant in *BRCA2*, enabling its classification as pathogenic (class 5, Fig. 45 E).

For the remaining three variants the minigene assay revealed abnormalities in splicing, ranging from alternative usage of canonical splice sites, for the c.441G>C variant in *BRCA1* (Fig. 45 C), usage of *de*

novo splice sites in the case of c.68-5A>G variant in *BRCA2* (Fig. 45 D) and of cryptic splice sites, as in c.213-14C>G variant in *BRCA1* (Fig. 45 A). However, a residual, and in one case a almost undetectable, production of the full-length wild-type transcript from the mutated allele, supports the classification of these variants as VUS (class 3). The results of this study have just been published (Gelli *et al*, 2019).

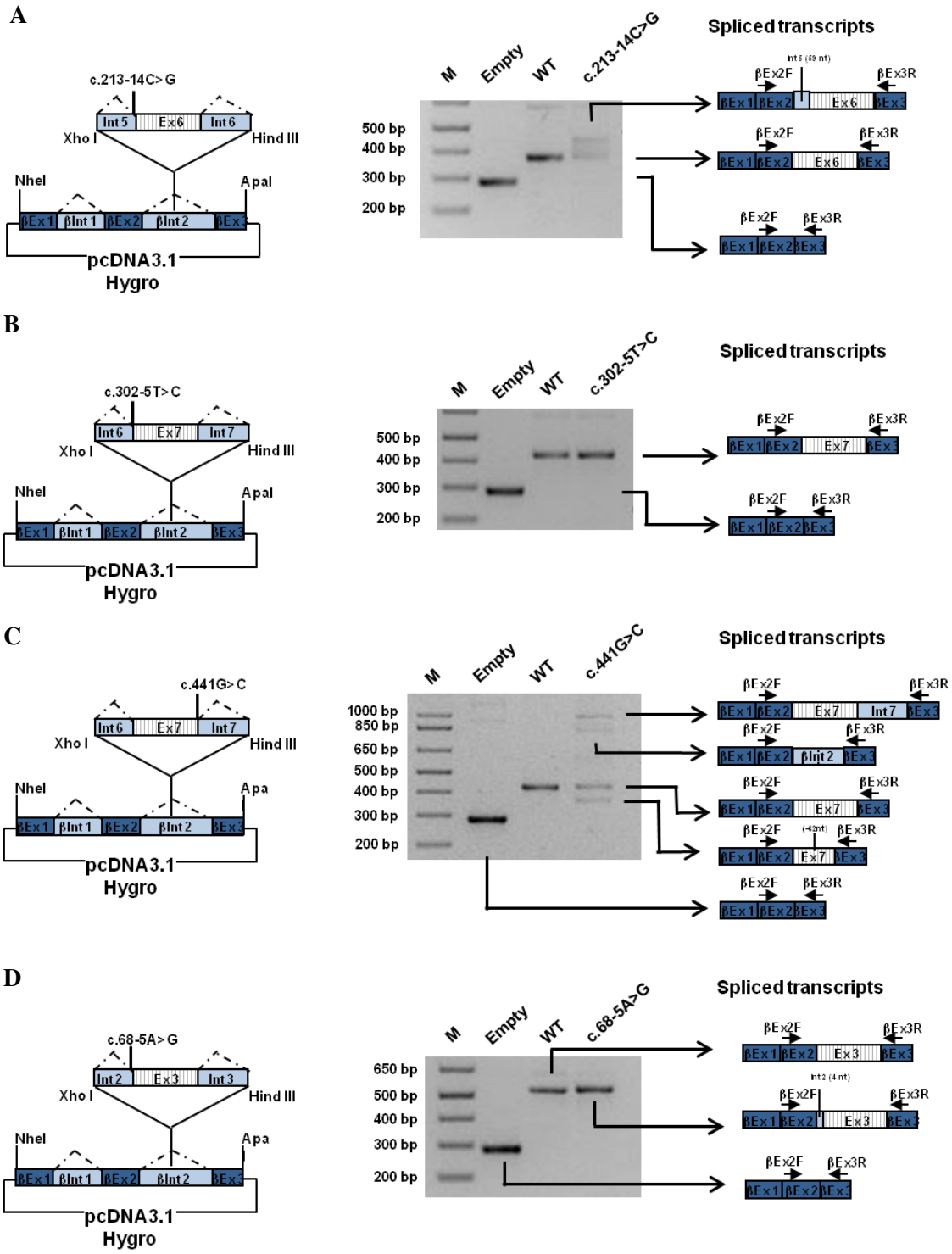

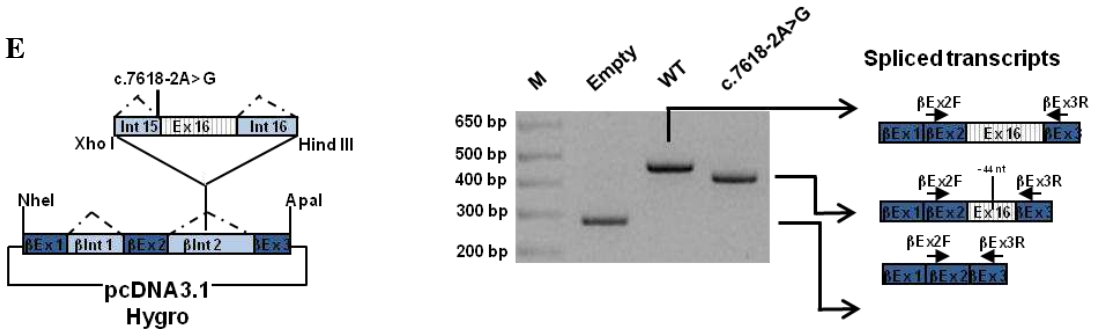

Fig. 45 RT-PCR analysis of the *BRCA1 and BRCA2* minigene constructs expressed in HeLA cells using vector specific primers. Each construct, schematically depicted on the left, contains the exon close to, or harboring the variant of interest and part of the upstream and downstream introns of *BRCA1* gene or *BRCA2* gene. In A), the construct contains the exon 6 of the *BRCA1* gene. Legend: M, 1 Kb plus molecular marker (ThermoFisher Scientific); Empty, empty β-globin-pCDNA3.1 vector; WT, wild type construct; c.213-14G>C, construct containing the c.213-14G>C variant. In B) and C), the construct contains exon 7 of the *BRCA1* gene. Legends as above, c.302-5T>C, construct containing the c.302-5T>C variant; c.441G>C, construct containing the c.441G>C variant. In D), the construct contains exon 3 of the *BRCA2* gene. c.68-5A>G, construct containing the c.68-5A>G variant. In E), the construct contains exon 16 of the *BRCA2* gene. c.7618-2A>G, construct containing the c.7618-2A>G variant (adapted from Gelli *et al*, 2019).

SECTION VIII

BIBLIOGRAPHY

Accili D, Arden KC. FoxOs at the crossroads of cellular metabolism, differentiation, and transformation. Cell. 2004 May 14;117(4):421-6.

Acin-Perez R, Enriquez JA. The function of the respiratory supercomplexes: the plasticity model. Biochim Biophys Acta. 2014 Apr;1837(4):444-5.

Aich A, Wang C, Chowdhury A, Ronsör C, Pacheu-Grau D, Richter-Dennerlein R, Dennerlein S, Rehling P. COX16 promotes COX2 metallation and assembly during respiratory complex IV biogenesis. Elife. 2018 Jan 30;7.

Adli M. The CRISPR tool kit for genome editing and beyond. Nat Commun. 2018 May 15;9(1):1911.

Ahringer, J., ed. Reverse genetics (April 6, 2006), WormBook, ed. The *C. elegans* Research Community, WormBook, doi/10.1895/wormbook.1.47.1.

Altun, Z.F. and Hall, D.H. 2010. Nervous system, neuronal support cells. In *WormAtlas*. doi:10.3908/wormatlas.1.19.

Altun, Z.F. and Hall, D.H. 2011. Nervous system, general description. In *WormAtlas*. doi:10.3908/wormatlas.1.18.

Ars E, Kruyer H, Morell M, Pros E, Serra E, Ravella A, Estivill X, Lázaro C. Recurrent mutations in the *NF1* gene are common among neurofibromatosis type 1 patients. J Med Genet. 2003 Jun;40(6):e82.

Avery L, Shtonda BB. Food transport in the *C. elegans* pharynx. J Exp Biol. 2003 Jul;206(Pt 14):2441-57.

Bacaj T, Lu Y, Shaham S. The conserved proteins CHE-12 and DYF-11 are required for sensory cilium function in *Caenorhabditis elegans*. Genetics. 2008 Feb;178(2):989-1002.

Badhwar R, Bagler G. Control of Neuronal Network in *Caenorhabditis elegans*. PLoS One. 2015 Sep 28;10(9):e0139204.

Bae YK, Barr MM. Sensory roles of neuronal cilia: cilia development, morphogenesis, and function in *C. elegans.* Front Biosci. 2008 May 1;13:5959-74.

Balsa E, Marco R, Perales-Clemente E, Szklarczyk R, Calvo E, Landázuri MO, Enríquez JA. NDUFA4 is a subunit of complex IV of the mammalian electron transport chain. Cell Metab. 2012 Sep 5;16(3):378-86.

Bargmann, C.I. Chemosensation in *C. elegans* (October 25, 2006), WormBook, ed. The *C. elegans* Research Community, WormBook, doi/10.1895/ wormbook.1.123.1.

Barr MM, Sternberg PW. A polycystic kidney-disease gene homologue required for male mating behaviour in *C. elegans*. Nature. 1999 Sep 23;401(6751):386-9.

Barrière A, Félix MA. Isolation of *C. elegans* and related nematodes. WormBook. 2014 May 2:1-19. doi: 10.1895/wormbook.1.115.2.

Bettencourt-Dias M, Hildebrandt F, Pellman D, Woods G, Godinho SA. Centrosomes and cilia in human disease. Trends Genet. 2011 Aug;27(8):307-15.

Bhaskaran S, Butler J A, Becerra S, Fassio V, Girotti M, Rea S L. Breaking *Caenorhabditis elegans* The Easy Way Using The Balch Homogenizer – An Old Tool For a New Application. Anal Biochem. 2011 Jun 15; 413(2): 123–132.

Blau HM, Chiu CP, Webster C. Cytoplasmic activation of human nuclear genes in stable heterocaryons. Cell. 1983 Apr;32(4):1171-80.

Braeckman BP, Houthoofd K, Vanfleteren JR. Intermediary metabolism (February 16, 2009), WormBook, ed. The *C. elegans* Research Community, WormBook, doi/10.1895/wormbook.1.146.1.

Brenner, S. (1974). Genetics 77, 71.

Burdine R, Stern M J. Easy RNA isolation from *C. elegans*: A TRIZOL based method. Worm Breeder's Gazette; 1996; 14: 10–10.

Burgering BM. A brief introduction to FOXOlogy. Oncogene. 2008 Apr 7;27(16):2258-62.

C. elegans Sequencing Consortium. Genome sequence of the nematode *C. elegans*: a platform for investigating biology. Science. 1998 Dec 11;282(5396):2012-8.

Caminsky N, Mucaki EJ, Rogan PK. Interpretation of mRNA splicing mutations in genetic disease: review of the literature and guidelines for information-theoretical analysis. F1000Res. 2014 Nov 18;3:282.

Carlson CG, Barrientos A, Tzagoloff A, Glerum DM. *COX16* encodes a novel protein required for the assembly of cytochrome oxidase in *Saccharomyces cerevisiae*. J Biol Chem. 2003 Feb 7;278(6):3770-5.

Cartegni L, Chew SL, Krainer AR. Listening to silence and understanding nonsense: exonic mutations that affect splicing. Nat Rev Genet. 2002 Apr;3(4):285-98.

Casarin A, Giorgi G, Pertegato V, Siviero R, Cerqua C, Doimo M, Basso G, Sacconi S, Cassina M, Rizzuto R, Brosel S, M Davidson M, Dimauro S, Schon EA, Clementi M, Trevisson E, Salviati L. Copper and bezafibrate cooperate to rescue cytochrome *c* oxidase deficiency in cells of patients with *SCO2* mutations. Orphanet J Rare Dis. 2012 Apr 19;7:21.

Cassada RC, Russell RL. The dauer larva, a post-embryonic developmental variant of the nematode *Caenorhabditis elegans*. Dev Biol. 1975 Oct;46(2):326-42.

Cerqua C, Morbidoni V, Desbats MA, Doimo M, Frasson C, Sacconi S, Baldoin MC, Sartori G, Basso G, Salviati L, Trevisson E. *COX16* is required for assembly of cytochrome *c* oxidase in human cells and is involved in copper delivery to COX2. Biochim Biophys Acta Bioenerg. 2018 Apr;1859(4):244-252.

Chalfie M, Tu Y, Euskirchen G, Ward WW, Prasher DC. Green fluorescent protein as a marker for gene expression. Science. 1994 Feb 11;263(5148):802-5.

Chang JT, Kumsta C, Hellman AB, Adams LM, Hansen M. Spatiotemporal regulation of autophagy during *Caenorhabditis elegans* aging. Elife. 2017 Jul 4;6.

Chang JT, Hansen M. Age-associated and tissue-specific decline in autophagic activity in the nematode *C. elegans*. Autophagy. 2018;14(7):1276-1277.

Chapin HC, Okada M, Merz AJ, Miller DL. Tissue-specific autophagy responses to aging and stress in *C. elegans*. Aging (Albany NY). 2015 Jun;7(6):419-34.

Chiba CM, Rankin CH. A developmental analysis of spontaneous and reflexive reversals in the nematode *Caenorhabditis elegans*. J Neurobiol. 1990 Jun;21(4):543-54.

Chicherin IV, Dashinimaev E, Baleva M, Krasheninnikov I, Levitskii S, Kamenski P. Cytochrome *c* Oxidase on the Crossroads of Transcriptional Regulation and Bioenergetics. Front Physiol. 2019 May 24;10:644.

Chiu H, Alqadah A, Chuang CF, Chang C. *C. elegans* as a genetic model to identify novel cellular and molecular mechanisms underlying nervous system regeneration. Cell Adh Migr. 2011 Sep-Oct;5(5):387-94.

Cohen-Fix O, Askjaer P. Cell Biology of the *Caenorhabditis elegans* Nucleus. Genetics. 2017 Jan;205(1):25-59.

Cong L, Ran FA, Cox D, Lin S, Barretto R, Habib N, Hsu PD, Wu X, Jiang W, Marraffini LA, Zhang F. Multiplex genome engineering using CRISPR/Cas systems. Science. 2013 Feb 15;339(6121):819-23.

Cook SJ, Jarrell TA, Brittin CA, Wang Y, Bloniarz AE, Yakovlev MA, Nguyen KCQ, Tang LT, Bayer EA, Duerr JS, Bülow HE, Hobert O, Hall DH, Emmons SW. Whole-animal connectomes of both *Caenorhabditis elegans* sexes. Nature. 2019 Jul;571(7763):63-71.

Corsi A.K., Wightman B., and Chalfie M. A Transparent window into biology: A primer on *Caenorhabditis elegans* (June 18, 2015), WormBook, ed. The *C. elegans* Research Community, WormBook, doi/10.1895/wormbook.1.177.1.

Das A, Dickinson DJ, Wood CC, Goldstein B, Slep KC. Crescerin uses a TOG domain array to regulate microtubules in the primary cilium. Mol Biol Cell. 2015 Nov 15;26(23):4248-64.

Devlin LA, Sayer JA. Renal ciliopathies. Curr Opin Genet Dev. 2019 Jun;56:49-60.

Diaz F, Thomas CK, Garcia S, Hernandez D, Moraes CT. Mice lacking COX10 in skeletal muscle recapitulate the phenotype of progressive mitochondrial myopathies associated with cytochrome *c* oxidase deficiency. Hum Mol Genet. 2005 Sep 15;14(18):2737-48.

Diaz F. Cytochrome *c* oxidase deficiency: patients and animal models. Biochim Biophys Acta. 2010 Jan;1802(1):100-10.

Dikic I, Elazar Z. Mechanism and medical implications of mammalian autophagy. Nat Rev Mol Cell Biol. 2018 Jun;19(6):349-364.

Dimaras H, Kimani K, Dimba EA, Gronsdahl P, White A, Chan HS, Gallie BL. Retinoblastoma. Lancet. 2012 Apr 14;379(9824):1436-46.

DiMauro S, Schon EA. Mitochondrial respiratory-chain diseases. N Engl J Med. 2003 Jun 26;348(26):2656-68.

DiMauro S. Mitochondrial diseases. Biochim Biophys Acta. 2004 Jul 23;1658(1-2):80-8.

DiMauro S, Tanji K, Schon EA. The many clinical faces of cytochrome *c* oxidase deficiency. Adv Exp Med Biol. 2012;748:341-5.

Doroquez DB, Berciu C, Anderson JR, Sengupta P, Nicastro D. A high-resolution morphological and ultrastructural map of anterior sensory cilia and glia in *Caenorhabditis elegans*. Elife. 2014 Mar 25;3:e01948.

Emmanuele V, López LC, Berardo A, Naini A, Tadesse S, Wen B, D'Agostino E, Solomon M, DiMauro S, Quinzii C, Hirano M. Heterogeneity of coenzyme Q10 deficiency: patient study and literature review. Arch Neurol. 2012 Aug;69(8):978-83.

Emmons, S.W. Male development (November 10, 2005), WormBook, ed. The *C. elegans* Research Community, WormBook, doi/10.1895/wormbook.1.33.1.

Fallerini C, Dosa L, Tita R, Del Prete D, Feriozzi S, Gai G, Clementi M, La Manna A, Miglietti N, Mancini R, Mandrile G, Ghiggeri GM, Piaggio G, Brancati F, Diano L, Frate E, Pinciaroli AR, Giani M, Castorina P, Bresin E, Giachino D, De Marchi M, Mari F, Bruttini M, Renieri A, Ariani F. Unbiased next generation sequencing analysis confirms the existence of autosomal dominant Alport syndrome in a relevant fraction of cases. Clin Genet. 2014 Sep;86(3):252-7.

Fallerini C, Baldassarri M, Trevisson E, Morbidoni V, La Manna A, Lazzarin R, Pasini A, Barbano G, Pinciaroli AR, Garosi G, Frullanti E, Pinto AM, Mencarelli MA, Mari F, Renieri A, Ariani F. Alport syndrome: impact of digenic inheritance in patients management. Clin Genet. 2017 Jul;92(1):34-44.

Fay D.S. Classical genetic methods (December 30, 2013), WormBook, ed. The *C. elegans* Research Community, WormBook, doi/10.1895/wormbook.1.165.1.

Ferner RE, Gutmann DH. Neurofibromatosis type 1 (NF1): diagnosis and management. Handb Clin Neurol. 2013;115:939-55.

Fire A, Xu S, Montgomery MK, Kostas SA, Driver SE, Mello CC. Potent and specific genetic interference by double-stranded RNA in *Caenorhabditis elegans*. Nature. 1998 Feb 19;391(6669):806-11.

Fontanesi F, Soto IC, Barrientos A. Cytochrome *c* oxidase biogenesis: new levels of regulation. IUBMB Life. 2008 Sep;60(9):557-68.

Forzan M, Salviati L, Pertegato V, Casarin A, Bruson A, Trevisson E, Di Gianantonio E, Clementi M. Is *CFTR* 621+3 A>G a cystic fibrosis causing mutation? J Hum Genet. 2010 Jan;55(1):23-6.

Friend SH, Bernards R, Rogelj S, Weinberg RA, Rapaport JM, Albert DM, Dryja TP. A human DNA segment with properties of the gene that predisposes to retinoblastoma and osteosarcoma. Nature. 1986 Oct 16-22;323(6089):643-6.

Gelli E, Colombo M, Pinto AM, De Vecchi G, Foglia C, Amitrano S, Morbidoni V, Imperatore V, Manoukian S, Baldassarri M, Lo Rizzo C, Catania L, Frullanti E, Tagliafico E, Cortesi L, Spaggiari F, Mencarelli MA, Trevisson E, Radice P, Renieri A, Ariani F. Usefulness and Limitations of

Comprehensive Characterization of mRNA Splicing Profiles in the Definition of the Clinical Relevance of *BRCA1/2* Variants of Uncertain Significance. Cancers (Basel). 2019 Mar 1;11(3).

Gems D, Sutton AJ, Sundermeyer ML, Albert PS, King KV, Edgley ML, Larsen PL, Riddle DL. Two pleiotropic classes of *daf-2* mutation affect larval arrest, adult behavior, reproduction and longevity in *Caenorhabditis elegans*. Genetics. 1998 Sep;150(1):129-55.

Genuardi M, Klutz M, Devriendt K, Caruso D, Stirpe M, Lohmann DR. Multiple lipomas linked to an *RB1* gene mutation in a large pedigree with low penetrance retinoblastoma. Eur J Hum Genet. 2001 Sep;9(9):690-4.

Ghezzi D, Zeviani M. Assembly factors of human mitochondrial respiratory chain complexes: physiology and pathophysiology. Adv Exp Med Biol. 2012;748:65-106.

Gieseler K., Qadota H., and Benian G. M. Development, structure, and maintenance of *C. elegans* body wall muscle. (April 13, 2017), WormBook, ed. The *C. elegans* Research Community, WormBook, 10.1895/wormbook.1.81.2.

Gómez-Orte E, Cornes E, Zheleva A, Sáenz-Narciso B, de Toro M, Iñiguez M, López R, San-Juan JF, Ezcurra B, Sacristán B, Sánchez-Blanco A, Cerón J, Cabello J. Effect of the diet type and temperature on the *C. elegans* transcriptome. Oncotarget. 2017 Dec 21;9(11):9556-9571.

Glick D, Barth S, Macleod KF. Autophagy: cellular and molecular mechanisms. J Pathol. 2010 May;221(1):3-12.

Grad LI, Sayles LC, Lemire BD. Isolation and functional analysis of mitochondria from the nematode *Caenorhabditis elegans*. Methods Mol Biol. 2007;372:51-66.

Grishok A. RNAi mechanisms in *Caenorhabditis elegans*. FEBS Lett. 2005 Oct 31;579(26):5932-9.

Gubler MC. Inherited diseases of the glomerular basement membrane. Nat Clin Pract Nephrol. 2008 Jan;4(1):24-37.

Gusarov I, Pani B, Gautier L, Smolentseva O, Eremina S, Shamovsky I, Katkova-Zhukotskaya O, Mironov A, Nudler E. Glycogen controls *Caenorhabditis elegans* lifespan and resistance to oxidative stress. Nat Commun. 2017 Jun 19;8:15868.

Hartill V, Szymanska K, Sharif SM, Wheway G, Johnson CA. Meckel-Gruber Syndrome: An Update on Diagnosis, Clinical Management, and Research Advances. Front Pediatr. 2017 Nov 20;5:244.

Hedgecock EM, Sulston JE, Thomson JN. Mutations affecting programmed cell deaths in the nematode *Caenorhabditis elegans*. Science. 1983 Jun 17;220(4603):1277-9.

Hedgecock EM, White JG. Polyploid tissues in the nematode *Caenorhabditis elegans*. Dev Biol. 1985 Jan;107(1):128-33.

Hillier LW, Coulson A, Murray JI, Bao Z, Sulston JE, Waterston RH. Genomics in *C. elegans*: so many genes, such a little worm. Genome Res. 2005 Dec;15(12):1651-60.

Hildebrandt F, Benzing T, Katsanis N. Ciliopathies. N Engl J Med. 2011 Apr 21;364(16):1533-43.

Hirsh D, Vanderslice R. Temperature-sensitive developmental mutants of *Caenorhabditis elegans*. Dev Biol. 1976 Mar;49(1):220-35.

Hobert, O. Specification of the nervous system (August 8, 2005), WormBook, ed. The *C. elegans* Research Community, WormBook, doi/10.1895/wormbook.1.12.1.

Hobert O. The neuronal genome of *Caenorhabditis elegans* (August 13, 2013), WormBook, ed. The *C. elegans* Research Community, WormBook, doi/10.1895/wormbook.1.161.1.

Hope I A. *C. elegans: A Practical Approach.* Oxford University Press, Oxford. 1999.

Hsin H, Kenyon C. Signals from the reproductive system regulate the lifespan of *C. elegans*. Nature. 1999 May 27;399(6734):362-6.

Hsu PD, Lander ES, Zhang F. Development and applications of CRISPR-Cas9 for genome engineering. Cell. 2014 Jun 5;157(6):1262-78.

Hudson BG. The molecular basis of Goodpasture and Alport syndromes: beacons for the discovery of the collagen IV family. J Am Soc Nephrol. 2004 Oct;15(10):2514-27.

Hüttemann M, Lee I, Grossman LI, Doan JW, Sanderson TH. Phosphorylation of mammalian cytochrome *c* and cytochrome *c* oxidase in the regulation of cell destiny: respiration, apoptosis, and human disease. Adv Exp Med Biol. 2012;748:237-64.

Imperatore V, Pinto AM, Gelli E, Trevisson E, Morbidoni V, Frullanti E, Hadjistilianou T, De Francesco S, Toti P, Gusson E, Roversi G, Accogli A, Capra V, Mencarelli MA, Renieri A, Ariani F. Parent-of-origin effect of hypomorphic pathogenic variants and somatic mosaicism impact on phenotypic expression of retinoblastoma. Eur J Hum Genet. 2018 Jul;26(7):1026-1037.

Inglis P.N. et al. The sensory cilia of *Caenorhabditis elegans* (March 8, 2007), WormBook, ed. The *C. elegans* Research Community, WormBook, doi/10.1895/wormbook.1.126.2.

Jacobi AM, Rettig GR, Turk R, Collingwood MA, Zeiner SA, Quadros RM, Harms DW, Bonthuis PJ, Gregg C, Ohtsuka M, Gurumurthy CB, Behlke MA. Simplified CRISPR tools for efficient genome

editing and streamlined protocols for their delivery into mammalian cells and mouse zygotes. Methods. 2017 May 15;121-122:16-28.

Jiang P, Mizushima N. Autophagy and human diseases. Cell Res. 2014 Jan;24(1):69-79.

Kaletta T, Hengartner MO. Finding function in novel targets: *C. elegans* as a model organism. Nat Rev Drug Discov. 2006 May;5(5):387-98.

Kanber D, Berulava T, Ammerpohl O, Mitter D, Richter J, Siebert R, Horsthemke B, Lohmann D, Buiting K. The human retinoblastoma gene is imprinted. PLoS Genet. 2009 Dec;5(12):e1000790.

Kang C, You YJ, Avery L. Dual roles of autophagy in the survival of *Caenorhabditis elegans* during starvation. Genes Dev. 2007 Sep 1;21(17):2161-71.

Kenyon C, Chang J, Gensch E, Rudner A, Tabtiang R. A *C. elegans* mutant that lives twice as long as wild type. Nature. 1993 Dec 2;366(6454):461-4.

Kim SK, Horvitz HR. The *Caenorhabditis elegans* gene *lin-10* is broadly expressed while required specifically for the determination of vulval cell fates. Genes Dev. 1990 Mar;4(3):357-71.

Kimura KD, Tissenbaum HA, Liu Y, Ruvkun G. *daf-2*, an insulin receptor-like gene that regulates longevity and diapause in *Caenorhabditis elegans*. Science. 1997 Aug 15;277(5328):942-6.

Klionsky DJ *et al*, Guidelines for the use and interpretation of assays for monitoring autophagy. Autophagy. 2012 Apr;8(4):445-544.

Kuchenbaecker KB *et al*, Risks of Breast, Ovarian, and Contralateral Breast Cancer for *BRCA1* and *BRCA2* Mutation Carriers. JAMA. 2017 Jun 20;317(23):2402-2416.

Kulkarni A, Chen J, Maday S. Neuronal autophagy and intercellular regulation of homeostasis in the brain. Curr Opin Neurobiol. 2018 Aug;51:29-36.

Lee SJ, Murphy CT, Kenyon C. Glucose shortens the life span of *C. elegans* by downregulating DAF-16/FOXO activity and aquaporin gene expression. Cell Metab. 2009 Nov;10(5):379-91.

Lee S, Dong HH. FoxO integration of insulin signaling with glucose and lipid metabolism. J Endocrinol. 2017 May;233(2):R67-R79.

Lemire, B. Mitochondrial genetics (September 14, 2005), WormBook, ed. The *C. elegans* Research Community, WormBook, doi/10.1895/ wormbook.1.25.1.

Liang Y. Emerging Concepts and Functions of Autophagy as a Regulator of Synaptic Components and Plasticity. Cells. 2019 Jan 9;8(1).

Lin K, Dorman JB, Rodan A, Kenyon C. *daf-16*: An HNF-3/forkhead family member that can function to double the life-span of *Caenorhabditis elegans*. Science. 1997 Nov 14;278(5341):1319-22.

Lin XX, Sen I, Janssens GE, Zhou X, Fonslow BR, Edgar D, Stroustrup N, Swoboda P, Yates JR 3rd, Ruvkun G, Riedel CG. DAF-16/FOXO and HLH-30/TFEB function as combinatorial transcription factors to promote stress resistance and longevity. Nat Commun. 2018 Oct 23;9(1):4400.

Lithgow GJ, White TM, Melov S, Johnson TE. Thermotolerance and extended life-span conferred by single-gene mutations and induced by thermal stress. Proc Natl Acad Sci U S A. 1995 Aug 1;92(16):7540-4.

Liu Q, Kidd PB, Dobosiewicz M, Bargmann CI. *C. elegans* AWA Olfactory Neurons Fire Calcium-Mediated All-or-None Action Potentials. Cell. 2018 Sep 20;175(1):57-70.e17.

Luo F, Tao YH. Nephronophthisis: A review of genotype-phenotype correlation. Nephrology (Carlton). 2018 Oct;23(10):904-911.

Maglioni S, Ventura N. *C. elegans* as a model organism for human mitochondrial associated disorders. Mitochondrion. 2016 Sep;30:117-25.

Maillard PV, van der Veen AG, Poirier EZ, Reis E Sousa C. Slicing and dicing viruses: antiviral RNA interference in mammals. EMBO J. 2019 Apr 15;38(8).

Mammucari C, Milan G, Romanello V, Masiero E, Rudolf R, Del Piccolo P, Burden SJ, Di Lisi R, Sandri C, Zhao J, Goldberg AL, Schiaffino S, Sandri M. FoxO3 controls autophagy in skeletal muscle in vivo. Cell Metab. 2007 Dec;6(6):458-71.

Martinez-Lopez N, Athonvarangkul D, Singh R. Autophagy and aging. Adv Exp Med Biol. 2015;847:73-87.

Martins R, Lithgow GJ, Link W. Long live FOXO: unraveling the role of FOXO proteins in aging and longevity. Aging Cell. 2016 Apr;15(2):196-207.

Masyukova SV, Landis DE, Henke SJ, Williams CL, Pieczynski JN, Roszczynialski KN, Covington JE, Malarkey EB, Yoder BK. A Screen for Modifiers of Cilia Phenotypes Reveals Novel *MKS* Alleles and Uncovers a Specific Genetic Interaction between *osm-3* and *nphp-4*. PLoS Genet. 2016 Feb 10;12(2):e1005841.

Mathiassen SG, De Zio D, Cecconi F. Autophagy and the Cell Cycle: A Complex Landscape. Front Oncol. 2017 Mar 31;7:51.

Maupas, E. Modes et formes de reproduction des nématodes. Arch. Zool. Exp. 1900; 8: 463-624.

Meissner B, Rogalski T, Viveiros R, Warner A, Plastino L, Lorch A, Granger L, Segalat L, Moerman DG. Determining the sub-cellular localization of proteins within *Caenorhabditis elegans* body wall muscle. PLoS One. 2011;6(5):e19937.

Meléndez A, Tallóczy Z, Seaman M, Eskelinen EL, Hall DH, Levine B. Autophagy genes are essential for dauer development and life-span extension in *C. elegans*. Science. 2003 Sep 5;301(5638):1387-91.

Meléndez, A. and Levine, B. Autophagy in *C. elegans* (August 24, 2009), *WormBook*, ed. The *C. elegans* Research Community, WormBook, doi/10.1895/wormbook.1.147.1.

Mencarelli MA, Heidet L, Storey H, van Geel M, Knebelmann B, Fallerini C, Miglietti N, Antonucci MF, Cetta F, Sayer JA, van den Wijngaard A, Yau S, Mari F, Bruttini M, Ariani F, Dahan K, Smeets B, Antignac C, Flinter F, Renieri A. Evidence of digenic inheritance in Alport syndrome. J Med Genet. 2015 Mar;52(3):163-74.

Menzies FM, Fleming A, Caricasole A, Bento CF, Andrews SP, Ashkenazi A, Füllgrabe J, Jackson A, Jimenez Sanchez M, Karabiyik C, Licitra F, Lopez Ramirez A, Pavel M, Puri C, Renna M, Ricketts T, Schlotawa L, Vicinanza M, Won H, Zhu Y, Skidmore J, Rubinsztein DC. Autophagy and Neurodegeneration: Pathogenic Mechanisms and Therapeutic Opportunities. Neuron. 2017 Mar 8;93(5):1015-1034.

Merris M, Kraeft J, Tint GS, Lenard J. Long-term effects of sterol depletion in *C. elegans*: sterol content of synchronized wild-type and mutant populations. J Lipid Res. 2004 Nov;45(11):2044-51.

Michel H. The mechanism of proton pumping by cytochrome *c* oxidase. Proc Natl Acad Sci U S A. 1998 Oct 27;95(22):12819-2.

Milan G, Romanello V, Pescatore F, Armani A, Paik JH, Frasson L, Seydel A, Zhao J, Abraham R, Goldberg AL, Blaauw B, DePinho RA, Sandri M. Regulation of autophagy and the ubiquitin-proteasome system by the FoxO transcriptional network during muscle atrophy. Nat Commun. 2015 Apr 10;6:6670.

Milenkovic D, Blaza JN, Larsson NG, Hirst J. The enigma of the respiratory chain supercomplex. Cell Metab. 2017 Apr 4;25(4):765-776.

Mizushima N. Autophagy: process and function. Genes Dev. 2007 Nov 15;21(22):2861-73.

Mourier A, Larsson NG. Tracing the trail of protons through complex I of the mitochondrial respiratory chain. PLoS Biol. 2011 Aug;9(8):e1001129.

Murphy CT, McCarroll SA, Bargmann CI, Fraser A, Kamath RS, Ahringer J, Li H, Kenyon C. Genes that act downstream of DAF-16 to influence the lifespan of *Caenorhabditis elegans*. Nature. 2003 Jul 17;424(6946):277-83.

Nigon, V. Polyploïdie expérimentale chez un nématode libre, *Rhabditis elegans* Maupas. Bull. Biol. Fr. Belg. 1951; 85: 187-225.

Nigon, V.M., and Félix, M.-A. History of research on *C. elegans* and other free-living nematodes as model organisms. (September, 07, 2017), *WormBook*, ed. The *C. elegans* Research Community, WormBook, doi/10.1895/wormbook.1.181.1.

Paix A, Folkmann A, Rasoloson D, Seydoux G High Efficiency, Homology-directed genome editing in *Caenorhabditis elegans* Using CRISPR-Cas9 ribonucleoprotein complexes. Genetics. 2015 Sep;201(1):47-54.

Paix A, Folkmann A, Seydoux G. Precision genome editing using CRISPR-Cas9 and linear repair templates in *C. elegans*. Methods. 2017 May 15;121-122:86-93.

Palmisano NJ, Meléndez A. Detection of Autophagy in *Caenorhabditis elegans*. Cold Spring Harb Protoc. 2016 Feb 1;2016(2):pdb.top070466.

Panowski SH, Dillin A. Signals of youth: endocrine regulation of aging in *Caenorhabditis elegans*. Trends Endocrinol Metab. 2009 Aug;20(6):259-64.

Parsons MT *et al*. Large scale multifactorial likelihood quantitative analysis of *BRCA1* and *BRCA2* variants: An ENIGMA resource to support clinical variant classification. Hum Mutat. 2019 May 27.

Perkins LA, Hedgecock EM, Thomson JN, Culotti JG. Mutant sensory cilia in the nematode *Caenorhabditis elegans*. Dev Biol. 1986 Oct;117(2):456-87.

Petruzzella V, Tiranti V, Fernandez P, Ianna P, Carrozzo R, Zeviani M. Identification and characterization of human cDNAs specific to *BCS1*, *PET112*, *SCO1*, *COX15*, and *COX11*, five genes involved in the formation and function of the mitochondrial respiratory chain. Genomics. 1998 Dec 15;54(3):494-504.

Pierron D, Wildman DE, Hüttemann M, Letellier T, Grossman LI. Evolution of the couple cytochrome *c* and cytochrome *c* oxidase in primates. Adv Exp Med Biol. 2012;748:185-213.

Possik E, Pause A. Measuring oxidative stress resistance of *Caenorhabditis elegans* in 96-well microtiter plates. J Vis Exp. 2015 May 9;(99):e52746.

Rak M, Bénit P, Chrétien D, Bouchereau J, Schiff M, El-Khoury R, Tzagoloff A, Rustin P. Mitochondrial cytochrome *c* oxidase deficiency. Clin Sci (Lond). 2016 Mar;130(6):393-407.

Ramzan R, Weber P, Kadenbach B, Vogt S. Individual biochemical behaviour versus biological robustness: spotlight on the regulation of cytochrome *c* oxidase. Adv Exp Med Biol. 2012;748:265-81.

Rea SL, Ventura N, Johnson TE. Relationship between mitochondrial electron transport chain dysfunction, development, and life extension in *Caenorhabditis elegans*. PLoS Biol. 2007 Oct 2;5(10):e259.

Reiter JF, Leroux MR. Genes and molecular pathways underpinning ciliopathies. Nat Rev Mol Cell Biol. 2017 Sep;18(9):533-547.

Richards S, Aziz N, Bale S, Bick D, Das S, Gastier-Foster J, Grody WW, Hegde M, Lyon E, Spector E, Voelkerding K, Rehm HL; ACMG Laboratory Quality Assurance Committee. Standards and guidelines for the interpretation of sequence variants: a joint consensus recommendation of the American College of Medical Genetics and Genomics and the Association for Molecular Pathology. Genet Med. 2015 May;17(5):405-24.

Rubinsztein DC, Mariño G, Kroemer G. Autophagy and aging. Cell. 2011 Sep 2;146(5):682-95.

Saeki S, Yamamoto M, Iino Y. Plasticity of chemotaxis revealed by paired presentation of a chemoattractant and starvation in the nematode *Caenorhabditis elegans*. J Exp Biol. 2001 May;204(Pt 10):1757-64.

Salviati L, Hernandez-Rosa E, Walker WF, Sacconi S, DiMauro S, Schon EA, Davidson MM. Copper supplementation restores cytochrome *c* oxidase activity in cultured cells from patients with *SCO2* mutations. Biochem J. 2002 Apr 15;363(Pt 2):321-7.

Sammut M, Cook SJ, Nguyen KCQ, Felton T, Hall DH, Emmons SW, Poole RJ, Barrios A. Glia-derived neurons are required for sex-specific learning in *C. elegans*. Nature. 2015 Oct 15;526(7573):385-390.

Sandri M, Sandri C, Gilbert A, Skurk C, Calabria E, Picard A, Walsh K, Schiaffino S, Lecker SH, Goldberg AL. Foxo transcription factors induce the atrophy-related ubiquitin ligase atrogin-1 and cause skeletal muscle atrophy. Cell. 2004 Apr 30;117(3):399-412.

Sanz DJ, Acedo A, Infante M, Durán M, Pérez-Cabornero L, Esteban-Cardeñosa E, Lastra E, Pagani F, Miner C, Velasco EA. A high proportion of DNA variants of *BRCA1* and *BRCA2* is associated with aberrant splicing in breast/ovarian cancer patients. Clin Cancer Res. 2010 Mar 15;16(6):1957-67.

Sawin ER, Ranganathan R, Horvitz HR. *C. elegans* locomotory rate is modulated by the environment through a dopaminergic pathway and by experience through a serotonergic pathway. Neuron. 2000 Jun;26(3):619-31.

Schafer W. Nematode nervous systems. Curr Biol. 2016 Oct 24;26(20):R955-R959.

Schulz TJ, Zarse K, Voigt A, Urban N, Birringer M, Ristow M. Glucose restriction extends *Caenorhabditis elegans* life span by inducing mitochondrial respiration and increasing oxidative stress. Cell Metab. 2007 Oct;6(4):280-93.

Seligman AM, Karnovsky MJ, Wasserkrug HL, Hanker JS. Nondroplet ultrastructural demonstration of cytochrome oxidase activity with a polymerizing osmiophilic reagent, diaminobenzidine (DAB). J Cell Biol. 1968 Jul;38(1):1-14.

Senchuk MM, Dues DJ, Schaar CE, Johnson BK, Madaj ZB, Bowman MJ, Winn ME, Van Raamsdonk JM. Activation of DAF-16/FOXO by reactive oxygen species contributes to longevity in long-lived mitochondrial mutants in *Caenorhabditis elegans*. PLoS Genet. 2018 Mar 9;14(3):e1007268.

Signes A, Fernandez-Vizarra E. Assembly of mammalian oxidative phosphorylation complexes I-V and supercomplexes. Essays Biochem. 2018 Jul 20;62(3):255-270.

Simmer F, Tijsterman M, Parrish S, Koushika SP, Nonet ML, Fire A, Ahringer J, Plasterk RH. Loss of the putative RNA-directed RNA polymerase RRF-3 makes *C. elegans* hypersensitive to RNAi. Curr Biol. 2002 Aug 6;12(15):1317-9.

Sinkler CA, Kalpage H, Shay J, Lee I, Malek MH, Grossman LI, Hüttemann M. Tissue- and condition-specific isoforms of mammalian cytochrome *c* oxidase subunits: from function to human disease. Oxid Med Cell Longev. 2017;2017:1534056.

Slep KC. The role of TOG domains in microtubule plus end dynamics. Biochem Soc Trans. 2009 Oct;37(Pt 5):1002-6.

Son JH, Shim JH, Kim KH, Ha JY, Han JY. Neuronal autophagy and neurodegenerative diseases. Exp Mol Med. 2012 Feb 29;44(2):89-98. doi: 10.3858/emm.2012.44.2.031.

Starich TA, Herman RK, Kari CK, Yeh WH, Schackwitz WS, Schuyler MW, Collet J, Thomas JH, Riddle DL. Mutations affecting the chemosensory neurons of *Caenorhabditis elegans*. Genetics. 1995 Jan;139(1):171-88.

Stiernagle, T. Maintenance of *C. elegans* (February 11, 2006), WormBook, ed. The *C. elegans* Research Community, WormBook, doi/10.1895/wormbook.1.101.1.

Sulston J, Hodgkin J. 1988. Methods, The nematode *C. elegans,* edited by W.B. Wood. Cold Spring Harbor. Laboratory Press, Cold Spring Harbor, NY.

Sulston JE, Schierenberg E, White JG, Thomson JN. The embryonic cell lineage of the nematode *Caenorhabditis elegans*. Dev. Biol. Dev Biol. 1983 Nov;100(1):64-119.

Suspitsin E, Imyanitov EN. Bardet-Biedl Syndrome. Mol Syndromol. 2016 May; 7(2): 62–71.

Suthammarak W, Yang YY, Morgan PG, Sedensky MM. Complex I function is defective in complex IV-deficient *Caenorhabditis elegans*. J Biol Chem. 2009 Mar 6;284(10):6425-3.

Suthammarak W, Morgan PG, Sedensky MM. Mutations in mitochondrial complex III uniquely affect complex I in *Caenorhabditis elegans*. J Biol Chem. 2010 Dec 24;285(52):40724-31.

Thomas S, Boutaud L, Reilly ML, Benmerah A. Cilia in hereditary cerebral anomalies. Biol Cell. 2019 Sep;111(9):217-231.

Thorburn A. Autophagy and disease. J Biol Chem. 2018 Apr 13;293(15):5425-5430.

Timmons L, Court DL, Fire A. Ingestion of bacterially expressed dsRNAs can produce specific and potent genetic interference in *Caenorhabditis elegans*. Gene. 2001 Jan 24;263(1-2):103-12.

Tissenbaum HA. Using *C. elegans* for aging research. Invertebr Reprod Dev. 2015 Jan 30;59(sup1):59-63.

Tóth ML, Sigmond T, Borsos E, Barna J, Erdélyi P, Takács-Vellai K, Orosz L, Kovács AL, Csikós G, Sass M, Vellai T. Longevity pathways converge on autophagy genes to regulate life span in *Caenorhabditis elegans*. Autophagy. 2008 Apr;4(3):330-8.

Trevisson E, Morbidoni V, Forzan M, Daolio C, Fumini V, Parrozzani R, Cassina M, Midena E, Salviati L, Clementi M. The Arg1038Gly missense variant in the *NF1* gene causes a mild phenotype without neurofibromas. Mol Genet Genomic Med. 2019 May;7(5):e616.

Tsang WY, Lemire BD. The role of mitochondria in the life of the nematode, *Caenorhabditis elegans*. Biochim Biophys Acta. 2003 Jul 14;1638(2):91-105.

Tyson JR, O'Neil NJ, Jain M, Olsen HE, Hieter P, Snutch TP. MinION-based long-read sequencing and assembly extends the *Caenorhabditis elegans* reference genome. Genome Res. 2018 Feb;28(2):266-274.

van der Bliek AM, Sedensky MM, Morgan PG. Cell Biology of the Mitochondrion. Genetics. 2017 Nov;207(3):843-871.

Ventura N, Rea SL. *Caenorhabditis elegans* mitochondrial mutants as an investigative tool to study human neurodegenerative diseases associated with mitochondrial dysfunction. Biotechnol J. 2007 May;2(5):584-95.

Vidoni S, Harbour ME, Guerrero-Castillo S, Signes A, Ding S, Fearnley IM, Taylor RW, Tiranti V, Arnold S, Fernandez-Vizarra E, Zeviani M. MR-1S Interacts with PET100 and PET117 in module-based assembly of human cytochrome *c* oxidase. Cell Rep. 2017 Feb 14;18(7):1727-1738.

Wallace DC. Mitochondrial DNA mutations in disease and aging. Environ Mol Mutagen. 2010 Jun;51(5):440-50.

Wallis D, Li K, Lui H, Hu K, Chen MJ, Li J, Kang J, Das S, Korf BR, Kesterson RA. Neurofibromin (NF1) genetic variant structure-function analyses using a full-length mouse cDNA. Hum Mutat. 2018 Jun;39(6):816-821.

Warburton-Pitt SR, Jauregui AR, Li C, Wang J, Leroux MR, Barr MM. Ciliogenesis in *Caenorhabditis elegans* requires genetic interactions between ciliary middle segment localized NPHP-2 (inversin) and transition zone-associated proteins. J Cell Sci. 2012 Jun 1;125(Pt 11):2592-603.

Ward S, Carrel JS. Fertilization and sperm competition in the nematode *Caenorhabditis elegans*. Dev Biol. 1979 Dec; 73(2):304-21.

Waters AM, Beales PL. Ciliopathies: an expanding disease spectrum. Pediatr Nephrol. 2011 Jul;26(7):1039-56.

White JG, Southgate E, Thomson JN, Brenner S. The structure of the nervous system of the nematode *Caenorhabditis elegans*. Philos Trans R Soc Lond B Biol Sci. 1986 Nov 12;314(1165):1-340.

Whitfield CW, Bénard C, Barnes T, Hekimi S, Kim SK. Basolateral localization of the *Caenorhabditis elegans* epidermal growth factor receptor in epithelial cells by the PDZ protein LIN-10. Mol Biol Cell. 1999 Jun;10(6):2087-100.

Wong-Riley MT. Bigenomic regulation of cytochrome *c* oxidase in neurons and the tight coupling between neuronal activity and energy metabolism. Adv Exp Med Biol. 2012;748:283-304.

Yin H, Song CQ, Suresh S, Wu Q, Walsh S, Rhym LH, Mintzer E, Bolukbasi MF, Zhu LJ, Kauffman K, Mou H, Oberholzer A, Ding J, Kwan SY, Bogorad RL, Zatsepin T, Koteliansky V, Wolfe SA, Xue W, Langer R, Anderson DG. Structure-guided chemical modification of guide RNA enables potent non-viral in vivo genome editing. Nat Biotechnol. 2017 Dec;35(12):1179-1187.

Yu S, Avery L, Baude E, Garbers DL. Guanylyl cyclase expression in specific sensory neurons: a new family of chemosensory receptors. Proc Natl Acad Sci U S A. 1997 Apr 1;94(7):3384-7.

Zarkower, D. Somatic sex determination (February 10, 2006), WormBook, ed. The *C. elegans* Research Community, WormBook, doi/10.1895/wormbook.1.84.1.

Zhang X, Tang N, Hadden TJ, Rishi AK. Akt, FoxO and regulation of apoptosis. Biochim Biophys Acta. 2011 Nov;1813(11):1978-86.

Zhang H, Chang JT, Guo B, Hansen M, Jia K, Kovács AL, Kumsta C, Lapierre LR, Legouis R, Lin L, Lu Q, Meléndez A, O'Rourke EJ, Sato K, Sato M, Wang X, Wu F. Guidelines for monitoring autophagy in *Caenorhabditis elegans*. Autophagy. 2015;11(1):9-27.

ACKNOWLEDGEMENTS

My sincere appreciation goes to those who have supported me in one way or the other during these three years.

First of all I would like to thank my supervisor Dr. Eva Trevisson, for giving me the possibility to enroll in the PhD program of the Translational Specialistic Medicine "G.B. Morgagni" school, which has been extremely formative: first of all, I could expand my technical skills and had the opportunity to approach the use of *C. elegans* as model of study, being to my knowledge the only group in Padua with this expertise so far. Moreover, I am grateful to her since I had the possibility to be involved in several stimulating projects, and she supported and allowed me to grow as a research scholar.

I also thank Prof. Leonardo Salviati, the head of the Genetics Lab, my colleagues of the research group, Cristina, Cristina and Elisa, for our collaborative sharing of ideas and skills, and all the people in the diagnostics division. I'm also grateful to past lab members Laura, Luis, Manuel, Marian and Roberta for their help and suggestions.

I would like to thank Prof. Marco Sandri and Anaïs Franco-Romero for the opportunity to be involved in an exciting research project and the friendly collaboration that we have established.

Moreover a special thank goes to Simone Martinelli and Luca Pannone, who helped us with the genome-editing experiments and provided me many useful technical tips. I also had to opportunity to visit their lab in Roma, meet their group and to be trained by Luca in *C. elegans* microinjection.

Finally, I'm grateful to Prof. Kevin Slep for his useful suggestions and kind help with the Crescerin project.